# Problems in Cosmology and Numerical Relativity

Bishop Mongwane




Thesis presented for the Degree of
DOCTOR OF PHILOSOPHY
in the Department of Mathematics and Applied Mathematics
UNIVERSITY OF CAPE TOWN
South Africa
October 2014

Supervisor: Prof Peter K. S. Dunsby

# Declaration

The work presented in this thesis is based on works done by the author at the University of Cape Town under the supervision of Prof. Peter K. S. Dunsby. The list below identifies chapters which are partly based on the listed publications/preprints:

- Chapter 5

  "Cosmic Electromagnetic Fields due to Perturbations in the Gravitational Field"
  Bishop Mongwane, Peter K. S. Dunsby, Bob O. Osano
  Journal-ref: Phys. Rev. D 86, 083533 (2012)

- Chapter 9

  "On Convergence of High Order Runge-Kutta Time Discretizations for Non-Linear Hyperbolic Problems"
  Bishop Mongwane
  Journal-ref: Submitted to SIAM (2014)

- Chapter 10

  "Toward a Consistent Framework for High Order Mesh Refinement Schemes in Numerical Relativity"
  Bishop Mongwane
  Journal-ref: Submitted to CQG (2014)

I hereby declare that this thesis has not been submitted, either in the same or different form, to this or any other university for a degree and that it represents my own work.

Bishop Mongwane
October 2014

# Abstract

A generic feature of most inflationary scenarios is the generation of primordial perturbations. Ordinarily, such perturbations can interact with a weak magnetic field in a plasma, resulting in a wide range of phenomena, such as the parametric excitation of plasma waves by gravitational waves. This mechanism has been studied in different contexts in the literature, such as the possibility of indirect detection of gravitational waves through electromagnetic signatures of the interaction. In this work, we consider this concept in the particular case of magnetic field amplification. Specifically, we use non-linear gauge-invariant perturbation theory to study the interaction of a primordial seed magnetic field with density and gravitational wave perturbations in an almost Friedmann-Lemaître-Robertson-Walker (FLRW) spacetime with zero spatial curvature. We compare the effects of this coupling under the assumptions of poor conductivity, perfect conductivity and the case where the electric field is sourced via the coupling of velocity perturbations to the seed field in the ideal magnetohydrodynamic (MHD) regime, thus generalizing, improving on and correcting previous results. We solve our equations for long wavelength limits and numerically integrate the resulting equations to generate power spectra for the electromagnetic field variables, showing where the modes cross the horizon. We find that the interaction can seed Electric fields with non-zero curl and that the curl of the electric field dominates the power spectrum on small scales, in agreement with previous arguments.

The second focus area of the thesis is the development a stable high order mesh refinement scheme for the solution of hyperbolic partial differential equations. It has now become customary in the field of numerical relativity to couple high order finite difference schemes to mesh refinement algorithms. This approach combines the efficiency of local mesh refinement with the robustness and accuracy of higher order methods. To this end, different modifications of the standard Berger-Oliger adaptive mesh refinement algorithm have been proposed. In this work we present a new fourth order convergent mesh refinement scheme with subcycling in time for numerical relativity applications. One of the distinctive features of our algorithm is that we do not use buffer zones to deal with refinement boundaries, as is cur-

rently done in the literature, but explicitly specify boundary data for refined grids instead. We argue that the incompatibility of the standard mesh refinement algorithm with higher order Runge Kutta methods is a manifestation of order reduction phenomena which is caused by inconsistent application of boundary data in the refined grids. Indeed, a peculiar feature of high order explicit Runge Kutta schemes is that they behave like low order schemes when applied to hyperbolic problems with time dependent Dirichlet boundary conditions. We present a new algorithm to deal with this phenomenon and through a series of examples demonstrate fourth order convergence. Our scheme also addresses the problem of spurious reflections that are generated when propagating waves cross mesh refinement boundaries. We introduce a transition zone on refined levels within which the phase velocity of propagating modes is allowed to decelerate in order to smoothly match the phase velocity of coarser grids. We apply the method to test problems involving propagating waves and show a significant reduction in spurious reflections.

# Dedication

***This work is dedicated to my mother:***

Lethušang Suzan Mongwane.

# Acknowledgments

It is a pleasure to thank my supervisor Prof. Peter Dunsby who provided much support, guidance and encouragement through my years as a PhD student at UCT. I have had the pleasure to collaborate with Dr. Bob Osano in the early years of my study and I am grateful for all the insights he provided. I am greatly indebted to Dr. Denis Pollney whose valuable comments and advice has made my journey through Numerical Relativity less confusing. I also thank Prof. Chris Clarkson for his help and general discussions.

My heartfelt thanks to the Astronomy department for all the free coffee I have enjoyed over the years. It has been a great pleasure to interact with my colleagues in the Mathematics department at various levels: At the risk of leaving out some names, I mention Dr. Obinna Umeh, Dr. Sean February, Dr. Anne-Marie Nzioki, Dr. Mohammed Abdelwahab and others (I sure do know a lot of doctors).

I gratefully acknowledge the financial support from the National Research Foundation (South Africa). Some analytic computations in this paper were performed with the help of the computer package xAct [277]. Some of the computations were performed using facilities provided by the University of Cape Town's ICTS High Performance Computing team.

I would like to thank *in a special way* Zara Randriamanakoto whose companionship and support has helped keep me sane. My thanks are due to my family, Lethusang Suzan Mongwane, Confidance Mongwane, Peter Mongwane, Nkateko Cynthia Mongwane and Kunene Khoza for putting up with my seemingly endless years of study and their inspiration in general. I appreciate the support I have received from my home-away-from-home, Brackendale and my church Mowbray Baptist church. Above all I thank my Lord Jesus Christ for my very existence.

# Contents

# List of Figures

# List of Tables

# Chapter 1

# Introduction

This thesis is composed of two distinct and self-contained parts, which constitute important developments in the fields of Cosmology and Numerical Relativity. In Part I, we focus on the issue of cosmic magnetism, a problem that has attracted significant attention in recent years. In Part II we tackle the subject of high order mesh refinement for three dimensional numerical relativity simulations. This Chapter gives a brief outline of the thesis.

## 1.1 Cosmology

Charged plasmas are ubiquitous in many astrophysical and cosmological environments. It is expected that the interplay between gravity and electromagnetism in the non linear regime may be at the heart of several phenomena such as gamma-ray bursts [285]. In the first part of the thesis, we study the interaction of gravitational fluctuations with magnetic fields in a cosmological setting. In particular, we look at density perturbations and gravitational wave perturbations as a means of amplifying preexisting magnetic fields. This study has the potential to yield a proper treatment of general relativistic plasmas in a cosmological setting through the machinery of non linear perturbation theory.

In general, theoretical studies of cosmic magnetism can be subdivided into Generation mechanisms and Amplification mechanisms. Generation mechanisms deal with phenomena that seek to generate magnetic fields without relying on the existence of a seed field. This is commonly referred to as Magnetogenesis and many such mechanisms have been proposed in the literature, see [46, 141, 175] for comprehensive reviews. The much celebrated Biermann battery effect falls into this category. On the other hand, Amplification mechanisms deal with the amplification of a preexisting weak field through some physical process. Popular paradigms in this category include the dynamo mechanism and the adiabatic compression of

a magnetized cloud [184]. The work presented here falls under the latter category. This forms part of ongoing efforts aimed at using non-linear perturbation theory to study magnetic field amplification by gravitational fluctuations [123, 65, 417]. Our treatment differs from previous contributions in a number of areas:

- ***Gauge invariance***

  We employ a two parameter perturbative scheme [85, 352, 123, 304, 305] with expansion parameter $\epsilon_B$ characterizing magnetic field perturbations and $\epsilon_g$ characterizing the amplitude of gravitational field perturbations. It is well known that relativistic perturbation theory is prone to spurious gauge modes as a consequence of the general covariance in the theory of general relativity, see for example [292, 358, 154, 268]. We carry out our analysis in a manner that is free of spurious gauge modes by utilizing suitably defined gauge-invariant variables.

- ***Interactions with scalar degrees of freedom***

  Studies of the effects of magnetic fields on density perturbations have been pursued by several authors in the literature [376, 208, 45]. Particularly interesting is the generation and amplification of density perturbations by a preexisting magnetic field [230]. In contrast, the phenomenon whereby a preexisting magnetic seed field undergoes amplification following an interaction with density perturbations has received little attention. By including scalar perturbations in the shear tensor, one opens the possibility of density perturbations to enter the Einstein-Maxwell system at non linear order in perturbation theory. This issue is dealt with in more detail in Chapter 5.

- ***Conductivity***

  We present the equations governing the interaction under several assumptions on the conductivity of the cosmic medium. In particular, we consider the cases of poor, finite and infinite conductivity. We also consider the one-fluid plasma description of the ideal MHD approximation that is relevant for the dust dominated epoch, and present the concomitant equations.

The first part of the thesis is structured as follows: In Chapter 2 we present some elements of modern cosmology. We summarize the Friedmann-Lemaitre-Robertson-Walker (FLRW) model of cosmology which describes the expansion (or contraction) of a homogeneous and isotropic universe. We introduce the parameters characterizing the geometry, expansion and matter composition of the FLRW spacetime. These parameters are linked through the

Einstein field equations of general relativity. In §2.3 we summarize cosmic inflation and primordial perturbations. Aspects of cosmic magnetism such as observational probes are covered in §2.5.

Chapters 3 and 4 are dedicated to gathering the necessary tools that we employ in Part I of this thesis. Chapter 3 focuses on the 1+3 Covariant approach to cosmology. We present the propagation and constraint equations characterizing the gravitational and electromagnetic fields. In §3.7, we give a covariant characterization of the FLRW models covered in Chapter 2. In Chapter 4 we discuss aspects of cosmological perturbation theory and the concept of gauge invariance. After a brief review of metric-based perturbation theory in §4.3, we present our perturbative framework in terms of covariantly defined quantities. We detail the two parameter perturbative scheme in §4.7.

In Chapter 5 we present the Einstein-Maxwell equations given in terms of gauge invariant quantities. We set up and discuss the main equations describing the interaction of gravitational fields with electromagnetic fields in a FLRW background. Following numerical integrations, we compute the power spectrum for the interaction variables. Finally we present some conclusions and future outlook in Chapter 6.

## 1.2 Numerical Relativity

There are several avenues which one could follow within the field of numerical relativity. In the second part of the thesis we tackle the issue of mesh refinement, a problem of clear interest in numerical relativity and numerical analysis of PDEs in general [342, 22, 413, 334, 248, 33, 112]. In particular, we focus on coupling higher order finite difference schemes to the fixed mesh refinement algorithm. We concentrate on the case where refinement occurs both in space and time, a configuration that is commonly referred to as Berger-Oliger time stepping [59]. Although we will naturally restrict the higher order operators to fourth order, the algorithms presented in this thesis apply to orders higher than fourth order with minimal modifications. In addition, our methods are not restricted to any particular formulation of the Einstein field equations.

The issue of high order mesh refinement within the field of Numerical Relativity has been pursued by several authors with differing levels of complexity [131, 248, 80]. The implementation presented in this thesis differs from previous contributions in two major respects, relating to the treatment of interface boundary conditions. We summarize these as follows:

- ***Stability and order reduction***

  The conceptual framework of our mesh refinement algorithm begins with a resolution of an old yet somewhat obscure problem of Runge Kutta order reduction [100, 1, 306]. In a nutshell, high order Runge Kutta schemes have a tendency to behave like second order schemes when used to integrate non linear hyperbolic PDEs with time dependent boundary conditions. Concerning the stability of mesh refinement algorithms, the treatment of interface boundaries can be reduced to the problem of treating time dependent boundary conditions. It has been argued that the manner in which time dependent boundaries are imposed can affect the stability and convergence of a simulation, even when employing unigrid runs [100].

  In Chapter 9, we present an algorithm for applying time dependent boundary conditions for non linear hyperbolic PDEs in a way that retains the stability and convergence properties of the underlying Runge Kutta method. We adopt this method in the treatment of interface boundaries in Chapter 10. Of course, the applications of our algorithm go beyond mesh refinement, see Chapter 9 for details.

- ***Spurious reflections***

  Another important issue is how one deals with spurious reflections that are known to plague mesh refinement algorithms. High order finite difference schemes are known to incur lower truncation errors. Consequently at these orders, the dominant source of error emanates from spurious reflections off refinement boundaries.

  In Chapter 10, we present a mechanism to significantly minimize reflections off refinement boundaries. Our approach is inspired by considering that propagating modes travel at phase speeds that are influenced by the step size of a given grid. In a mesh refinement setting, phase speeds vary across mesh refinement boundaries, becoming slower as they move from fine to coarse grids. The problem arises because the phase speed change is abrupt at the coarse-fine grid interface. We introduce the use of a transition zone at refinement boundaries that facilitate a smooth propagation of modes across the fine-coarse grid interface.

Part II of the thesis is structured as follows: In Chapter 7 we present some of the key conceptual underpinnings of numerical relativity. In all discussions, a broad general knowledge of the theory of general relativity is assumed, see for example the specialized texts [281, 393, 209] on the subject. Section 7.2 introduces the concept of foliating a spacetime, which is a starting point for any 3+1 formulation of the Einstein field equations. The stan-

dard ADM formulation is presented in §7.3.1. After a brief discussion about Hyperbolicity and Well-Posedness of a PDE (§7.4), we present the BSSN formulation in §7.6.

Chapter 8 is dedicated to numerical issues arising from an implementation of a numerical relativity code. This includes a detailed outline of the mesh refinement algorithm in §8.8. The development of a reliable mesh refinement algorithm, which is a key part of this thesis, relies on efficient 3D interpolation operators which we outline in §8.8.5. Types of (outer) boundary conditions that are supported in our code are presented in §8.7.

In Chapters 9 and 10 we address the main objectives of Part II of this thesis. In Chapter 9 we deal with the issue of order reduction and how to avoid it. The chapter also covers several aspects of explicit Runge Kutta schemes. Most notably, the subject of Dense Output (§9.8) which offers an elegant alternative to polynomial interpolation in time. Chapter 10 carries to completion the full mesh refinement algorithm. In this chapter we present the treatment of coarse-fine interface boundaries. The notion of a Transition zone is introduced in §10.3.2. Throughout the thesis we give a detailed presentation of our methods, augmented with numerical examples where necessary.

## 1.3 Notation and Conventions

In the rest of this thesis, we follow [281, 393] by adopting the more geometrically motivated metric signature $(-+++)$. Unless purposefully retained, we employ geometrized units with $8\pi G = c = 1$, where $G$ is the gravitational constant and $c$ is the speed of light in vacuum. We use $\nabla_a$ to denote the four dimensional covariant derivative, $\mathrm{D}_a$ for the three dimensional covariant derivative and $\partial_a$ for partial differentiation. Time derivatives are denoted by an overdot in the first part of the thesis and by $\partial_t$ in the second part. We adopt the Einstein notation and imply a sum over repeated indices. Cosmological quantities indexed by a '0' subscript are evaluated at the present time $t_0$, e.g. $a_0 = a(t_0)$.

Metric signature:

$$(-+++) \tag{1.1}$$

Units:

$$8\pi G = c = k_B = \hbar = 1 \tag{1.2}$$

Curvature tensors:

$$R^a_{bcd} = \partial_c \Gamma^a{}_{bd} - \partial_d \Gamma^a{}_{bc} + \Gamma^e{}_{bd}\Gamma^a{}_{ce} - \Gamma^f{}_{bc}\Gamma^a{}_{df} \tag{1.3}$$

$$R_{ab} = g^{ac} R_{abcd} \tag{1.4}$$

$$R = g^{ab} R_{ab} \tag{1.5}$$

Commonly used Acronyms:

| | |
|---|---|
| ADM | Arnowitt-Deser-Misner |
| AMR | Adaptive Mesh Refinement |
| BSSN | Baumgarte-Shapiro-Shibata-Nakamura |
| CDM | Cold Dark Matter |
| CFL | Courant-Friedrichs-Lewy |
| CMB | Cosmic Microwave Background |
| EFE | Einstein Field Equation |
| EGS | Ehlers-Geren-Sachs |
| EH | Einstein-Hilbert |
| EM | Electromagnetic |
| FLRW | Friedmann-Lemaitre-Robertson-Walker |
| FMR | Fixed Mesh Refinement |
| GR | General Relativity |
| MHD | Magnetohydrodynamics |
| MPI | Message Passing Interface |
| ODE | Ordinary Differential Equation |
| OOP | Object-Oriented Programming |
| PDE | Partial Differential Equation |
| PSTF | Projected Symmetric Trace Free |
| SKA | Square Kilometer Array |

Tensor symmetries:

$$S_{(ab)} = \tfrac{1}{2}(S_{ab} + S_{ba}) \tag{1.6}$$

$$S_{[ab]} = \tfrac{1}{2}(S_{ab} - S_{ba}) \tag{1.7}$$

Alternating (volume) tensor:

$$\eta_{abcd} = \sqrt{-g}\, \delta^0{}_{[a}\delta^1{}_b\delta^2{}_c\delta^3{}_{d]} \tag{1.8}$$

$$g = \det(g_{ab}) \tag{1.9}$$

# Part I

# Cosmology

# Chapter 2

# Review of Modern Cosmology

## 2.1 The Homogeneous and Isotropic Universe

### 2.1.1 The Robertson-Walker Metric

The standard model of cosmology is founded on the Cosmological Principle. There are two basic assumptions underlying the Cosmological Principle, i.e. isotropy and homogeneity. In particular, one assumes that the universe is isotropic and spatially homogeneous on sufficiently large scales i.e at any particular time, the universe looks the same from all positions in space and all directions at any point are equivalent. This somewhat crude assumption, which greatly simplifies general relativistic studies of cosmology, is justified by observations of the distribution of galaxies and the near-isotropy of the cosmic microwave background (CMB). We refer the reader to [202, 209, 284, 327] for a thorough discussion on this topic.

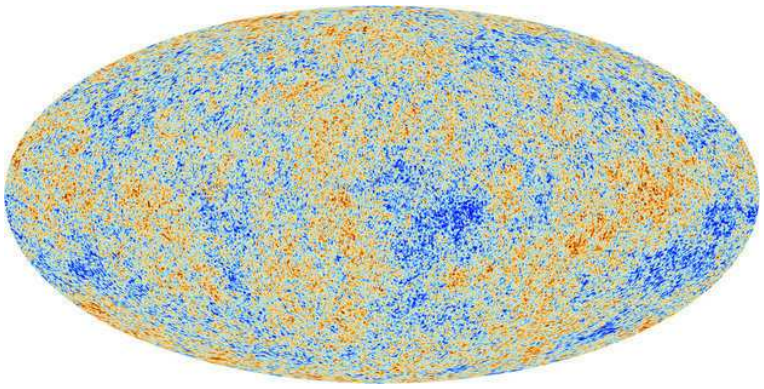

Figure 2.1: *Fluctuations in the cosmic microwave background temperature, as determined from the Planck satellite.*

The general line element $ds^2 = g_{ab}dx^a dx^b$ consistent with such an assumption is given by

the Robertson-Walker (RW) metric, which in spherical coordinates $(r, \theta, \phi)$ takes the form,

$$ds^2 = -c^2dt^2 + a(t)^2\left[\frac{dr^2}{1-kr^2} + r^2(d\theta^2 + \sin^2\,\theta d\phi^2)\right] , \tag{2.1}$$

where the function $a(t)$ is the cosmic scale factor and is a function only of cosmic time $t$, with its present day value normalized to unity $a(t_0) = 1$. The constant $k$ characterizes the mean spatial curvature of the spatial slices. In this case $k$ can take on either of the three values $-1, 0, +1$, where $k = -1$ corresponds to an open universe, $k = 0$ corresponds to a flat universe and $k = 1$ corresponds to a closed universe. The line element (2.1), is often succinctly written as,

$$ds^2 \equiv -dt^2 + a(t)^2\gamma_{ij}dx^i dx^j , \tag{2.2}$$

$$= a(\eta)^2\left[-d\eta^2 + \gamma_{ij}dx^i dx^j\right] , \tag{2.3}$$

where $\gamma_{ij}$ is the metric of the spatial surfaces and $\eta$ is a conformal time related to the cosmic time $t$ via

$$\eta = \int \frac{dt}{a(t)} . \tag{2.4}$$

It is important to note that the FLRW metric results from the assumption of the Cosmological principle and is independent of the theory of gravity adopted.

Of course, the observed universe contains structure and is not perfectly homogeneous. The general approach to physical cosmology is to study the global dynamics of the universe with the homogeneous and isotropic metric (2.1), which has become synonymous with the standard model of cosmology. The observed inhomogeneities are then treated as perturbations of the FLRW metric. We discuss cosmological perturbations in Chapter 4.

### 2.1.2 Hubble Law

The FLRW metric (2.1) describes an expanding or contracting cosmological spacetime depending on whether the scale factor $a(t)$ is increasing or decreasing with time. Among the first observational indications pointing toward an expanding universe was the Hubble law, obtained from recession velocities of local galaxies [214]. Neglecting the peculiar velocities of individual galaxies, the Hubble law is given by the relation,

$$v = H_0 d , \tag{2.5}$$

Figure 2.2: *Hubble Ultra Deep Field... [53]*

where $v$ (in km $s^{-1}$) is the recession velocity of a galaxy at distance $d$ (in Mpc). The proportionality constant $H_0$ (in km $\text{s}^{-1}$ $\text{Mpc}^{-1}$), generally referred to as the Hubble constant, has consequences for time and length scales in a given cosmological model. The implication of (2.5) was that the further away the galaxy is measured to be, the faster was its recession velocity. This discovery lent objective credence to the then notion of an expanding universe.

To put the Hubble law into a cosmological perspective, we introduce the concept of a cosmological redshift. Consider a photon emitted by a source 's' (e.g. a galaxy) moving with 4-velocity $u^a_s$. Suppose such a photon was observed by an observer 'o' moving with 4-velocity $u^a_o$. The frequency shift of the propagating photon as expressed by the ratio of their corresponding wavelengths $\lambda_o/\lambda_s$ satisfies the relation

$$\frac{\lambda_o}{\lambda_s} = \frac{(k_a u^a)_o}{(k_a u^a)_s} = 1 + z \ , \tag{2.6}$$

where $k^a$ is the photon 4-vector and $z$ is the redshift. In a FLRW spacetime, this expression reduces to (see for example [209, 393])

$$1 + z = \frac{a(t_o)}{a(t_e)} \ , \tag{2.7}$$

where $a(t)$ is the scale factor at cosmic time $t$. For an expanding universe $a(t_0) > a(t_e)$ resulting in the wavelength being shifted to the 'red' towards longer wavelengths, hence the name redshift. Similarly, $a(t_0) < a(t_e)$ in a contracting universe. In that case, the wavelengths are shifted towards the blue, hence the name blueshift. From the relation (2.7) we note that

the shift in the spectral lines of galaxies is caused by the expanding spacetime and not by a Doppler shift resulting from the relative motion of the source and observer. This means one should not view the consequences of the Hubble law as implying necessarily that galaxies are receding from one another, but simply that spacetime itself is expanding, thereby causing the apparent motion of galaxies.

In order to deal with the uncertainties involved in measuring the value of $H_0$, it is customary to parametrize the Hubble constant today in terms of a dimensionless parameter $h$ such that $H_0$ becomes

$$H_0 = 100\ h\ \mathrm{km\,s^{-1}Mpc^{-1}} \tag{2.8}$$

$$= \frac{h}{9.77\ \mathrm{Gyr}} \tag{2.9}$$

$$= \frac{h}{2998\ \mathrm{Mpc}} \qquad (\text{in units of } c = 1)\ , \tag{2.10}$$

where, historically, $h$ was thought to be between 0.5 and 1. This factor-of-two uncertainty persisted for much of the $20th$ century, see for example [257]. Figure 2.3 shows the value of $H_0$ for some recent surveys with the most up to date observations constraining the value of $h$ to be in the neighborhood of 0.67 [8]. Accordingly, an object with a measured recession velocity of 6700 $\mathrm{km\,s^{-1}}$ is expected to be at a distance $v/H_0 = 100$ Mpc. It is worth noting that Hubble originally measured a Hubble constant of $H_0 = 500$ km $\mathrm{s^{-1}Mpc^{-1}}$, corresponding to the value $h = 5$, see [231] for more historical values of $H_0$.

### 2.1.3 Scale Factor Dynamics

The scale factor $a(t)$ is the only dynamical variable in the FLRW metric (2.1). As a result, time variation of $a(t)$ can be used to completely characterize the dynamics of a homogeneous and isotropic cosmological model. From the scale factor $a$, one can define a useful quantity, the Hubble parameter $H$ characterizing the rate of expansion,

$$H = \frac{\dot{a}}{a}\ , \tag{2.11}$$

where the overdot denotes differentiation with respect to cosmic time $t$. A positive value of the Hubble parameter $H > 0$ indicates an expanding universe, while a negative value $H < 0$ indicates a collapsing universe. The present day value of $H$, denoted by $H(t_0) = H_0$ is the Hubble constant appearing in the Hubble law (2.5).

In addition, one is also interested in whether the cosmic expansion is slowing down or

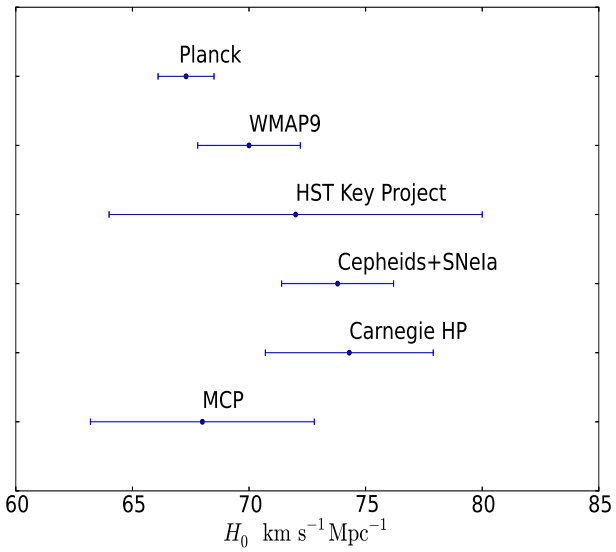


Figure 2.3: *The value of $H_0$ from recent surveys [8].*

accelerating. To quantify this behavior, one defines the deceleration parameter $q$,

$$q = -\frac{\ddot{a}}{aH^2} \,, \tag{2.12}$$

with a present day value of $q(t_0) = q_0$. The sign of $q$ determines whether the expansion is slowing down or speeding up. In particular, a negative sign for the deceleration parameter $q < 0$ is indicative of accelerated expansion, while a positive sign $q > 0$ indicates cosmic expansion that is decelerating. The values for $H_0$ and $q_0$ can be determined observationally (see §2.1.5). In a similar manner, one defines higher order derivatives of the scale factor in terms of dimensionless parameters. The jerk $j$ and snap $s$ parameters, representing the third and fourth derivatives are defined as follows,

$$j = \frac{\dddot{a}}{aH^3} \,, \tag{2.13}$$

$$s = \frac{\ddddot{a}}{aH^4} \,. \tag{2.14}$$

The parameters (2.13)–(2.14) are valid for any cosmic time $t$, with present day values denoted as $j(t_0) = j_0$ and $s(t_0) = s_0$. Using these, the scale factor can be written as a Taylor expansion

about the present time $t_0$ as follows[391],

$$a(t) = a_0 \left[1 + H_0(t-t_0) - \frac{1}{2}q_0 H_0^2 (t-t_0)^2 + \frac{1}{6} j_0 H_0^3 (t-t_0)^3 + \frac{1}{24} s_0 H_0^4 (t-t_0)^4 + \mathcal{O}(\{t-t_0\}^5)\right] \tag{2.15}$$

### 2.1.4 Cosmological Field Equations

To study the dynamics of the FLRW cosmological model, one needs a model for the cosmic fluid that permeates the cosmological spacetime. This can be specified in a general relativistic manner through an energy momentum tensor $T_{ab}$. The isotropy and homogeneity postulates of the cosmological principle are consistent with the perfect fluid form of the energy momentum tensor,

$$T_{ab} = (\mu + p)\, u_a u_b - p g_{ab} \ , \tag{2.16}$$

where $u_a$ is the cosmological fluid 4-velocity, $\mu$ and $p$ are the rest frame energy density and isotropic pressure respectively, as measured by an observer in a locally inertial frame, comoving with the fluid, and $c$ is the speed of light.

To relate the matter content to the metric of the space time, one invokes the Einstein field equations.

$$G_{ab} \equiv R_{ab} - \frac{1}{2} g_{ab} R = T_{ab} - \Lambda g_{ab} \ , \tag{2.17}$$

where $G_{ab}$ is the Einstein tensor, $R_{ab}$ is the Ricci tensor, $R = g^{ab} R_{ab}$ is the curvature scalar and $\Lambda$ is a cosmological constant. The field equations (2.17), correspond to the Einstein-Hilbert action $S_{EH}$ in the variational approach to general relativity. The action $S$ for general relativity is given by

$$S = S_{EH} + S_M = \frac{1}{2} \int d^4x \sqrt{-g} R + \int d^4x \mathcal{L}_M \ , \tag{2.18}$$

where $g$ is the determinant of the metric tensor $g_{ab}$ and $\mathcal{L}_M$ is the matter Lagrangian. In terms of the Lagrangian formulation of the field equations, the energy momentum tensor $T_{ab}$ is given by

$$T_{ab} = -\frac{2}{\sqrt{-g}} \frac{\delta \mathcal{L}_M}{\delta g^{ab}}. \tag{2.19}$$

Built within the Einstein field equations, is the conservation of matter, characterized by the vanishing of the divergence of the energy-momentum tensor

$$\nabla_b T^{ab} = 0 \ . \tag{2.20}$$

This does not need to be a separate assumption, but follows as a direct consequence of the Bianchi identities which are given by,

$$\nabla_b G^{ab} = 0 \, . \tag{2.21}$$

This feature differs from the Trace-Free Einstein equations where the energy momentum conservation is a separate assumption [158].

By plugging in the perfect fluid form of the energy momentum tensor (2.16), into the field equations (2.17), along with the FLRW metric (2.1), one arrives at a coupled set of evolution equations, governing the dynamics of the scale factor $a(t)$. These are the Friedmann and Raychaudhuri equations, respectively given by,

$$H^2 = \frac{8\pi G}{3}\mu - \frac{k}{a^2} + \frac{\Lambda}{3} \, , \tag{2.22a}$$

$$\frac{\ddot{a}}{a} = -\frac{4\pi G}{3}\left(\mu + 3p\right) + \frac{\Lambda}{3} \, , \tag{2.22b}$$

while the energy conservation equation results in the following dynamical equation for the energy density $\mu$,

$$\dot{\mu} = -3H\left(\mu + p\right) \, . \tag{2.23}$$

The energy conservation equation (2.23) is also referred to as the continuity equation.

Assuming a barotropic description of the cosmic fluid, one can relate the pressure and energy density of the matter constituents through the equation of state

$$p = w\mu \, , \tag{2.24}$$

where $w$ is the equation of state parameter whose value depends on the type of matter under consideration. In principle, the equation of state parameter $w$ is not restricted to constant values; it is possible to have a non-constant equation of state parameter. In this case, one can recover an evolution equation for $w$ from the energy conservation equation (2.23)

$$\dot{w} = 3H(1+w)(w - c_s^2) \, , \tag{2.25}$$

where $c_s^2 = \partial p/\partial\mu$ is the adiabatic speed of sound. Using the barotropic equation of state (2.24) with constant $w$ and assuming vanishing curvature $k = 0$, one can analytically solve the equations (2.23) and (2.22a) summarizing the dynamics of FLRW spacetimes. The energy

density and scale factor evolve as,

$$\mu(t) \propto a^{-3(1+w)} \,, \tag{2.26a}$$

$$a(t) \propto t^{\frac{2}{3(1+w)}} \,. \tag{2.26b}$$

In the standard model of cosmology, there are three dominant types of matter that assume a constant equation of state parameter. In particular, we have the following:

- ***Relativistic matter***

  For relativistic matter the equation of state parameter is given by $w = 1/3$. This type of matter includes photons and relativistic neutrinos. It is often collectively called radiation.

- ***Non relativistic matter***

  For non relativistic matter the equation of state parameter is $w = 0$. Note that this implies $p = 0$, hence this type of matter is often referred to as pressureless dust or simply dust. The non relativistic matter contribution is assumed to be made up of baryons and cold dark matter. The baryons are composed of Hydrogen and Helium, while cold dark matter is matter that does not interact with light, and only couples gravitationally to other matter species. While the properties of baryonic matter are well understood, the nature of dark matter is still somewhat a mystery. Current favored dark matter candidates include axions, sterile neutrinos, supersymmetric and Kaluza-Klein particles [60, 63]. There has been several experiments aimed at searching for dark matter particles. The status of such experiments is reviewed in, for example, [27, 116, 360].

- ***Cosmological constant***

  Effectively the cosmological constant acts as a fluid with energy density $\mu_\Lambda = \Lambda c^2/8\pi G$, and equation of state parameter $w = -1$. The cosmological constant, which is repulsive in nature, was originally introduced by Einstein in the quest to construct a static model of the universe, as was desired at the time. Observations of recession velocities of galaxies would later disfavor the static universe, thus rendering the cosmological constant unnecessary.

  The relevance of $\Lambda$ today comes as a result of the Dark energy problem (§2.2). The cosmological constant has been reintroduced and incorporated into the cosmic energy budget as a possible means to account for the late time accelerated expansion of the

Universe. We note from (2.22b) that any value of the equation of state parameter that satisfies $w < -1/3$ guarantees that $q < 0$ leading to accelerated expansion.

One can make some qualitative inferences from (2.26): the FLRW universe must have passed from a radiation dominated epoch ($\mu \propto a^{-4}$, $a \propto t^{1/2}$) through to a matter dominated epoch ($\mu \propto a^{-3}$, $a \propto t^{2/3}$) at early times. For this to happen, that means there is a time $t_{eq}$ where the energy density of radiation and matter were equal, $\mu_r = \mu_m$. This era is known as the matter-radiation equality. If one is willing to extrapolate the solution to much earlier times, then one is led to the following singularity theorem:

| Fluid | $w$ | $\mu(a)$ | $a(t)$ |
|---|---|---|---|
| Radiation | $1/3$ | $a^{-4}$ | $t^{1/2}$ |
| Dust | $0$ | $a^{-3}$ | $t^{2/3}$ |
| $\Lambda$ | $-1$ | $a^{0}$ | $e^{Ht}$ |

Table 2.1: *Solutions for the evolution of the scale factor and energy density in a flat FLRW universe.*

**Theorem 2.1.1 (FLRW Universe Singularity Theorem [150, 157])** *In a FLRW universe with $\Lambda \leq 0$ and $\mu + 3p/c^2 > 0$ at all times, at any instant $t_0$ when $H_0 > 0$ there is a finite time $t_*$ where $t_0 - (1/H_0) < t < t_0$ such that $a(t) \to 0$ as $t \to t_*$. The universe starts at a space time singularity with density $\mu \to \infty$ and temperature $T \to \infty$ if $\mu + p/c^2 > 0$.*

### 2.1.5 Cosmological Parameters

In a multi-fluid setting, where more than one matter species contributes to the energy density, then the density $\mu$ and pressure $p$ are understood to mean the sum over all such species. For observational purposes, it is convenient to work instead with dimensionless density parameters $\Omega_i$, defined as

$$\Omega_i \equiv \frac{\mu_i}{\mu_{critic}} \equiv \frac{8\pi G}{3H^2}\mu_i. \tag{2.27}$$

where $\mu_{critic} = 3H^2/8\pi G$ is the critical density at which the cosmological model is spatially flat, and has a present day value of

$$\mu_{critic,0} = 2.775 \times 10^{11}\ h^2\ \mathrm{M}_\odot\mathrm{Mpc}^{-3}\ , \tag{2.28}$$

$$= 1.9 \times 10^{-29} h^2\ \mathrm{g\ cm}^{-3}\ . \tag{2.29}$$

The index $i$ stands for the individual components of the cosmological fluid. In particular, $i = m$ for non-relativistic matter, $i = r$ for relativistic matter and $i = \Lambda$ for the cosmological

constant. From the solution (2.26), we see that the density parameter evolves as,

$$\Omega_i = \left(\frac{H_0}{H}\right)^2 \Omega_{i,0} a^{-3(1+w_i)}. \tag{2.30}$$

where we have denoted by $\Omega_{i,0}$, the present day value of $\Omega_i$. We can then write the Friedmann equation (2.22a), in a particularly elegant form,

$$\Omega_m + \Omega_r + \Omega_\Lambda + \Omega_k = 1 \ , \tag{2.31}$$

where we have defined the curvature density parameter $\Omega_k$ as,

$$\Omega_k = -\frac{k}{H^2 a^2} \ . \tag{2.32}$$

One can then relate the total energy density to the local geometry as in Table 2.2.

| Criterion | Curvature | Description |
|---|---|---|
| $\Omega < 1$ | $k = -1$ | Open spatial geometry |
| $\Omega = 1$ | $k = 0$ | Flat spatial geometry |
| $\Omega > 1$ | $k = +1$ | Closed spatial geometry |

Table 2.2: *Relationships between the total density parameter and the curvature of spacetime.*

In terms of the density parameters, the dynamical equations (2.22) now reduce to,

$$E(z) \equiv \frac{H(z)}{H_0} = [\Omega_{r,0}(1+z)^4 + \Omega_{m,0}(1+z)^3 + \Omega_{k,0}(1+z)^2 + \Omega_\Lambda]^{1/2} \ , \tag{2.33}$$

$$q(z) = \frac{1}{2}\left(\frac{H_0}{H(z)}\right)^2 [2\Omega_{r,0}(1+z)^4 + \Omega_{m,0}(1+z)^3 - 2\Omega_\Lambda] \ , \tag{2.34}$$

where we have used the expression (2.7) to rewrite the scale factor $a$ in terms of redshift $z$. In practice, the radiation contribution to the present day energy density is negligible, $\Omega_{r,0} \approx 5 \times 10^{-5}$. Using the parameter $h$ (defined in §2.1.2), the dimensionless density parameters are sometimes written in terms of physical density parameters defined as $\omega_b = \Omega_b h^2$ for baryons and $\omega_c = \Omega_c h^2$ for cold dark matter. Current CMB observations from the Planck experiment favor the parameter values outlined in Table 2.3, which translate to $\omega_b = 0.02207 \pm 0.00033$, $\omega_c = 0.1196 \pm 0.0031$ in terms of physical density parameters [8]. Measuring and constraining these parameters has been the subject of several experiments [54, 354, 8].

| Parameter | 68% limits |
|---|---|
| $H_0$ | $67.4 \pm 1.4$ |
| $\Omega_m$ | $0.314 \pm 0.020$ |
| $\Omega_k$ | 0 |
| $\Omega_\Lambda$ | $0.686 \pm 0.020$ |

Table 2.3: *Cosmological parameter values from the Planck experiment. The errors are quoted at the* 68% *confidence interval. The value of* $H_0$ *is given in units of* $km\,s^{-1}Mpc^{-1}$.

## 2.2 Dark Energy

When studying cosmological models, one is concerned not only with the expansion history but also the future fate of a given model. For example, a cosmological model may indicate that the universe will expand indefinitely, becoming cooler and less dense with time. Alternatively the universe may expand, having started in a big bang, and then recolapse in a big-crunch. These scenarios depend on the energy density of the universe.

Current observations suggest that about 68% of the energy composition is in the form of dark energy, a mysterious component with negative pressure [310, 325, 354, 8, 309]. There has been several options proposed to describe the nature of this mysterious component. Among them are:

- ***Cosmological constant***

  At the core of the standard ΛCDM model is the assumption that gravitational interactions are described by Einstein's theory of general relativity, with the cosmological constant $\Lambda$ acting as the repulsive field accounting for the apparent accelerated expansion of the universe.

  Within the realm of quantum field theory, the cosmological constant is interpreted as the intrinsic energy density of vacuum $\rho_{vac}$. This interpretation of $\Lambda$ is well exposed to experimental confrontation. Comparing the observed value for $\rho_\Lambda$ and the one predicted from quantum field theory leads to embarrassing results: the comparison is off by between 60–120 orders of magnitude! This discrepancy is known in the literature as the cosmological constant problem [275, 101, 103, 102].

- ***Quintessence***

  An alternative to the cosmological constant is Quintessence models, also quantified by a negative equation of state parameter $w_q = p_q/\mu_q < 0$. In these models, the accelerated expansion is caused by a slow rolling scalar field [322, 384, 414, 92]. While

the cosmological constant is time independent and spatially homogeneous, quintessence is dynamic in time and spatially inhomogeneous. The principles behind quintessence models are much similar to that of new inflation [193, 13] in which the inflaton drives a short period of superluminal expansion in the early universe (§2.3). However they differ in their associated energy and time scales. In particular, the energy scale of quintessence is smaller than that of inflation while the time scale of quintessence is longer than that of inflation.

- ***Inhomogeneity effects***

  The basic idea behind these models come from the fact that the observed universe contains non linear structures whose effects on the large-scale dynamics may not be well captured by FLRW models. In fact, by assuming the FLRW model as the background metric of the universe, one implies the existence of some spatial averaging procedure through which one smoothes over the small scale inhomogeneities. The process of averaging over structure results in backreaction effects that could in principle account for the apparent present-day cosmic acceleration [320, 120]. On the other hand, local inhomogeneities have the potential to affect the propagation of light, thus affecting cosmological observations [153, 118]. In this case, one can interpret the apparent late time acceleration of the universe, as inferred from the dimming of Type Ia supernovae as an inhomogeneity effect [118, 164, 319, 172].

  It is worth noting that it is observationally difficult to test the homogeneity postulate of the Cosmological Principle. The general approach is to assume the Copernican principle, which states that we are not occupying a special place in the universe. With this assumption, isotropy implies homogeneity. Therefore, it is possible to relax the homogeneity assumption without compromising much of the underpinnings of modern cosmology. Moving away from the homogeneity assumptions of the FLRW models, one is led to a variety of inhomogeneous cosmological models such as the Lemaítre-Tolman-Bondi, Szekeres, etc[361, 68, 338].

- ***Modified gravity***

  It is also possible to interpret the observed accelerated expansion as a breakdown of the general theory of relativity on large scales. The procedure here is to modify the Einstein-Hilbert action of general relativity to admit a more general structure. In particular, the Ricci scalar $R$ in (2.18) is substituted by a generic function $f(R)$ which reduces to $f(R) = R$ in the GR limit. This is the avenue pursued in $f(R)$ theories of gravity, see for example [135, 353, 124]. The idea here is that the modification will

result in an effective curvature fluid that can mimic a fluid with a dark equation of state parameter $w < -1/3$ as required for late time acceleration.

## 2.3 Inflationary Cosmology

Inflation is, quite simply, a phase of accelerated superluminal expansion of the early universe. This stage of evolution was introduced in the early 1980s to iron out several issues with the standard big bang cosmology [193, 13, 236, 250, 42]. The aim of inflation is not to replace the Big bang model, but is merely supplementary to the model. At the end of the inflationary era, one still requires that the evolution return to the standard model of cosmology through some reheating process [234].

### 2.3.1 Limitations of The Big Bang Model

- ***The flatness problem***

  Current observations favor an almost flat universe with the density parameter $\Omega$ close to unity. From the Friedmann equation (2.31) we have that,

$$1 - \Omega = \Omega_k \tag{2.35}$$

$$\equiv -\frac{k}{a^2 H^2}. \tag{2.36}$$

  Since during the radiation or matter dominated epochs, the comoving Hubble radius $(aH)^{-1}$ is expected to increase in a FLRW cosmological model, the quantity $|1 - \Omega|$ will be driven away from zero.

  To elucidate the problem further, we look at the evolution of the spatial curvature $\Omega_k$. One can show that the time evolution is given by

$$\dot{\Omega}_k = 2\Omega_k H q. \tag{2.37}$$

  Therefore, if the universe is flat at some early cosmic time, it remains so for all time. However, if $\Omega_k$ is different from zero it will evolve away from being flat. Thus we require that the quantity $|1 - \Omega|$ be extremely close to zero at early times. In fact, in order to be consistent with current observations, one would require that $|1 - \Omega| \lesssim 10^{-16}$ at Nucleosynthesis ($t = 1$ $s$) and that $|1 - \Omega| \lesssim 10^{-60}$ at the Planck epoch ($t = 10^{-43}$ $s$), for example. The flatness problem is the question of how likely such fine tuning is [138].

The problem can be solved by requiring that the comoving Hubble radius $(aH)^{-1}$ decrease at early times in order to drive the curvature to zero.

- ***The horizon problem***

  The horizon problem is related to the fact that vastly separated patches in the sky appear to have the same physical properties [282]. The problem arises because according to standard cosmology, such patches would not have had enough time to interact at early times because they are not in causal contact due to the existence of particle horizons.

  In particular, the Hubble distance $H^{-1}$ at the surface of last scattering subtends an angle of approximately one degree today. The hot big bang model offers no prospect, within itself, to explain the homogeneity of the temperature fluctuations in the CMB, as observed from patches in the sky that are separated by more than a degree. This problem can be solved by requiring that the Universe is inside the horizon at the beginning of inflation. In this case, the Hubble length is initially large, and decreases at the onset of inflation leaving the observable Universe within the smooth patch that will have formed through causal interactions [260], see Figure 2.4 for a schematic representation.

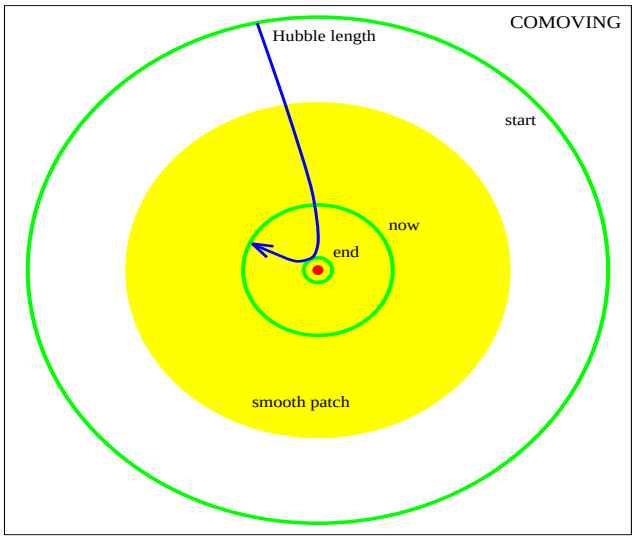


Figure 2.4: *An illustration of the inflationary solution to the horizon problem. During inflation, the comoving Hubble length decreases, thus allowing the observable Universe to lie within the smooth patch [249].*

- ***Relic particle abundances***

  The relic particle abundance problem is related to the fact that if the universe was very hot at early times as required by the standard Big Bang model, then a variety of

stable exotic interacting particles, such as magnetic monopoles, gravitinos, topological defects, domain walls, etc, would be produced. These would contribute to the present energy density $\Omega$ and somewhat alter the evolution of the FLRW model. However, to date, no such relics have been detected.

The role of inflation in solving this problem is that the superluminal expansion phase brought in by inflation will dilute the number density of such particles, such that their interaction rate is lowered. This, of course, assumes that the relics were produced before the inflationary phase [260].

### 2.3.2 Inflationary Dynamics

The problems identified in the previous section can be solved by a brief period of accelerated expansion at early times, before the radiation dominated epoch. This requirement can be stated in terms of the scale factor as

$$\ddot{a} > 0 \, . \tag{2.38}$$

An equivalent and perhaps more physically transparent representation of the accelerated expansion is given in terms of the comoving Hubble radius $(aH)^{-1}$ as the condition [209],

$$\frac{d}{dt}\left(\frac{1}{aH}\right) < 0 \, . \tag{2.39}$$

The implication of (2.39) is that the comoving Hubble radius must decrease with time. As a result, causal contact is maintained at early times such that the now vastly separated patches in the sky get enough time to exchange physical information.

The dynamics of the inflationary phase are thought to have been dominated by some scalar field $\phi$ that is able to attain negative pressure. Assuming the general theory of relativity as the theory of gravity, an action $S$ representing such dynamics is given by [42]

$$S \equiv S_{EH} + S_{\phi} \, , \tag{2.40}$$

$$= \frac{1}{2\kappa}\int d^4x\sqrt{-g}R + \int d^4x \left[\frac{1}{2}g^{ab}\partial_a\phi\partial_b\phi - V(\phi)\right] \, , \tag{2.41}$$

where $S_{EH}$ is the familiar Einstein-Hilbert action, and $V(\phi)$ is some scalar field potential. In this context, $\phi$ is referred to as the inflaton field. The dynamics of $\phi$ are governed by the Klein-Gordon equation

$$\Box^2\phi + \frac{d}{d\phi}V(\phi) = 0 \, , \tag{2.42}$$

where $\Box^2 = g^{ab}\nabla_a\nabla_b$ is the covariant d'Alembertian operator. Varying the action (2.41) results in an effective energy momentum tensor $T^{(\phi)}_{ab}$ for the scalar field $\phi$

$$T^{(\phi)}_{ab} \equiv -\frac{2}{\sqrt{-g}}\frac{\delta\mathcal{L}_\phi}{\delta g^{ab}} = \partial_a\phi\partial_b\phi - g_{ab}\left(\frac{1}{2}\partial_c\phi\partial^c\phi + V(\phi)\right) , \tag{2.43}$$

with energy density $\mu_\phi$ and pressure $p_\phi$ respectively given by,

$$\mu_\phi = \frac{1}{2}\dot{\phi}^2 + V(\phi) , \tag{2.44}$$

$$p_\phi = \frac{1}{2}\dot{\phi}^2 - V(\phi) . \tag{2.45}$$

From (2.44) and (2.45), one can define an equation of state parameter for the scalar field as

$$w_\phi = \frac{\frac{1}{2}\dot{\phi}^2 - V(\phi)}{\frac{1}{2}\dot{\phi}^2 + V(\phi)} . \tag{2.46}$$

In order to have a negative equation of state parameter $w_\phi < 0$, as is required for accelerated expansion, the potential $V(\phi)$ has to dominate over the kinetic term $\dot{\phi}^2$ such that

$$V(\phi) > \dot{\phi}^2 . \tag{2.47}$$

If the inflaton is minimally coupled then it independently obeys the continuity equation (2.23) in the form,

$$\dot{\mu}_\phi = -3H\left(\mu_\phi + p_\phi\right) . \tag{2.48}$$

Upon using the expressions (2.44) and (2.45), the continuity equation (2.48) reduces to

$$\ddot{\phi} + 3H\dot{\phi} + \frac{d}{d\phi}V(\phi) = 0 , \tag{2.49}$$

which is equivalent to the Klein-Gordon equation (2.42). The Friedmann and Raychaudhuri equations reduces to the following,

$$H^2 = \frac{1}{3}\left[\frac{1}{2}\dot{\phi} + V(\phi)\right] , \tag{2.50a}$$

$$\frac{\ddot{a}}{a} = \dot{H} + H^2 = (1-\epsilon)H^2 , \tag{2.50b}$$

where the parameter $\epsilon = -\dot{H}/H^2$ is a slow roll parameter. In terms of $\epsilon$, the condition for inflation to occur is $\epsilon < 1$. Another useful slow roll parameter is $\eta = \dot{\epsilon}/\epsilon H$ [42].

### 2.3.3 The Slow Roll Approximation

Within the slow roll approximation, characterized by the condition $V(\phi) \gg \dot{\phi}^2$, one can have analytic solutions for the equations (2.49)–(2.50). Upon differentiation, the slow roll approximation results in $dV/d\phi \gg \ddot{\phi}$. With this approximation, the dynamical equations (2.49) and (2.50) reduce to the following system

$$3H\dot{\phi} = -\frac{d}{d\phi}V(\phi) \ , \tag{2.51}$$

$$H^2 = \frac{1}{3}V(\phi) \ , \tag{2.52}$$

$$\dot{H} = -\frac{1}{2}\dot{\phi}^2 \ . \tag{2.53}$$

Moreover, the slow roll parameters $\epsilon$ and $\eta$ can be given in terms of the potential $V(\phi)$ and its derivatives [42, 9],

$$\epsilon \equiv \frac{1}{2}\left[\frac{1}{V(\phi)}\frac{dV(\phi)}{d\phi}\right]^2 \ll 1 \ , \tag{2.54}$$

$$\eta \equiv \left[\frac{1}{V(\phi)}\frac{d^2V(\phi)}{d\phi^2}\right]^2 \ll 1 \ . \tag{2.55}$$

Solutions of the system (2.51)–(2.53) suggest that the Hubble parameter is held constant while the scale factor grows exponentially during the inflationary phase,

$$a(t) \propto e^{\sqrt{H}t} \ , \tag{2.56}$$

or in terms of the potential $V(\phi)$

$$a(t) \propto \exp\left(\sqrt{\tfrac{1}{3}V(\phi)}t\right) \ . \tag{2.57}$$

The epoch of inflation will last as long as the condition (2.47) is satisfied. Naturally, as the inflaton rolls down the potential $V(\phi)$, the condition will inevitably no longer be satisfied and inflation ends. A fundamental concept in inflationary theories is that of the number of $e$-foldings $N$ of the scale factor. This number quantifies the amount of inflation that occurs. It is expressed through the ratio of the scale factor at the end of inflation to its value at the

beginning of inflation, according to

$$N = \ln \frac{a(t_{end})}{a(t)} \, . \tag{2.58}$$

Within the slow roll approximation, the number of $e$-foldings that result as the scalar field rolls from $\phi_1$ to $\phi_2$ is given by

$$N = \int_{t_1}^{t_2} H dt \, , \tag{2.59}$$

$$= \int_{\phi_1}^{\phi_2} \frac{H}{\dot{\phi}} d\phi \, . \tag{2.60}$$

The number of $e$-foldings that are necessary to solve the problems outlined in §2.3.1 can be shown to be, $N \gtrsim 60 - 70$.

There are other proposed inflationary paradigms other than the single field inflation, see [255, 147, 146, 258, 38, 289, 254] for detailed discussions. [147, 146], power law inflation [258], intermediate inflation [38, 289] and hybrid inflation [254].

### 2.3.4 Primordial Fluctuations

The inflationary phase is crucial to the success of the standard model of cosmology. Although it was initially postulated to solve the problems outlined in §2.3.1, it has several by-products which makes it even more appealing to cosmology. In particular, inflationary theories present a mechanism for the generation of scalar and tensor fluctuations at horizon exit. Such fluctuations will generally manifest themselves as density and gravitational wave perturbations, respectively. It is possible for these perturbations to interact with a preexisting weak magnetic field, thus providing an amplification mechanism for the latter. We deal with this phenomenon in Chapter 5.

#### Scalar Fluctuations

The quantum fluctuations of the inflaton field generated during the slow-roll phase will freeze in and become classical at horizon exit [86, 106, 42]. In general, inflation predicts a scale-invariant power law form for the power spectrum of scalar fluctuations,

$$\mathcal{P}_{\mathcal{R}} = A_s \left( \frac{k}{k_0} \right)^{n_s - 1} \, , \tag{2.61}$$

where $k_0$ is a pivot scale, the parameters $A_s$ and $n_s$ are the amplitude of the primordial fluctuations and the scalar spectral index respectively. The amplitude $A_s$ is related, during the slow roll approximation, to the potential via,

$$A_s = \frac{V(\phi)}{24\pi^2 M_{\rm pl}^4\,\epsilon}\ . \tag{2.62}$$

On the other hand, the scalar spectral index $n_s$ can be written in terms of the slow roll parameters $\epsilon$ and $\eta$ as

$$n_s = 1 - 6\epsilon + 2\eta\ . \tag{2.63}$$

Thus constraints on the scalar spectral index immediately translate into constraints for the inflationary potential $V(\phi)$ (cf. equations 2.54 and 2.55). We note that since during the slow rolling phase $\epsilon \ll 1$ and $\eta \ll 1$, the scalar spectral index is almost unity, $n_s \approx 1$, thus guaranteeing the scale invariance of (2.61). CMB Constraints from Planck set the following bounds on the inflationary parameters [9],

$$\ln(10^{10} A_s) = 3.089^{+0.024}_{-0.027}\ , \tag{2.64}$$

$$n_s = 0.9603 \pm 0.0073\ . \tag{2.65}$$

Figure 2.5 shows joint $1\sigma$ and $2\sigma$ confidence regions for the scalar spectral index $n_s$ and tensor-to-scalar ratio $r_{0.002}$ (see below) using Planck data compared to predictions of some selected inflationary models [9].

### Tensor Fluctuations

In a similar fashion, a generic feature of inflationary scenarios is the production of primordial gravitational waves. The power spectrum of inflationary tensor fluctuations is given by,

$$\mathcal{P}_T = A_T \left(\frac{k}{k_0}\right)^{n_T}\ , \tag{2.66}$$

where $k_0$ is the pivot scale, $A_T$ is the tensor amplitude and $n_T$ is the tensor spectral index. In terms of the potential $V(\phi)$, the tensor amplitude takes the form,

$$A_T = \frac{2V(\phi)}{3\pi^2 M_{\rm pl}^4}\ . \tag{2.67}$$

The tensor spectral index $n_T$ on the other hand is related the slow roll parameter $\epsilon$ through

$$n_T \equiv \frac{d\ \ln \mathcal{P}_h(k)}{d\ \ln k}\ , \tag{2.68}$$

$$= -2\epsilon\ , \tag{2.69}$$

and is expected to be small, in accordance with the slow roll approximation. It is worth noting that for the simple case of single field inflation, the tensor spectrum is not independent of the other inflationary parameters. In particular, we define the tensor-to-scalar ratio $r$ in the slow roll limit according to,

$$r \equiv \frac{\mathcal{P}_T(k)}{\mathcal{P}_s(k)} \approx 16\epsilon \approx -8n_T\ . \tag{2.70}$$

which is commonly referred to as the consistency relation.

Primordial tensor modes can be observed through their signatures in the CMB. In particular, the tensor modes are expected to induce temperature fluctuations along with E- and B-mode polarization in the CMB. Several CMB experiments have been commissioned with prospects of detecting primordial B-mode polarization. Of particular interest in this context is the BICEP2[1] experiment, which has recently announced the detection of a primordial B-mode signal in the CMB [7]. This result amounts to a somewhat indirect detection of primordial gravitational waves. The constraint on the tensor-to-scalar ratio $r$ as reported in [7] is,

$$r = 0.20^{+0.07}_{-0.05}\ , \tag{2.71}$$

at the pivot scale $k = 0.05\ \text{Mpc}^{-1}$, with $r = 0$ excluded at the $7\sigma$ confidence level. However, there has since been doubt cast over the reliability of the BICEP2 results owing to the fact that Galactic dust, whose effects were underestimated in [7], can mimic the B-mode signal. See [7, 313] for more detail and rigor on this topic.

## 2.4 Distances in Cosmology

Because cosmological observations are made on our past null cone, physical distances are no longer measurable and one has to be clear what is meant by 'distances' in cosmology. The common convention in observational cosmology is to define distances operationally, i.e. in terms of observable quantities. There are several notions of distance in observational cosmol-

[1] Background Imaging of Cosmic Extragalactic Polarization.

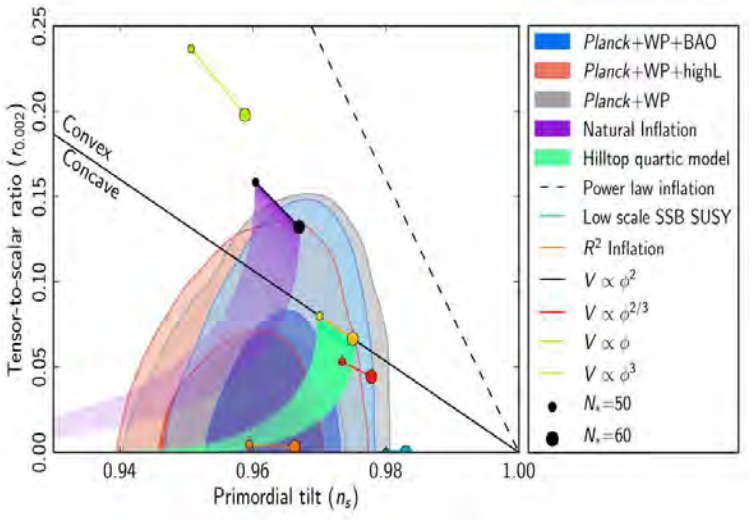


Figure 2.5: *Constraints for $n_s$ and $r_{0.002}$ at the $1\sigma$ and $2\sigma$ confidence levels from Planck (in combination with other datasets) [9].*

ogy see [105] for definitions. The two most commonly used distances are the Luminosity and Angular diameter distances which are respectively defined as [395, 209]

$$d_L = (L/4\pi F)^{1/2} \qquad \text{and} \qquad d_A = R/\alpha \ , \tag{2.72}$$

where $L$ is the Luminosity of the source, $F$ is the flux measured by the observer, $R$ is the proper size of the object and $\alpha$ is the angle it subtends on the sky. These definitions exploit the notion of,

- ***Standard Candles***

  These are objects of known intrinsic luminosity, such that flux measurements will readily determine their distance. Type Ia supernovae fall into this category [332, 325, 310]. These are thought to occur when a white dwarf accretes enough matter to reach a mass close to the Chandrasekhar limit of $1.44\,M_\odot$. This is the largest possible mass that can be supported by electron degeneracy pressure. Further accretion, within this limit, leads to a range of physical processes that ultimately result in a thermonuclear supernova explosion. Because the exploding star always has a mass close to the Chandrasekhar limit, there is very little variation in the absolute luminosities of the supernovae of this kind. This property makes them good standard candles, subject to

calibration [375, 242, 265].

- ***Standard Rulers***

  These are objects of known diameter scales. A representative example in this category is Baryon Acoustic Oscillations [151, 43, 128, 176]. Before decoupling, photons and baryons are thought to have formed a tightly coupled photon-baryon fluid supporting a standing wave acoustic oscillation. This oscillation is induced, in some overdense region of the cosmic plasma, by rarefactions and compressions as a result of the counteracting forces of gravity and the repulsive pressure created as the photons interact with matter through Thomson scattering. Once photons decoupled from the baryons, they traveled freely without much interactions with matter. These free-streaming photons make up the CMB and have, encoded within their distribution, the snapshot of the oscillation just before decoupling.

These and other types of distance measurements play a major role in extragalactic astronomy and cosmology, see for instance [395, 396] on this topic. In practice, the expressions (2.72) need to be modified to account for curvature and expansion of spacetime in a cosmological setting. In a FLRW cosmological model, the Luminosity distance is given by

$$d_L = \frac{c(1+z)}{H_0\sqrt{-\Omega_k}} \sin\left[\sqrt{-\Omega_k}\int_0^z \frac{dz'}{E(z')}\right] , \tag{2.73}$$

where the quantity $E(z)$ is given by Equation (2.33). The angular diameter distance can be obtained in a similar manner by using the fact that the Luminosity distance $d_L$ and angular distance $d_A$ are linked by the distance duality relation [159]:

$$d_L = (1+z)^2 d_A \, . \tag{2.74}$$

It is important to note that the distance duality relation (2.74), sometimes referred to as the reciprocity relation, is independent of the adopted theory of gravity and matter content of the space time [104]. Because they are given in terms of cosmological parameters, the Luminosity and Area distance measures play a major role in cosmological parameter estimation methods. standard candles and standard rulers with known luminosity and angular size properties respectively. The Luminosity distance measures are used in connection with Type Ia supernovae observations. Similarly the angular diameter distance is used in connection with Baryon Acoustic Oscillations (BAO) observations.

Using the expression (2.15), one can rewrite the Luminosity distance in terms of a series expansion in redshift, resulting in the expression [110, 391],

$$d_L = \frac{cz}{H_0}\left[1 + \frac{1}{2}(1-q_0)z + \frac{1}{6}(q_0 + 3q_0^2 - j_0 - \Omega_{k,0})z^2 \right. \\ \left. + \frac{1}{24}\left(2 - 2q_0 - 15q_0^2 - 15q_0^3 + 10j_0q_0 + 5j_0 + s_0 + 2\Omega_{k,0} + 3q_0\Omega_{k,0}\right)z^3 + \mathcal{O}(z^4)\right] . \quad (2.75)$$

The distance-redshift relation is an important concept in observational cosmology, particularly supernovae cosmology [29, 326]. It is interesting to note that for low redshift sources, the luminosity distance-redshift relation (2.75) becomes linear,

$$d_L \simeq \frac{cz}{H_0} , \quad (2.76)$$

which is the Hubble law (2.5) with recession velocity $v = cz$. As a result, the expression (2.75) is sometimes referred to as the Hubble relation. One can derive new versions for the Hubble relation by using other distance measures other than the Luminosity distance $d_L$ [105]. In fact, the traditional redshift expansion (2.75) breaks down and fails to converge for redshifts $z > 1$, and other parametrizations become necessary, see [105] for rigor and detail.

We conclude this section with the following theorem (see also [200, 119]) that highlights the importance of the Hubble relation in establishing issues of isotropy:

**Theorem 2.4.1 (*Hasse and Perlick Theorem [200]*)** *Consider a Lorentzian manifold $(\mathcal{M}, g)$ with an observer field $V$. Then $(\mathcal{M}, g, V)$ admits an isotropic Hubble law of third order at every point $p \in \mathcal{M}$ if and only if $(\mathcal{M}, g, V)$ is either redshift free or a FLRW model (locally around every point $p \in \mathcal{M}$).*

## 2.5 Electromagnetic Fields

Electromagnetic field effects are often neglected in studies of galaxy formation and other cosmological studies. This is often justified by the assumption of charge neutrality in the cosmic plasma along with the fact that the gravitational force is expected to dominate over cosmological scales, compared to the Electromagnetic force. However, there is growing interest in the area of cosmic electromagnetism, in light of observations indicating the presence of magnetic fields in a wide range of astrophysical objects. Large scale magnetic fields of varying amplitudes have been observed in entire galaxy clusters, individual galaxies and other high redshift condensations. These fields are observed on characteristic scales of $\sim 1$ Mpc and

are of micro-Gauss strength, $10^{-7} - 10^{-5}$ G [240, 397]. The existence of such fields poses fundamental problems for cosmology [37], given that vector modes are expected to decay with the cosmological expansion. There are a variety of candidate mechanisms proposed to explain the origin and evolution of such fields, spanning different theories of physics [46].

### 2.5.1 Magnetic Field Observations

Of great importance in understanding the role and nature of magnetic fields in galaxy formation and cosmology in general is the observation of such fields at high redshifts, especially in galaxy clusters and the intergalactic medium. Observational techniques of magnetic fields rely on the following physical principles,

- ***Faraday rotation***

  A polarized electromagnetic wave traveling through a magnetized plasma will undergo a rotation of its plane of polarization. The rotation measure $RM$ for a source at some cosmological distance $l_s$ is proportional to the strength of the permeating line-of-sight magnetic field $B_{\parallel}$ according to,

$$RM = 8.12 \times 10^5 \int_0^{l_s} \frac{n_e(z) B_{\parallel}(z)}{(1+z)^2} dl(z) \qquad (\text{rad m}^{-2}) \,, \tag{2.77}$$

  where $n_e$ is the number density of electrons in $cm^{-3}$ and the $(1+z)^{-2}$ factor accounts for the fact that the electromagnetic waves will be redshifted as they travel from the source to the observer. In the equation (2.77), $B_{\parallel}$ is measured in $\mu$G and the distance is given in Mpc. In a standard flat $\Lambda$CDM cosmological model, the distance element $dl$ is related to the cosmological redshift through the relation,

$$dl(z) = \frac{dz}{H_0(1+z)\sqrt{\Omega_{m,0}(1+z)^3 + \Omega_{\Lambda}}} \,, \tag{2.78}$$

  where $H_0$ is the Hubble constant, $\Omega_{m,0}$ and $\Omega_{\Lambda}$ are the present day energy densities of matter and dark energy.

  By studying the Faraday rotation measures of polarized high redshift radio sources, and given the distribution of free electrons in the intergalactic medium, it is possible to place upper limits on uniform cosmological and intergalactic magnetic fields [350, 75, 235, 12].

- ***Synchrotron radiation***

  Relativistic cosmic-ray electrons propagating in a magnetized medium will spiral along magnetic field lines due to the Lorentz force acting on them. The accelerating charged particles induce non-thermal synchrotron emission in the radio region of the electromagnetic spectrum. For example, the diffuse radio emission from the Milky-Way has been attributed to cosmic rays traveling in interstellar magnetic fields [167, 52]. As a result, radio-faint galaxies tend to have weaker magnetic fields compared to their radio-loud counterparts, see [224] for a review on the subject. By exploiting this phenomenon one can study magnetic fields in astrophysical systems like pulsars, galaxies and clusters.

- ***Zeeman splitting***

  The presence of a magnetic field introduces a preferred direction such that the electronic energy levels of an atom are no longer independent of the angular momentum vector. As a result, spectral lines are split into several components, a phenomenon known as Zeeman splitting. Zeeman splitting offers a more direct way of measuring the strength of astrophysical magnetic fields, as opposed to rotation measures and synchrotron radiation which measure the line-of-sight component. The line shift associated with the energy splitting is given by,

  $$\frac{\Delta\nu}{\nu} = 1.4\, g \frac{B}{\nu}\,, \tag{2.79}$$

  where $B$ is measured in $\mu$G, $\nu$ is measured in $Hz$ and the parameter $g$ is the Lande factor relating the angular momentum of an atom to its magnetic moment.

  Observations of magnetic fields relying on the Zeeman effect have been carried out for a number of astrophysical objects like galaxies, star forming regions, Masers, HII regions etc [226, 323, 399, 328], see also [389].

### 2.5.2 Constraining Primordial Magnetic Fields

One can constrain the strength of primordial magnetic fields by studying their effects on the Big bang Nucleosynthesis (BBN) process. Any magnetic fields that existed during the BBN epoch would have certain effects on the main predictions of the BBN process [397, 185, 279]. In particular, one expects that the energy density of magnetic fields will induce a faster cosmological expansion rate, thus decreasing the time scale over which the BBN epoch will

last. In addition, in the presence of strong magnetic fields, one expects the nuclear reaction rates to be altered. These effects have been studied by several authors in the literature [107, 183, 227, 108]. Numerical studies calculating the element abundances, with the presence of homogeneous magnetic fields, lead to upper limits of order $10^{-6}$ G.

It is known that Primordial magnetic fields can seed, and in turn amplify, density perturbations in the baryonic plasma through the Lorentz force acting on the weakly ionized cosmic plasma [230]. These secondary perturbations are seeded independently from the standard adiabatic mode. Since after the recombination epoch, the baryonic fluid is gravitationally bound to cold dark matter, these perturbations are likely to leave an imprint on the dark matter fluid. As a result, one expects the effect of Primordial magnetic fields to leave a signature in the form of distortions in the linear matter power spectrum. In principle, the presence of a primordial magnetic field of nano-Gauss strength can induce fluctuations in the density field that are large enough to produce stronger clustering power of Ly$\alpha$ clouds, bigger cosmic shear, a larger number of galaxy clusters and other phenomena. Therefore, one can use such signatures as potential probes of the strength and statistics of Primordial magnetic fields [394, 134, 340, 93].

Observations of the CMB anisotropies can also be used to constrain primordial magnetic fields. In this case one exploits the fact that a homogeneous magnetic field in a slightly anisotropic universe will cause the universe to expand at different rates in different directions. This trait is due to the fact that expansion along the direction parallel to the field lines is somewhat disfavored because of the opposing magnetic tension. On the other hand, expansion in directions orthogonal to the field lines is favored because of the magnetic pressure [264, 408, 39]. Current limits on a stochastic primordial magnetic field from the cosmic microwave background radiation constrains the amplitude to be $B < 3.4 \times 10^{-9}$ G at the 1 Mpc scale, with a spectral index $n_B < 0$ [8, 301, 341]. In this case, one parametrizes the amplitude of such a field as

$$B_\lambda^2 = \int_0^\infty \frac{dk k^2}{2\pi^2} e^{-k^2\lambda^2} p_B(k) \,, \tag{2.80}$$

$$= \frac{A}{4\pi^2 \lambda^{n_B+3}} \Gamma\left(\frac{n_B+3}{2}\right) \,, \tag{2.81}$$

where the constraint $n_B > -3$ has to be imposed to avoid infrared divergences. In principle, more stringent constraints can be obtained from the CMB trispectrum. For example, in [374], a present day limit of $B < 0.05 \times 10^{-9}$ G was found.

It is also possible to constrain primordial magnetic fields by looking at Faraday rotation in the polarization signal of the CMB [238]. In [96, 97] it was also argued that the anisotropy

generated by a stochastic primordial magnetic field would have a significant effect on the production of gravitational waves in the early universe. Thus using constraints on the amplitude of gravitational waves from, say the Nucleosynthesis epoch, one can constrain the strength of magnetic fields allowed at early times.

### 2.5.3 Challenges for Primordial Magnetic Fields

To date, no detection of magnetic fields has been classified as cosmological. The observed fields are often tied to some gravitationally bound systems like galaxies and galaxy clusters. However, there is increasing speculation that such fields could be of primordial origin [213]. This consideration is in line with the observed hemispherical power asymmetry in the CMB [10, 132, 187, 286, 337, 245] and is further substantiated by the observation of magnetic fields in galaxies at high redshift and in the intergalactic medium [223, 61, 366, 23]. The problem in this scenario is that the presence of cosmological magnetic fields is not consistent with the cosmological principle. While it is possible to have uniform magnetic fields permeating a homogeneous cosmological spacetime, such a spacetime is no longer isotropic as there will be preferred directions along the field lines. In other words, one may have to abandon the simple ΛCDM cosmological model which is based on the homogeneous and isotropic FLRW spacetime.

The main problem however may be to explain the physical origin and subsequent evolution of primordial magnetic fields in an expanding universe. It is now widely believed that the structure of magnetic fields in spiral galaxies is consistent with magnetic field amplification and ordering via the magnetohydrodynamic (MHD) dynamo mechanism [330]. The MHD dynamo mechanism can produce amplification factors of up to $\sim 10^8$ but requires a seed field as large as $10^{-20} - 10^{-30}$ G in order to explain the observed galactic fields [133]. As a result the mechanism cannot in itself explain the origin of primordial magnetic fields. Additionally, adiabatic contraction of magnetic flux lines during cosmological structure formation can enhance galactic fields by a factor of $\sim 10^3$. Again, this mechanism requires a seed field that has to have been generated by some process pre-dating the epoch of structure formation.

Among the physical mechanisms proposed to explain the origin of the seed field is one due to Harrison [199]. This mechanism rests on the fact that non-zero vorticity in the pre-recombination photon-baryon plasma can generate weak magnetic fields of about $\sim 10^{-25}$ G. However, vorticity is not a generated mode at first order in perturbation theory and has to be put in as an initial condition. Second order treatments of the pre-recombination plasma in terms of a Kinetic theory description has also been used to generate the required seed fields [178, 166, 232, 219, 363, 266]. The key idea is a preferential Thompson scattering of photons

off free electrons, over the scattering off protons (the scattering off protons is suppressed by a factor $(m_e/m_p)^2$) which induces differences in the proton and electron velocity fields. Electric fields are then induced to counter charge separation between the electrons and protons. The generated electric fields will then feed in the magnetic induction equation to generate magnetic fields at second order in perturbation theory. The photon anisotropic stress also couples to the electron velocities and contributes to the magnetic field sources. In addition, other arguments relying on electroweak and QCD phase transitions [210, 98, 386, 207, 11], topological defects [211], velocity perturbations [64] etc. have been proposed as candidate mechanisms, see also [46, 141]. The generated fields, however, are usually too weak to leave any detectable imprint on the CMB [166]. This is not surprising given the form of the fluid quantities of a magnetic field (see §3.3.2). In particular, the energy density $\mu_B = B^2/2$, the isotropic pressure $p_B = B^2/6$ and the anisotropic pressure $\Pi_{ab} = B_{\langle a}B_{b\rangle}$ of a field generated at second order will manifest at fourth order in perturbation theory, which is not relevant for CMB anisotropies.

In addition to meeting the right strengths, the generated fields must be of the right scale to match those observed today. One of the problems of primordial generation mechanisms in general is that although some may reach the required strengths, they are causal in nature. This means that their coherence scales cannot exceed the Hubble scale during the time of magnetic field generation. By comparison, the galactic scale today is well outside the Hubble scale at such early epochs. Moreover, the small scale fields i.e, those that are already sub-horizon before matter-radiation equality cannot reach the recombination epoch due to micro-physical mechanisms such as magnetic and photon diffusion processes [46]. A possible solution to the scale problem may be the inverse cascade process, whereby magnetic energy is transferred to increasingly larger scales [129, 351, 74]. This mechanism however, requires strongly helical magnetic fields. On the other hand, Inflation and other pre-Big Bang models capable of causally producing super horizon perturbations are often invoked to circumvent the scale problem. However, the residual magnetic fields surviving the exponential expansion accompanying many inflationary models are thought to be too weak to be of cosmological relevance.[2]. This is a consequence of the fact that electromagnetic fields are conformally coupled to gravity. It is nevertheless possible to break the conformal invariance through some non standard couplings of electromagnetic fields to other fields such as the dilaton field to avoid the accompanying exponential dilution of the magnetic fields during the inflationary era [385, 321, 276, 173]. The primordial fields are also constrained by the fact that the

[2]This is not a generic feature of all Friedmann universes however. It is possible to 'preserve' primordial magnetic fields in an open Friedmann universe; the hyperbolic geometry can slow down the adiabatic decay of the field leading to superadiabatic amplification [41, 382], see also [6].

anisotropic stress of the produced magnetic fields contains a spin-2 component and will result in an overproduction of gravitational waves at horizon crossing which is inconsistent with standard BBN constraints [96, 97]. In essence, strong primordial magnetic fields are not consistent with limits from the BBN epoch, CMB anisotropies and gravitational wave limits. This feature favors the idea that the primordial seed field may have been weak and subsequently amplified by some other mechanism.

# Chapter 3

# 1+3 Covariant Approach to Cosmology

## 3.1 Preliminaries

Spacetimes are commonly described through the metric approach, where solutions of the field equations involve specifying the metric functions $g_{ij}(x^k)$ which are described in some coordinate system. However, coordinate independent approaches are possible. For example, one can use the Covariant formalism, based on a 1+3 decomposition of geometric quantities with respect to a fundamental four velocity $u^a$. One of the attractive aspects of this approach to General Relativity is that the underlying dynamical equations have a stronger appeal from a geometric standpoint, when compared to the quasi-linear, second-order partial differential equation form, which the Einstein field equations take in the metric based approach. Alternatively, one can adopt the 1+3 orthonormal frame (ONF) formalism which contains the 1+3 Covariant equations as a subset, while simultaneously guaranteeing the existence of a corresponding metric. For a review on the cosmological applications of the 1+3 covariant approach, the reader is referred to [152, 156, 160]

In the Covariant approach, we assume the existence of a unique timelike vector field $u^a$, representing the average 4-velocity matter at each point,

$$u_a = \frac{dx^a}{d\tau}, \qquad u_a u^a = -1 \ , \tag{3.1}$$

where the $x^a$ are general coordinates and $\tau$ measures the proper time along the world line. The key equations governing the full structure of the spacetime are derived from the Ricci and the once and twice contracted Bianchi identities applied to the 4-velocity vector $u^a$. The

Einstein field equations, in this case, play a lesser role than in the metric based approach. One invokes them simply to relate the curvature of spacetime to the local matter content. This feature makes the Covariant approach appealing in certain cases, especially when modified gravity theories are involved. This splitting uniquely defines two projection tensors $U^a$ and $h^a{}_b$ which project along and orthogonal to the 4-velocity $u^a$. These projection tensors are defined by,

$$U^a{}_b = -u^a u_b, \tag{3.2}$$

$$h^a{}_b = \delta^a{}_b + u^a u_b \ , \tag{3.3}$$

such that the following relations hold,

$$U^a{}_c U^c{}_b = U^a{}_b, \qquad U^a{}_a = 1, \qquad U_{ab}u^b = u_a \ , \tag{3.4}$$

$$h^a{}_c h^c{}_b = h^a{}_b, \qquad h^a{}_a = 3, \qquad h_{ab}u^b = 0 \ . \tag{3.5}$$

We define two projected covariant derivatives: the convective time derivative along $u^a$ and the spatially projected covariant derivative

$$\dot{Q}^{a\cdots b}{}_{c\cdots d} \equiv u^e \nabla_e Q^{a\cdots b}{}_{c\cdots d} \ , \tag{3.6}$$

$$\mathrm{D}_e Q^{a\cdots b}{}_{c\cdots d} \equiv h^a{}_p \cdots h^b{}_q \, h^r{}_c \cdots h^s{}_d \, h^f{}_e \nabla_f Q^{p\cdots q}{}_{r\cdots s} \ , \tag{3.7}$$

respectively. The two derivatives generally do not commute, see §3.9. In addition, one can identify a unique effective volume element $\epsilon_{abc}$ on the rest spaces

$$\epsilon_{abc} = \eta_{abcd} u^d \ , \tag{3.8}$$

where, $\eta_{abcd}$ is the alternating tensor of the full space time and is given by,

$$\eta_{abcd} = -\sqrt{|g|}\, \delta^0{}_{[a}\delta^1{}_b\delta^2{}_c\delta^3{}_{d]}, \qquad \eta^{abcd}\eta_{pqrs} = 4!\delta_p{}^{[a}\delta_q{}^b\delta_r{}^c\delta_s{}^{d]} \ . \tag{3.9}$$

By contracting on the Levi-Civita tensor of the spatial hypersurface $\epsilon_{abc}$, one arrives at the

following identities,

$$\epsilon_{abc}\epsilon^{def} = 3!h^{[a}{}_{d}h^{b}{}_{e}h^{c]}{}_{f} \ , \tag{3.10}$$

$$\epsilon_{abc}\epsilon^{cef} = 2!h^{[a}{}_{e}h^{b]}{}_{f} \ , \tag{3.11}$$

$$\epsilon_{abc}\epsilon^{bcf} = 2!h^{a}{}_{f} \ , \tag{3.12}$$

$$\epsilon_{abc}\epsilon^{abc} = 3! \ . \tag{3.13}$$

In addition, the following relations are useful.

$$\mathrm{D}_a h_{bc} = 0, \qquad \mathrm{D}_a \epsilon_{bcd} = 0, \qquad \dot{h}_{ab} = 2u_{(a}\dot{u}_{b)}, \qquad \dot{\epsilon}_{abc} = 3u_{[a}\epsilon_{bc]d}\dot{u}^{d} \ . \tag{3.14}$$

We generally use angular brackets on free indices to indicate orthogonal projection of vectors and the orthogonally projected symmetric trace free (PSTF) part of tensors,

$$V_{\langle a\rangle} = h_{a}{}^{b}V_{b}, \qquad T_{\langle ab\rangle} = [h^{c}{}_{(a}h^{d}{}_{b)} - \frac{1}{3}h^{cd}h_{ab}]T_{cd} \ . \tag{3.15}$$

One can use the orthogonal projected covariant derivative to define covariant divergence *div* and *curl* operators akin to standard three dimensional vector calculus. These operators are defined as,

$$\mathrm{div}\ V = \mathrm{D}^{a}V_{a}, \qquad (\mathrm{div}\ T)_{a} = \mathrm{D}^{b}T_{ab} \ , \tag{3.16}$$

for the divergence, and

$$\mathrm{curl}\ V_{a} = \epsilon_{abc}\mathrm{D}^{b}V^{c}, \qquad \mathrm{curl}\ T_{ab} = \epsilon_{cd\langle a}\mathrm{D}^{c}T_{b\rangle}{}^{d} \ , \tag{3.17}$$

for the curl operator.

## 3.2 Kinematic Quantities

The basic equations are then characterized by the irreducible parts of the first covariant derivative of the time like vector $u_a$

$$\nabla_{a}u_{b} = -u_{a}\mathcal{A}_{b} + \mathrm{D}_{a}u_{b} = -u_{a}\mathcal{A}_{b} + \frac{1}{3}\Theta h_{ab} + \sigma_{ab} + \omega_{ab} \ , \tag{3.18}$$

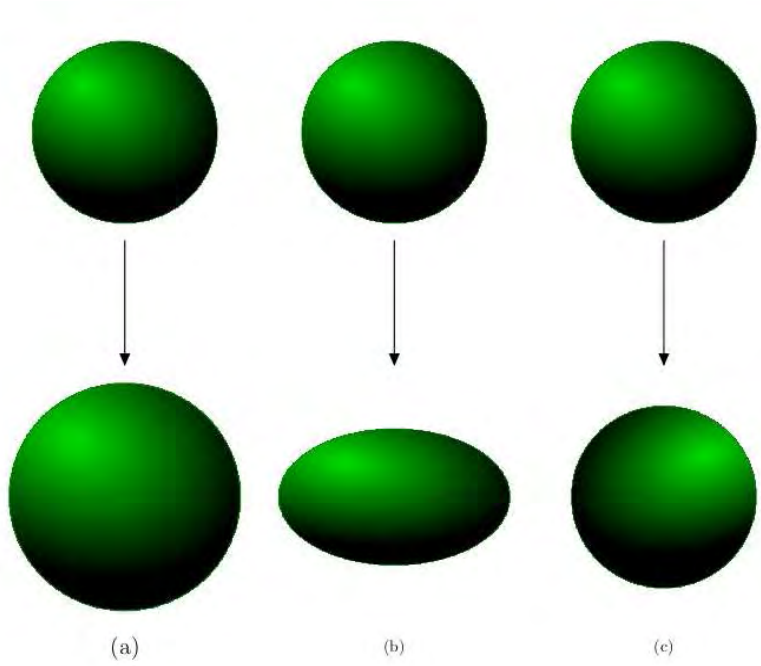


Figure 3.1: *A representation of the action of (a) expansion, (b) shear and (c) vorticity on a fluid sphere during a small time interval.*

This characterization of the kinematic quantities dates back to works by Raychaudhuri, Schüking and Ehlers, see for example [150][1]. The dynamical variables on the right hand side of Equation (3.18) have a physical meaning. Consider a sphere of fluid particles. The possible dynamics of such a sphere can be broken down into,

- ***Acceleration***

  The quantity $\mathcal{A}_a$ defined as

  $$\mathcal{A}_b = u^a \nabla_a u_b \,, \tag{3.19}$$

  is the relativistic acceleration vector representing the effect of forces other than gravity alone on the fluid sphere.

- ***Expansion***

  The rate of volume expansion $\Theta$ is defined as

  $$\mathrm{D}_a u^a = \Theta \,. \tag{3.20}$$

  The action of $\Theta$ alone transforms the fluid sphere to a similar sphere with a different

[1] This is actually the English translation of the original 1961 article.

volume. This corresponds to case (a) in Figure 3.1. The variable $\Theta$ is related to the Hubble parameter in a FLRW cosmological model by

$$H \equiv \frac{\dot{a}}{a} = \frac{1}{3}\Theta \, . \tag{3.21}$$

- ***Vorticity***

  The antisymmetric vorticity tensor $\omega_{[ab]}$ defined via

  $$\omega_{ab} = \mathrm{D}_{[a}u_{b]} \, , \tag{3.22}$$

  describes the rigid rotation of the fluid relative to a non-rotating frame. It is common to define the vorticity vector $\omega_a$,

  $$\omega_a = \frac{1}{2}\epsilon_{abc}\omega^{bc} \qquad \Rightarrow \qquad \omega_a u^a = 0, \qquad \omega_{ab} = \epsilon_{abc}\omega^c \, . \tag{3.23}$$

  Thus the action of $\omega_a$ alone on the fluid sphere will rotate the sphere along some axis, leaving the volume invariant. This corresponds to case (c) in Figure 3.1

- ***Shear***

  The symmetric trace-free rate of shear tensor $\sigma_{\langle ab\rangle}$ defined as

  $$\sigma_{ab} = \mathrm{D}_{\langle a}u_{b\rangle} \tag{3.24}$$

  describes the rate of distortion of the fluid flow. The action of $\sigma_{ab}$ alone on the fluid sphere will distort the sphere, without changing its overall volume. This corresponds to case (b) in Figure 3.1.

## 3.3 The Energy-Momentum Tensor

An arbitrary energy momentum tensor $T_{ab}$ of matter sources in the phenomenological fluid description can be decomposed into its irreducible parts relative to the fundamental congruence $u_a$ as,

$$T_{ab} = \mu u_a u_b + p h_{ab} + 2q_{(a}u_{b)} + \pi_{ab}. \tag{3.25}$$

This represents an imperfect, self gravitating fluid that is comoving with the preferred timelike vector field $u_a$. The quantities appearing in (3.25) have a physical interpretation. We make

the following identifications,

$$\mu = T_{ab}u^a u^b \ , \tag{3.26}$$

$$p = \frac{1}{3}T_{ab}h^{ab} \ , \tag{3.27}$$

$$q_q = -T_{bc}u^b h^{ca} \ , \tag{3.28}$$

$$\pi_{ab} = T_{cd}h^c_{\langle a}h^d_{b\rangle} \ , \tag{3.29}$$

where $\mu$ is the relativistic energy density, $p$ is the isotropic pressure, $q_a$ is the relativistic momentum density, representing the energy flux relative to the congruence $u_a$, and $\pi_{ab}$ is the anisotropic pressure. We note that a perfect fluid is characterized by a vanishing momentum density and anisotropic stress, $q_a = 0 = \pi_{ab}$.

In a thermodynamic context, in addition to the energy momentum tensor $T_{ab}$, one needs the particle flux $N_a$ and the entropy flux $S_a$. The energy momentum tensor is required to satisfy the Bianchi identities while $S_a$ satisfies the Second law of thermodynamics, i.e

$$\nabla^a T_{ab} = 0, \qquad \nabla_a S^a \geq 0 \ . \tag{3.30}$$

A simpler description arises when one assumes a barotropic equation of state $p = p(\mu)$. This is often given in the form

$$p = w\mu \ , \tag{3.31}$$

where for cosmological relevance, the equation of state parameter $w$ assumes the values $-1, 0, 1/3$ corresponding to the cosmological constant $\Lambda$, pressureless dust and radiation fluid respectively.

### 3.3.1 Scalar Fields

Scalar fields are of theoretical importance in cosmology. They play a role in inflationary theories in the early universe, and in quintessence models to explain the late time accelerated expansion of the universe. A minimally coupled scalar field $\phi$ has energy momentum tensor of the form,

$$T_{ab} = \nabla_a\phi\nabla_b\phi - g_{ab}\left(\frac{1}{2}\nabla_c\phi\nabla^c\phi + V(\phi)\right) \ . \tag{3.32}$$

We can interpret this as a perfect fluid with energy density and pressure given respectively by,

$$\mu = -\frac{1}{2}\nabla_a\phi\nabla^a\phi + V(\phi) \ , \tag{3.33}$$

$$p = -\frac{1}{2}\nabla_a\phi\nabla^a\phi - V(\phi) \ . \tag{3.34}$$

The dynamics of $\phi$ are governed by the Klein-Gordon equation

$$\nabla_a\nabla^a\phi - \frac{\partial V}{\partial\phi} = 0 \ , \tag{3.35}$$

which is a direct consequence of the conservation equation $\nabla^a T_{ab} = 0$, with the energy momentum tensor $T_{ab}$ given by (3.32). Within the covariant approach, we can choose the fundamental four velocity $u_a$ to be the unique timelike vector (with unit magnitude),

$$u^a = \frac{\nabla^a\phi}{\sqrt{-\nabla_b\phi\nabla^b\phi}} \ . \tag{3.36}$$

Having chosen the four velocity field $u_a$, one can proceed to calculate the kinematical quantities $\{\Theta, \omega_a, \sigma_{ab}\}$ of §3.2 in order to present a formal description of the scalar field dynamics in terms of fluid variables.

### 3.3.2 Electromagnetic Fields

The Maxwell field tensor $F_{ab}$ decomposes relative to the fundamental observer as,

$$F_{ab} = 2u_{[a}E_{b]} + \epsilon_{abc}B^c \ , \tag{3.37}$$

where,

$$E_a = F_{ab}u^b \qquad \text{and} \qquad B_a = \frac{1}{2}\epsilon_{abc}F^{bc} \tag{3.38}$$

are respectively the Electric and Magnetic field as measured by the fundamental observer moving with 4-velocity $u^a$. These are 3-vectors on the spacelike hypersurface, $E_a u^a = 0 = B_a u^a$.

It is also possible to give a fluid description of electromagnetic fields. In this case the energy momentum tensor of the electromagnetic field is given in terms of the Faraday tensor. This assumes the form,

$$T_{ab} = F_{ac}F^c_{\ b} - \frac{1}{4}g_{ab}F^{cd}F_{cd} \ . \tag{3.39}$$

Using the expression (3.37) for the Faraday tensor, one can write (3.39) as,

$$T_{ab} = \frac{1}{2}(E^2 + B^2)u_a u_b + \frac{1}{6}(E^2 + B^2)h_{ab} + 2u_{(a}\epsilon_{b)cd}E^c B^d - (E_{\langle a}E_{b\rangle} + B_{\langle a}B_{b\rangle}) \ , \tag{3.40}$$

where $E^2 = E_a E^a$ and $B^2 = B_a B^a$ are the magnitudes of the fields $E_a$ and $B_a$ respectively. This expression corresponds to an imperfect fluid with energy density $\mu$, isotropic pressure $p$, heat flux $\mathcal{Q}_a$ and anisotropic stress $\mathcal{P}_{ab}$ given respectively by

$$\mu = \frac{1}{2}(E^2 + B^2) \ , \tag{3.41}$$

$$p = \frac{1}{6}(E^2 + B^2) \ , \tag{3.42}$$

$$\mathcal{Q}_a = \epsilon_{abc}E^b B^c \ , \tag{3.43}$$

$$\mathcal{P}_{ab} = -(E_{\langle a}E_{b\rangle} + B_{\langle a}B_{b\rangle}) \ . \tag{3.44}$$

### 3.3.3 Energy Conditions

For standard matter, it is customary to impose certain conditions on the energy momentum tensor $T_{ab}$ in a quest to capture certain canons of standard physics, such as the the fact that energy is never negative. These energy conditions are summarized in Table 3.1.

It is interesting to note that the Strong Energy Condition (SEC) has to be violated by the inflaton field during the inflationary era and also by a cosmological constant $\Lambda$. In fact, from the Raychaudhuri equation (2.22b), we conclude that accelerated expansion occurs when $\mu + 3p < 0$ which in terms of the equation of state parameter $w$ translates into $w < -1/3$.

## 3.4 The Gravitational Field

In the geometric description of gravity, spacetime curvature is encoded in the Riemann tensor $R_{abcd}$. This tensor is defined through the Ricci identity,

$$\nabla_{[a}\nabla_{b]}u^c = R_{abcd}u^d \ . \tag{3.45}$$

The Riemann tensor can be algebraically decomposed into a trace part represented by the Ricci tensor $R_{ab} = R^c{}_{acb}$ and a trace-free part $C_{abcd}$ as,

$$R_{abcd} = C_{abcd} + g_{a[c}R_{d]b} - g_{b[c}R_{d]a} - \frac{1}{3}Rg_{a[c}g_{d]b}. \tag{3.46}$$

| Energy condition | Criteria | |
|---|---|---|
| Weak | $T_{ab}u^a u^b \geq 0$ , | $\begin{array}{rcl}\mu & \geq & 0 \\ \mu + p & \geq & 0\end{array}$ |
| Null | $T_{ab}k^a k^b \geq 0$ , | $\mu + p \geq 0$ |
| Strong | $T_{ab}u^a u^b + 1/2T^a_{\ a} \geq 0$ , | $\begin{array}{rcl}\mu + 3p & \geq & 0 \\ \mu + p & \geq & 0\end{array}$ |
| Dominant | $-T^a_{\ b}u^b$ , | $\begin{array}{rcl}\mu & \geq & 0 \\ \mu & \geq & \lvert p_i\rvert\end{array}$ |

Table 3.1: *In this table, we give a summary of the energy conditions, where the vectors $u^a$ and $k^a$ are arbitrary timelike and null respectively.*

where the trace part $R_{ab}$ can be determined from the Einstein field equations and the trace-free part $C_{abcd}$, commonly referred to as the Weyl tensor cannot be determined from the Einstein field equations. This is clear because upon contracting on (3.46), which is necessary to recover the Ricci tensor, the Weyl tensor vanishes and so cannot be part of the field equations. Thus the Weyl tensor encodes tidal forces which cannot be determined locally by dynamical sources; it represents the free gravitational field, enabling gravitational action at a distance. Upon using the Bianchi identities $\nabla_{[a}R_{ab]cd} = 0$ one arrives at the relation,

$$\nabla^d C_{abcd} = -\nabla_{[a}\left(R_{b]c} - \frac{1}{6}R\, g_{b]c}\right) . \tag{3.47}$$

In analogy with splitting the Maxwell field tensor $F_{ab}$ into a magnetic and an electric field, the Weyl tensor $C_{abcd}$ can be split covariantly into a 'magnetic' part $H_{ab}$ and an 'electric' part $E_{ab}$, relative to the timelike congruence $u_a$.

$$E_{ab} = C_{abcd}u^c u^d \qquad E^a_{\ a} = 0, \qquad E_{ab}u^b = 0 , \tag{3.48}$$

$$H_{ab} = \frac{1}{2}\epsilon_{ade}C^{de}_{\ \ bc}u^c \qquad H^a_{\ a} = 0, \qquad H_{ab}u^b = 0 . \tag{3.49}$$

The electric part of the Weyl tensor describes tidal effects, akin to the tidal tensor associated with the Newtonian potential, while the magnetic part describes the propagation of gravita-

tional radiation and has no Newtonian counterpart. With this identification, the Weyl tensor takes the form

$$C_{abcd} = (4g_{a[p}g_{q]b}g_{c[r}g_{s]d} - \eta_{abpq}\eta_{cdrs})u^p u^r E^{qs} \tag{3.50}$$

$$+ 2(\eta_{abpq}g_{c[r}g_{s]d} + g_{a[p}g_{q]b}\eta_{cdrs})u^p u^r H^{qs} \ . \tag{3.51}$$

Finally, using these decompositions, along with the Einstein field equations, one can cast the Riemann tensor in a form

$$R^{abcd} = R^{abcd}_P + R^{abcd}_I + R^{abcd}_H + R^{abcd}_E \ , \tag{3.52}$$

where,

$$R^{abcd}_P = \frac{2}{3}(\mu + 3p - 2\Lambda)u^{[a}u_{[c}h^{b]}_{\ \ d]} + \frac{2}{3}(\mu + \Lambda)h^{[a}_{\ \ [c}h^{b]}_{\ \ d]} \ , \tag{3.53a}$$

$$R^{abcd}_I = -2u^{[a}h^{b]}_{\ \ [c}q_{d]} - 2u_{[c}h^{[a}_{\ \ d]}q^{b]} - 2u^{[a}u_{[c}\pi^{b]}_{\ \ d]} + 2h^{[a}_{\ \ [c}\pi^{b]}_{\ \ d]} \ , \tag{3.53b}$$

$$R^{abcd}_H = 2\epsilon^{abe}u_{[c}H_{d]e} + 2\epsilon_{cde}u^{[a}H^{b]e} \ , \tag{3.53c}$$

$$R^{abcd}_E = 4u^{[a}u_{[c}E^{b]}_{\ \ d} + 4h^{[a}_{\ \ [c}E^{b]}_{\ \ d]} \ . \tag{3.53d}$$

The above equations (3.53) show the relative contributions to the Riemann tensor $R^{abcd}$ coming from the perfect ($R^{abcd}_P$) and imperfect ($R^{abcd}_I$) fluid component of the Energy-momentum tensor, while $R^{abcd}_H$ and $R^{abcd}_E$ are the contributions from the Magnetic and Electric part of the Weyl tensor, respectively.

## 3.5 Propagation and Constraint Equations

***Propagation***

Evolution equations for the kinematic variables $\{\Theta, \omega_a, \sigma_{ab}\}$ are obtained by separating out the parallel projected part of the Ricci identity (3.45) into its irreducible components. We refer the reader to [152] for an outline of the derivation. This results in the following equations,

$$\dot{\Theta} - \mathrm{D}_a\mathcal{A}^a = -2\sigma_{ab}\sigma^{ab} + 2\omega_a\omega^a + \mathcal{A}_a\mathcal{A}^a - \tfrac{1}{3}\Theta^2 - \tfrac{1}{2}(\mu + 3p) + \Lambda \ , \tag{3.54}$$

$$\dot{\omega}_{\langle a\rangle} - \tfrac{1}{2}\epsilon_{abc}\mathrm{D}^b\mathcal{A}^c = -\tfrac{2}{3}\Theta\omega_a + \sigma_{ab}\omega^b \ , \tag{3.55}$$

$$\dot{\sigma}_{\langle ab\rangle} - \mathrm{D}_{\langle a}\mathcal{A}_{b\rangle} = -\sigma_{c\langle a}\sigma_{b\rangle}{}^c - \omega_{\langle a}\omega_{b\rangle} + \mathcal{A}_{\langle a}\mathcal{A}_{b\rangle} - \tfrac{2}{3}\Theta\sigma_{ab} - E_{ab} + \tfrac{1}{2}\pi_{ab} \ . \tag{3.56}$$

Equation (3.54), commonly referred to as the Raychaudhuri equation, is the basic equation of gravitational attraction and underlies the singularity theorem (Theorem 2.1.1 in §2.1.4). The repulsive nature of the cosmological constant and the identification of $\mu + 3p$ as the active gravitational mass density is evident from the Raychaudhuri equation. The vorticity term $\omega^{ab}\omega_{ab}$ acts to hold the matter apart, while the shear term $\sigma^{ab}\sigma_{ab}$ acts by pulling the world lines together.

From the Bianchi identities, one recovers the following propagation equations for the Electric and Magnetic parts of the Weyl tensor,

$$\begin{aligned}\left(\dot{E}_{\langle ab\rangle} + \tfrac{1}{2}\dot{\pi}_{\langle ab\rangle}\right) - \text{curl } H_{ab} + \tfrac{1}{2}\mathrm{D}_{\langle a}q_{b\rangle} &= -\tfrac{1}{2}(\rho + p)\sigma_{ab} - \Theta\left(E_{ab} - \tfrac{1}{6}\pi_{ab}\right) - A_{\langle a}q_{b\rangle} \\ &\quad + 2A^{c}\epsilon_{cd(a}H_{b)}{}^{d} + 3\sigma_{c\langle a}E_{b\rangle}{}^{c} - \omega^{c}\epsilon_{cd(a}E_{b)}{}^{d} \\ &\quad - \tfrac{1}{2}\sigma^{c}{}_{\langle a}\pi_{b\rangle c} - \tfrac{1}{2}\omega^{c}\epsilon_{cd(a}\pi_{b)}{}^{d}\ , \end{aligned} \tag{3.57}$$

and

$$\begin{aligned}\dot{H}_{\langle ab\rangle} + \text{curl } E_{ab} - \tfrac{1}{2}\text{curl } \pi_{ab} &= -\Theta H_{ab} + 3\sigma^{c}_{\langle a}H_{b\rangle c} + \tfrac{3}{2}\omega_{\langle a}q_{b\rangle} \\ &\quad - \epsilon_{cd\langle a}\left[2\mathcal{A}^{c}E_{b\rangle}{}^{d} - \tfrac{1}{2}\sigma_{b\rangle}{}^{c}q^{d} - \omega^{c}H_{b\rangle}{}^{d}\right]\ , \end{aligned} \tag{3.58}$$

respectively. These equations, showing the propagation of gravitational radiation, represent the gravitational counterparts of Maxwell equations (§3.6).

We also need propagation equations for the matter variables. These are derived from the conservation of matter $\nabla_a T^{ab} = 0$. Projecting along and orthogonal to the 4-velocity $u^a$ results in the energy conservation equation,

$$\dot{\mu} + \mathrm{D}_a q^a = -\Theta(\mu + p) - 2\mathcal{A}_a q^a - \sigma_{ab}\pi^{ab}\ , \tag{3.59}$$

and respectively, the momentum conservation equation

$$\dot{q}^a + \mathrm{D}^a p + \mathrm{D}_b \pi^{ab} = -\tfrac{4}{3}q^a - \sigma^a q^b - (\mu + p)\mathcal{A}^a - \mathcal{A}_b\pi^{ab} - \epsilon^{abc}\omega_b q_c\ . \tag{3.60}$$

### *Constraints*

To complement the system (3.54)–(3.58), we give the following constraint equations which must be satisfied at each hypersurface during propagation. By projecting the Ricci identities (3.45) orthogonal to the 4-velocity $u^a$ we obtain the constraints (3.61), (3.62) and (3.62). Similarly, from the Bianchi identiies one recovers the constraints (3.64) and (3.64).

$$0 = (C_1)_a = \mathrm{D}^b\sigma_{ab} - \tfrac{2}{3}\mathrm{D}_a\Theta + \epsilon_{abc}[\mathrm{D}^b\omega^c + 2\mathcal{A}^b\omega^c] + q_a \ , \tag{3.61}$$

$$0 = (C_2) = \mathrm{D}_a\omega^a - \mathcal{A}_a\omega^a \ , \tag{3.62}$$

$$0 = (C_3)_{ab} = H_{ab} + 2\mathcal{A}_{\langle a}\omega_{b\rangle} + \mathrm{D}_{\langle a}\omega_{b\rangle} - \mathrm{curl}\ \sigma_{ab} \ , \tag{3.63}$$

$$\begin{aligned} 0 = (C_4)_a = \mathrm{D}^b\left(E_{ab} + \tfrac{1}{2}\pi_{ab}\right) - \tfrac{1}{3}\mathrm{D}_a\mu + \tfrac{1}{3}\Theta q_a - \tfrac{1}{2}\sigma_{ab}q^b - 3\omega^b H_{ab} - \\ \epsilon_{abc}\left[\sigma^{bd}H^c{}_d - \tfrac{3}{2}\omega^b q^c\right] \ , \end{aligned} \tag{3.64}$$

$$\begin{aligned} 0 = (C_5)_a = \mathrm{D}^b H_{ab} + (\mu + p)\omega_a + 3\omega^b\left(E_{ab} - \tfrac{1}{6}\pi_{ab}\right) + \\ \epsilon_{abc}\left[\tfrac{1}{2}\mathrm{D}^b q^c + \sigma^{bd}\left(E^c{}_d + \tfrac{1}{2}\pi^c{}_d\right)\right] \ . \end{aligned} \tag{3.65}$$

## 3.6 Maxwell Field Equations

The dynamics of the Faraday tensor $F_{ab}$ as governed by Maxwell's equations are given by

$$\nabla_{[a}F_{bc]} = 0 \ , \tag{3.66}$$

$$\nabla^b F_{ab} = J_a \ , \tag{3.67}$$

where $F_{ab} = 2\nabla_{[a}A_{b]}$ is the Faraday tensor, $A_{ab}$ is the 4-potential and $J_a$ is the 4-current. These equations can be decomposed covariantly into propagation and constraint equations according to [377, 40, 152]

$$\dot{E}_{\langle a\rangle} - \mathrm{curl}\ B_a = -\frac{2}{3}\Theta E_a + \sigma_{ab}E^b + \epsilon_{abc}(\mathcal{A}^b B^c + \omega^b E^c) - \mu_0\mathcal{J}_{\langle a\rangle} \ , \tag{3.68a}$$

$$\dot{B}_{\langle a\rangle} + \mathrm{curl}\ E_a = -\frac{2}{3}\Theta B_a + \sigma_{ab}B^b + \epsilon_{abc}(\mathcal{A}^b E^c + \omega^b B^c) \ , \tag{3.68b}$$

$$0 = \mathrm{D}_a E^a - 2\omega_a B^a - \frac{\rho_c}{\epsilon_0} \ , \tag{3.68c}$$

$$0 = \mathrm{D}_a B^a + 2\omega_a E^a \ . \tag{3.68d}$$

where $\rho_c = -j_a u^a$ characterizes the charge density. From (3.67), one can write down a wave equation for the Maxwell field tensor $F_{ab}$,

$$\nabla^2 F_{ab} = -2R_{abcd}F^{cd} + R_a{}^c F_{cb} + F_a{}^c R_{cb} + \nabla_b J_a - \nabla_a J_b \ , \tag{3.69}$$

from which one can derive wave equations for the electric $E_a$ and magnetic $B_a$ field variables.

In the absence of gravitational interactions, the Maxwell's equations (3.68)–(3.68d) reduce to their usual form,

$$\dot{E}_{\langle a\rangle} - \text{curl}\, B_a = -\mu_0 \mathcal{J}_{\langle a\rangle} \ , \tag{3.70}$$

$$\dot{B}_{\langle a\rangle} + \text{curl}\, E_a = 0 \ , \tag{3.71}$$

$$\mathrm{D}_a E^a = \frac{\rho_c}{\epsilon_0} \ , \tag{3.72}$$

$$\mathrm{D}_a B^a = 0 \ . \tag{3.73}$$

The covariant form of the Maxwell equations set the stage for studying interactions with gravitational phenomena. In particular, we note the following interactions

- ***Expansion***

  The coupling of the electromagnetic fields with expansion gives rise to the possibility of damping or amplification of a test field. For example, in a cosmological setting, the action of expansion alone serves to dilute any magnetic fields that may be present in the cosmic medium.

  Conversely, one expects that the action of contraction alone will serve to amplify any preexisting magnetic fields in the cosmic medium. It is fairly established that the universe is expanding, so this feature is not relevant for cosmological spacetimes at late times. However, in astrophysical contexts where a star can collapse into a neutron star or a charged black hole, this phenomenon is expected to play a role.

- ***Rotation***

  Rotation is not expected to play a role in a FLRW spacetime. In fact, like the magnetic field, vorticity is diluted by the cosmological expansion. However, in astrophysical situations where neutrons stars or charged black holes have high angular momenta, the interaction with rotation is expected to become important.

  Moreover, in cases involving gravitational perturbations of high order, it has been shown that vorticity can be sourced. This phenomenon will not only induce interactions with preexisting fields, but has the potential within itself, to source electromagnetic fields.

- ***Shear***

  The action of the shear alone serves to amplify any preexisting magnetic field in the cosmic medium. Since gravitational waves are encoded in the shear tensor $\sigma_{ab}$, this phenomenon incorporates the possibility of observable electromagnetic signatures following an interaction with a gravitational wave. The study of interactions of preexisting fields with gravitational waves is the subject of Chapter 5.

- ***Non inertial acceleration***

  Non inertial acceleration can be linked to changes in the pressure of the cosmic fluid, which can in turn be linked to perturbations in the density field. The fact that magnetic fields have a non zero coupling with acceleration accommodates the possibility that density perturbations can affect the dynamics of magnetic fields in a cosmological setting. Again, we treat this phenomenon in Chapter 5.

## 3.7 Covariant Characterization of FLRW Models

To describe FLRW models within the covariant approach, we note that the the spatially homogeneous and isotropic FLRW line element (2.1), reduces to,

$$ds^2 = -dt^2 + a(t)^2 h_{ab} dx^a dx^b. \tag{3.74}$$

We refer the reader to [160] for a thorough treatment of the FLRW model in the covariant approach. For this metric, we have that the 4-velocity field is given by

$$u^0 = 1, \qquad u^i = 0, \qquad i = 1, 2, 3 \tag{3.75}$$

from which we can compute the kinematical variables, starting from

$$\nabla_a u_b = \frac{\dot{a}}{a} h_{ab} = -u_a \mathcal{A}_b + \frac{1}{3}\Theta h_{ab} + \sigma_{ab} + \omega_{ab} \,, \tag{3.76}$$

This immediately suggests that

$$\Theta = 3\frac{\dot{a}}{a}, \qquad \mathcal{A}_a = 0, \qquad \sigma_{ab} = 0, \qquad \omega_a = 0 = \omega_{ab} \,. \tag{3.77}$$

Thus, relative to the congruence $u_a$, the kinematical variables have to be locally isotropic. Moreover, the FLRW spacetime is characterized by a perfect fluid matter tensor, i.e

$$\pi_{ab} = 0, \qquad q_a = 0 \, . \tag{3.78}$$

Spatial homogeneity implies that the spatial gradients of the energy density $\mu$, pressure $p$, and the expansion $\Theta$ vanish, i.e

$$\mathrm{D}_a\mu = 0, \qquad \mathrm{D}_a p = 0, \qquad \mathrm{D}_a\Theta = 0 \, . \tag{3.79}$$

These restrictions imply that the spacetime is conformally flat leading to the vanishing of the Weyl tensor,

$$C_{abcd} = 0 \qquad \Rightarrow \qquad E_{ab} = 0, \qquad \text{and} \qquad H_{ab} = 0 \, . \tag{3.80}$$

The key background equations characterizing an isotropic and homogeneous cosmological model are recovered from covariant propagation equations by imposing the above conditions. In particular, the energy conservation equation (3.59) reduces to

$$\dot{\mu} = -(1+w)\Theta\mu, \tag{3.81}$$

the Raychaudhuri equation (3.54) reduces to

$$\dot{\Theta} = -\frac{1}{3}\Theta^2 - \frac{1}{2}\mu(1+3w) + \Lambda, \tag{3.82}$$

where $w = p/\mu$ and finally the Friedmann equation

$$\mu + \Lambda = \frac{1}{3}\Theta^2 + \frac{3k}{a^2}. \tag{3.83}$$

In Chapter 5, we focus mainly on flat models $k = 0$ with vanishing cosmological constant $\Lambda = 0$. In this case, the scale factor evolution as recovered from the Raychaudhuri equation (3.82) is given by,

$$\frac{\ddot{a}}{a} = -\frac{1}{2}(1+3w)\left(\frac{\dot{a}}{a}\right)^2 \, . \tag{3.84}$$

One can integrate (3.84), with initial values set at some arbitrary initial time $t_i$, such that $\Theta(t_i) = \Theta_i$. This leads to the following,

$$\frac{\dot{a}}{a} = \frac{2H_i}{3H_i(1+w)(t-t_i)+2} \,, \tag{3.85}$$

where we have used the fact that $\Theta_i = 3H_i$, where $H_i$ is the Hubble parameter at the initial time $t_i$. Of course, (3.85) is only an intermediate step, we continue the integration to recover the following solution for the scale factor,

$$a = a_i \left[\tfrac{3}{2}H_i(1+w)(t-t_i)+1\right]^{\frac{2}{3(1+w)}} \,. \tag{3.86}$$

It is convenient at this time to define a dimensionless time variable $\tau$

$$\tau = \frac{3}{2}H_i(1+w)(t-t_i)+1 \,, \tag{3.87}$$

such that Equation (3.86) reduces to

$$a = a_i \tau^{\frac{2}{3(1+w)}} \,. \tag{3.88}$$

We will employ this time variable in Chapter 5.

## 3.8 The Ehlers-Geren-Sachs Theorem

Unlike spatial homogeneity, the isotropy postulate of the Cosmological principle is a directly observable quality. Indeed, observational data shows that the CMB is isotropic about us to within one part in $10^5$. Given information about the isotropy of the CMB, one can make certain deductions about spatial homogeneity. One of the most important results in this regard is the Ehlers-Geren-Sachs (EGS) theorem [149, 202].

**Theorem 3.8.1 (Ehlers-Geren-Sachs (EGS)[149])** *If a family of fundamental observers in a dust spacetime measure the background radiation to be everywhere exactly isotropic, then the spacetime is locally exactly FLRW.*

For a proof of the EGS theorem, see for example [119]. This theorem has since been generalized to several contexts, including modified gravity theories [163]. The EGS theorem and its generalizations, along with the Copernican principle, provide a basis for the assumption of spatial homogeneity, given the isotropy of the CMB. However, the CMB is only approximately

isotropic and not exactly isotropic as required by Theorem 3.8.1. We state the almost-EGS version in §4.5.

## 3.9 Commutator Relations

In general, the derivatives introduced in §3.1 do not commute. However, one can derive commutator relations between them. A starting point to derive these relations is through the following,

$$\nabla_{[a}\nabla_{b]}S = 0 \,, \tag{3.89}$$

$$2\nabla_{[a}\nabla_{b]}S^{c} = R_{ab}{}^{c}{}_{d}S^{d} \,, \tag{3.90}$$

$$2\nabla_{[a}\nabla_{b]}S^{cd} = -R_{ab}{}^{ec}S_{e}{}^{d} - R_{ab}{}^{ed}S^{c}{}_{e} \,, \tag{3.91}$$

which are the Ricci identities for scalars $S$, first rank tensors $S^{a}$ and second rank tensors $S^{ab}$ respectively. Upon projecting onto the spatial slices, one will need the expression of the 3-Riemann tensor. This is given by the Gauss equation,

$${}^{(3)}R_{abcd} = h^{p}{}_{a}h^{q}{}_{b}h^{r}{}_{c}h^{s}{}_{d}\,{}^{(4)}R_{pqrs} - K_{ac}K_{bd} + K_{bc}K_{ad} \,, \tag{3.92}$$

relating the full spatial projection of the Riemann tensor of the full spacetime to the induced three dimensional Riemann tensor ${}^{(3)}R_{abcd}$. The symmetric tensor $K_{ab}$ appearing in (3.92) is called the second fundamental form, or extrinsic curvature. It is given in terms of the kinematical variables as,

$$K_{ab} = \frac{1}{3}\Theta h_{ab} + \sigma_{ab} \,. \tag{3.93}$$

We give the commutation relations for 3-scalar, 3-vector and second rank 3-tensor derivatives in Appendix A.3.

# Chapter 4

# Cosmological Perturbation Theory

## 4.1 Introduction

In relativistic cosmology, gravitational interactions are modeled by the theory of general relativity. This paradigm features solutions of the Einstein field equations under certain assumptions of cosmological relevance. In general, there are a number of prevalent methods in which one can solve or analyze the Einstein field equations. We briefly mention these below:

- ***Analytical***,

  The FLRW spacetime and the Lemaître-Tolman-Bondi (LTB) metric are examples of cosmological exact solutions. Analytical methods, or more appropriately, exact solutions of the Einstein field equations were among the first approaches used in studying general relativistic spacetimes. We refer the reader to [356, 222] for a more extensive treatment of this subject. It is worth mentioning that because of the non linearity of the Einstein field equations, general exact solutions for arbitrary matter distributions are analytically intractable. For this reason, one often has to impose high degrees of symmetries in order to simplify the problem at hand. This is often undesirable in many situations of interest. In such cases, one resorts to some of the methods mentioned below. Nevertheless, this form of generating solutions has provided invaluable insights, by for example, providing the groundwork for testing observational predictions of general relativity. In addition, exact solutions form the bedrock for perturbation theory, by providing a background about which one introduces perturbations.

- ***Numerical***.

  This class of methods proceed by formulating the Einstein field equations as an initial-boundary value problem to be integrated in time using numerical methods. An attractive feature of this approach is that no symmetry assumptions are necessary. In principle, one needs only provide initial and boundary data for the metric elements, having assumed a particular gauge. Numerical methods for solving the Einstein field equations form the basis of Numerical Relativity and are discussed in Part II of this thesis.

- ***Qualitative***

  Within this class, one is interested in inferring evolutionary properties of general classes of cosmological models. For example, the Dynamical System approach has been adopted in the field of cosmology to study spatially homogeneous cosmological space times [392, 125, 362, 262, 99]. In this case the governing equations can be reduced to a finite system of autonomous ordinary differential equations. The Piece-wise approximation methods along with Hamiltonian methods also fall within this subclass and they find application in analyzing various aspects of cosmological models [392].

- ***Perturbative***

  A fundamental assumption in relativistic perturbation theory is the existence of a parametric family of spacetimes that can be Taylor expanded around some background. The general idea behind perturbative methods is to represent the sought after solution $g_{ab}$ in terms of some known background solution ${}^{(0)}g_{ab}$, plus perturbations,

$$g_{ab} = {}^{(0)}g_{ab} + \delta g_{ab} \ . \tag{4.1}$$

  One then uses the field equations to derive equations of motion for the new fields $\delta g_{ab}$. We note that analytical or exact solutions are used in characterizing the background solution ${}^{(0)}g_{ab}$. Linear perturbations of spatially homogeneous and isotropic cosmological models were first studied in the 1940s by Lifshitz [251, 252] and later extended by several authors. In the following, we make the common assumption in the literature that the perturbed spacetimes have the same manifold as the background spacetime i.e. we consider the perturbations $\delta g_{ab}$ as fields propagating on the background spacetime [357, 352]. In this treatment, therefore, we restrict the possibility that the perturbations may alter the differential structure of the background manifold and so we neglect issues of backreaction.

In this Chapter we focus on perturbative methods. In particular, we present the main equations that represent a perturbed FLRW spacetime. The Chapter itself is structured as follows: We begin by summarizing the essence of gauge invariance in §4.2 followed by a recap of metric based perturbation theory in §4.3. In §4.4 we present the main equations describing gravitational perturbations within the 1+3 Covariant formalism. The equations presented in the aforementioned section are a key component of our study as they will be later used to characterize gravitational degrees of freedom in Chapter 5. We follow up in §4.6 with a method to compute perturbed (covariant) kinematic variables in terms of metric variables. Finally, we present the details of our two parameter perturbation scheme that is central to our study of cosmological magnetic fields within the FLRW spacetime (see Chapter 5).

## 4.2 Gauge Invariance

A recurrent theme within relativistic perturbation theory is that of gauge invariance. In this section, we aim to elucidate this concept. From Equation (4.1), we note that one will routinely have to compare tensors in the background spacetime $(\mathcal{M}, \bar{g}_{ab})$ with those of the perturbed spacetime $(\mathcal{M}, g_{ab})$ in order to quantify the deviation from the background solution. We are thus led to define a diffeomorphism $\Phi$ such that $\Phi : \mathcal{M} \to \mathcal{M}$ which relates points of the background spacetime with those of the perturbed spacetime. This choice of coordinates is referred to as a gauge choice, and any change in $\Phi$ is referred to as a gauge transformation. Consider a quantity $Q$ defined in the perturbed spacetime $(\mathcal{M}, g_{ab})$, with the corresponding quantity $\bar{Q}$ defined in the background spacetime $(\mathcal{M}, \bar{g}_{ab})$. We define a perturbation $\delta Q$ of $Q$ at the point $p \in \bar{\mathcal{M}}$ as follows

$$\delta Q(p) = Q(p) - \bar{Q}(\Phi^{-1}(p)) \,, \tag{4.2}$$

where $\bar{Q}(\Phi^{-1}(p))$ is the pull-back. From this we note that the perturbation $\delta Q(p)$ is not unique as it depends on the mapping $\Phi$ of points between the background and perturbed spacetimes. To illustrate this further, consider a change in the mapping $\Phi$, such that the new correspondence is given by a diffeomorphism $\tilde{\Phi}$, the perturbation is now given by,

$$\delta \tilde{Q}(p) = Q(p) - \tilde{Q}(\tilde{\Phi}^{-1}(p)) \,. \tag{4.3}$$

Comparison with (4.2) reveals the gauge artifact $\Delta Q(p)$ which is given by,

$$\Delta Q(p) = \delta \tilde{Q}(p) - \delta Q(p) = \tilde{Q}(\tilde{\Phi}^{-1}(p)) - Q(\Phi^{-1}(p)) \,. \tag{4.4}$$

Perturbations where this artifact vanishes are referred to as gauge-invariant. We state without proof the following result [358],

**Lemma 4.2.1 (*Stewart-Walker Lemma*)** *The linear perturbation $Q_1$ of a quantity $Q_0$ on $(\mathcal{M}, g)$ is gauge invariant if and only if one of the following holds*

1. *$Q_0$ vanishes.*
2. *$Q_0$ is a constant scalar.*
3. *$Q_0$ is a constant linear combination of Kronecker deltas.*

The Stewart & Walker Lemma has since been generalized to contexts involving non linear and in general N-parameter perturbations [85, 352]. For example, in the case of a two parameter perturbation scheme up to order $(n, n')$, the criteria for gauge invariance is given as follows [85, 352],

**Lemma 4.2.2** *The perturbation $Q$ of a quantity $Q_0$ on $(\mathcal{M}, g)$ is gauge invariant at order $(n, n')$ if and only if one of the following holds*

1. *$Q_0$ and all its perturbations of order lower than $(n, n')$ vanish.*
2. *$Q_0$ and all its perturbations of order lower than $(n, n')$ are constant scalars.*
3. *$Q_0$ and all its perturbations of order lower than $(n, n')$ are constant linear combinations of Kronecker deltas.*

In characterizing the interaction of gravitational fields with electromagnetic fields, we employ a two parameter perturbative scheme. Lemma 4.2.2 becomes relevant in establishing gauge invariance in this context. We describe this in more detail in §4.7.

## 4.3 Metric-Based Perturbation Theory

The framework employed in metric based perturbation theory was among the first attempts made to study perturbed solutions of the Einstein field equations [251, 252]. Within this approach, one starts from a known background solution, and explicitly add perturbations to the resulting metric. We refer the reader to [233, 144] for a thorough treatment of the subject. In general, one has the option of considering perturbations in a particular gauge, or considering the gauge invariant method of Bardeen [36].

### 4.3.1 Metric Tensor

We consider linear perturbations about a flat FLRW metric. In the Poisson gauge, such perturbations are given through the line element by,

$$ds^2 = a^2 \left[-(1+2\Phi)d\eta^2 + 2\omega_i dx^i d\eta + [(1-2\Psi)\gamma_{ij} + h_{ij}]dx^i dx^j\right] \ , \tag{4.5}$$

where we employ conformal time $\eta$, which is related to cosmic time via $dt = a\, d\eta$. In this gauge, the quantities $\Phi$ and $\Psi$ correspond to the gauge-invariant Bardeen potentials. We proceed by performing a scalar-vector-tensor (SVT) decomposition of the perturbation variables as follows,

$$\omega_i = \partial_i B + B_i \tag{4.6}$$

$$h_{ij} = 2E_{ij} + 2\partial_{(i}E_{j)} + 2\partial_i\partial_j E \tag{4.7}$$

where the quantities $B_i$, $E_i$ and $E_{ij}$ are transverse and $E_{ij}$ is in addition traceless, i.e.

$$\partial^i B_i = 0 \ , \qquad \partial^i E_i = 0, \tag{4.8a}$$

$$\partial^i E_{ij} = 0 \ , \qquad E^i{}_i = 0 \ . \tag{4.8b}$$

In essence, the 10 degrees of freedom in the perturbations are composed of 4 scalar degrees of freedom ($\Phi$, $\Psi$, $B$, $E$), 4 vector degrees of freedom ($B_i$, $E_i$, together with the constraints (4.8a)) and 2 tensor degrees of freedom ($E_{ij}$, together with (4.8b)).

### 4.3.2 Energy-Momentum Tensor

As mentioned in the introductory sections (2.1.4), the FLRW cosmological models are consistent with the perfect fluid form of the energy momentum tensor,

$$T_{ab} = (\mu + p)\, u_a u_b + p g_{ab} \ , \tag{4.9}$$

where $u_a$ is the cosmological fluid 4-velocity, $\mu$ and $p$ are the rest frame energy density and isotropic pressure respectively, as measured by an observer in a locally inertial frame, comoving with the fluid. For convenience, we express the background energy momentum tensor with one index raised, and the other lowered

$$T^a_{\ b} = (\mu + p) u^a u_b + p \delta^a_{\ b} \ . \tag{4.10}$$

We then proceed to perturb the energy density and pressure as

$$\mu(\eta, x^i) = \bar{\mu} + \delta\mu(\eta, x^i) \,, \tag{4.11a}$$

$$p(\eta, x^i) = \bar{p} + \delta p(\eta, x^i) \,. \tag{4.11b}$$

Under the assumption of an equation of state of the form $p = p(\mu, S)$ where $S$ is the entropy, the pressure perturbation $\delta p$ can be expanded as

$$\delta p = \frac{\partial p}{\partial S}\Big|_{\mu} \delta S + \frac{\partial p}{\partial \mu}\Big|_{S} \delta\mu \,, \tag{4.12}$$

where $\delta S$ is the entropy perturbation. If one assumes adiabatic perturbations, then the Entropy perturbation vanishes $\delta S = 0$ and the pressure perturbation reduces to $\delta p = c_s^2 \delta\mu$, where $c_s^2 = \partial p/\partial\mu$ is the adiabatic speed of sound. To find the perturbed 4-velocity, we invoke the normalization condition $u^a u_a = -1$ to recover the relations

$$a u^0 = (1 - \Phi), \tag{4.13}$$

$$a u^i = v^i, \tag{4.14}$$

where $v^i$ is the spatial 3-velocity of the fluid. The contravariant components of the 4-velocity can be derived from the condition $u_a = g_{ab} u^b$,

$$u_0 = -a(1 + \Phi) \,, \tag{4.15}$$

$$u_i = a(v_i + \omega_i) \,. \tag{4.16}$$

We are now in a position to perturb the energy momentum tensor (4.10). Using the expressions (4.11a)–(4.15) leads to the following perturbations,

$$\delta T^0{}_0 = -\delta\mu \,, \tag{4.17}$$

$$\delta T^0{}_j = (\mu + p)(v_i + \omega_i) \,, \tag{4.18}$$

$$\delta T^j{}_0 = -(\mu + p) v^i \,, \tag{4.19}$$

$$\delta T^i{}_j = \delta p \delta^i{}_j + \Pi^i{}_j \,, \tag{4.20}$$

where we have included an anisotropic stress contribution $\Pi^i{}_j$ in the perturbed energy momentum tensor.

### 4.3.3 Einstein Field Equations

The perturbed Einstein field equations are given by

$$\delta G^a{}_b = \delta T^a{}_b \,, \tag{4.21}$$

where $\delta G^a{}_b$ is the perturbed Einstein tensor. From (4.21), one can derive equations of motion for the perturbed variables. In general, it is customary to split the perturbation variables into scalar, vector and tensor parts. At first order in perturbation theory, scalar, vector and tensor modes decouple from each other and thus evolve independently. However, at higher order, one can have non-trivial couplings. For example, first order scalar perturbations can source tensor perturbations at second order in perturbation theory.

The resulting equations are presented below, see for example [269] for details on the derivation.

**Scalar**

$$3\mathcal{H}(\Phi' + \mathcal{H}\Phi) - \nabla^2\Phi = -4\pi G a^2 \delta\mu \,, \tag{4.22}$$

$$\Phi' + \mathcal{H}\Phi = -4\pi G a^2 (\mu + p) v \,, \tag{4.23}$$

$$\Phi'' + 3\mathcal{H}\Phi' + (2\mathcal{H}' + \mathcal{H}^2)\Phi = 4\pi G a^2 \delta p \,. \tag{4.24}$$

When considering adiabatic perturbations, the pressure perturbation is related to the density perturbation through $\delta p = c_s^2$. In this case, one can write a master equation for the Bardeen potential $\Phi$ as,

$$\Phi'' - \nabla^2\Phi + 3\mathcal{H}(1 + c_s^2)\Phi' + [2\mathcal{H}' + \mathcal{H}^2(1 + 3c_s^2)]\Phi = 0 \,. \tag{4.25}$$

**Vector**

$$\omega_i' + 2\mathcal{H}\omega_i = 0 \,. \tag{4.26}$$

**Tensor**

$$h_{ij}'' + 2\mathcal{H}h_{ij}' - \nabla^2 h_{ij} = 8\pi G a^2 p \Pi_{ij} \,. \tag{4.27}$$

## 4.4 Covariant Perturbations

The basic approach to perturbation theory in the covariant formalism is to start with the exact non linear system of the physical spacetime, then 'linearize' about some chosen background [201, 259, 297, 154]. This is in contrast to the metric based approach of §4.3, where one starts with an idealized background, then add perturbations. For almost FLRW spacetimes, the quantities

$$\{\Theta, \mu, p\} \tag{4.28}$$

and their time derivatives are non vanishing in the background, we therefore designate them as zero-th order in perturbation theory. On the other hand, the quantities,

$$\{\mathcal{A}_a, \sigma_{ab}, \omega_a, q_a, \pi_{ab}, E_{ab}, H_{ab}\} \tag{4.29}$$

and their time and spatial derivatives are designated as first order in perturbation theory. Since they vanish in the background space time, they are gauge invariant by the Stewart and Walker lemma 4.2.1.

### Scalar Perturbations

Scalar perturbations in cosmology are linked to growing inhomogeneities [288]. In order to characterize scalar density perturbations, we begin by defining the first order gauge invariant variables,

$$\mathcal{X}_b = a\mathrm{D}_b\mu \ , \tag{4.30a}$$

$$\mathcal{Z}_b = a\mathrm{D}_b\Theta \ , \tag{4.30b}$$

where $a$ is the scale factor. In the case of vanishing vorticity $\omega_a = 0$, the variables (4.30) contain only scalar degrees of freedom. The variables (4.30) are related to the shear tensor $\sigma_{ab}$ and electric part of the Weyl tensor through the linearized relations,

$$a\mathrm{D}^c\sigma_{bc} = \frac{2}{3}\mathcal{Z}_b \ , \tag{4.31a}$$

$$a\mathrm{D}^c E_{bc} = \frac{1}{3}\mathcal{X}_b \ . \tag{4.31b}$$

We note that Equation (4.31b) presents a relativistic analogue of the Newtonian Poisson equation. Now, the system governing the scalar gravitational perturbations is given by the

following propagation equations,

$$\dot{\sigma}_{\langle ab\rangle} + \frac{2}{3}\Theta\sigma_{ab} = \mathrm{D}_{\langle a}\mathcal{A}_{b\rangle} - E_{ab} \ , \tag{4.32a}$$

$$\dot{E}_{\langle ab\rangle} + \Theta E_{ab} = -\frac{1}{2}\mu(1+w)\sigma_{ab} \ , \tag{4.32b}$$

$$\dot{\mathcal{Z}}_{\langle a\rangle} + \frac{2}{3}\Theta\mathcal{Z}_a = -\frac{1}{2}\mu\mathcal{X}_a - \frac{w}{3(1+w)}\left(-\frac{1}{3}\Theta^2 + \mu + \Lambda\right)\mathcal{X}_a - \frac{w}{1+w}\mathrm{D}^2\mathcal{X}_a \ , \tag{4.32c}$$

$$\dot{\mathcal{X}}_{\langle a\rangle} - \Theta w\mathcal{X}_a = -(1+w)\mathcal{Z}_a \ , \tag{4.32d}$$

which is obtained by linearizing the exact equations given in §3.5. In the above we have set the vorticity to zero ($\omega_a = 0$), see also [122]. The system (4.32) is not independent. In particular, the scalar part of the shear $\sigma_{ab}$ and Electric part of the Weyl tensor $E_{ab}$ couple to density perturbations and are related to the clumping of matter via the constraints (4.31).

By differentiating (4.32a) and using (4.32b) and one of the constraints (4.31b) to substitute for $E_{ab}$, one arrives at a forced wave equation for the shear,

$$\ddot{\sigma}_{\langle ab\rangle} - \mathrm{D}^2\sigma_{ab} + \frac{5}{3}\Theta\dot{\sigma}_{\langle ab\rangle} + \left[\frac{1}{9}\Theta^2 + \frac{1}{6}\mu - \frac{3}{2}p + \frac{5}{3}\Lambda\right]\sigma_{ab} = -\frac{w}{a^2(1+w)}\left[\dot{\mathcal{X}}_{ab} + \frac{1}{3}\Theta\mathcal{X}_{ab}\right] \tag{4.33}$$

where $\mathcal{X}_{ab} = -(1+w)a^2\mathrm{D}_{\langle a}\mathcal{A}_{b\rangle}/w = a\mathrm{D}_{\langle a}\mathcal{X}_{b\rangle}$. We need an evolution equation for $\mathcal{X}_{ab}$ in order to close Equation (4.33). One can start from (4.32d) and (4.32c) to write a wave equation for $\mathcal{X}_a$ then taking the comoving spatial gradient of the resulting wave equation. This procedure yields the following:

$$\ddot{\mathcal{X}}_{ab} - w\mathrm{D}^2\mathcal{X}_{ab} - \left(w - \frac{2}{3}\right)\Theta\dot{\mathcal{X}}_{ab} + \frac{1}{2}\mu(3w+1)(w-1)\mathcal{X}_{ab} - 2w\Lambda\mathcal{X}_{ab} = 0 \ . \tag{4.34}$$

In including scalar perturbations, we have explicitly coupled the scalar part of the shear tensor to density perturbations. This shows that density gradients source distortions in the Weyl curvature and vice versa. Hence, knowing the shear allows one to compute density gradients and knowing density gradients one can compute the scalar part of the shear [84].

### Vector Perturbations

At first order in gravitational perturbation theory, the only source of vector modes is the vorticity $\omega_a$. However, this is a decaying mode which is damped by the expansion of the universe without any source terms,

$$\dot{\omega}_{\langle a\rangle} + \frac{2}{3}\Theta\omega_a = 0 \ . \tag{4.35}$$

For this reason, vector modes are not of practical interest at first order. We do note however, that it is possible to source vorticity at second order in perturbation theory [291, 115].

When included, magnetic fields can also be a source of vector modes. The background FLRW spacetime (§3.7) does not contain any magnetic fields. We therefore treat the seed magnetic field as a first order perturbation to the spacetime (§4.7). In principle, the seed field may have its origins in inflation or other mechanisms based on string cosmology, in which electromagnetic vacuum fluctuations are amplified due to a dynamical dilaton or an inflaton field [173]. We assume that at order first order, electric fields are small compared to the magnetic fields, i.e $E^2 \ll B^2$. Thus, in the absence of diffusive losses or amplification, the induction equation (3.68b) takes the frozen-in form,

$$\dot{\tilde{B}}_{\langle a\rangle} + \frac{2}{3}\Theta\tilde{B}_a = 0 \,, \tag{4.36}$$

regardless of the equation of state or plasma properties of the cosmic fluid. It follows then that the magnetic field decays adiabatically as $\tilde{B}_a \propto a^{-2}$, where $a$ is the cosmological scale factor. This adiabatic decay arises from the expansion of the Universe which conformally dilutes the field lines due to flux conservation. The frozen-in condition (4.36) does not discriminate between homogeneous ($\mathrm{D}_a\tilde{B}_b = 0$) and inhomogeneous ($\mathrm{D}_a\tilde{B}_b \neq 0$) magnetic fields. For an inhomogeneous field the spatial gradients of the seed magnetic field $\mathrm{D}_b\tilde{B}_a$ are of the same order as $\tilde{B}_a$ and evolve according to $\mathrm{D}_b B_a \propto a^{-3}$.

### Tensor Perturbations

Tensor perturbations encode information about the propagation of gravitational waves. In the covariant approach, the electric $E_{ab}$ and magnetic $H_{ab}$ part of Weyl tensor are used in the description of gravitational waves. Stripping these tensors of scalar modes results in the constraints,

$$\mathrm{D}^a\sigma_{ab} = 0, \qquad \mathrm{D}^a E_{ab} = 0, \qquad \mathrm{D}^a H_{ab} = 0, \qquad H_{ab} = \mathrm{curl}\ \sigma_{ab} \,. \tag{4.37}$$

At first order in perturbation theory, the equations governing the evolution of the tensor modes are given through,

$$\dot{\sigma}_{\langle ab\rangle} + \frac{2}{3}\Theta\sigma_{ab} = -E_{ab} \,, \tag{4.38}$$

$$\dot{E}_{\langle ab\rangle} + \Theta E_{ab} = \mathrm{curl}\ (\mathrm{curl}\ \sigma_{ab}) - \frac{1}{2}\mu(1+w)\sigma_{ab} \,, \tag{4.39}$$

$$\dot{H}_{\langle ab\rangle} + \Theta H_{ab} = -\mathrm{curl}\ E_{ab} \,. \tag{4.40}$$

One can eliminate the $H_{ab}$ equation through the constraint $H_{ab} = \text{curl}\,\sigma_{ab}$. Differentiating (4.38) in time and using (4.39), one arrives at the wave equation,

$$\ddot{\sigma}_{\langle ab\rangle} - \mathrm{D}^2\sigma_{ab} + \frac{5}{3}\Theta\dot{\sigma}_{\langle ab\rangle} + \left(\frac{1}{9}\Theta^2 + \frac{1}{6}\mu - \frac{3}{2}p + \frac{5}{3}\Lambda\right)\sigma_{ab} = 0\ , \tag{4.41}$$

where we have used the identity

$$\text{curl curl}\ S_{ab} = -\mathrm{D}^2 S_{ab} + \frac{3}{2}\mathrm{D}_{\langle a}\mathrm{D}^c S_{b\rangle c} + \left(\mu + \Lambda - \frac{1}{3}\Theta^2\right) S_{ab}\ . \tag{4.42}$$

The shear tensor $\sigma_{ab}$ was shown to characterize gravitational waves in the Covariant approach [143].

## 4.5 The *Almost* Ehlers-Geren-Sachs Theorem

In §3.8 we stated the EGS theorem, allowing deductions of spatial homogeneity given (*i*) the high isotropy of the CMB at our spacetime position and (*ii*) the Copernican principle, that we are not at a privileged position in the Universe. It has been show that the EGS theorem 3.8.1 is stable, leading to a more realistic basis for spatial homogeneity of the Universe.

**Theorem 4.5.1 (Almost EGS [359])** *If the Einstein-Liouville equations are satisfied in an expanding Universe model, where there is present pressure-free matter with 4-velocity vector field $u^a$ such that freely propagating background radiation is everywhere almost isotropic relative to $u^a$ in some domain $U$, then the spacetime is almost-FLRW in $U$.*

The proof of the almost-EGS theorem can be found in [359, 156].

Interestingly, several 'counterexamples' of Theorem 4.5.1 have been presented in the literature. Most notably [294] presents a class of Bianchi type $VII_0$ dust models that are not almost FLRW, even though they have almost isotropic CMB temperature. However, as stated by the authors, this does not contradict the results of [359] because the proof of the almost EGS theorem requires additional assumptions on the (dimensionless) time and spatial derivatives of the multipoles, which are not valid for the cases presented in [294]. In addition, [121] highlights the role of the acceleration of the fundamental observers in the theorem. The theorem remains valid, with the additional clause that the acceleration vanishes.

## 4.6 Perturbed Kinematic Quantities

Cases may arise where one needs to compute the covariant kinematic variables, given a particular metric. Starting from the perturbed 4-velocity (4.15) along with the metric (4.5), one can compute the perturbed kinematic quantities introduced in §3.2. See [84] for a more rigorous discussion of this prospect in the context of the Bardeen formalism. The kinematic variables in terms of the metric variables are given as follows,

$$^{(0)}\Theta = 3\frac{\mathcal{H}}{a} \,, \tag{4.43}$$

$$^{(1)}\Theta = \frac{1}{a}\Big(2\Phi' - 3\Psi' + \mathrm{D}^i v_i\Big) \,, \tag{4.44}$$

$$^{(0)}\sigma_{ij} = 0 \,, \tag{4.45}$$

$$^{(1)}\sigma_{ij} = \frac{1}{2}ah'_{ij} + a\mathrm{D}_{\langle i}v_{j\rangle} + a\mathrm{D}_{\langle i}\omega_{j\rangle} \,, \tag{4.46}$$

$$^{(0)}\omega_{ij} = 0 \,, \tag{4.47}$$

$$^{(1)}\omega_{ij} = \frac{1}{2}a\Big(\mathrm{D}_{[i}v_{j]} + \mathrm{D}_{[i}\omega_{j]}\Big) \,, \tag{4.48}$$

$$^{(0)}\mathcal{A}_i = 0 \,, \tag{4.49}$$

$$^{(1)}\mathcal{A}_i = \frac{1}{2}\Big(\omega'_i + \omega_i\mathcal{H} + v'_i + v_i\mathcal{H}\Big) + \mathrm{D}_i\Phi \,. \tag{4.50}$$

## 4.7 Two Parameter Non-Linear Perturbations

When dealing with relativistic perturbations, the choice of background is often motivated by the physics at hand. Ideally one would like to select a background that is complex enough the capture the relevant dynamics, yet simple enough to remain analytically tractable. This is particularly the case in cosmological perturbation theory where flat FLRW spacetimes are often the preferred background. However, the situation gets complicated when one is interested in including cosmological electromagnetic fields. As already mentioned in the introductory paragraphs (§2.5.3), a FLRW spacetime cannot readily host magnetic fields, as

the induced anisotropic stresses $\Pi_{ab} = \tilde{B}_{\langle a}\tilde{B}_{b\rangle} \neq 0$ will break the isotropy. This feature motivates the adoption of a two parameter perturbative scheme, where we treat the background magnetic field $\tilde{B}_a$ as a first order perturbation of amplitude $\epsilon_{\tilde{B}}$ to the isotropic spacetime. Such an approach results in the energy density, the isotropic and anisotropic pressure of the field being second order quantities in perturbation theory, see §3.3.2.

We proceed by essentially adopting a two parameter perturbative framework [85, 352, 123, 304, 305]. Fundamentally, this consists of separately parametrizing the gravitational and Maxwell field perturbations in two expansion parameters $\epsilon_g$ and $\epsilon_{\tilde{B}}$, representing the amplitudes of the gravitational and electromagnetic field perturbations, respectively [123, 65, 417]. Using this parametrization, any quantity $Q^{\cdots}{}_{\cdots}$ in the physical spacetime can be expanded in the form,

$$Q^{\cdots}{}_{\cdots} = \epsilon_g^0\epsilon_{\tilde{B}}^0\, \overset{(0,0)}{Q}{}^{\cdots}{}_{\cdots} + \epsilon_g^1\epsilon_{\tilde{B}}^0\, \overset{(1,0)}{Q}{}^{\cdots}{}_{\cdots} + \epsilon_g^0\epsilon_{\tilde{B}}^1\, \overset{(0,1)}{Q}{}^{\cdots}{}_{\cdots} + \epsilon_g^1\epsilon_{\tilde{B}}^1\, \overset{(1,1)}{Q}{}^{\cdots}{}_{\cdots} + \mathcal{O}(\epsilon_g^2\,, \epsilon_{\tilde{B}}^2)\,, \tag{4.51}$$

where the first term on the right represents the background term; the first and second terms represent the first order gravitational and electromagnetic perturbations respectively; the fourth term represents the non-linear coupling we're looking to investigate; the higher order terms represent self-coupling terms of order $\epsilon_g^m$ and $\epsilon_{\tilde{B}}^n$, $m, n \geq 2$. In general, terms describing the coupling will be of the form $\epsilon_g^m\epsilon_{\tilde{B}}^n$, where, in this work, we restrict the perturbative order to $\mathcal{O}(\epsilon_g^1\epsilon_B^1)$ and therefore neglect terms of order $\mathcal{O}(\epsilon_g^2\epsilon_B^1)$, $\mathcal{O}(\epsilon_g^1\epsilon_B^2)$ and higher, resulting from the self-coupling of the fields; this includes gravitational couplings with the magnetic anisotropy $\Pi_{ab} = -\tilde{B}_{\langle a}\tilde{B}_{b\rangle}$, which leads to $\mathcal{O}(\epsilon_g^1\epsilon_B^2)$ terms. We will generally refer to quantities of order $\mathcal{O}(\epsilon_g^1\epsilon_B^1)$ simply as non-linear and reserve the designation 'second order' for terms that are of order $\epsilon_g^2$ and $\epsilon_{\tilde{B}}^2$. As in [123, 65, 417], one can visualize this framework as a hierarchy of spacetimes to label the different perturbative orders.

Since the interaction terms are of order $\mathcal{O}(\epsilon_g^1\epsilon_B^1)$ we have that the induced magnetic field $B_a$ will be of the same order. In addition, we assume that the electric field $E_a$ will be of the same order as the induced magnetic field. Clearly $B_a$ does not satisfy the criteria for gauge invariance at $\mathcal{O}(\epsilon_g^1\epsilon_{\tilde{B}}^1)$ since it is neither vanishing nor a constant scalar at $\mathcal{O}(\epsilon_g^0\epsilon_{\tilde{B}}^1)$. To this end, we make use of the same auxiliary variable $\beta_a$ identified in [123, 65, 417]. The incentive behind this choice comes from the induction equation (4.36)

$$\beta_a \equiv \dot{\tilde{B}}_a + \frac{2}{3}\Theta\tilde{B}_a = 0\,. \tag{4.52}$$

Since $\beta_a$ vanishes at lower perturbative orders $\mathcal{O}(\epsilon_g^0\epsilon_B^0)$, $\mathcal{O}(\epsilon_g^1\epsilon_B^0)$ and $\mathcal{O}(\epsilon_g^0\epsilon_B^1)$, it follows that it is a gauge invariant quantity by the Stewart & Walker lemma [358, 85, 352]. We do not

however integrate $\beta_a$ to recover the induced gauge-dependent magnetic field $B_a$ as was done in for example [65]. Instead, we treat the variable $\beta_a$ as the fundamental variable whose deviation from zero quantifies deviation from the adiabatic decay of the magnetic field. This deviation thus quantifies amplification in an unambiguous manner. Having gathered the necessary tools in the this and the previous chapters, we are now in a position to study the amplification of cosmological magnetic fields, which is the subject of the next Chapter.

# Chapter 5

# Cosmic Magnetic Fields

## 5.1 Introduction

A generic feature of inflationary cosmology is the generation of primordial gravitational waves and density perturbations (see §2.3.4). The role and evolution of these perturbations is well understood within the framework of linear perturbation theory about a FLRW background. In general, gravitational waves can be viewed as relevant both in cosmology and astrophysics. From a cosmological viewpoint, primordial gravitational wave data may provide a new window to early universe physics, such as placing constraints on the inflationary potential [215, 355, 47, 73, 267]. From an astrophysical perspective, measurements of gravitational waveforms from binary black hole collisions can be used to study signatures of modified gravity and other relevant relativistic effects. Such waveforms can now be accurately modeled within the realm of non linear general relativity, employing post Newtonian (PN) methods and the framework of numerical relativity [50, 14]. On the other hand, density perturbations are linked to growing modes that bolster cosmological structure formation at late times.

It is a well accepted understanding that interactions of gravitational degrees of freedom with a pre-existing magnetic field offers the potential to generate electromagnetic waves [373, 335, 271, 77, 34, 273, 381, 65, 165]. Traditionally, this mechanism has often been studied in the context of amplification of the seed magnetic field or as a means of indirect detection of gravitational waves through electromagnetic waves accompanying the interaction. Most of these studies however have been restricted to focusing on the interaction of magnetic fields with tensor perturbations, characterizing gravitational radiation. In this work we revisit and extend the work presented in [273, 65, 417], to include scalar modes in the interaction and thus opening an avenue for amplification of magnetic fields through density perturbations. Interestingly, the presence of magnetic fields can induce and amplify density fluctuations in a

baryonic plasma through the action of the Lorentz force on the constituent ions and electrons. Nevertheless, we restrict our attention to the case where the magnetic field is the one that undergoes amplification following interactions with scalar perturbations. The gravitational perturbations we employ in this work are cosmological in nature and have been described in Chapter 4 in the case of a FLRW background.

When using perturbation theory about a FLRW background to study the interplay between gravitation and electromagnetism, one is immediately faced with the question of how to embed the seed magnetic field into the background spacetime. The isotropy of the FLRW spacetime does not readily allow for any direction preference that may be introduced by a vector field. In principle, one could simply consider an anisotropic background like Bianchi or Kantowski-Sachs models [225]. Within these models one can naturally embed magnetic fields without disrupting the concomitant symmetries of the background spacetime. In fact, this avenue has been explored by several authors. For example [383] considers cosmological perturbations in a magnetized Bianchi class I background. However, due to motivations of spatial isotropy from observations of CMB and large-scale structure, one would ideally want to consider an isotropic background.

There are several ways in which one can deal with magnetic fields in an isotropic background. For example, one can treat the seed magnetic field as a zeroth order quantity, subject to the assumption that the energy density of the field be small compared to the energy density of matter $B^2 \ll \mu$ and that the anisotropic stress is negligible $\Pi_{ab} = B_{\langle a}B_{b\rangle} \approx 0$. With these approximations, the energy density of the magnetic field cannot alter the gravitational dynamics of the background spacetime; this approach is often referred to as the weak-field approximation. Alternatively, one can treat the seed field as a statistically homogeneous and isotropic random field. In this case, the properties of the magnetic field are studied in terms of their Fourier components,

$$\mathbf{B}(\mathbf{k}, t) = \int d^3x \mathbf{B}(\mathbf{x}, t) e^{i\mathbf{k}\cdot\mathbf{x}} \, . \tag{5.1}$$

The isotropy and homogeneity of the FLRW spacetime implies that the expectation values cannot depend on any vector or tensor, except the vector $\mathbf{k}$ and tensors $\delta_{ij}$, $\epsilon_{ijk}$ and their linear combinations. As a result the seed field does not introduce any directional dependence in the background spacetime. One can then easily employ statistical methods to quantify the dynamics of the field. A third possibility is to leave the background spacetime untouched but instead treat the seed field as a first order perturbation, using a two parameter approximation scheme to characterize the perturbations in the electromagnetic and gravitational degrees of

freedom; this is the approach we adopt in this work.

One can go a long way in comparing the different perturbation schemes. For example, in the weak-field approximation, the induced magnetic field will be at first order, a well understood regime in perturbation theory. While in the two parameter case, the induced field will be at second order[1], a regime that is not so well developed. Nevertheless, for the purposes of our work, the two approaches are mathematically equivalent. The apparent differences between them is as a result of relabeling of spacetimes, i.e. 'First order' in the weak-field approximation corresponds to 'second order' in the two parameter case. Indeed, Maxwell's equations and thus the Einstein-Maxwell system takes the same mathematical form in both of these approaches. They both use the machinery of relativistic perturbation theory and are thus equally prone to gauge issues, see [212, 383] for example.

This Chapter is structured as follows: After a presentation of the interaction equations in §5.3, we present the derivation of the equations describing the induction of EM fields in §5.4.1 and §4.4 for a general current and a note on how to evaluate the induced electrical current in §5.4.3. We present the power spectra of the induced magnetic field variable in §5.6. The details of our two-parameter perturbative framework have already been presented in §4.1.

## 5.2 Gauge Invariant Perturbation Variables

The Einstein-Maxwell equations (3.68) contain terms that couple the electromagnetic fields to the gravitational fields. The system can be written at perturbative order $\mathcal{O}(\epsilon_g^1\epsilon_{\tilde{B}}^1)$ by discarding higher order terms. This approximation scheme results in the two propagation equations,

$$\dot{B}_{\langle a\rangle} + \frac{2}{3}\Theta B_a = \sigma_{ab}\tilde{B}^b - \text{curl } E_a \,, \tag{5.2a}$$

$$\dot{E}_{\langle a\rangle} + \frac{2}{3}\Theta E_a = \text{curl } B_a + \epsilon_{abc}\mathcal{A}^b\tilde{B}^c - \mathcal{J}_a \,, \tag{5.2b}$$

subject to the constraints, $\mathrm{D}_a E^a = 0 = \mathrm{D}_a B^a$. Following [122] we make the following comments:

1. The magnetic field $\tilde{B}_a$ appearing in the equations (5.2a) and (5.2b) multiplied by the gravitational variables should not be the same as the $B_a$ appearing alone. The variable

[1]For the purposes of this argument, we refer to perturbations of order $\epsilon_g\epsilon_{\tilde{B}}$ as second order, with evident misuse of terminology. In the rest of the work, we will refer to quantities of this order simply as non-linear and reserve the designation 'second order' to quantities of order $\epsilon_g^2$ and $\epsilon_{\tilde{B}}^2$

$B^a$ is a mixture of linear and non-linear quantities (the seed magnetic field and the induced field) while the terms involving $\tilde{B}^a$ are a product of first order quantities. One has to keep this in mind when integrating the equations.

2. The system is not gauge-invariant as already mentioned in § 4.7. This can be attributed to the mixture of linear and non-linear terms in the system. In the covariant approach to perturbation theory, the solution of perturbed differential operators is never sought, one can get around this by making sure that the differential operators involved operate on quantities of the corresponding perturbative order.

In an attempt to cast the system (5.2) in a consistent and gauge invariant manner, we introduce the following non-linear variables: The fundamental variable $\beta_a$ measuring deviation from adiabatic decay, $I_a$ describing the interaction with shear distortions and $\xi_a$ describing interaction with density perturbations. These are defined as follows,

$$\beta_a = \dot{B}_{\langle a\rangle} + \frac{2}{3}\Theta B_a \,, \tag{5.3a}$$

$$I_a = \sigma_{ab}\tilde{B}^b \,, \tag{5.3b}$$

$$\xi_a = \epsilon_{abc}\mathcal{A}^b\tilde{B}^c \,. \tag{5.3c}$$

Rewriting the Einstein-Maxwell system (5.2) in terms of the new variables (5.3) results in the following system,

$$\beta_a = I_a - \mathscr{E}_a \,, \tag{5.4}$$

$$\dot{E}_{\langle a\rangle} + \frac{2}{3}\Theta E_a = \mathscr{B}_a + \xi_a - \mathcal{J}_a \,, \tag{5.5}$$

where we have written curl $E_a = \mathscr{E}_a$ and curl $B_a = \mathscr{B}_a$ for brevity.

## 5.3 Evolution of Interaction Variables

The Maxwell fields couple to Weyl curvature through the shear term and density perturbations through the acceleration terms and the non-linear identity (5.9). In the case of pure tensor modes in the shear tensor, the interaction variable $I_a = \sigma^T_{ab}\tilde{B}^b$ was shown to satisfy a closed wave equation, for both a homogeneous [65] and an inhomogeneous [417] seed field $\tilde{B}_a$. Here, we include contributions from scalar perturbations in the shear, which give rise to source terms due to coupling with density perturbations. In this case $I_a$ satisfies a forced

wave equation,

$$\ddot{I}_{\langle a\rangle} - \mathrm{D}^2 I_a + 3\Theta\dot{I}_{\langle a\rangle} + \left[\frac{13}{9}\Theta^2 - \frac{1}{6}\mu - \frac{5}{2}\mu w + \frac{7}{3}\Lambda\right] I_a = \mathcal{C}_a^I \,, \tag{5.6}$$

where the forcing term $\mathcal{C}_a^I$ is given by,

$$\mathcal{C}_a^I = -\frac{w}{a^2(1+w)}\left(\dot{S}_{\langle a\rangle} + \Theta S_a\right). \tag{5.7}$$

where $w$ is the equation of state parameter and $a$ is the cosmic scale factor. To close the above system, we give the companion wave equation for $S_a = a\tilde{B}^b \mathrm{D}_{\langle a}\mathcal{X}_{b\rangle}$ as,

$$\ddot{S}_a - w\mathrm{D}^2 S_a + (2-w)\Theta\dot{S}_a + \left[\frac{2}{3}(1-w)(\Lambda+\Theta^2) + \frac{1}{6}\mu(1+3w)(3w-5)\right] S_a = 0. \tag{5.8}$$

We note, for later convenience (§ 4.4) that the forcing term $\mathcal{C}_a^I$ vanishes in a matter dominated universe ($w = 0$) i.e $I_a$ decouples from $S_a$ when $w = 0$.

## 5.4 Induction of Electromagnetic Fields

In the following, we introduce non-linear gravitationally induced 'effective current' terms $\mathcal{C}_a^E$, $\mathcal{C}_a^{\mathscr{E}}$ and $\mathcal{C}_a^{\beta}$ which are made up of the coupling between density and gravitational wave perturbations; these will act as driving forces of the induced Maxwell fields.

### 5.4.1 The Electric Field

In this section, we show how the coupling of gravitational perturbations with the seed magnetic field can induce Electric fields. To this end, we give wave equations for the induced Electric field $E_a$ and its rotation $\mathscr{E}_a$. In deriving the wave equation for $E_a$, we differentiate (5.5) and equate the result to the non-linear identity,

$$\dot{(\mathrm{curl}\, B_a)} = \mathrm{curl}\,\beta_a - \Theta\,\mathrm{curl}\, B_a + H_{ab}\tilde{B}^b + \frac{1}{3a(1+w)}\epsilon_{abc}\tilde{B}^b\left(\Theta w\mathcal{X}^c - 2\dot{\mathcal{X}}^c\right) \,, \tag{5.9}$$

obtained from the commutation relations (Appendix A.3) and we have used Equation (4.32d) to rewrite the acceleration terms. The resulting wave equation is found to be,

$$\ddot{E}_{\langle a\rangle} - \mathrm{D}^2 E_a + \frac{5}{3}\Theta\dot{E}_a + \left[\frac{2}{9}\Theta^2 + \frac{1}{3}\mu(1-3w) + \frac{4}{3}\Lambda\right] E_a = \mathcal{C}_a^E \,, \tag{5.10}$$

where $\mathcal{C}_a^E$ is a gravitationally induced source term given by,

$$\begin{aligned}\mathcal{C}_a^E &= \text{curl}\, I_a + H_{ab}\tilde{B}^b \\ &+ \frac{1}{a(1+w)}\epsilon_{abc}\left[\left(w-\frac{2}{3}\right)(\tilde{B}^b\mathcal{X}^c)^{\cdot} + \Theta\left(w-\frac{4}{9}\right)\tilde{B}^b\mathcal{X}^c\right] - \Theta\mathcal{J}_a - \dot{\mathcal{J}}_a\,,\end{aligned} \tag{5.11}$$

and $\mathcal{J}_a$ is the 3-current. The terms involving the Levi-Civita tensor $\epsilon_{abc}$ in $\mathcal{C}_a^E$ vanish when the magnetic field $\tilde{B}^a$ is parallel to the fractional density gradient $\mathcal{X}^a$. Taking the curl of (5.10) results in the equation governing the rotation of $E_a$,

$$\ddot{\mathscr{E}}_a - \mathrm{D}^2\mathscr{E}_a + \frac{7}{3}\Theta\dot{\mathscr{E}}_a + \left[\frac{7}{9}\Theta^2 + \frac{1}{6}\mu(1-9w) + \frac{5}{3}\Lambda\right]\mathscr{E}_a \;=\; \mathcal{C}_a^{\mathscr{E}}\,, \tag{5.12}$$

where the source term $\mathcal{C}_a^{\mathscr{E}} = \text{curl}\,\mathcal{C}_a^E$ is given by,

$$\begin{aligned}\mathcal{C}_a^{\mathscr{E}} &= -(\text{curl}\,\mathcal{J}_a)^{\cdot} - \frac{4}{3}\Theta\text{curl}\,\mathcal{J}_a + 2\,\mathrm{D}^b\mathrm{D}_{[a}I_{b]} + \epsilon_{acd}\tilde{B}_b\mathrm{D}^cH^{db} \\ &+ \frac{2}{a^2(1+w)}\left[\left(w-\frac{2}{3}\right)(a\tilde{B}_{[a}\mathrm{D}^b\mathcal{X}_{b]})^{\cdot} + \Theta\left(w-\frac{4}{9}\right)a\tilde{B}_{[a}\mathrm{D}^b\mathcal{X}_{b]}\right]\,.\end{aligned} \tag{5.13}$$

### 5.4.2 The Magnetic Field

As already mentioned, the induced magnetic field will be characterized via the variable $\beta_a = \dot{B}_a + \frac{2}{3}\Theta B_a$. On using (5.4), (5.6) and (5.12), one can write a second-order equation governing the evolution of the fundamental variable $\beta_a$. This can be written in either of two forms: in terms of $I_a$ or $\mathscr{E}_a$, corresponding to using (5.4) as a constraint to either of (5.12) or (5.6) respectively. Recall that both $I_a$ and $\mathscr{E}_a$ satisfy wave equations of the form $\mathcal{L}[I_a] = \mathcal{C}_a^I$ and $\mathcal{L}[\mathscr{E}_a] = \mathcal{C}_a^{\mathscr{E}}$, where the $\mathcal{C}_a^i$s are source terms.

Using covariant harmonics [84], one can already notice from (5.6) and (5.12) that the eigenfunctions used to harmonically decompose $I_a$ and $\mathscr{E}_a$ are not the same for a general perturbation [2]. Consider the induction equation (5.4), and write it as $\beta_a = \sum_k(\mathcal{P}_aI_{(k)} - \mathcal{Q}_a\mathscr{E}_{(k)})$, where $\mathcal{P}_a$ and $\mathcal{Q}_a$ are distinct eigenfunctions of the Laplace-Beltrami operator, i.e $\mathcal{P}_a \neq \mathcal{Q}_a$. For the separation of variables technique to work for $\beta_a$, one must eliminate either $I_a = \mathcal{P}_aI_{(k)}$, along with its source terms $\mathcal{C}_a^I$ or $\mathscr{E}_a = \mathcal{Q}_a\mathscr{E}_{(k)}$ along with its source terms $\mathcal{C}_a^{\mathscr{E}}$. In this way, $\beta_a$ can then be expanded in terms of one set of complete eigenfunctions. This presents a problem: since both $I_a$ and $\mathscr{E}_a$ are coupled to source terms $\mathcal{C}_a^I$ and $\mathcal{C}_a^{\mathscr{E}}$ respectively at second-

[2] In particular, for scalar perturbations, we expand $I_a$ as $I_a = \tilde{B}_{(n)}\sigma_{(k)}\tilde{\mathcal{H}}^a_{(n)}\mathrm{D}_{\langle a}\mathrm{D}_{b\rangle}\mathcal{Q}^{(k)}$ and $\mathscr{E}_a$ as $\mathscr{E}_a = \mathscr{E}_{(\ell)}\tilde{\mathcal{H}}^{(n)}_{[a}\mathrm{D}^b\mathrm{D}_{b]}\mathcal{Q}^{(k)}$; these are evidently not the same eigenfunctions. Implicitly, $\mathcal{C}_a^I$ will be expanded in the same harmonics as $I_a$, and similarly for $\mathscr{E}_a$ and $\mathcal{C}_a^{\mathscr{E}}$.

order, both $\mathcal{C}_a^I$ and $\mathcal{C}_a^{\mathscr{E}}$ will still couple to the $\beta_a$ equation at this order, thereby introducing the differing set of eigenfunctions $\mathcal{P}_a$ and $\mathcal{Q}_a$. A similar problem arose in [155], due to the inclusion of a vorticity term.

It is possible to do away with $\mathcal{C}_a^I$ in equation (5.6) by requiring that $w = 0$ and this alleviates the problem [3]. We shall then henceforth restrict to the pressureless dust ($w = 0$) case and write the $\beta_a$ wave equation in terms of $\mathscr{E}_a$. This results in,

$$\ddot{\beta}_{\langle a\rangle} - \mathrm{D}^2\beta_a + 3\Theta\dot{\beta}_{\langle a\rangle} + \left[\frac{13}{9}\Theta^2 - \frac{1}{6}\mu + \frac{7}{3}\Lambda\right]\beta_a \;=\; \mathcal{C}_a^{\beta}\,, \tag{5.14}$$

where,

$$\begin{aligned}\mathcal{C}_a^{\beta} = &-\frac{2}{3}\Theta\dot{\mathscr{E}}_a + \left[-\frac{2}{3}\Theta^2 + \frac{1}{3}\mu - \frac{2}{3}\Lambda\right]\mathscr{E}_a + (\mathrm{curl}\,\mathcal{J}_a)^{\cdot} + \frac{4}{3}\Theta\,\mathrm{curl}\,\mathcal{J}_a - 2\,\mathrm{D}^b\mathrm{D}_{[a}I_{b]}\\ &- \epsilon_{acd}\tilde{B}_b\mathrm{D}^c H^{db} - \frac{2}{a^2}\left[-\frac{2}{3}(a\tilde{B}_{[a}\mathrm{D}^b\mathcal{X}_{b]})^{\cdot} - \frac{4}{9}\Theta(a\tilde{B}_{[a}\mathrm{D}^b\mathcal{X}_{b]})\right]\,.\end{aligned} \tag{5.15}$$

Note that while we keep $S_a = a\tilde{B}^b\mathrm{D}_{\langle a}\mathcal{X}_{b\rangle}$ distinct from $a\tilde{B}_{[a}\mathrm{D}^b\mathcal{X}_{b]}$ in real space, their evolution equations can be made equivalent in harmonic space by a suitable choice of eigenfunctions[4]. We shall thus write $S_{(\ell)}$ in place of $\tilde{B}_{(n)}\mathcal{X}_{(k)}$ to avoid introducing another letter to denote the latter. This should not lead to any ambiguities.

### 5.4.3 The Electric Current

#### Limiting cases: poor and perfect conductivity

To close the above system, one needs to take care of the current term $\mathcal{J}_a$ appearing in (5.11), (5.13) and (5.15). Naturally, this term depends on the electrical properties of the medium. It is given in terms of the Electric field $E_a$ via Ohm's law,

$$\mathcal{J}_a = \varsigma E_a, \tag{5.16}$$

[3] This is not to say that $w = 0$ is any more special than $w = 1/3$, we simply invoke it here to decouple (5.6) from the source terms; indeed, any other method to achieve this would suffice. As a matter of fact, when considering only tensor perturbations, (5.6) does not couple to any source terms, even for a general $w$. Moreover, when including vector perturbations, Equation (5.6) does couple to a source term $\frac{3}{2}\tilde{B}^b\mathrm{D}_{\langle a}\mathrm{D}^c\sigma_{b\rangle c}$, even when $w = 0$.

[4] In particular, expanding $a\tilde{B}^b\mathrm{D}_{\langle a}\mathcal{X}_{b\rangle}$ in terms of $a^2\tilde{\mathcal{H}}^b\mathrm{D}_{\langle a}\mathrm{D}_{b\rangle}\mathcal{Q}$ and $a\tilde{B}_{[a}\mathrm{D}^b\mathcal{X}_{b]}$ in terms of $a^2\tilde{\mathcal{H}}_{[a}\mathrm{D}^b\mathrm{D}_{b]}\mathcal{Q}$ will yield the same harmonic components $S_{(\ell)} \equiv \tilde{B}_{(n)}\mathcal{X}_{(k)}$; $a^2\tilde{\mathcal{H}}^b\mathrm{D}_{\langle a}\mathrm{D}_{b\rangle}\mathcal{Q}$ and $a^2\tilde{\mathcal{H}}_{[a}\mathrm{D}^b\mathrm{D}_{b]}\mathcal{Q}$ are eigenfunctions of the Laplace-Beltrami operator.

where $\varsigma$ is the electrical conductivity of the medium. In this section, we consider only the limiting cases of very high ($\varsigma \to \infty$) and very poor conductivity ($\varsigma \to 0$). Under the assumption of poor conductivity, the currents vanish $\mathcal{J}_a = 0$, despite the presence of a non-zero electric field. In this case, one solves equations (5.10), (5.12) and (5.14), with the current terms set to zero. At the opposite end, the case of perfect conductivity, the electric fields vanish and the currents keep the magnetic field frozen in with the fluid. In this case, the current term satisfies the following evolution equation,

$$\begin{aligned}(\mathrm{curl}\ \mathcal{J}_a)^{\cdot} + \frac{4}{3}\Theta \mathrm{curl}\ \mathcal{J}_a = 2\,\mathrm{D}^b\mathrm{D}_{[a}I_{b]} + \epsilon_{acd}\tilde{B}_b\mathrm{D}^c H^{db} \\ + \frac{2}{a^2}\left[-\frac{2}{3}(a\tilde{B}_{[a}\mathrm{D}^b\mathcal{X}_{b]})^{\cdot} - \frac{4}{9}\Theta(a\tilde{B}_{[a}\mathrm{D}^b\mathcal{X}_{b]})\right],\end{aligned} \tag{5.17}$$

and (5.10) and (5.12) are no longer relevant. One can verify that using this relation reduces equation (5.14) to $\beta_a = I_a$, as can be confirmed also from the induction equation (5.4).

One can also invoke the magnetohydrodynamic MHD approximation, which is valid for cold plasmas (pressureless dust can be well approximated by a cold plasma treatment) [228] . Cold plasmas have components with non-relativistic velocities and are thus mathematically easier to deal with [417, 243, 272]. We consider a two component electron-ion plasma and assume that the motion properties of the plasma on macroscopic scales are captured by the center of mass 3-velocity $v^a$ of the system i.e the difference in mean velocities of the individual species is small compared with the overall fluid velocity. We also assume charge neutrality of the cosmic plasma, i.e., the number densities of the electrons and ions $n_e$ and $n_i$ are roughly equal, $n_e \approx n_i$. This assumption guarantees the vanishing of the total charge $\rho_c = -e(n_e - n_i) \approx 0$ and the background 3-current $\mathcal{J}_a \approx 0$. In this case, the generalized Ohm's law is given by

$$\mathcal{J}_{\langle a\rangle} = \varsigma(E_a + \epsilon_{abc}v^b\tilde{B}^c)\,, \qquad v^a = \frac{\mu_e v_e^a + \mu_i v_i^a}{\mu_e + \mu_i}\,, \tag{5.18}$$

where the subscripts $e$ and $i$ denote quantities for electrons and ions respectively. The center of mass 3-velocity $v_a$ of the electron-ion plasma can be shown to satisfy the linearized Euler equation,

$$\dot{v}_{\langle a\rangle} + \frac{1}{3}\Theta v_a = 0\,. \tag{5.19}$$

In the ideal-MHD environment, the conductivity of the medium is very high ($\varsigma \to \infty$), then $E_a + \epsilon_{abc}v^b\tilde{B}^c \to 0$ in order to keep the current $\mathcal{J}_a$ finite. This readily gives the Electric field $E_a$ and its rotation $\mathscr{E}_a$ as, $E_a = -\epsilon_{abc}v^b\tilde{B}^c$ and $\mathscr{E}_a = 2\tilde{B}_{[a}\mathrm{D}^b v_{b]}$. Using (4.36) and (5.19),

one can show that,

$$\dot{E}_{\langle a\rangle} + \Theta E_a = 0, \qquad \text{and} \qquad \dot{\mathscr{E}}_a + \frac{4}{3}\Theta\,\mathscr{E}_a = 0\,. \tag{5.20}$$

With these, the 3-current $\mathcal{J}_a$ satisfies the following evolution equation,

$$\begin{aligned}(\mathrm{curl}\,\mathcal{J}_a)^{\cdot} + \frac{4}{3}\Theta\mathrm{curl}\,\mathcal{J}_a = 2\,\mathrm{D}^b\mathrm{D}_{[a}I_{b]} + \epsilon_{acd}\tilde{B}_b\mathrm{D}^c H^{db} + \frac{2}{a^2}\Big[-\frac{2}{3}(a\tilde{B}_{[a}\mathrm{D}^b\mathcal{X}_{b]})^{\cdot} \\ -\frac{4}{9}\Theta(a\tilde{B}_{[a}\mathrm{D}^b\mathcal{X}_{b]})\Big] + \mathrm{D}^2\mathscr{E}_a - \left(-\frac{1}{9}\Theta^2 + \frac{5}{6}\mu + \frac{1}{3}\Lambda\right)\mathscr{E}_a\,.\end{aligned} \tag{5.21}$$

The wave equation for the fundamental variable $\beta_a$ within this approximation is obtained by substituting (5.21) into (5.14), resulting in

$$\ddot{\beta}_{\langle a\rangle} - \mathrm{D}^2\beta_a + 3\Theta\dot{\beta}_{\langle a\rangle} + \left[\frac{13}{9}\Theta^2 - \frac{1}{6}\mu + \frac{7}{3}\Lambda\right]\beta_a \;=\; \mathrm{D}^2\mathscr{E}_a + \left[\frac{1}{3}\Theta^2 - \frac{1}{2}\mu - \Lambda\right]\mathscr{E}_a\,. \tag{5.22}$$

The application of the ideal MHD approximation in cosmology has often been criticized as rather being of practical appeal rather than of physical one [367]. Ideally, the curl of $E_a$ should be the outcome of a rigorous treatment of the physics of the particle interactions in terms of a kinetic theory description, see for example [219, 363].

**Intermediate case: Finite conductivity**

The case of poor conductivity may not be much relevant in the post recombination epoch as the universe then acquires very high conductivity. The perfect conductivity case, while relevant, may be thought of as an idealized notion. We thus turn to the finite conductivity case. The conductivity of the post decoupling era can be modeled by,

$$\varsigma = \frac{n_e^2 e^2}{m_e n_\gamma \sigma_T} \approx 10^{11}\,\mathrm{s}^{-1} \tag{5.23}$$

where, $n_e$ is the density of free electrons, $e$ is the electric charge of an electron, $m_e$ is the mass of an electron, $n_\gamma$ is the density of photons and $\sigma_T$ is the collision crossection. For a perfect fluid, the ratio $n_\gamma/n_e$ is constant, see [44] for example.

Assuming that Ohm's law (5.16) holds, we may write the current terms in Equation (5.15) as,

$$(\mathrm{curl}\,\mathcal{J}_a)^{\cdot} + \frac{4}{3}\Theta\mathrm{curl}\,\mathcal{J}_a = \varsigma\dot{\mathscr{E}}_a + \frac{4}{3}\Theta\,\varsigma\mathscr{E}_a \tag{5.24}$$

where we have assumed that spatial gradients of the conductivity may be neglected ($\mathrm{D}_a\varsigma \approx 0$) and that the conductivity is constant in time ($\dot{\varsigma} \approx 0$). Substituting (5.24) in the wave equation (5.14) for $\beta_a$ results in,

$$\ddot{\beta}_{\langle a\rangle} - \mathrm{D}^2\beta_a + 3\Theta\dot{\beta}_{\langle a\rangle} + \left[\frac{13}{9}\Theta^2 - \frac{1}{6}\mu + \frac{7}{3}\Lambda\right]\beta_a \;=\; \mathcal{C}_a^{\beta}\,, \tag{5.25}$$

where the source term $\mathcal{C}_a^{\beta}$ is now given by,

$$\begin{aligned}\mathcal{C}_a^{\beta} \;=\;& \left(\frac{\varsigma}{\Theta} - \frac{2}{3}\right)\Theta\dot{\mathscr{E}}_a + \left[\left(2\frac{\varsigma}{\Theta} - 1\right)\frac{2}{3}\Theta^2 + \frac{1}{3}\mu - \frac{2}{3}\Lambda\right]\mathscr{E}_a - 2\,\mathrm{D}^b\mathrm{D}_{[a}I_{b]} - \epsilon_{acd}\tilde{B}_b\mathrm{D}^c H^{db} \\ -\;& \frac{2}{a^2}\left[-\frac{2}{3}(a\tilde{B}_{[a}\mathrm{D}^b\mathcal{X}_{b]})^{\cdot} - \frac{4}{9}\Theta(a\tilde{B}_{[a}\mathrm{D}^b\mathcal{X}_{b]})\right]\,.\end{aligned} \tag{5.26}$$

Note that the electric currents $\mathcal{J}_a$, electric fields $E_a$ and the conductivity $\varsigma$ are all simultaneously finite. The simplifications that arise due to the characterization of the limiting cases ($\mathcal{J}_a = 0$ for poor conducting mediums and $E_a = 0$ for perfect conducting mediums) are no longer applicable in the case of finite conductivity. One then needs a proper model for the electric currents to ensure that the initial conditions for $\mathcal{J}_a$ and $E_a$ are not chosen independently. There are several ways in which one can model electric currents, all resulting in terms of perturbative order $\epsilon_g^2$, see [266] for example. While these terms can be seamlessly accommodated in our framework, they have the undesirable effect of seeding magnetic fields. This will lead us away from the isolated effects of the amplification of an already existing field. Inclusion of such terms will therefore lead us to overestimate the effect of the amplification. With this in mind, we restrict to the limiting cases of presented above.

## 5.5 The Induced Fields

We now treat separately the induction of electromagnetic fields due to interaction with *scalar* and *tensor* perturbations. To this end, we expand the perturbation variables in terms of a helicity basis (Appendix A.2). In addition, we use a unified time variable whose defining equation is $\dot{\tau} = \frac{3}{2}H_i$ instead of proper time, to re-write the relevant equations [5]. We have to substitute for $\mu$, $\Theta$ and $a$, appearing in the perturbed equations, from the zeroth order equations. We restrict our treatment to zero cosmological constant $\Lambda = 0$ and flat spatial sections $K = 0$. Under these assumptions, Friedmann equation reduces to $\mu = \Theta^2/3$, where $\Theta$ is given by $\Theta = 3H_i/\tau$ and the scale factor $a$ evolves as $a = a_i\tau^{2/3}$.

[5] The subscript $i$ marks some initial time $\tau = 1$, see [65] for details.

### 5.5.1 EM Induction due to Scalar Perturbations

In this case, the coupling of a seed field with gravitational perturbations is described by the variable $I_a$ and $S_a$; these variables become sources of electromagnetic fields.

- ***Interaction terms***

  Equations (5.6) and (5.8) for the interaction variables $I_a$ and $S_a$, respectively become,

$$\frac{9}{4}I''_{(\ell)} + \frac{27}{2\tau}I'_{(\ell)} + \frac{25}{2\tau^2}I_{(\ell)} = 0, \tag{5.27a}$$

$$\frac{9}{4}S''_{(\ell)} + \frac{9}{\tau}S'_{(\ell)} + \frac{7}{2\tau^2}S_{(\ell)} = 0\ , \tag{5.27b}$$

  Note that since $w = 0$, the entire system has decoupled from $a\tilde{B}^b \mathrm{D}_{\langle a}\mathcal{X}_{b\rangle}$, however we still need an equation for $S_{(\ell)}$ because of the coupling with $a\tilde{B}_{[a}\mathrm{D}^b\mathcal{X}_{b]}$ in Equations (5.13) and (5.15). These interaction variables have the general solutions,

$$I_{(\ell)}(\tau) = C_1\tau^{-10/3} + C_2\tau^{-5/3}\ , \tag{5.28a}$$

$$S_{(\ell)}(\tau) = \frac{1}{5}C_3\tau^{-7/3} + \frac{1}{5}C_4\tau^{-2/3}\ , \tag{5.28b}$$

  where the $C_i$'s are integration constants.

- ***Electromagnetic fields***

  Equation (5.10) for the Electric field $E_a$ becomes,

$$\frac{9}{4}E''_{(\ell)} + \frac{15}{2\tau}E'_{(\ell)} + \left[\left(\frac{\ell}{a_iH_i}\right)^2\tau^{-4/3} + \frac{3}{\tau^2}\right]E_{(\ell)} = \pm\frac{(k+n)}{3a_iH_i^2}I_{(\ell)}\tau^{-2/3} \mp \frac{1}{H_i}S'_{(\ell)} \mp \frac{4}{3H_i\tau}S_{(\ell)}\ . \tag{5.29}$$

  In general, it is much easier to solve for $\beta_{(\ell)}$ from the induction equation

$$\beta_{(\ell)} = I_{(\ell)} \mp \frac{\ell}{a_i\tau^{2/3}}E_{(\ell)}\ , \tag{5.30}$$

  once $I_{(\ell)}$ and $E_{(\ell)}$ are known, rather than from the wave equation (5.14).

### 5.5.2 EM Induction due to Tensor Perturbations

In this case, the transverse and trace-free parts of the shear tensor $\sigma_{ab}$ characterize gravitational waves. The interaction with a seed field is then purely described by the variable

$I_a$ without any contribution from either density or velocity perturbations. The generalized Ohm's law (5.18) in the MHD approximation also reduces to (5.16). We thus only need the equations for $\beta_a$, $I_a$ and $E_a$.

- ***Interaction variable***

  Equation (5.6) for the interaction variable $I_a$ becomes,

$$\frac{9}{4}I''_{(\ell)} + \frac{27}{2\tau}I'_{(\ell)} + \left[\left(\frac{\ell}{a_i H_i}\right)^2 \tau^{-4/3} + \frac{25}{2\tau^2}\right] I_{(\ell)} = 0 \,, \tag{5.31}$$

  with the general solution,

$$I_{(\ell)}(\tau) = \tau^{-5/2}\left[C_1 J_1\left(\frac{5}{2}, \frac{\ell}{a_i H_i}\frac{2}{\tau^{1/3}}\right) + C_2 J_2\left(\frac{5}{2}, \frac{\ell}{a_i H_i}\frac{2}{\tau^{1/3}}\right)\right] \,, \tag{5.32}$$

  where $C_1$ and $C_2$ are integration constants, $J_1$ and $J_2$ are Bessel functions of the second kind.

- ***Electromagnetic Fields***

  Equation (5.10) for the electric field variable $E_a$ becomes,

$$\frac{9}{4}E''_{(\ell)} + \frac{15}{2\tau}E'_{(\ell)} + \left[\left(\frac{\ell}{a_i H_i}\right)^2 \tau^{-4/3} + \frac{3}{\tau^2}\right] E_{(\ell)} = \pm\frac{(2k+n)}{H_i^2 a_i} I_{(\ell)} \tau^{-2/3} \tag{5.33}$$

  and we once again determine $\beta_{(\ell)}$ from the induction equation

$$\beta_{(\ell)} = I_{(\ell)} \mp \frac{\ell}{a_i \tau^{2/3}} E_{(\ell)} \tag{5.34}$$

  instead of using the wave equation (5.14).

## 5.6 Numerical Integrations

We need initial conditions in order to solve the equations presented in the previous section. The conditions are adapted as follows: for $\beta_a$ we invoke Maxwell's equation (5.4)

$$\beta_a = I_a - \mathscr{E}_a, \tag{5.35}$$

which upon differentiating in time results in the initial condition for $\dot{\beta}_a$

$$\dot{\beta}_a = \dot{I}_a - \dot{\mathscr{E}}_a \,. \tag{5.36}$$

For the interaction variable $I_a$, we use the definition (5.3)

$$I_a = \sigma_{ab}\tilde{B}^b \,, \tag{5.37}$$

which can be differentiated to yield the initial condition for $\dot{I}_a$. Using Leibniz rule, this result in

$$\dot{I}_a = \dot{\sigma}_{ab}\tilde{B}^b + \sigma_{ab}\dot{\tilde{B}}^b \,. \tag{5.38}$$

One can then use the evolution of the background magnetic field (4.36) to substitute for $\dot{\tilde{B}}_a$,

$$\dot{\tilde{B}}_a = -\frac{2}{3}\Theta\tilde{B}_a \,. \tag{5.39}$$

For the rotation of the Electric field $\mathscr{E}_a$ [6], we use Maxwell's equation (5.5) and the commutation relation (A.16) to get,

$$\dot{\mathscr{E}}_a \;=\; -\Theta\mathscr{E}_a + \mathcal{R}_{ab}\tilde{B}^b - \mathrm{D}^2 B_a \,, \tag{5.40}$$

where in this case $B_a$ (without the tilde) is the induced magnetic field, and we have written the first order perturbed 3-Ricci tensor $\mathcal{R}_{ab}$ as [152, 156]

$$\mathcal{R}_{ab} = -\dot{\sigma}_{\langle ab\rangle} - \Theta\sigma_{ab} \,. \tag{5.41}$$

We require that the gravitationally induced field variables $E_a$ (and hence $\mathscr{E}_a$) and $B_a$ be zero initially. This leads to the following initial conditions for the perturbation variables:

$$\begin{aligned}
I^i_{(\ell)} &= \sigma^i_{(k)}\tilde{B}^i_{(n)} \,, & I'_{i(\ell)} &= \sigma'_{i(\ell)}\tilde{B}^i_{(n)} - \tfrac{4}{3}\sigma^i_{(k)}\tilde{B}^i_{(n)} \,, \\
\mathscr{E}^i_{(\ell)} &= 0 \,, & \mathscr{E}'_{i(\ell)} &= -2\mathscr{E}^i_{(\ell)} - \left(\sigma'_{i(\ell)} + 2\sigma^i_{(k)}\right)\tilde{B}^i_{(n)} \,, \\
\beta^i_{(\ell)} &= \sigma^i_{(k)}\tilde{B}^i_{(n)} \,, & \beta'_{i(\ell)} &= 2\sigma'_{i(k)}\tilde{B}^i_{(n)} + \tfrac{2}{3}\sigma^i_{(k)}\tilde{B}^i_{(n)} + 2\mathscr{E}^i_{(\ell)} \,.
\end{aligned} \tag{5.42}$$

Following [381, 378, 243], we adopt the initial condition for the shear from $(\sigma/H)_i \sim 10^{-6}$. We choose the seed field to be $\tilde{B}^i = 10^{-20}$ G, as typical of those produced around the recombination era [363].

[6] Note that the Electric field $E_a$ and its curl $\mathscr{E}_a$ are related by a factor of $\ell$ when expanded in terms of the helicity basis described in Appendix A.2. In particular $\mathscr{E}_a = \pm(\ell/a_i)\tau^{-2/3}E^{(\pm)}e_a^{(\pm)}$

Given the system of initial conditions (5.42), one can notice that the interaction variable $I_a$ plays the fundamental role in the interaction process. In particular, if we set $I_a = 0$ initially, then no amplification takes place. We show the time evolution $I_a(\tau)$ in Figure 5.1 on a log-log scale. A noteworthy feature in the figure is the rapid decay of $I_a$ for both scalars and tensors. Although the interaction with scalar perturbations decays slightly slower, it essentially follows the same trend as the interaction with gravitational waves. We are thus led to conclude that even including scalar perturbations in the interaction, we reach the same conclusion as [165] and [243] that there is no significant amplification of electromagnetic fields coming from the interaction.

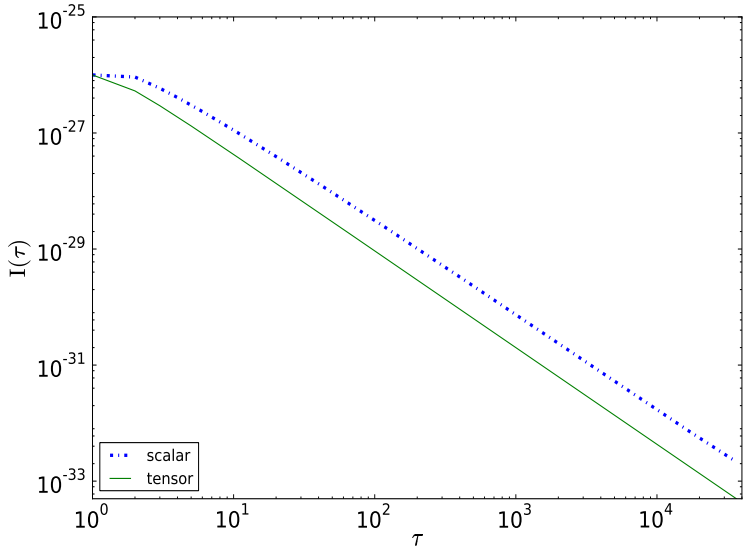


Figure 5.1: *Time evolution of the interaction variable in log-log axes. Note that for the interaction with scalars, the decay is slightly slower than for tensors.*

The effect of the gravitational perturbations on the interaction is thought to be largest at the point where the modes enter the horizon. This is clearly evident in Figures 5.2(a) and 5.2(b). A couple of features are worth noting from Figure 5.2(a). One is that the spectrum for the interaction variable mimics that of gravitational waves. It is also consistent with the fact that gravitational waves start oscillating at horizon crossing. This is to be expected since although for a spatially inhomogeneous magnetic field $\tilde{B}_a$, the product $I_{(\ell)} = \tilde{B}_{(n)}\sigma_{(k)}$ becomes a convolution in Fourier space, $I(k) = \sum_n B(n)\sigma(k-n)$, we have only considered the mode-mode coupling case, $I(k) = B(k)\sigma(k)$.

The power spectra for the case of interaction with scalars are not as interesting. There is no scale dependence on the interaction variable $I_a$, cf equation (5.27a). This is because

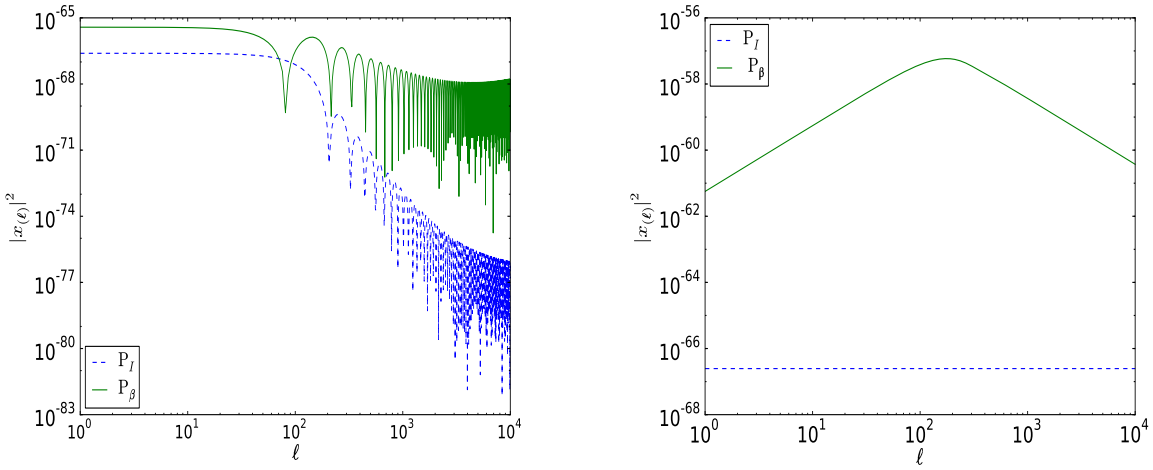


(a) (b)

Figure 5.2: *Plots of Power vs scale ($\ell$); we define the power as $P_x = |x(\ell)^2|$. (a): Power spectra of the magnetic field variable $\beta_{(\ell)}$ (green, solid), and the interaction variable $I_{(\ell)}$ (blue, dashed) at redshift $z = 0$ for the tensor case. (b): Power spectra of the magnetic field variable $\beta_{(\ell)}$ (green, solid), and the interaction variable $I_{(\ell)}$ (blue, dashed) at redshift $z = 0$ for the scalar case.*

the Laplacian term for scalar perturbations comes from the acceleration vector which is identically zero in the dust case $\mathcal{A}_b = 0$.

It would be interesting to generalize our treatment to include the case of non-zero pressure. This will lend us to the radiation dominated era where one can incorporate photons in the plasma and can consider collisional effects as was done in [219, 363] for example. One could treat the interesting case of simultaneous generation and amplification of magnetic fields by coalescing these phenomena.

# Chapter 6

# Conclusions and Future Outlook

## 6.1 Conclusions

Interactions of gravitational radiation with electromagnetic fields in laboratory, astrophysical and cosmological environments have been studied using a variety of formalisms by several authors in the literature [373, 335, 271, 77, 34, 273, 381, 65, 165]. The studies have generally focused on the effects of gravitational waves on electromagnetic fields as a viable mechanism to amplify weak magnetic fields. Other studies have studied the effects of electromagnetic fields on gravitational radiation. Such effects include, for example, the gravitational analogue of cyclotron damping, Landau damping, Faraday rotation of gravitational waves etc. (see for example [339, 261] and references therein).

In this work, we have used the 1+3 Covariant formalism to carry out an analysis of the coupling between gravitational perturbations with electromagnetic fields as a possible means for magnetic field amplification in a cosmological setting. This carries to completion the work began in [65] and [417]. In agreement with the work of [165] and [243] we argue that there is no significant amplification resulting from the interaction of magnetic field with gravitational waves. Even with the inclusion of density perturbations, the induced fields may still be orders of magnitude smaller than those required by the galactic dynamo mechanism. This justifies the perturbative treatment and our neglect of backreaction effects.

The induction of electromagnetic fields due to the interaction of a test magnetic field with gravitational waves was studied in [273] using the weak-field approximation. We included this study here as a subset, treating the background magnetic field as a first order perturbation and recovered similar results. This shows that there is no fundamental difference between the two approaches, apart from a labeling of spacetimes, which should not affect physical results. We also extended this study by using a proper non-linear perturbative framework.

This framework was applied in [65], but an erroneous argument there led to the neglect of the rotation of the Electric field, thus restricting the study to perfectly conducting environments. This result, which led to the conclusion that the interaction was independent of the conductivity of the medium, was subsequently refuted in [380]. In fact, upon inspection of the initial conditions (5.42) one can conclude that even if one initially sets the rotation of the Electric field to zero, $\mathscr{E}_i = 0$ there are non-zero terms on the right hand side of the initial conditions for $\dot{\mathscr{E}}$ that will seed a non-zero $\mathscr{E}$. We also carry to completion the work presented in [417] by doing a proper extraction of the scalar and tensor modes in the perturbation equations and including numerical integrations. In terms of the conductivity of the cosmic medium, [273] restricted their study to poor conducting mediums, [65] to perfectly conducting mediums and [417] treated the MHD approximation. We carried our analysis for all three cases. We find that for tensor perturbations, the ideal MHD approximation is just the same as the perfect conductivity assumption of the fluid treatment. For scalar perturbations, we find an additional source term in the induced field (compared with perfectly conducting environments) due to the coupling of the seed field with scalar velocity perturbations. The current term $\mathcal{J}_a$ was neglected at all orders in [65], in an attempt, presumably, to uphold the background magnetic field's homogeneity condition $\mathrm{D}_a\tilde{B}_b = 0$. However, this is not necessary since introducing the current term at the non-linear order does not break the condition $\mathrm{D}_a\tilde{B}_b = 0$. Also, one cannot consistently invoke Ohm's law for poor and perfect conducting environments without a current term. In [417], an inhomogeneous seed field was assumed thereby requiring a first order current $\mathcal{J}^a = \rho_e v_e^a + \rho_i v_i^a = -e(n_e v_e^a - n_i v_i^a)$ to uphold the condition $\mathrm{D}_a\tilde{B}_b \neq 0$. However, after decoupling (which is the era considered there), Thompson scattering is no longer efficient. Thus electrons and ions are tightly coupled by coulomb scattering at first order. Their velocity fields are therefore equal as they form a perfectly coupled baryon fluid [179, 278]. There can be therefore no currents generated at this order and the condition curl $\tilde{B}_a = \mathcal{J}_a \approx 0$ will render the seed field homogeneous.

Both [65] and [417] integrate $\beta_a$ to recover the amplified magnetic field, after specifying a frame $u^a$. While this procedure takes into account the frame dependence of the induced magnetic field $B_a$, it invalidates gauge invariance as the recovered $B_a$ remains gauge dependent and takes the same value and form as it would have without the introduction of $\beta_a$. This is already pointed out in [380], see also [66] and [379]. In this work, we do not integrate $\beta_a$ to recover the induced field. Instead we simply note that one can assign a physical meaning to the magnetic field variable $\beta_a$ by noting that $\beta_a = 0$ describes the background adiabatic decay of the fields. Any deviation from $\beta_a = 0$ would then imply amplification of the background field. Moreover, $\beta_a$ is a linear combination of terms that source magnetic fields through the

induction equation (5.4). Thus we can estimate the relative importance of each source term through $\beta_a$ without having to integrate it to recover the gauge-dependent $B^a$. For example, we see from Figure 5.2(a) that the rotation of the electric field dominates at small scales compared to the interaction term. Observations of cosmological magnetic fields are difficult enough as it is, a new cosmological observable would lead to better understanding of studies in magnetic fields. While $\beta_a$ may not be that quantity, it does arise naturally from Maxwell's equations.

Mechanisms that seek to generate magnetic fields, relying on non-linear perturbation theory are attractive for several reasons [145]. Among these is that they can easily blend in with known physics as they become relevant around the recombination era. This makes it possible to quantitatively evaluate the generated fields using CMB constraints. In this work, we have restricted our gravitational field perturbations to first order in our treatment. In [77] the interaction of a strong non linear gravitational wave with electromagnetic fields was studied, leading to new phenomena that are otherwise absent in the linearized treatment. Progress in non-linear perturbation theory will allow us to investigate these non-linear effects in a manner that is free of spurious gauge modes [122, 117].

## 6.2 Future Outlook

The characterization of the observed large scale magnetic fields as 'primordial' remains open to question. Despite the growing interest and our increasing understanding of cosmological electromagnetism, many fundamental questions on their possible origin and subsequent evolution remain unanswered. Current observations of galactic magnetic fields is not enough to constrain the properties of a primordial magnetic field. This is as a result of the uncertainties in the theory of galaxy formation, and the fact that the MHD dynamo mechanism and other non linear effects are likely to alter the nature of any seed field present at the onset of galaxy formation. To circumvent this issue, more observation is required to map out the strength and evolution of magnetic fields at cosmological distances. Intergalactic magnetic field observations may also provide a setting where the seed field has not been affected by astrophysical processes. Large modern radio astronomy telescopes like the SKA [51] and LOFAR [21] have identified the issue of cosmic magnetism as one of their key science projects.

As already mentioned in the introductory paragraphs, Magnetogenesis by second order effects, have the tendency of generating fields with energy densities at fourth order in perturbation theory. Such methods, though attractive for their simplicity and physical appeal, cannot in general be constrained by CMB anisotropies. On the other hand, one can look to

study secondary effects of the generated magnetic fields as a viable means of constraining theories of magnetogenesis. This could be a fruitful enterprise given the current proliferation of magnetogenesis theories [46].

In general, first order perturbation methods can be used to get an impression of the underlying physics of a given problem. However they are plagued by gauge issues at non linear orders. This feature paves a way for the study of electromagnetism in curved spacetimes by numerical methods. It would be interesting to carry out studies of magnetic field amplification by numerically integrating the non linear GRMHD equations within the framework of numerical relativity. Furthermore, the collision of a neutron star with a black hole provides a rich arena for the interplay between gravity and electromagnetism. It is not unreasonable to think that signatures from such phenomena could be observed with the next generation of interferometric detectors.

# Part II

# Numerical Relativity

# Chapter 7

# Rudiments of Numerical Relativity

## 7.1 Historical Context

General relativity, unlike Newtonian theory of gravity, describes gravitational interactions by adopting a geometric picture of spacetime. Within this description, matter moves according to the curvature of spacetime, which is in turn curved by the very presence of matter. An added level of intricacy is the fact that the gravitational field acquires its own dynamical properties even in the absence of matter, a feature which is clearly demonstrated by the collapse of pure gravitational waves into a black hole [4, 17]. These aspects present a non linearity within the concomitant field equations of gravity. As a result, the Einstein field equations

$$G_{ab} \equiv R_{ab} - \frac{1}{2} g_{ab} R = 8\pi T_{ab} \ , \tag{7.1}$$

are challenging to solve for general spacetimes whose exact forms are not analytically known. This deceptively simple system (7.1) is actually a set of ten quasi-linear coupled partial differential equations for the ten components of the four dimensional metric tensor $g_{ab}$. Analytical solutions of the field equations are limited to simplified spacetimes, which are often endowed with unrealistic symmetry assumptions. The aim of numerical relativity is to set up the field equations (7.1) as an initial-boundary value problem, and evolve the metric functions numerically in time. This approach allows for more realistic simulations of systems involving strong gravitational fields, where perturbative approximations would naturally break down or otherwise cumbersome to manipulate.

One of the most important problems involving strong gravitational fields in relativity is the evolution of black hole spacetimes. The first numerical simulations of black hole dynamics were attempted nearly 50 years ago [194, 349]. With the advent of the computer age and

a growing interest in the field of black hole and gravitational physics in general, the field of numerical relativity emerged. Subsequent advances in the field over the years has since made it possible to simulate the final stages of highly relativistic colliding binary black holes and other compact objects like neutron star binaries. One of the original motivations for pursuing black hole spacetime evolutions was to provide templates of gravitational waveforms for current and future generation interferometric gravitational wave observatories. This enterprise has helped mature the field and in turn spawned other interests within the realm of numerical and mathematical relativity. As a result, there are now several independent numerical relativity codes currently in use within the community [400, 82, 333, 203, 140, 32, 95]. In addition to the computational advances, there has been progress in commissioning state-of-the-art interferometric observatories like LIGO [2], VIRGO [5], TAMA [364], GEO600 [186], etc. with prospects of directly detecting gravitational wave bursts from compact sources. Another thrust along this direction is the establishment of several collaborations between members of the numerical relativity, gravitational wave data analysis communities and other communities specializing in analytical methods, culminating in the NINJA and NRAR projects [30]. Several reviews have been compiled on the current status of the binary black hole problem, see for example [206].

Aside from colliding binaries, numerical relativity can also be used to shed some light on various other issues of physical interest. For example, Choptuik's study of spherically symmetric collapse of massless scalar fields using numerical techniques led to the discovery of critical phenomena [113, 189]. There has also been progress in studying event and apparent horizons and approaches to spacetime singularities during gravitational collapse. Such studies pave a way towards numerical investigations of Penrose's cosmic censorship hypothesis [307, 308]. Another area of interest has been the interplay between electromagnetism and gravity in curved spacetimes [295, 174, 290]. This offers the possibility of detecting electromagnetic signatures of black hole mergers or ringdown in the presence of magnetic fields [287, 123, 410]. These and other issues, which were previously only limited to perturbative or post-Newtonian approximation treatment, are now routine applications for most numerical relativity codes. Although the field may have a certain astrophysical disposition, there is nothing inherent within numerical relativity techniques that would restrict their application to astrophysical problems. As a matter of fact, numerical methods are being increasingly employed in studying various aspects of cosmological models. A fascinating paradigm in this division is the simulation of a black hole lattice universe [55, 56, 403]. These types of cosmological models have certain implications on the overall understanding of inhomogeneity and backreaction effects in cosmology [256, 83]. Moreover, there is growing interest in

applications of numerical relativity tools beyond standard general relativity [331, 303] and higher dimensional theories [411, 398, 345].

With a history that spans just over half a century, numerical relativity is a somewhat complex subject, drawing from different facets of geometry, computational science and general relativity. However, the apparent complexity has simpler underpinnings. A typical recipe for any simulation involves a choice of formulation for the Einstein field equations. Of course, there are, in addition, problem-dependent issues such as initial data and boundary conditions. The reduction of the field equations (7.1) into a standard PDE system involves several aspects such as the main evolution equations, the system of constraint equations and the gauge system which represents the coordinate choice. These components give rise to a range of evolution formalisms. A general evolution mechanism for the Einstein field equations can be classified largely as either Cauchy, Characteristic or Hyperboloidal. This classification is based on the type of initial value problem that each class solves. In this work, we restrict our attention to the widely adopted Cauchy formulation, in particular the 3+1 type formulations (see §7.2 and §7.3). There has been significant progress in finding well posed formulations which avoid issues such as constraint instabilities and other computational nightmares that result in early termination of numerical relativistic simulations [346, 324]. Also common to all numerical relativity codes is the use of discretization procedures. A popular method of choice in this category has been the use of second order accurate finite difference stencils with iterative Crank-Nicholson time integration within the method of lines framework. Other methods that have recently entered the mainstream are finite elements [237, 109], spectral methods [182, 229, 71] and higher order finite difference schemes. These choices ultimately have a bearing on significant issues such as ease of implementation, stability, well-posedness, physical appropriateness, long term behavior and overall efficiency.

Withing the guise of general relativity, isolated systems like black holes and other compact objects of astrophysical interest are well approximated by asymptotically flat spacetimes. In studying these systems, one is immediately confronted with the outer boundary condition, which is typically the radiation boundary condition. At the theoretical level, such boundary conditions must be imposed at infinity, a configuration which is not computationally feasible. One has several options to deal with this issue. For example, through compactification methods, it is possible to adopt a coordinate system that maps spatial infinity to some finite coordinate value [169]. A simpler alternative involves setting the boundary conditions at a sufficiently large distance from the source. In this case, one proceeds by adopting a discretization procedure that is capable of resolving the fine scale features in the vicinity of the source while simultaneously allowing the grid to stretch to large distances. One such

example is the Fish eye coordinate system [95, 413]. This can be viewed as a mapping from a uniform coordinate system to a warped coordinate system that concentrates more grid points in the vicinity of the source, and rarefies grid points away from the source. The scheme allows the use of moderate grid sizes in the simulation of compact sources. Another novel technique to deal with the large range of length scales is mesh refinement, where the grid spacing is chosen locally according to the accuracy requirements of a specific region in the computational grid [263, 298, 334, 137, 409]. Numerical integrations with mesh refinement are typically carried out on a hierarchy of (Cartesian) nested grids, see §8.8 for more details. It is known that during the implementation of such algorithms, several issues related to scalability, loss of convergence, spurious reflections and loss of conservation[1] may arise [22, 413, 334, 248, 33, 112]. In this second part of the thesis, we focus on the issue of convergence and spurious reflections. The problems of scalability and loss of conservation do not arise in our work because (*i*) Our mesh refinement implementation is not yet fully parallel and (*ii*) We are dealing with the vacuum Einstein field equations (which are not in conservative form). However, these issues will be addressed in future work.

## 7.2 Foliations of Spacetime

In this section we outline how one can cast the seemingly abstract tensorial form of the field equations (7.1) into a Cauchy or initial value problem amenable to numerical treatment. This amounts to decomposing the four dimensional spacetime $(\mathcal{M}, g_{ab})$ into a group of non intersecting Cauchy hypersurfaces $\Sigma$, by using a timelike vector $n^a$, normal to $\Sigma$. Within this configuration, the hypersurfaces $\Sigma$ coincide with the level surfaces of some parameter $t$, which can be interpreted as coordinate time. This setup induces a spatial metric $\gamma_{ab}$ on the 3-dimensional hypersurfaces $\Sigma$ such that,

$$\gamma_{ab} = g_{ab} + n_a n_b, \qquad \gamma^{ab} = g^{ab} + n^a n^b \ . \tag{7.2}$$

Like the four dimensional metric $g_{ab}$, the 3-metric $\gamma_{ab}$ is symmetric in the indices $a$ and $b$. Quantities on $(\mathcal{M}, g_{ab})$ are decomposed with respect to the foliation through projection tensors $N^a{}_b$ and $\gamma^a{}_b$ which project along and orthogonal to the timelike 4-vector $n^a$, respectively.

[1] In this case the 'conservation' refered to here is the requirement that fluxes into the fine grid across a coarse-fine cell boundary must equal the flux out of the coarse cell.

These projection tensors are defined as,

$$N^a_{\ b} = -n^a n_b \ , \tag{7.3}$$

$$\gamma^a_{\ b} = \delta^a_{\ b} + n^a n_b \ , \tag{7.4}$$

such that,

$$N^a_{\ c} N^c_{\ b} = N^a_{\ b}, \qquad N^a_{\ a} = 1, \qquad N_{ab} n^b = n_a \ , \tag{7.5}$$

$$\gamma^a_{\ c} \gamma^c_{\ b} = \gamma^a_{\ b}, \qquad \gamma^a_{\ a} = 3, \qquad \gamma_{ab} n^b = 0 \ . \tag{7.6}$$

We define a spatially projected covariant derivative, compatible with the induced metric $\gamma_{ab}$, as

$$\mathrm{D}_e Q^{a\cdots b}_{\quad c\cdots d} \equiv \gamma^a_{\ p} \cdots \gamma^b_{\ q} \, \gamma^r_{\ c} \cdots \gamma^s_{\ d} \, \gamma^f_{\ e} \nabla_f Q^{p\cdots q}_{\quad r\cdots s} \ . \tag{7.7}$$

One can easily show that $\mathrm{D}_a \gamma_{bc} = 0$ as required. The Einstein field equations (7.1) are given in terms of four dimensional quantities. In order to decompose the field equations in 3+1 form, we will need 3-dimensional expressions for the tensors involved. We therefore continue and define the 3-dimensional Riemann tensor associated with the induced metric $\gamma_{ab}$ as,

$$R_{abc}^{\quad\ d} = \partial_b \Gamma^d_{\ ac} - \partial_a \Gamma^d_{\ bc} + \Gamma^f_{\ ac} \Gamma^d_{\ fb} - \Gamma^f_{\ bc} \Gamma^d_{\ fa} \ , \tag{7.8}$$

where the $\Gamma^a_{\ bc}$ are the associated 3-dimensional connection coefficients defined through the 3-metric $\gamma_{ab}$ as,

$$\Gamma^a_{\ bc} = \frac{1}{2} \gamma^{ad} (\partial_c \gamma_{db} + \partial_b \gamma_{dc} - \partial_d \gamma_{bc}) \ . \tag{7.9}$$

The 3-dimensional Riemann tensor as given by (7.8) is a purely spatial tensor encoding information about the curvature intrinsic to the spatial slice $\Sigma$. To get a full picture of the curvature information, we need to know how the 3-dimensional hypersurface $\Sigma$ is embedded in the 4-dimensional manifold. This information is encoded in the extrinsic curvature $K_{ab}$. We define $K_{ab}$ through spatial projections of the gradient of the timelike 4-vector,

$$K_{ab} = -\gamma^c_{\ a} \gamma^d_{\ b} \nabla_c n_d \ . \tag{7.10}$$

It is not difficult to see that $K_{ab}$ is also symmetric in the indices $a$ and $b$. The extrinsic curvature can also be written as a Lie derivative along the timelike 4-vector $n^a$,

$$K_{ab} = -\frac{1}{2} \mathcal{L}_n \gamma_{ab} \ . \tag{7.11}$$

If the 4-vector $n^a$ is along the time direction, then equation (7.11) provides a propagation equation for the 3-metric $\gamma_{ab}$. However, in general this is not the case since $n^a \nabla_a t = \alpha^{-1} \neq 1$, where $t$ is a scalar function that can be interpreted as a global time function. We thus consider instead the vector,

$$t^a = \alpha n^a + \beta^a \,, \tag{7.12}$$

such that $t^a \nabla_a t = 1$. Here, $\alpha$ and $\beta^a$ are the lapse function and shift vector respectively. The vector $t^a$ can be interpreted as connecting points with the same spatial coordinates from one hypersurface to the next. With this identification, one can interpret the lapse function $\alpha$ as a measure of the lapse of proper time between hypersurfaces, while the shift vector $\beta^a$ measures how coordinates shift within a hypersurface with respect to the 4-vector $n^a$. Finally, the line element $ds^2 = g_{ab} dx^a dx^b$ of the 4-dimensional spacetime is split according to,

$$ds^2 = -(\alpha^2 - \beta_i \beta^i) dt^2 + 2\beta_i dt dx^i + \gamma_{ij} dx^i dx^j \,, \tag{7.13}$$

where $\beta_i = \gamma_{ij} \beta^j$. In this coordinate system, one can identify the components of the timelike 4-vector $n^a$ as,

$$n^a = \left(1/\alpha, -\beta^i/\alpha\right) , \qquad n_a = (-\alpha, 0) \,. \tag{7.14}$$

Given the space time quantities $\gamma_{ab}$, $\beta^a$ and $\alpha$, one can reconstruct the 4 dimensional metric $g_{ab}$ as,

$$g_{ab} = \begin{pmatrix} -\alpha^2 + \beta_k \beta^k & \beta_i \\ \beta_j & \gamma_{ij} \end{pmatrix} , \qquad g^{ab} = \begin{pmatrix} -1/\alpha^2 & \beta^i/\alpha^2 \\ \beta^j/\alpha^2 & \gamma^{ij} - \beta^i \beta^j/\alpha^2 \end{pmatrix} . \tag{7.15}$$

In addition, the determinant of the 4-metric $g = \det g_{ab}$ is related to that of the 3-metric $\gamma = \det \gamma_{ij}$ by

$$\sqrt{-g} = \alpha \sqrt{\gamma} \,. \tag{7.16}$$

This reconstruction of the 4-metric becomes necessary when, for example, one solves the geodesic equation (7.89).

## 7.3 3+1 Form of the Field Equations

Throughout all the thesis, we are considering the vacuum Einstein field equations, characterized by the vanishing of the energy momentum tensor $T_{ab} = 0$. The Einstein field equations can be recast in 3+1 form by considering projections along and orthogonal to the 4-vector $n^a$. The only possible projections are:

1. Full projection along $n^a$,

2. Full projection onto the spatial slice $\Sigma$ (orthogonal to $n^a$)

3. Mixed projection, where one index is projected along and the other orthogonal to $n^a$.

Considering all three possibilities leads to the following system of equations,

$$\gamma^c{}_a \gamma^d{}_b R_{cd} = 0\,, \tag{7.17}$$

$$n^a n^b \left(R_{ab} - \tfrac{1}{2} R g_{ab}\right) = 0\,, \tag{7.18}$$

$$\gamma^c{}_a n^b \left(R_{cb} - \tfrac{1}{2} R g_{cb}\right) = 0\,. \tag{7.19}$$

In order to proceed, we need expressions for the terms on the left hand side in terms of three dimensional quantities. Starting from the Ricci identity

$$\mathrm{D}_a \mathrm{D}_b v^c - \mathrm{D}_b \mathrm{D}_a v^c = R_{abcd} v^d\,, \tag{7.20}$$

where $v^a$ is a 3-vector orthogonal to the timelike vector $n^a$ and the 3-Riemann tensor $R_{abcd}$ is given by (7.8), one recovers Gauss relation (after some manipulation) relating the full Riemann tensor to the spatial Riemann tensor,

$$\left({}^{(4)}R^c{}_{dab}\right)_\perp = R^c{}_{dab} + K^c{}_a K_{db} - K^c{}_b K_{ad}\,, \tag{7.21}$$

where $[\cdots]_\perp$ indicates spatial projection along all the free indices. We are interested instead in the relation between the four dimensional Ricci tensor and the spatial Ricci tensor. To this end, we contract (on the indices $c$ and $a$) to recover the contracted Gauss relation,

$$\gamma^c{}_a \gamma^d{}_b \, {}^{(4)}R_{cd} + \gamma_{ad} n^d \gamma^\rho{}_b n^\sigma \, {}^{(4)}R^\mu{}_{d\rho\sigma} = R_{ab} + K K_{ab} - K_{ad} K^d{}_b\,. \tag{7.22}$$

Further contraction, leads to the following scalar Gauss equation, relating the Ricci scalar of the full spacetime to that of the spatial slice,

$${}^{(4)}R + 2\, {}^{(4)}R_{cd} n^c n^d = R + K^2 - K_{cd} K^{cd}\,. \tag{7.23}$$

We need one more relation, to accommodate the mixed projection (7.19). For this, we turn to the Ricci identity of the full space time,

$$\nabla_a \nabla_b v^c - \nabla_b \nabla_a v^c = R_{abcd} v^d\,. \tag{7.24}$$

Carrying out a mixed projection on (7.24) and some manipulations leads to the Codazzi-Mainardi relation

$$\gamma^{c}{}_{r} n^{s} \gamma^{p}{}_{a} \gamma^{q}{}_{b} \, {}^{(4)}R^{r}{}_{spq} = \mathrm{D}_b K^{c}{}_{a} - \mathrm{D}_a K^{c}{}_{b} \, . \tag{7.25}$$

To recover the relation in terms of the Ricci tensor, we contract over $a$ and $c$ to get the contracted Codazzi-Mainardi relation,

$$\gamma^{p}{}_{a} n^{q} \, {}^{(4)}R_{pq} = \mathrm{D}_a K - \mathrm{D}_p K^{p}{}_{a} \, . \tag{7.26}$$

We can now plug (7.22), (7.23) and (7.26) into (7.17)–(7.19), respectively to arrive at a 3+1 formulation of the field equations. We refer the reader to [180, 49, 393] for insight and detailed derivations of the geometric relations presented in this section.

### 7.3.1 Evolution and Constraint equations

With the preliminaries presented above, we now present the explicit form of the Einstein field equations (7.17)–(7.19) in terms of 3+1 decomposed quantities. The resulting system of equations is often referred to as the Arnowitt-Deser-Misner (ADM) form, in reference to the ideas presented in [28]. Equation (7.17) results in six evolution equations for the six independent components of the extrinsic curvature $K_{ab}$, while (7.18) and (7.19) lead to one constraint equation (Hamiltonian or energy constraint), and three constraint equations respectively (momentum constraint). The entire system is supplemented by (7.11) for the propagation of the three metric and is given as,

***Propagation:***

$$\partial_t g_{ij} = -2\alpha K_{ij} + \mathrm{D}_i \beta_j + \mathrm{D}_j \beta_i \, , \tag{7.27a}$$

$$\begin{aligned} \partial_t K_{ij} = &- \mathrm{D}_i \mathrm{D}_j \alpha + \alpha (R_{ij} - 2K_{i\ell} K^{\ell}{}_{j} + K K_{ij}) \\ &+ \beta^k \partial_k K_{ij} + K_{kj} \partial_i \beta^k + K_{ik} \partial_j \beta^k \, . \end{aligned} \tag{7.27b}$$

***Constraint:***

$$\mathcal{H} \equiv R - K_{ij} K^{ij} + K^2 = 0 \, , \tag{7.28a}$$

$$\mathcal{M}_i \equiv \mathrm{D}_j K^{j}{}_{i} - \mathrm{D}_i K = 0 \, , \tag{7.28b}$$

which are the Hamiltonian and momentum constraints respectively. In (7.27), $\mathrm{D}_i$ is the 3-dimensional covariant derivative associated with the 3-metric $\gamma_{ij}$, $R_{ij}$ and $R$ are the three-dimensional Ricci tensor and Ricci scalar, respectively given by

$$R_{ij} = \frac{1}{2}\gamma^{k\ell}\left(\gamma_{kj,i\ell} + \gamma_{i\ell,kj} - \gamma_{k\ell,ij} - \gamma_{ij,k\ell}\right) + \gamma^{k\ell}\left(\Gamma^{m}{}_{i\ell}\Gamma_{mkj} - \Gamma^{m}{}_{ij}\Gamma_{mk\ell}\right) , \tag{7.29}$$

$$R = \gamma^{ij}R_{ij} . \tag{7.30}$$

Given initial and boundary conditions for the fields $(\gamma_{ij}, K_{ij})$, the propagation equations (7.27) describe the time evolution of the system and can be numerically integrated. It is noteworthy that although the evolution system (7.27) involves the shift vector $\beta^i$ and the lapse function $\alpha$, it does not provide any equations for these variables. As a result, the system is underdetermined and cannot, as it stands, provide a unique solution. This feature is related to the gauge freedom in general relativity. A gauge fixing procedure must be augmented to the system in order to form a genuine PDE problem. We discuss several gauge choices in §7.7.

### 7.3.2 Constraints Conservation

From a theoretical standpoint, it is important to assess the consistency of the system (7.27)–(7.28). The constraints equations (7.28) do not involve time derivatives. More importantly, they do not depend on the gauge functions $\alpha$ and $\beta^i$. They refer to a given spatial surface $\Sigma_t$, and must be satisfied at all other hypersurfaces during evolution.

To analyze the consistency of the ADM equations, it is important to investigate how constraint violations propagate in time. For the Hamiltonian constraint $\mathcal{H}$, one recovers the following propagation equation,

$$\begin{aligned}(\partial_t - \beta^i\partial_i)\mathcal{H} = {} & 2\alpha K\mathcal{H} - 2\alpha\gamma^{ij}\partial_i\mathcal{M}_j - 4\gamma^{ij}\partial_j\alpha\mathcal{M}_i \\ & + \alpha\partial_l\gamma_{mk}(2\gamma^{ml}\gamma^{kj} - \gamma^{mk}\gamma^{lj})\mathcal{M}_j .\end{aligned} \tag{7.31}$$

For the momentum constraint $\mathcal{M}$, one arrives at the following propagation equation,

$$\begin{aligned}(\partial_t - \beta^j\partial_j)\mathcal{M}_i = {} & -\frac{1}{2}\alpha\partial_i\mathcal{H} - \mathcal{H}\partial_i\alpha + \alpha K\mathcal{M}_i \\ & - \beta^i\gamma^{jl}\partial_i\gamma_{lk}\mathcal{M}_j + \partial_i\beta_k\gamma^{kj}\mathcal{M}_j .\end{aligned} \tag{7.32}$$

Clearly, the constraints are conserved during evolution. We note from (7.31) and (7.32) that if the constraints are satisfied initially, $\mathcal{H} = 0$ and $\mathcal{M} = 0$, they remain so during evolution.

However, this is only true theoretically in an analytical setting. Because of round off and truncation error, the constraints are never exactly zero in a numerical evolution. This opens room for constraint violating modes to grow in time. In fact, numerically, the ADM system is prone to such constraint violation modes. The ability of a system to numerically conserve the constraint equations is related to a property referred to as Well-Posedness, which we discuss in the next section.

## 7.4 Hyperbolicity and Well-Posedness

In order to establish issues of existence, uniqueness and stability of solutions of the Einstein field equations one invokes some results on the theory of PDEs [162, 191]. An important property to consider in the formulations of the Einstein field equations or in general PDEs is that of well-posedness, which is the property that the solution of the system depend continuously on the initial data. In such cases small perturbations in the initial data will accordingly correspond to small perturbations in the solution. This property is given by the following definition [191],

**Definition 7.4.1** *A system is well-posed if there exists some norm $\|\cdot\|$, such that the norm of the solution vector is bounded for all time $t \geq 0$ by*

$$\|\mathbf{u}(t, x^i)\| \leq k e^{\alpha t} \|\mathbf{u}(0, x^i)\| \ , \tag{7.33}$$

*where $k$ and $\alpha$ are constants that do not depend on the initial data of the solution. We say a system is ill-posed if it is not well-posed.*

By definition, not all PDE systems are well-posed, however there are classes of PDEs that are well-posed. To gain further insight into this class, we look at some general classifications of PDEs. A second order PDE is classified as being parabolic, elliptic or hyperbolic based on the following generic model PDE in two variables,

$$A u_{xx} + 2B u_{xy} + C u_{yy} + D u_x + E u_y = F \ , \tag{7.34}$$

where $A$, $B$ and $C$ are functions of $x$ and $t$. In analogy with the analysis of conic sections, the discriminant $\Delta = B^2 - 4AC$ plays an important role in the classification of PDEs. In particular, the classification is based on whether the discriminant is less, equal or greater than zero. This classification system is summarized in Table 7.1. Because the discriminant of hyperbolic PDEs is positive, they have real characteristics, as opposed to the Elliptic

| Category | Criterion | Example |
|---|---|---|
| Hyperbolic | $B^2 - 4AC > 0$ | Wave equation $\partial_{tt} u = c^2 \partial_{xx} u$ |
| Parabolic | $B^2 - 4AC = 0$ | Heat equation $\partial_t u = \alpha \partial_{xx} u$ |
| Elliptic | $B^2 - 4AC < 0$ | Laplace equation $\partial_{xx} u = 0$ |

Table 7.1: *Classification of partial differential equations.*

PDEs, which have imaginary characteristics. The Einstein field equations of course are more complicated than the examples given in Table 7.1. However, one can manipulate them in such a manner that they fall into one of the classes. For example, the Parabolized ADM (PADM) equations are a parabolic formulation of the Einstein field equations, while the ADM and BSSN formulations are hyperbolic in nature. The constraint equations, on the other hand, are Elliptic as they apply on the instantaneous 3-spaces $\Sigma$.

Hyperbolicity is further classified into weakly hyperbolic, strongly hyperbolic or symmetric hyperbolic based on the eigenvalues of the characteristic matrix of the PDE system under consideration. Consider the quasilinear hyperbolic PDE system,

$$\partial_t \mathbf{u} = \mathbf{A}^i(\mathbf{u}) \partial_i \mathbf{u} + \mathbf{S}(\mathbf{u}) \ , \tag{7.35}$$

where $\mathbf{u}$ is the solution vector with $n$ components, each matrix $\mathbf{A}^i$ is an $n \times n$ matrix, and $\mathbf{S}$ is a source term. The characteristic matrix $\mathbf{P}$ is formed from $\mathbf{P} = \mathbf{A}^i n_i$, where $n_i$ is some arbitrary unit vector. The system (7.35) is said to be:

- Weakly hyperbolic if the characteristic matrix $\mathbf{P}$ has real eigenvalues, but does not posses a complete set of eigenvectors.
- Strongly hyperbolic if the eigenvalues of the characteristic matrix $\mathbf{P}$ are real, and $\mathbf{P}$ is diagonalizable for all unit vectors $n_i$.

- Symmetric hyperbolic if the characteristic matrix $\mathbf{P}$ is Hermitian. All symmetric hyperbolic systems are, by extension, strongly hyperbolic.

This classification relates to the well posedness of a system in that, strongly hyperbolic systems are well-posed, while weakly hyperbolic systems are ill-posed. One therefore expects strongly hyperbolic formulations of the Einstein field equations to conserve the constraint equations during evolution. In fact, several authors have dedicated a significant amount of effort to cast the Einstein field equations into strongly hyperbolic formulations — under suitable gauge conditions [346, 324].

## 7.5 Conformal Decompositions

The study of conformal transformations is important not only in 3+1 numerical relativity but in the field of general relativity as a whole. One can often gain insight into certain problems by studying conformal decompositions of the metric [222]. This method is used in deriving new formulations of the Einstein field equations (cf. BSSN formulation, see §7.6), and also in the construction of initial data (cf. York-Lichnerowicz conformal decompositions, see §7.9). Consider the following conformal transformation of the metric,

$$\gamma_{ij} = \psi^4 \bar{\gamma}_{ij} \qquad \gamma^{ij} = \psi^{-4} \bar{\gamma}^{ij} \ , \tag{7.36}$$

where $\tilde{\gamma}_{ij}$ is referred to as the conformal metric. For instance, the conformal metric in the BSSN formulation is given by,

$$\tilde{\gamma}_{ij} = \gamma^{-1/3} \gamma_{ij} \ . \tag{7.37}$$

This absorbs one degree of freedom into the conformal factor, leaving five degrees of freedom in the conformally related metric. The particular choice of the scaling factor in Equation (7.37) leads to the conformal metric having unit determinant $\tilde{\gamma} = 1$, but is otherwise freely chosen. Under the conformal transformation (7.36), the connection coefficients transform according to,

$$\Gamma^i_{jk} = \tilde{\Gamma}^i_{jk} + 2(\delta^i_j \tilde{\mathrm{D}}_k \ln\psi + \delta^i_k \bar{\mathrm{D}}_j \ln\psi - \tilde{\gamma}_{jk} \tilde{\gamma}^{il} \tilde{\mathrm{D}}_l \ln\psi) \ , \tag{7.38}$$

where $\tilde{\Gamma}^i_{jk}$ is the conformal connection associated with the conformal metric $\tilde{\gamma}_{ij}$. One can go further and define a covariant derivative $\tilde{\mathrm{D}}_a$ associated with the conformal connection, such

that $\tilde{\mathrm{D}}_a\tilde{\gamma}_{bc} = 0$. In a similar manner, the Ricci tensor $R_{ab}$ transforms as,

$$\begin{aligned} R_{ij} = \tilde{R}_{ij} - 2\left(\tilde{\mathrm{D}}_i\mathrm{D}_j \ln\psi + \tilde{\gamma}_{ij}\tilde{\gamma}^{lm}\tilde{\mathrm{D}}_l\tilde{\mathrm{D}}_m \ln\psi\right) \\ + 4\left(\bar{\mathrm{D}}_i \ln\psi\ \tilde{\mathrm{D}}_j \ln\psi - \tilde{\gamma}_{ij}\tilde{\gamma}^{lm}\tilde{\mathrm{D}}_l \ln\psi\ \tilde{\mathrm{D}}_m \ln\psi\right) \ , \end{aligned} \tag{7.39}$$

while the Ricci scalar $R$ transforms according to

$$R = \psi^{-4}\bar{R} - 8\psi^{-5}\bar{\mathrm{D}}^2\psi \ . \tag{7.40}$$

Having presented the conformal decompositions of the metric, we now turn our attention to the decompositions of the extrinsic curvature $K_{ij}$. It is customary to separate the trace $K$ and trace-free parts $A_{ij}$ of the extrinsic curvature $K_{ij}$ as

$$K_{ij} = A_{ij} + \frac{1}{3}\gamma_{ij}K \ . \tag{7.41}$$

We then introduce a conformal transformation on the traceless part $A_{ij}$ as

$$A^{ij} = \psi^{\alpha}\bar{A}^{ij} \ , \tag{7.42}$$

Where the exponent $\alpha$ is normally taken to be $\alpha = -4$ or $\alpha = -10$. This concludes the issue of conformal decompositions. The idea of conformal transformations forms the basis for the BSSN formulation (§7.6).

## 7.6 The BSSN Formulation

Despite their simplicity, the ADM equations are not commonly used in long term numerical evolution of general relativistic spacetimes. This system is actually only weakly hyperbolic and thus, it is ill-posed. The Baumgarte-Shapiro-Shibata-Nakamura (BSSN) [344, 48] formulation on the other hand has been shown to be strongly hyperbolic and thus well-posed for certain gauge choices [67, 190]. In order to present the BSSN system of equations, we

begin by introducing the following conformal variables, which are key in the formulation,

$$\tilde{\gamma}_{ij} = e^{-4\phi}\gamma_{ij} \,, \tag{7.43a}$$

$$\tilde{A}_{ij} = e^{-4\phi}\left(K_{ij} - \frac{1}{3}\gamma_{ij}K\right) \,, \tag{7.43b}$$

$$\phi = \frac{1}{12}\ln\,\gamma \,, \tag{7.43c}$$

$$\tilde{\Gamma}^i \equiv \tilde{\gamma}^{jk}\tilde{\Gamma}^i{}_{jk} = -\tilde{\gamma}^{ij}{}_{,j} \,, \tag{7.43d}$$

where $\gamma = \det(\gamma_{ij})$ is the determinant of the physical metric $\gamma_{ij}$. The conformal factor in (7.43a) is chosen such that the determinant of the conformal metric $\tilde{\gamma}_{ij}$ is unity, cf. Equation 7.43c. The new variables are tensor densities with weight 1/6 for $\phi$ and $-2/3$ for $\tilde{\gamma}_{ij}$ and $\tilde{A}_{ij}$. In total, the BSSN system consists of 17 variables $\{\phi, K, \tilde{\gamma}_{ij}, \tilde{A}_{ij}, \tilde{\Gamma}^i\}$ whose evolution in time is derived from the ADM system. This results in the following coupled system of PDEs,

$$\partial_t\phi = -\frac{1}{6}\alpha K + \beta^k\partial_k\phi + \frac{1}{6}\partial_k\beta^k \,, \tag{7.44}$$

$$\partial_t\tilde{\gamma}_{ij} = -2\alpha\tilde{A}_{ij} + \beta^k\partial_k\tilde{\gamma}_{ij} + \tilde{\gamma}_{ik}\partial_j\beta^k + \tilde{\gamma}_{jk}\partial_i\beta^k - \frac{2}{3}\tilde{\gamma}_{ij}\partial_k\beta^k, \,, \tag{7.45}$$

$$\partial_t K = \alpha\left(\tilde{A}_{ij}\tilde{A}^{ij} + \frac{1}{3}K^2\right) - \gamma^{ij}\mathrm{D}_i\mathrm{D}_j\alpha + \beta^k\partial_k K \,, \tag{7.46}$$

$$\begin{aligned}\partial_t\tilde{A}_{ij} = {}& \alpha\left(K\tilde{A}_{ij} - 2\tilde{A}_{ik}\tilde{A}^k{}_j\right) + e^{-4\phi}\big(\alpha R_{ij} - \mathrm{D}_i\mathrm{D}_j\alpha\big)^{TF} + \\ & \beta^k\partial_k\tilde{A}_{ij} + \tilde{A}_{ik}\partial_j\beta^k + \tilde{A}_{jk}\partial_i\beta^k - \frac{2}{3}\tilde{A}_{ij}\partial_k\beta^k \,,\end{aligned} \tag{7.47}$$

$$\begin{aligned}\partial_t\tilde{\Gamma}^i = {}& 2\alpha\left(\tilde{\Gamma}^i_{jk}\tilde{A}^{jk} - \frac{2}{3}\tilde{\gamma}^{ij}K_{,j} + 6\tilde{A}^{ij}\phi_{,j}\right) - 2\tilde{A}^{ij}\alpha_{,j} + \tilde{\gamma}^{jk}\beta^i{}_{,jk} + \frac{1}{3}\tilde{\gamma}^{ij}\beta^k{}_{,jk} + \beta^j\tilde{\Gamma}^i{}_{,j} \\ & -\tilde{\Gamma}^j\beta^i{}_{,j} + \frac{2}{3}\tilde{\Gamma}^i\beta^j{}_{,j} \,.\end{aligned} \tag{7.48}$$

The superscript $[\cdots]^{TF}$ denotes the trace-free part with respect to the physical metric $\gamma_{ij}$, and

$$\mathrm{D}_i\mathrm{D}_j\alpha = \partial_i\partial_j\alpha - 4\partial_{(i}\phi\partial_{j)}\alpha - \tilde{\Gamma}^k_{ij}\partial_k\alpha + 2\tilde{\gamma}_{ij}\tilde{\gamma}^{kl}\partial_k\phi\partial_l\alpha \,. \tag{7.49}$$

The Ricci tensor $R_{ij}$ is now written as a sum of two pieces

$$R_{ij} = \tilde{R}_{ij} + R^{\phi}_{ij} \,, \tag{7.50}$$

where $R^{\phi}_{ij}$ is derived from Equation (7.39) and is given by,

$$R^{\phi}_{ij} = -2\tilde{\mathrm{D}}_i\tilde{\mathrm{D}}_j\phi - 2\tilde{\gamma}_{ij}\tilde{\mathrm{D}}^k\tilde{\mathrm{D}}_k\phi + 4\tilde{\mathrm{D}}_i\phi\tilde{\mathrm{D}}_j\phi - 4\tilde{\gamma}_{ij}\tilde{\mathrm{D}}^l\phi\tilde{\mathrm{D}}_l\phi \,, \tag{7.51}$$

$$\tilde{R}_{ij} = -\frac{1}{2}\tilde{\gamma}^{mn}\tilde{\gamma}_{ij,mn} + \tilde{\gamma}_{k(i}\tilde{\Gamma}^k{}_{,j)} + \tilde{\Gamma}^k\tilde{\Gamma}_{(ij)k} + \tilde{\gamma}^{mn}\left(2\tilde{\Gamma}^k{}_{m(i}\tilde{\Gamma}_{j)kn} + \tilde{\Gamma}^k{}_{in}\tilde{\Gamma}_{kmj}\right) \,. \tag{7.52}$$

For this system to be analytically equivalent to the ADM system above, the introduced auxiliary variables have to satisfy the following constraints,

$$\bar{\gamma}^{ij}\bar{A}_{ij} = 0 \,, \tag{7.53}$$

$$\det\bar{\gamma}_{ij} = 1 \,, \tag{7.54}$$

$$\tilde{\Gamma}^i = \tilde{\gamma}^{jk}\tilde{\Gamma}^i_{jk} \,, \tag{7.55}$$

resulting from the definitions (7.43). These constraints can be enforced during evolution as follows,

- To enforce (7.53), replace $\tilde{A}_{ij}$ by

$$\tilde{A}_{ij} = \tilde{A}_{ij} - \frac{1}{3}\tilde{\gamma}_{ij}\tilde{\gamma}^{kl}\tilde{A}_{kl} \,, \tag{7.56}$$

  after every time step. This was shown to have improved stability properties in [20].

- For (7.54), scale the metric $\tilde{\gamma}_{ij}$ after every time step by

$$\tilde{\gamma}_{ij} = \tilde{\gamma}^{-1/3}\tilde{\gamma}_{ij} \,, \tag{7.57}$$

- Only use the variable $\tilde{\Gamma}^i$ in places where it is differentiated, and replace it by

$$\tilde{\Gamma}^i = \tilde{\gamma}^{jk}\tilde{\Gamma}^i_{jk} \,, \tag{7.58}$$

  everywhere else [20].

To complete the specification of the BSSN formulation, we present the Hamiltonian and momentum constraints. In the new variables, the constraints (7.28) are given as [401],

$$\mathcal{H} \equiv e^{-4\phi}\tilde{\gamma}^{ij}(\tilde{R}_{ij} + \tilde{R}^{\phi}_{ij}) - \tilde{A}_{ij}\tilde{A}^{ij} + \frac{2}{3}K^2 = 0 \,, \tag{7.59a}$$

$$\mathcal{M}^i \equiv \mathrm{D}_j\tilde{A}^{ij} + 6\tilde{A}^{ij}\phi_{,j} - \frac{2}{3}\tilde{\gamma}^{ij}K_{,j} = 0 \,, \tag{7.59b}$$

These constraints are not enforced during evolution, but merely used to monitor the evolution.

In general, formulations of the Einstein field equations in 3+1 form are not limited to the ADM or BSSN evolution equations. One can always add arbitrary multiples of the constraint equations to the right hand side of the 3+1 equations to recover new equations, possibly with differing levels of well-posedness, and hyperbolicity. Indeed, many formulations employing this procedure have been introduced in the literature. In addition, one can also introduce spatial derivatives of existing variables as new independent variables, effectively introducing new sets of subsidiary constraints. We refer the reader to [346, 324] for reviews on the formulation problem in numerical relativity.

## 7.7 Coordinate Conditions

The lapse function $\alpha$ and shift vector $\beta^i$, collectively referred to as gauge variables, encode information about the choice of coordinate system. There is no evolution equations for the gauge variables from the Einstein field equations, a feature representing the coordinate freedom in general relativity. These functions are thus freely specifiable and have to be specified before one can proceed with the evolution. The issue of gauge conditions in numerical relativity is quite involved, we discuss some common choices below and refer the reader to [180, 49] for the theoretical basis underlying these choices.

### Geodesic coordinates

The simplest choice of slicing is the geodesic slicing. This slicing, which corresponds to unit lapse, along with a vanishing shift constitute the geodesic coordinates (also Gaussian-normal coordinates),

$$\alpha = 1 \,, \tag{7.60a}$$

$$\beta^i = 0 \,. \tag{7.60b}$$

In this case, the coordinate time $t$ coincides with the proper time of Eulerian observers. This choice of gauge may seem appealing at first, due to its simplicity. But it is singularity seeking in nature, a feature that makes it a poor coordinate choice. To clarify, consider the evolution of the trace of the extrinsic curvature,

$$\partial_t K - \beta^i \mathrm{D}_i K = -\mathrm{D}^2\alpha + \alpha\left(K_{ij}K^{ij} + 4\pi(\rho + S)\right) \,. \tag{7.61}$$

Applying the gauge condition (7.60), results in

$$\partial_t K = \alpha \left( K_{ij} K^{ij} + 4\pi(\rho + S) \right) \ . \tag{7.62}$$

Because the terms on the right hand side of (7.62) are always positive[2], $K$ increases monotonically without bound. This has the implication that the volume element of the Eulerian observers approaches zero due to the relation,

$$\partial_t \ln \gamma^{1/2} = -K \ . \tag{7.63}$$

As a result, the Geodesic gauge is prone to formation of coordinate singularities.

### Maximal slicing

To circumvent problems associated with the Geodesic gauge condition, one can put a constraint in place to keep the volume elements of the Eulerian observers constant. A common choice along this line of thought is Maximal slicing, characterized by the imposition

$$K = 0 = \partial_t K \ , \tag{7.64}$$

which is valid for asymptotically flat space times. Equation (7.61), now results in an Elliptic equation for the lapse,

$$\mathrm{D}^2 \alpha = \alpha \left( K_{ij} K^{ij} + 4\pi(\rho + S) \right) \ . \tag{7.65}$$

Typically, one solves (7.65) while fixing $K$ constant by not evolving (7.46) within the BSSN formulation. This is done to constrain $K$ from drifting away from its initial value, due to numerical errors during evolution [20, 18]. The maximal slicing gauge has geometrical advantages over some gauge choices. Moreover, it is designed to be singularity avoiding. However, it requires the numerical solution of an Elliptic PDE during evolution. This is computational undesirable since the solution of (7.65) may dominate the computational effort, especially in 3D simulations.

### Harmonic coordinates

Harmonic coordinates are obtained by requiring that the spacetime coordinates satisfy the harmonic condition,

$$\nabla^a \nabla_a x^b = 0 \ , \tag{7.66}$$

[2] That the second term is positive is guaranteed by the strong energy condition.

where the d'Alembertian operator $\nabla^a\nabla_a$ is taken with respect to the full metric of the spacetime $g_{ab}$. Imposing the condition (7.66) is equivalent to the requirement that

$$g^{ab\,(4)}\Gamma^c{}_{ab} = 0 \,, \tag{7.67}$$

where $g_{ab}$ is the 4-metric of the spacetime, and ${}^{(4)}\Gamma^a{}_{bc}$ is the connection associated with $g_{ab}$. Through the condition (7.67), one can derive evolution equations for the lapse $\alpha$ and shift vector $\beta^i$, thereby prescribing the harmonic gauge. However, one is not constrained to do so, as the condition can be applied separately for the time coordinate,

$$\nabla^a\nabla_a t = 0 \Rightarrow g^{ab\,(4)}\Gamma^0{}_{ab} = 0 \,, \tag{7.68}$$

leading to the harmonic slicing condition,

$$\left(\partial_t - \beta^i\partial_i\right)\alpha = -K\alpha^2 \,. \tag{7.69}$$

In the case where the condition is applied to the full spacetime coordinates, the slicing condition (7.69) is supplemented by the shift condition

$$\left(\partial_t - \beta^i\partial_i\right)\beta^i = -\alpha^2\left(\gamma^{ij}\partial_j \ln\ \alpha + \gamma^{jk}\Gamma^i_{jk}\right) \,. \tag{7.70}$$

The gauge condition (7.69)–(7.70) reduces the Einstein field equations into a set of non-linear hyperbolic wave equations which can be appealing for certain problems [404, 247, 171].

### Bona-Massó slicing

This is a family of slicing conditions, for which the lapse is chosen to satisfy [69],

$$\left(\partial_t - \beta^i\partial_i\right)\alpha = -K\alpha^2 f(\alpha) \,. \tag{7.71}$$

There are several common choices for the arbitrary function $f(\alpha) \geq 0$. For the particular case of $f(\alpha) = 0$ we recover the Geodesic slicing condition, assuming that $\alpha = 1$ initially. With the choice $f(\alpha) \to \infty$, one recovers the maximal slicing condition. A particularly interesting choice is $f(\alpha) = 2/\alpha$. In this case, (7.71) reduces to

$$\left(\partial_t - \beta^i\partial_i\right)\alpha = -2K\alpha \,, \tag{7.72}$$

which is commonly referred to as $1 + \log$ slicing [69, 26]. This is a reference to the fact that for $\beta^i = 0$, Equation (7.72) can be analytically solved to yield,

$$\alpha = 1 + \ln \gamma \, . \tag{7.73}$$

The slicing (7.72) is typically used in black hole spacetimes, along with a gamma freezing condition for the shift vector $\beta^i$ [19],

$$\left(\partial_t - \beta^i \partial_i\right) \beta^i = \frac{3}{4} B^i \, , \tag{7.74a}$$

$$\left(\partial_t - \beta^i \partial_i\right) B^i = \partial_t \tilde{\Gamma}^i - \eta B^i \, , \tag{7.74b}$$

where $\eta$ is a constant, typically chosen to be $\eta = 1/(2M)$ for a black hole of mass $M$. The combination (7.72) with (7.74) leads to stable evolution of puncture black hole spacetimes along with the BSSN formulation.

## 7.8 Evolving Black Hole Spacetimes

### 7.8.1 Dealing with Singularities

Black holes have a curvature singularity at their core, where the curvature of spacetime becomes infinite. This is one of the most challenging features of general relativity, both from a theoretical and numerical perspective. When considering numerical simulations of black holes, one is confronted with the question of how to numerically represent the singularity. There are three avenues that one could consider and we list them below,

#### Singularity avoidance

When evolving initial data of Misner or Brill-Lindquist type, one is essentially presented with coordinate singularities, with the physical singularity due to appear later in the evolution. During evolution, there are means through which one can 'avoid' the singularity. The concept of singularity avoidance is achieved through the slicing condition. The key idea is to choose smaller values of the lapse function in regions of spacetime where a singularity is about to appear. Because the lapse function relates coordinate and proper time through,

$$d\tau = \alpha dt \, . \tag{7.75}$$

this strategy has the desirable effect of slowing down time closer to the singularity, and thus allowing longer evolution times,

$$t \to \infty \qquad \text{as} \qquad \alpha \to 0 \,. \tag{7.76}$$

Maximal slicing and the $1+\log$ slicing condition have better singularity avoidance properties. These slicing conditions usually lead to the collapse of the lapse effect [311]. When using the geodesic slicing condition, one does not avoid the singularity but in fact rapidly approaches it. It can be shown that with this slicing condition, one will encounter the singularity at time $t = \pi M$ for a single Schwarzschild black hole of mass $M$.

While the singularity avoidance technique is an attractive feature, it does lead to an undesirable effect on the overall evolution. This can be illustrated from the fact that since time is effectively frozen inside the black hole while being required to evolve outside, large gradients in the metric fields develop near the horizon, thereby requiring more grid points at the black hole throat to resolve the fields and determine the gradients with reliable accuracy. This phenomenon is called grid stretching and with finite computational resources will eventually cause the simulation to terminate.

### Excision

In the excision approach one excises the singularity, along with some region of spacetime within the apparent horizon, out of the computational domain. The technique itself relies on the fact that black hole interiors are causally disconnected from the surrounding exterior domain so that whatever dynamics inside the horizon cannot affect the physics outside of it. Numerically, excision is done by imposing ingoing boundary conditions on the excision boundary, a region of spacetime near the horizon. Of course in the case where the black hole is moving, one has to dynamically relocate the excision boundary. This procedure has been used successfully in stable evolutions of black hole spacetimes [369, 20, 126, 347, 316].

### Punctures

The puncture approach in its original form consisted of analytically factoring out the singular terms from the metric. These terms are then analytically differentiated, while the remaining terms are numerically differentiated without trouble. This is referred to as the static puncture method. Although this method works well in dealing with the singular terms in the metric, it forces the punctures to remain at a fixed coordinate position, even when the black holes involved in the simulation have non-zero linear momentum.

A breakthrough in long term simulations of black hole spacetimes came with the advent of the moving puncture method. In this method, the singularities are not factored out like in the static puncture method but are evolved directly, through a conformal factor in the BSSN formulation. Of course, one must ensure that the singular point corresponding to $r = 0$ does not align with a grid node during discretization. This amounts to using a staggered cell-centered grid, as opposed to a vertex centered grid. The puncture approach has become the method of choice for evolving black hole universes. These are cosmological models which are made up of a regular lattice of black holes [55, 402].

There are slight variations of the moving puncture method, related to which conformal factor one evolves within the BSSN evolution equations. Consider the conformal factor,

$$\psi = (\det \gamma_{ij})^{1/12} \, . \tag{7.77}$$

One has the following options,

- ***The $\phi$-method***

  This method is characterized by the choice

  $$\phi = \ln \psi \, , \tag{7.78}$$

  and one recovers the original BSSN system of equations (7.44)–(7.48). As a cautionary note for puncture evolutions, we note that $\phi$ has a $\mathcal{O}(\ln \, r)$ singularity at the puncture.

- ***The $\chi$-method***

  This method is characterized by the choice,

  $$\chi = \psi^{-4} \, , \tag{7.79}$$

  $$\partial_t \chi = \frac{2}{3} \chi \alpha K + \beta^i \partial_i \chi - \frac{2}{3} \chi \partial_i \beta^i \, . \tag{7.80}$$

  as was advocated in [94]. The variable $\chi$ is $C^4$ at the puncture and thus better behaved. However, the final BSSN equations resulting from the use of $\chi$ will include terms involving divisions by $\chi$. To avoid infinities during evolution, one must ensure that $\chi$ is never zero by consistently replacing it by some small positive number in cases when it gets too close to zero.

- ***The $W$-method***

This method is much similar in spirit to the $\chi$-method. In this case, the conformal factor is given by

$$W = \psi^{-2} \,, \tag{7.81}$$

$$\partial_t W = \frac{1}{3} W \alpha K + \beta^i \partial_i W - \frac{1}{3} W \partial_i \beta^i \,. \tag{7.82}$$

The major difference with the $\chi$-method, is that one does not have to manually ensure that the conformal factor, $W$ in this case, is non-zero [274]. This is our method of choice when evolving black hole spacetimes.

### 7.8.2 Locating Horizons

#### Apparent horizon

Finding apparent horizons is an important problem in numerical relativity, especially in the studies of black hole spacetimes or other relativistic collapse phenomena. An apparent horizon is defined simply as the outermost marginally trapped surface [202]. This is the surface where the expansion $H$ of outgoing null geodesics vanishes. Such a surface is given by [405, 188],

$$0 \equiv H = \mathrm{D}_i n^i + n^i n^j K_{ij} - K \,, \tag{7.83}$$

where $n^i$ is the outward pointing unit 3-vector normal to the horizon surface and $\mathrm{D}_i$ is the covariant derivative associated with the 3-metric $\gamma_{ij}$. It is useful to characterize the horizon surface as some level set of a scalar function

$$F(x^i) = 0 \,. \tag{7.84}$$

The unit normal vector $n^i$ can then be written in terms of $F$ as,

$$n^i = \frac{s^i}{\|s^k\|} \qquad \text{where} \qquad s^i = \gamma^{ij} \mathrm{D}_j F \,, \tag{7.85}$$

such that $n^i n_i = 1$ and $n^i s_i = 0$, and it is to be understood that the norm is taken with respect to the 3-metric, $\|s^k\| = \sqrt{\gamma^{ij} s_i s_j}$.

A common assumption in most apparent horizon finders is that the apparent horizon has $S^2$ topology, and is such that each radial coordinate line intersects the horizon at exactly one point. This configuration is referred to as a Strahlkörper shape [336, 370] and guarantees

that the function $h(\theta, \phi)$, in the parametrization of the horizon surface,

$$F(r, \theta, \phi) = r - h(\theta, \phi) \ , \tag{7.86}$$

will remain single-valued. One then proceeds to expand the function $h(\theta, \phi)$ in spherical harmonics

$$h(\theta, \phi) = \sum_{l=0}^{l_{max}} \sum_{m=-l}^{l} \sqrt{4\pi} a_{lm} Y_{lm}(\theta, \phi) \ . \tag{7.87}$$

The goal of minimization methods is to vary the $a_{lm}$, and compute a trial horizon surface through the computation of the function $F(r, \theta, \phi)$ in (7.86) and hence the expansion $H$ in (7.83). An apparent horizon is considered found if one can find coefficients $a_{lm}$'s that minimize the surface integral,

$$\mathcal{S} = \int H^2 d\Omega \ . \tag{7.88}$$

This method is appealing because of its simplicity and ease of implementation. However several caveats are in order. For one, minimization algorithms have a tendency to settle at local minima. Moreover, they can be quite slow compared to other methods within the literature, for example flow methods [15]. Nevertheless, it has been used successfully by several authors [15, 25, 76, 161].

### Event horizon

The geodesic equation plays an important role in the location of event horizons. This is because the event horizon of a black hole is traced out by out going null geodesics that never actually reach null future infinity. It is actually one of general relativity's precepts that a particle (including light) propagating in a spacetime naturally follows a geodesic. Simply put, a geodesic is a curve of shortest 'length' between two points in a manifold. The three major approaches in locating event horizons are [372, 24],

1. integrate null geodesics forwards in time.
2. integrate null geodesics backwards in time.
3. integrate null surfaces backwards in time.

The geodesic equation is given in terms of the 4-metric as [209],

$$\frac{d^2 x^a}{d\lambda^2} + {}^{(4)}\Gamma^a{}_{bc} \frac{dx^a}{d\lambda} \frac{dx^b}{d\lambda} = 0 \ . \tag{7.89}$$

where $\lambda$ is some affine parameter. When considering null-geodesics, one can split (7.89) in 3+1 form into the following system [216],

$$\frac{dx^i}{d\lambda} = \gamma^{ij}p_j - \beta^i p^0 \,, \tag{7.90}$$

$$\frac{dp_i}{d\lambda} = -\alpha\partial_i\alpha(p^0)^2 + \partial_i\beta^k p_k p^0 - \frac{1}{2}\partial_i\gamma^{lm}p_l p_m \,, \tag{7.91}$$

where,

$$p^i = \frac{dx^i}{d\lambda} \qquad \text{and} \qquad p^0 = \frac{\sqrt{\gamma^{ij}p_i p_j}}{\alpha} \,. \tag{7.92}$$

The last equality enforces the null condition $p^a p_a = 0$. A more general treatment of the geodesic equation in the 3+1 formalism can be found in [390]. In locating event horizons of numerically generated spacetimes, it is important to note that unlike apparent horizons, event horizons are a global property of a given spacetime. In general, one needs to know the full future evolution of a given slice before one can compute the event horizon there.

## 7.9 Initial Data Generation

A Cauchy formulation of the Einstein field equations require the specification of initial data. The procedure involves specifying the metric $\gamma_{ij}$ and extrinsic curvature $K_{ij}$ components on some initial spatial slice $\Sigma_0$, see [181, 127] for reviews on the subject. As we saw in §7, the ten components of the field equations reduce to six evolution and four constraint equations. Because of the constraint equations (7.28), it is not possible to freely specify all components of the fields $\gamma_{ij}$ and $K_{ij}$, as these must be chosen to satisfy (7.28). The constraint equations form a system of four coupled elliptic partial differential equations that must be solved to construct initial data for numerical space times. The four differential equations, are not enough to constrain all the twelve independent components $(\gamma_{ij}, K_{ij})$. This leaves eight undetermined components. We note that four of these represent the freedom to specify the lapse and shift. We are now left with four undetermined functions. These functions represent the two dynamical degrees of freedom characterizing the two polarization modes of gravitational waves. The constraint equations only constrain the longitudinal part of the gravitational field, leaving the transverse parts freely specifiable.

We note that there is no restriction on which of the twelve components $(\gamma_{ij}, K_{ij})$ are constrained by Equations 7.28. Under certain conditions, one can unambiguously separate out the longitudinal from the transverse parts of the fields. In general however, such a simplification is not possible. In this case one relies on decompositions of $\gamma_{ij}$ and $K_{ij}$ that often

allow, at least approximately, a convenient splitting of the longitudinal from the transverse parts. Typically, such decompositions also result in simpler Elliptic forms for the constraint equations that can be solved once appropriate boundary conditions are specified.

A simplification arises when one considers a moment of time symmetry. At the moment of time symmetry, the extrinsic curvature satisfies $K_{ij} = 0$, implying $K = 0$. This is because at this point, the line element of the full space time is invariant under time reversal $t \to -t$. This further implies the vanishing of the shift vector $\beta_i = 0$. In this case, the momentum constraint decouples from the Hamiltonian constraint and is trivially satisfied.

### 7.9.1 York Lichnerowicz Conformal Decomposition

Under the conformal transformation (7.36), the Hamiltonian constraint equation becomes

$$8\bar{\mathrm{D}}^2\psi - \psi\bar{R} - \psi^5 K^2 + \psi^5 K_{ij}K^{ij} = -16\pi\psi^5\rho \,, \tag{7.93}$$

where $\bar{\mathrm{D}}^2 = \tilde{\gamma}^{ij}\bar{\mathrm{D}}_i\bar{\mathrm{D}}_j$ is the Laplacian operator and $\bar{R}$ is the Ricci scalar associated with the conformal metric $\tilde{\gamma}_{ij}$. Incorporating the traceless decomposition of the extrinsic curvature $K_{ij}$ from (7.41) along with the conformal transformation (7.42) with $\alpha = -10$, the Hamiltonian constraint (7.93) reduces to the following Elliptic equation for the conformal factor $\psi$,

$$8\bar{\mathrm{D}}^2\psi - \psi\bar{R} - \frac{2}{3}\psi^5 K^2 + \psi^{-7}\bar{A}_{ij}\bar{A}^{ij} = -16\pi\psi^5\rho \,, \tag{7.94}$$

Now, given the conformal metric, the solution of (7.94) will allow a reconstruction of the physical metric $\gamma_{ij}$. However, unless one is considering time symmetric data, one cannot ignore the coupling with the extrinsic curvature terms.

To close the system, we now turn to the momentum constraint, which when written in terms of $\bar{A}_{ij}$ becomes,

$$\bar{\mathrm{D}}_j\bar{A}^{ij} - \frac{2}{3}\psi^6\bar{\mathrm{D}}_i K = 8\pi\psi^{10}j^i \,. \tag{7.95}$$

The momentum constraint can be further simplified by considering the Scalar-Vector-Tensor irreducible splitting of $A^{ij}$ i.e. the splitting of $A^{ij}$ into a transverse traceless part and a longitudinal part $A^{ij} = A^{ij}_{TT} + A^{ij}_{L}$. In such a splitting the longitudinal part is given as,

$$\bar{A}^{ij}_L = \bar{\mathrm{D}}^i W^j + \bar{\mathrm{D}}^j W^i - \frac{2}{3}\bar{\gamma}^{ij}\bar{\mathrm{D}}_j W^j \,, \tag{7.96}$$

in terms of the conformal metric $\bar{\gamma}_{ij}$. The rationale behind such a splitting lies in the fact that the transverse-traceless part satisfies $\bar{\mathrm{D}}_i\bar{A}^{ij}_{TT} = 0$ and thus drops out of the conservation

equation (7.95) and one is left with,

$$\bar{\Delta}_L \bar{W}^i - \frac{2}{3}\psi^6 \bar{\mathrm{D}}_i K = 8\pi\psi^{10} j^i \ , \tag{7.97}$$

where the vector Laplacian $\Delta_L$ operator is given as,

$$\Delta_L \bar{W}^i = \bar{\mathrm{D}}^2 \bar{W}^i + \frac{1}{3}\bar{\mathrm{D}}^i \bar{\mathrm{D}}_j + \bar{R}^i{}_j \bar{W}^j \ . \tag{7.98}$$

Equations (7.94) and (7.97) can now be solved for the conformal factor $\psi$ and the vector potential $W^i$ to generate initial data. However, one needs to specify the remaining variables, i.e. $A^{ij}_{TT}$, $\bar{\gamma}_{ij}$ and $K$. The choice of these should reflect the physics of one's problem, while simultaneously simplifying the resulting equations, where possible. Common choices include,

- ***Transverse traceless part of*** $A^{ij}$

  One can chose the condition,

  $$A^{ij}_{TT} = 0 \ . \tag{7.99}$$

  From a physical standpoint, this choice can be interpreted as requiring that the gravitational wave content in the initial data be minimal.

- ***Trace of the extrinsic curvature*** $K$

  One can choose that $K$ be constant. Note that with this choice, the momentum constraint equation (7.97) decouples from the Hamiltonian constraint equation (7.95). Apart from resulting in simpler equations, this choice is associated with the constant mean curvature spatial hypersurface. One can also use the gauge freedom at the initial slice to achieve $K = 0$ through the maximal slicing condition. A closely related assumption is that of time symmetry, characterized by the vanishing of the extrinsic curvature $K_{ij} = 0$. With these assumptions, one proceeds by first solving the Momentum constraint (7.95) and finally solving the Hamiltonian constraint separately.

  Without these simplifying assumptions, one can still proceed albeit with more complexity, as the constraint equations do not decouple [220].

- ***Conformal metric*** $\bar{\gamma}_{ij}$

  For most astrophysical problems, it is reasonable to assume conformal flatness, characterized by,

  $$\bar{\gamma}_{ij} = \delta_{ij} \ , \tag{7.100}$$

where $\delta_{ij}$ is the Kronecker delta symbol. This choice can be interpreted to mean that far from the source, the metric is only weakly curved, thus essentially flat.

To conclude this section we note that the decomposition of the Momentum constraint presented above is commonly referred to as the *Conformal transverse decomposition*, a reference to the fact that the decomposition was presented in terms of $\bar{A}^{ij}$. One can proceed in a similar manner starting from the Momentum constraint in terms of the physical $A^{ij}$ instead of the conformal $\bar{A}^{ij}$, which is given by

$$\mathrm{D}_j A^{ij} - \frac{2}{3}\mathrm{D}_i K = 8\pi j^i \,. \tag{7.101}$$

Following this route leads to what is referred to as the *Physical transverse decomposition*.

### 7.9.2 Conformal Thin Sandwich Approach

The Conformal thin sandwich approach can be viewed as an alternative to the York Lichnerowicz conformal decomposition approach to initial data generation [406, 127]

### 7.9.3 Black Hole Initial Data

The simplest black hole solution is the Schwarszchild solution, representing a static non rotating black hole. By applying the decomposition techniques described in the previous sections one can generate black hole spacetimes in a more systematic way. We present two such cases below, representing time symmetric and Bowen-York initial data.

#### Time symmetric data

For time symmetric data, characterized by the vanishing of the extrinsic curvature $K_{ij} = 0$, the momentum constraint is trivially satisfied. The Hamiltonian constraint equation (7.94) then reduces to,

$$\tilde{\mathrm{D}}^2\psi = \frac{1}{8}\psi\tilde{R} \,. \tag{7.102}$$

If we further assume that the spacetime is conformally flat

$$\tilde{\gamma}_{ij} = \delta_{ij} \,, \tag{7.103}$$

we are led to the vanishing of the associated Ricci tensor and Ricci scalar, $\tilde{R}_{ij} = 0 = \tilde{R}$. Using this fact reduces Equation (7.102) to the much simpler form,

$$\bar{\mathrm{D}}^2\psi = 0 \,. \tag{7.104}$$

This is in fact Laplace equation which can be analytically solved, given suitable boundary conditions. We are interested in solutions that describe asymptotically flat space times, $\psi|_\infty = 1$. Imposing this requirement leads to the solution,

$$\psi = 1 + \frac{\mathcal{M}}{2r} \,. \tag{7.105}$$

Reconstructing the spatial metric from this solution leads to the familiar vacuum Schwarszchild solution for a Schwarszchild black hole with mass $\mathcal{M}$, in isotropic coordinates,

$$dl^2 = \psi^4[dr^2 + r^2(d\theta^2 + \sin^2\theta d\phi^2)] \,, \tag{7.106}$$

$$= \psi^4 \delta_{ij} dx^i dx^j \,. \tag{7.107}$$

For binary black hole initial data, one simply uses the fact that the Laplace equation (7.104) is linear and thus the solution $\psi$ will be made up of the individual contributions of the two black holes,

$$\psi = 1 + \frac{\mathcal{M}_1}{2r_1} + \frac{\mathcal{M}_2}{2r_2} \,. \tag{7.108}$$

This solution is often used (along with the Puncture method) for the simulation of head-on collisions of binary black holes initially at rest at a moment of time symmetry.

### Bowen-York initial data

The time symmetric solution presented in the previous section does not accommodate the possibility of the black hole to have any linear momentum $P^i$ or spin $S^j$. Indeed, these quantities are encoded in the extrinsic curvature $A^{ij}$ which vanishes for time symmetric data. If we do away with the assumption of vanishing extrinsic $K_{ij} = 0$, and retain only the conformal flatness assumption $\bar{\gamma}_{ij} = \delta_{ij}$ and maximal slicing condition $K = 0$, the momentum constraint (7.97) reduces to,

$$\bar{\Delta}_L \bar{W}^i = 0 \,, \tag{7.109}$$

or in terms of $\bar{A}^{ij}$

$$\bar{\mathrm{D}}_j \bar{A}^{ij} = 0 \,. \tag{7.110}$$

This equation can be shown to admit the following solution for $\bar{A}^{ij}$,

$$\bar{A}^{ij} = \frac{3}{2r^2}\left[P^i n^j + P^j n^i - (\delta^{ij} - n^i n^j)P^k n_k\right] + \frac{3}{r^3}\left(\epsilon^{ikl} S_k n_l n^j + \epsilon^{jkl} S_k n_l n^i\right) \ , \tag{7.111}$$

where $n^i = x^i/r$ and $r = \sqrt{x^2 + y^2 + z^2}$. The solution (7.111) is known as the Bowen-York solution [70], from which one can reconstruct the extrinsic curvature $K_{ij} = \psi^{-2}\bar{A}_{ij}$, once a solution for $\psi$ has been obtained. For this, we return to the Hamiltonian constraint (7.94), which reduces to

$$\bar{\mathrm{D}}^2\psi + \frac{1}{8}\psi^{-7}\bar{A}_{ij}\bar{A}^{ij} = 0 \ . \tag{7.112}$$

Unlike in the time symmetric case, this equation does not admit any known analytic solutions. It is thus solved using a numerical Elliptic solver. Owing to the linearity of the Momentum constraint (7.110), one can generate solutions for multiple black holes by adding up the individual contributions, which in the binary black hole case becomes

$$\bar{A}^{ij} = \bar{A}_1^{ij} + \bar{A}_2^{ij} \ . \tag{7.113}$$

An important point worth mentioning is that while the time symmetric data for a single black hole reduces to a slice of the well known Schwarzschild solution, Bowen-York initial data for a single spinning black hole with $P^i = 0$ and $S_j \neq 0$ does not constitute a constant time slice of the Kerr spacetime as one would ordinarily expect [177]. This result should not seem overly strange, given our assumption of conformal flatness in the construction of Bowen-York initial data. It has been fairly established, under certain restrictions, that the Kerr spacetime does not admit any slicing that would render it conformally flat [170, 241]. The implication is that a Bowen-York rotating black hole is not static, but contains gravitational radiation, which when radiated away will asymptotically settle to a Kerr space time in the future.

# Chapter 8

# Elements of Numerical Implementation

## 8.1 Numerical Tensor Manipulation

### 8.1.1 Elementary Operations

One of the challenges in numerically solving the Einstein field equations is how to translate the associated tensorial quantities into computer code once a suitable formulation has been chosen. Ideally one would want a less error prone method that is also efficient computationally. Take for instance the evaluation of the following contraction,

$$T_{cd} \;=\; S^{ab} P_{abcd} \,, \tag{8.1}$$

where summation is implied over repeated indices according to Einstein summation convention. The components of the tensor $T_{ab}$ are understood to be given by,

$$T_{kl} = \sum_{i=0}^{2} \sum_{j=0}^{2} S^{ij} P_{ijkl} \,. \tag{8.2}$$

To compute this expression in C code for example, one would have to use loops, resulting in code that resembles the following snippet,

```
for(int c = 0; c < 3; c++)
{
   for(int d = 0; d < 3; d++)
   {
```

```
        T(c, d) = 0.0;
        for(int a = 0; a < 3; a++)
        {
            for(int b = 0; b < 3; b++)
            {
                T(c, d) += S(a, b) * P(a, b, c, d);
            }
        }
    }
}
```

Needless to say, this exercise is error prone. Coding the BSSN evolution equations (see §7.6) in this manner becomes a computational nightmare. In addition, switching to a different formulation of the Einstein field equations proves to be arduous as it entails a similar error prone exercise.

We deal with this complexity by developing a new Tensor Package especially designed to do numerical computation. One of the attractive features of this tensor package is that one can use abstract tensor notation to write numerical formulas. For example, to do the contraction (8.1) above, one only has to write the following snippet of code,

```
Index<'a'> a;
Index<'b'> b;
Index<'c'> c;
Index<'d'> d;

T(c, d) = S(a, b) * P(a, b, c, d);
```

The philosophy of our design is similar to that of FTensor [246] and LTensor [253] and relies heavily on principles of Expression Templates and Template Metaprogramming. We have incorporated within this package, elementary tensor operations like addition, subtraction, contraction and tensor product operations. The result is that writing tensor equations into computer code becomes as simple as writing them on paper. Other approaches that have been used within the numerical relativity community include the use of computer algebra packages such as Mathematica in the case of Kranc [218]. Kranc uses the built-in tensor operations within Mathematica to turn abstract tensorial equations into their corresponding components. The resulting system can then be converted to C or Fortran code.

When developing a tensor package, a question arises on whether to make a distinction between the tensors $T_{ab}, T^{a}{}_{b}, T_{a}{}^{b}$ and $T^{ab}$ while using the same symbol $\mathbf{T}$ for all of them

or to use different symbols for each one of them. In principle, such a distinction can be made possible. For example, one can use uppercase letters to indicate upper indices and lower case letters to indicate lower indices or some other analogous method. The problem with this approach is that one will have to specify a metric before defining tensors. While this is obvious from a theoretical standpoint, it can lead to programming difficulties in the implementation. We have thus opted to use a Cartesian tensor notation, where all indices appear as lower indices. The contraction (8.1) then becomes,

$$T_{cd} \quad = \quad S_{ab} P_{abcd} \; . \tag{8.3}$$

With this notation, separate symbols for each of $T_{ab}, T^{a}_{\ b}, T_{a}^{\ b}$ and $T^{ab}$ will have to be used, if required. This notation has (so far) not led to any difficulties.

### 8.1.2 Expression Templates

We utilize expression templates to unroll the loops associated with our compact representation of tensor operations. Expression templates are a feature of the C++ language. The technique itself was actually discovered by accident, and has since been adopted for optimizing numerical libraries [388]. There is a significant amount of jargon involved in any discussion of Expression Templates. We instead refer the reader to [387] and references therein.

### 8.1.3 Coordinate Transformations

Although the code itself does the integration on a Cartesian grid, it is possible to initialize or output tensor components in other coordinate systems. This functionality relies on the fact that transformation properties of tensors of a given rank are the same. For instance to transform the components of a rank-2 tensor $S_{ab}$ from coordinates $x^a$ to some other coordinates $x'^a$ one uses the transformation rule,

$$S'_{ab} = \frac{\partial x^c}{\partial x'^a} \frac{\partial x^d}{\partial x'^b} S_{cd} \; , \tag{8.4}$$

$$= T^{c}_{\ a} T^{d}_{\ b} S_{cd} \; , \tag{8.5}$$

where each of the $T^{c}_{\ a} = \partial x^c / \partial x'^a$ is a transformation matrix. In general, for a rank $k$ tensor, we have

$$S'_{ab\cdots k} = T^{c}_{\ a} T^{d}_{\ b} \cdots T^{l}_{\ k} S_{cd\cdots l} \tag{8.6}$$

As an example, to move from Spherical $(r, \theta, \phi)$ to Cartesian $(x, y, z)$ coordinates, we have the following relations,

$$x = r\sin(\theta)\cos(\phi)\,, \qquad r = \sqrt{x^2+y^2+z^2}\,, \tag{8.7}$$

$$y = r\sin(\theta)\sin(\phi)\,, \qquad \theta = \arctan\left(\frac{\sqrt{x^2+y^2}}{z}\right)\,, \tag{8.8}$$

$$z = r\cos(\theta)\,, \qquad \phi = \arctan\left(\frac{y}{x}\right)\,. \tag{8.9}$$

The transformation matrix ${T^c}_a$ can then be computed to be,

$${T^c}_a = \begin{pmatrix} \frac{x}{r} & \frac{xz}{r^2\sqrt{x^2+y^2}} & \frac{-y}{x^2+y^2} \\ \frac{y}{r} & \frac{yz}{r^2\sqrt{x^2+y^2}} & \frac{x}{x^2+y^2} \\ \frac{z}{r} & -\frac{x^2+y^2}{r^2\sqrt{x^2+y^2}} & 0 \end{pmatrix}\,. \tag{8.10}$$

Of course one has to be careful to avoid the singularity associated with the point $r = 0$, which is not a problem for us since we employ a staggered grid. This transformation is handled through the function call $Scart = \mathbf{sphToCart}(\&Ssph, x, y, z)$.

When dealing with the BSSN variables, one has to keep in mind that the tensor densities $\tilde{\gamma}_{ij}$ and $\tilde{A}_{ij}$ transform in a way which is slightly different from (8.6). As a matter of fact, when initializing in a coordinate system that is not Cartesian, we first initialize the ADM variables $\gamma_{ij}$ and $K_{ij}$ which transform as tensors. We then transform from the ADM to the BSSN variables.

## 8.2 Method of Lines and False Transients

A well known technique in the numerical solution of time dependent partial differential equations is the Method of Lines (MoL). Within this framework, one converts a system of time-dependent partial differential equations into a time continuous system of ordinary differential equations by first discretizing only in the space dimensions, leaving the time dimension continuous. Standard ordinary differential equation solvers with known stability properties can then be used to advance the resulting semi-discrete system in time. This configuration has the advantage that the resulting code can be modularized in a straightforward manner. In addition, the stability analysis of the resulting system is much simpler. To illustrate the MoL

approach, consider the linear (hyperbolic) advection equation

$$\partial_t u = -\partial_x u \ . \tag{8.11}$$

Employing the MoL discretization results in the following system of ODEs,

$$\frac{du_i}{dt} = \frac{u_i - u_{i-1}}{\Delta x} \qquad i = 1, 2, \cdots, n-1 \ , \tag{8.12}$$

where $u_0$ is given by the supplied inflow boundary, and we have used a first order upwind scheme for the spatial differentiation.

The Method of lines approach is well suited to treatment of hyperbolic and parabolic partial differential equations. For elliptic type PDEs, one does not have a time variable and the method is not readily applicable. Instead, one uses the method of false transients approach [270, 296]. This uses a similar principle to the method of lines. For instance, consider the Laplace equation in 2D,

$$\partial_{xx}\psi + \partial_{yy}\psi = 0 \ . \tag{8.13}$$

One approximates (8.13) by a similar transient equation by introducing a 'time' derivative as follows,

$$\partial_\tau \psi = \partial_{xx}\psi + \partial_{yy}\psi \ . \tag{8.14}$$

The solution of (8.14) will converge to the required solution provided the criterion

$$\lim_{\tau \to \infty} \partial_\tau \psi = 0 \ , \tag{8.15}$$

is met. The procedure is then to proceed from (8.14) using the method of lines approach. The method as presented above results in a parabolic PDE. For some problems, one can transform the Elliptic PDE by using terms proportional to $\partial_{\tau\tau}$ instead. In this case, the resulting transient equation will be hyperbolic. One would then need to be careful that reflections off the boundary does not spoil the convergence to the stationary solution. Although not identified as such, the method of false transients has appeared in the numerical relativity community in slightly different contexts and is the general idea behind most parabolic and hyperbolic gauge conditions presented in, for example [35, 343, 19].

## 8.3 Spatial Discretization

Spatial differentiation is handled through fourth order convergent explicit finite differencing. We also employ a pseudo spectral approximation on Gauss-Chebyshev-Lobatto points, but we do not use it for numerical relativistic spacetimes (see §9.9.1). Other approaches that have been successfully used in the field of numerical relativity are finite elements [237, 109] and spectral methods [182, 229, 71]. We discretize our spacetime into a three dimensional uniform grid such that the $(x, y, z)$ coordinates at a point $(i, j, k)$ in the grid are given by the cell-centered discretizations

$$x_i = x_L + (i - \tfrac{1}{2})\Delta x \qquad i = 0, 1, \cdots, N_x - 1 \tag{8.16}$$

$$y_j = y_L + (j - \tfrac{1}{2})\Delta y \qquad j = 0, 1, \cdots, N_y - 1 \tag{8.17}$$

$$z_k = z_L + (k - \tfrac{1}{2})\Delta z \qquad k = 0, 1, \cdots, N_z - 1 \tag{8.18}$$

where, by default the stepsizes are given by

$$\Delta x = \frac{x_R - x_L}{N_x}, \qquad \Delta y = \frac{y_R - y_L}{N_y} \qquad \text{and} \qquad \Delta z = \frac{z_R - z_L}{N_z}. \tag{8.19}$$

We note that in cases where mesh refinement is involved, this method of discretization is only applied to the base grid, all other nested grids will inherit the properties of the parent grid. We discuss mesh refinement in §8.8 and the full implementation in Chapter 10.

Following the discretization, we apply appropriate finite difference operators to compute numerical derivatives. In particular, the first and second derivatives are given by the following operators,

$$\partial_x f_{i,j,k} = \frac{1}{12dx}[f_{i-2,j,k} - 8f_{i-1,j,k} + 8f_{i+1,j,k} - f_{i+2,j,k}], \tag{8.20}$$

$$\partial_{xx} f_{i,j,k} = \frac{1}{12dx^2}[-f_{i+2,j,k} + 16f_{i+1,j,k} - 30f_{i,j,k} + 16f_{i-1,j,k} - f_{i-2,j,k}], \tag{8.21}$$

respectively. The cross (sometimes referred to as mixed) derivative is given by sequential application of (8.20). In the case of the $xy$ derivative, this results in the operator,

$$\partial_{xy} f_{i,j,k} = \frac{1}{12dx}[\partial_y f_{i-2,j,k} - 8\partial_y f_{i-1,j,k} + 8\partial_y f_{i+1,j,k} - \partial_y f_{i+2,j,k}]. \tag{8.22}$$

We use these centered stencils for all derivatives, except the advection terms (terms like $\beta^i \partial_i$)

for which we use the lop sided formulas,

$$\begin{aligned} \partial_x f_{i,j,k} &= \frac{1}{12dx}[-f_{i-3,j,k} + 6f_{i-2,j,k} - 18f_{i-1,j,k} + 10f_{i,j,k} + 3f_{i+1,j,k}], \qquad \beta^x < 0 \\ \partial_x f_{i,j,k} &= \frac{1}{12dx}[f_{i+3,j,k} - 6f_{i+2,j,k} + 18f_{i+1,j,k} - 10f_{i,j,k} - 3f_{i-1,j,k}], \qquad \beta^x > 0 \end{aligned} \tag{8.23}$$

These formulas can be generated by using the method derived by Fornberg [168]. For lop sided stencils, see §B.2. As one moves to higher convergence order, more points are needed in the neighboring regions to accommodate the larger stencils. This has several consequences: in cases involving parallelization, there is a communication overhead associated with high order stencils. Moreover, because more floating point operations are involved, the computations are affected more by round off error.

## 8.4 The Courant-Friedrichs-Lewy Condition

In all computations in this work, we have used explicit methods. In particular, the explicit finite difference formulas above, and explicit time stepping through Runge Kutta methods (Chapter 9). Directly relevant to the stability of explicit time stepping algorithms is the concept of the Courant-Friedrichs-Lewy (CFL) condition which couples the time and space step during discretization [130]. Ordinarily, the time step $\Delta t$ is not chosen independently of the space step $\Delta x$ in an evolution but is constrained through the relation

$$\Delta t = \frac{C\Delta x}{u} \ , \tag{8.24}$$

where $u$ is some characteristic speed of the modes under consideration and $C$ is some constant typically referred to as a CFL number and satisfies $0 < C \leq 1$. This can be interpreted as saying that the numerical domain of dependence must be larger than the physical domain of dependence to maintain stability. Put simply, the time step $\Delta t$ must be smaller than the amount of time it takes for a propagating wave to move one space step $\Delta x$. Unless otherwise specified, we typically use $\Delta t = 0.25\Delta x$ in our simulations.

## 8.5 Artificial Dissipation

It is customary in Numerical relativity to add artificial dissipation to the right hand side of the evolution equations in order to remove high frequency errors and thereby stabilize some problems. For example, to evolve the gauge wave (§10.4.2) and polarized Gowdy wave initial

data with the BSSN formulation, one needs artificial dissipation to obtain stable evolutions [31]. The added dissipation terms are required to converge fast enough so as not to affect the convergence properties of the evolution scheme employed. We adopt the standard Kreiss-Oliger dissipation operator [239] characterized by,

$$\partial_t Q \to \partial_t Q + (-1)^{r/2}\sigma \sum_i h_i^{r+1} \mathcal{D}_{i+}^{r/2+1} \mathcal{D}_{i-}^{r/2+1} Q \ , \tag{8.25}$$

for $r$-th order finite difference stencils where $\sigma$ is a constant to be chosen and serves to regulate the strength of the dissipation operator. In the equation (8.25), it is to be understood that $\mathcal{D}_{i+}^m \mathcal{D}_{i-}^m = \mathcal{D}_i^{2m}$ is a $2m$ order finite difference operator. In particular, for fourth order finite differencing in one dimension, we have,

$$\partial_t Q \to \partial_t Q + \sigma h^5 \mathcal{D}^{(6)} Q \ . \tag{8.26}$$

The Kreiss Oliger dissipation operator works well to suppress instabilities caused by high frequency modes, in the context of finite difference methods. For spectral methods, one commonly uses filtering methods [205].

## 8.6 Stability, Consistency and Convergence

The issues of stability, consistency and convergence of a discretization is unavoidable in the treatment of numerical solutions of PDEs, or in the field of numerical analysis in general. In reference to the numerical solution of PDEs, we make the following identifications, with respect to some discrete norm $\|\cdots\|_{*,k}$

- ***Stability***

  A discretization of a PDE by finite differences is called stable if there exists constants $K$ and $\alpha$ such that

  $$\|\mathbf{u}(t, x^i)\|_{*,h} \leq K e^{\alpha t_n} \|\mathbf{u}(0, x^i)\|_{*,h} \ . \tag{8.27}$$

  for all $n$ such that $t_n = nk$ [91]. This condition, which is reminiscent of that of well-posedness presented in §7.4, is essentially a discrete version of the well-posedness condition. The guarantee of the stability condition is that the solution is bounded as the grid is refined, i.e as $h \to 0$.

- ***Consistency***

The discretization is said to be consistent if the error satisfies

$$\lim_{k,h\to 0} \|u^n - u(t_n, x^i)\|_{*,h} = 0 \; . \tag{8.28}$$

Although ostensibly similar, this requirement is not the same as saying the discretization is convergent.

- ***Convergence***

  The discretization is said to be convergent of order $(p, q)$ if

$$\lim_{k,h\to 0} \|u^n - u(t_n, x^i)\|_{*,h} = \mathcal{O}(\Delta x^p, \Delta t^q) \; . \tag{8.29}$$

  It can be shown that consistency and stability of a discretization necessarily imply convergence [191].

In the following, we introduce two useful discrete norms, the $L_2$ and $L_\infty$ norm that play an important role in our convergence diagnostics. For a grid function $f$ at some time step $n$ in one spatial dimension, the $L_2$ norm is given by

$$\|f^n\|_2 = \sqrt{\Delta x \sum_{j=1}^{N} (f_j^n)^2} \; , \tag{8.30}$$

where $\Delta x$ is the spatial step size. The $L_\infty$ norm on the other hand is given by

$$\|f^n\|_\infty = \max_{j=1\cdots N} |f_j^n| \; . \tag{8.31}$$

Note that both (8.30) and (8.31) are non-negative.

## 8.7 Outer Boundary Conditions

The method of choice to impose boundary conditions in this study is through the ghost-point approach, where the computational domain is extended by a fictitious set of points that serve to 'hold' boundary data and thus preventing one to have to redefine the difference operators closer to the boundaries. This differs from the SBP-SAT method for difference operators satisfying summation by parts rules. In this case, one adds penalty terms on the right hand side of the PDE system close to the boundary, such that the SBP property is maintained, see for example [139, 1]. There are several types of boundary conditions that are in use

in the numerical relativity literature. We summaries below only those that are relevant to this study,

- ***Dirichlet***

  Dirichlet type boundary conditions are easy to implement in our code. These are often used to keep the evolution variables at prescribed values at the boundaries. These values may be constant in time, in which case, one simply fixes the values at the boundary to their initial values, or they may be time dependent, in which case they are specified by some time dependent function. The case of time dependent boundary conditions is not so straightforward to deal with and may in fact affect the convergence properties of one's solution, a phenomenon known as order reduction [100]. We revisit this issue in Chapter 9.

- ***Periodic***

  Periodic boundaries are used to impose periodicity on the grid. For a grid with points $x_1, x_2, \cdots, x_n$, with one ghost point on either side, we enforce

$$T^{\cdots}_{\cdots}(x_0) = T^{\cdots}_{\cdots}(x_n) \ , \tag{8.32}$$

$$T^{\cdots}_{\cdots}(x_{n+1}) = T^{\cdots}_{\cdots}(x_1) \ . \tag{8.33}$$

  This may be desirable for example when one is simulating large domains. In three spatial dimensions, this configuration is equivalent to integrating on a boundary-free 3-torus.

- ***Radiative (Sommerfeld)***

  We assume that close to the boundary, all fields behave as spherical waves of the form,

$$f = f_\infty + \frac{u(r - vt)}{r} \ , \tag{8.34}$$

  where $f_\infty$ is the asymptotic value of the dynamical variables. For practical implementation, we cast (8.34) in differential form, which in Cartesian coordinates becomes,

$$\partial_t f|_x = -v \left( \frac{r}{x} \partial_x f + \frac{f - f_\infty}{r} \right) \ , \tag{8.35}$$

  where $r = \sqrt{x^2 + y^2 + z^2}$. We set the value $f_\infty = 1$ for the lapse $\alpha$, and diagonal metric components $\tilde{\gamma}_{ii}$, and $f_\infty = 0$ for all other variables. The wave speed is set to $v = 1$ for $\tilde{A}_{ij}$, $\tilde{\gamma}_{ij}$. We leave the conformal connection functions $\tilde{\Gamma}^i$ fixed to their initial values.

- ***Mirror symmetry***

  Octant symmetry is imposed by using a mirror symmetry boundary condition along the $x = 0$, $y = 0$ and $z = 0$ planes,

$$T^{\cdots}_{\cdots}(x) = T^{\cdots}_{\cdots}(-x) \ . \tag{8.36}$$

  This can also be viewed as special case of a coordinate transformation.

## 8.8 Adaptive Mesh Refinement

At the heart of this thesis is the concept of mesh refinement [58, 59]. This numerical technique is now a common component of most numerical relativity codes [334, 248, 112, 114, 79]. A full 3D implementation of Adaptive Mesh Refinement (AMR) is non-trivial to code, especially when parallelization is desired. One of the most important aspects of a mesh refinement implementation is the issue of how one handles mesh refinement boundaries which we address in Chapter 10. In this section, we briefly present some of the traits of the algorithm and other aspects which are required for a successful implementation.

### 8.8.1 Grid Layout

The grid hierarchy, upon which the numerical integration is carried out, is arranged by first discretizing the spatial domain into a relatively coarse uniform mesh that covers the entire computational domain, by following the method outlined in §8.3. This constitutes the base or root grid ${H^0}_0$ with a mesh size that we will denote by $h_0$. Finer grid patches with progressively smaller mesh sizes are then overlaid as required to the base grid with each grid at level $l$ having mesh size $h_l$ given by the relation

$$h_l = \frac{h_{l-1}}{r} \ , \tag{8.37}$$

where $h_{l-1}$ is the mesh size of the previous level, and $r$ is a refinement factor typically chosen to be $r = 2$ or $r = 4$. In general, more than one grid patch can be added in a given level. This forms a tree or a hierarchy of grids ${H^l}_p$, where the indices $l$ and $p$ represent the level and patch number respectively. Evidently, the basic building blocks of the grid hierarchy are uniform grids of differing resolution. This configuration is depicted in Figure 8.1. It is at this point that we emphasize that each grid in a given level $l$ has its own solution vector and is evolved independently of all other grids. Of course it has to depend on the parent grid,

within which it is nested, for boundary data.

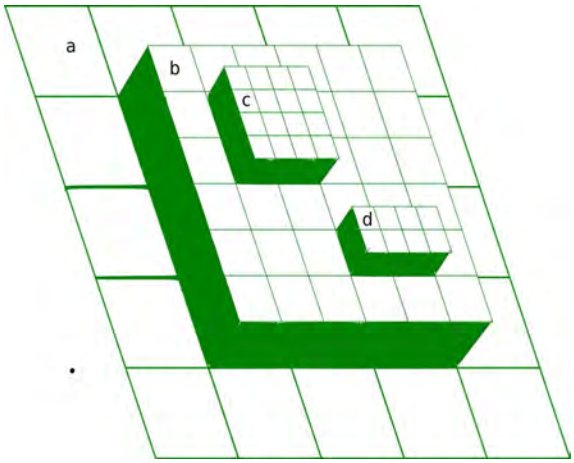


Figure 8.1: *A grid hierarchy demonstrating proper nesting. A single grid* $H^0{}_0$ *covering the entire domain is marked by 'a'. There is one refinement grid* $H^1{}_0$ *at level one marked by 'b'. Two disjoint refinement grids are* $H^2{}_0$ *and* $H^2{}_1$ *are marked by 'c' and 'd' respectively. Note that the ghost zones are not included in the grids. This figure is used to emphasize that the grid hierarchy is not some complex data structure, but that the overlaid grids are independently stored in memory.*

In principle, there is some freedom in the overlaying of the grids. However for practical considerations some restrictions may be necessary. Each grid patch added at a given level must satisfy the following conditions:

- The idea of proper nesting: A fine grid at level $l$ must start and end at the corner of a cell belonging to level $l-1$.
- Moreover, grids at higher levels cannot 'float'. This means that if there is a grid at level $l+2$, it must be contained in a grid at level $l+1$ that is itself properly nested on a grid at level $l$.
- The refinement factor $r$ must be an integer, and is the same for all levels. This results in a constant CFL number for all added levels, thus the same integration routine of the base level is stable on all levels, if it is stable on level 0. It also implies that grids at some higher level $l$ require $r^l$ time steps to catch up with a single time step of the base grid.
- The overlaid grids must be Cartesian. By this we mean that grids must be rectangular in two dimensions and cubic in three dimensions. Moreover, no rotation is allowed so that the edges of a grid at level $l$ are parallel to edges of grids at level $l-1$. In earlier implementations of the AMR algorithm, grids were allowed to rotate in space

to minimize the overall number of grids needed to cover a specific area. However, this leads to an unnecessary complexity in the implementation.

In cases where a given grid patch ${H^l}_p$ in some level $l$ has a neighboring grid patch ${H^l}_{p+1}$, there must be a routine that will allow exchange of the common data points. This mechanism will ensure that the interface boundary between the two grid patches is only artificial and no interpolation from previous grids is necessary to get boundary conditions for the common points.

To advance the grid hierarchy ${H^l}_p$ in time, a certain order in the integration of the levels must be maintained. The base grid is advanced one time step to time $t + \Delta t_0$. The next level is then advanced to the same time level, given by time $t + r\Delta t_1$. This goes on until the last level $l$, which is to be integrated to the same time as the base level which is given by $t + r^l \Delta t_l$. The control algorithm that is responsible for the time evolution of the entire grid hierarchy is orchestrated by a recursive procedure, which we summarize in Algorithm 1.

**Algorithm 1:** *A simple illustration of the AMR integration algorithm with refinement factor $r$.*

```
Procedure propagate()
Input: int level
Output: void
advanceLevel(level) ;
if level < max_level then
    foreach iteration j = 1, r do
        propagate(level + 1) ;
return ;
```

### 8.8.2 Inter-Level Communication

Each grid in a given level $l$ can be indexed independently by its own $(i_l, j_l, k_l)$ coordinate system. However, for reasons of inter-level communications, there is a mapping from the ${H^l}_p$ coordinates $(i_l, j_l, k_l)$ to the ${H^{l-1}}_p$ coordinates $(i_{l-1}, j_{l-1}, k_{l-1})$ and vice-versa. We express this relation via,

$$i_{l-1} = \frac{i_l - \mathbf{mod}(i_l, r)}{r} \,, \tag{8.38}$$

for a staggered grid hierarchy. Such communications are necessary for the computation of initial conditions, boundary conditions and for updating the coarse grid with the fine grid solution upon completion of a time step.

Initial data for the refined grid patches can be generated by spatial interpolation from the previous grid level (*prolongation*) or by calling the same initialization routine that was used to initialize the base grid, assuming that the grid hierarchy is fixed. In the context of FMR all levels are added and initialized at the same initial time $t_0$. The basis for the AMR approach is that data at higher levels in the grid hierarchy is more accurate than that at lower levels. Therefore, once all levels have been integrated to the same time, data in the finer meshes is used to update data in the coarse levels through the use of interpolation operators, a process called *restriction*. We present the interpolation operators we use in our code in §8.8.5.

It is important to note that with the mapping of indices given by Equation (8.38), all fine grid points are staggered about coarse grid points at lower levels. This choice has the advantage that if the base grid is discretized strategically to 'avoid' certain points $(x, y, z) \in \mathbb{R}^3$, (e.g. by using a cell centered grid to avoid dealing explicitly with the points on the edges) such points remain avoided in all refined levels. However, from a computational standpoint, this may be an expensive setup because communicating data across different levels requires three dimensional interpolation all the time. This is different from cases where some points in the fine grids are allowed to coincide with the ones from coarser levels. For such cases, inter-level communication can occur via *injection*, where data is simply copied to corresponding points at a given level.

### 8.8.3 The Flagging Step

Up to now, we have discussed how the grid hierarchy is built and integrated. This information is enough when the grid hierarchy is to remain fixed for the duration of a given simulation. However, the crux of AMR is that the grid hierarchy adapt to reflect and improve upon the local error in the computed solution. The idea behind the AMR algorithm is to have an error estimation routine that will serve to indicate which points in a given grid patch require refinement. The decision to refine or not is based on whether or not the estimated local error is within some error tolerance supplied by the user at the beginning of the simulation. A simple error estimation technique is the Richardson method, see [58, 59]. The error estimation is done typically every four time steps for second order accurate numerical integration.

Points in the grid requiring refinement are flagged or tagged for refinement. As an example we show the essence of the flagging operation for a two dimensional grid in Table (8.1). The points marked with a red-cross represent areas in the grid which exhibit a higher local error and the ones marked with the green ticks have acceptable errors. This is essentially a binary image that can be represented in a much simpler way through the use of zeros and ones. The operation is commonly accomplished by having some grid of integers $\mathcal{C}$ that is otherwise

of the same size as the grid on which one is doing the integration. If a point in the grid $H^l_p(i,j,k)$ is indicated to exhibit a local error that is higher than the specified tolerance, the corresponding point $\mathcal{C}(i,j,k)$ will be flagged with a '1', and will be flagged with a '0' otherwise, this is show in Table 8.2.

The points flagged as having high error will need to be reintegrated with a higher resolution. However, in general, such points will not necessarily form a regular grid. They may well be scattered throughout the grid $\mathcal{C}$. At the end of the flagging step, one then uses a clustering algorithm to generate subgrids out of the flagged points. These subgrids will be refined, initialized and reintegrated at the new resolution.

.

| | a | b | c | d | e | f | g | h | i | j | k | l | m | n | o | p | q | r |
|---|---|---|---|---|---|---|---|---|---|---|---|---|---|---|---|---|---|---|
| 1 | ✓ | ✓ | ✓ | ✓ | ✓ | ✓ | ✓ | ✓ | ✓ | ✓ | ✓ | ✓ | ✓ | ✓ | ✓ | ✓ | ✓ | ✓ |
| 2 | ✓ | ✓ | ✓ | ✓ | ✓ | ✓ | ✓ | ✓ | ✗ | ✗ | ✓ | ✓ | ✓ | ✓ | ✓ | ✓ | ✓ | ✓ |
| 3 | ✓ | ✓ | ✓ | ✓ | ✓ | ✓ | ✓ | ✗ | ✗ | ✗ | ✗ | ✓ | ✓ | ✓ | ✓ | ✓ | ✓ | ✓ |
| 4 | ✓ | ✓ | ✓ | ✓ | ✓ | ✓ | ✗ | ✗ | ✗ | ✗ | ✗ | ✗ | ✓ | ✓ | ✓ | ✓ | ✓ | ✓ |
| 5 | ✓ | ✓ | ✓ | ✓ | ✓ | ✗ | ✗ | ✗ | ✓ | ✓ | ✗ | ✗ | ✗ | ✓ | ✓ | ✓ | ✓ | ✓ |
| 6 | ✓ | ✓ | ✓ | ✓ | ✗ | ✗ | ✗ | ✓ | ✓ | ✓ | ✓ | ✗ | ✗ | ✗ | ✓ | ✓ | ✓ | ✓ |
| 7 | ✓ | ✓ | ✓ | ✗ | ✗ | ✗ | ✓ | ✓ | ✓ | ✓ | ✓ | ✓ | ✗ | ✗ | ✗ | ✓ | ✓ | ✓ |
| 8 | ✓ | ✓ | ✗ | ✗ | ✗ | ✓ | ✓ | ✓ | ✓ | ✓ | ✓ | ✓ | ✓ | ✗ | ✗ | ✗ | ✓ | ✓ |
| 9 | ✓ | ✗ | ✗ | ✗ | ✓ | ✓ | ✓ | ✓ | ✓ | ✓ | ✓ | ✓ | ✓ | ✓ | ✗ | ✗ | ✗ | ✓ |
| 10 | ✓ | ✗ | ✗ | ✗ | ✓ | ✓ | ✓ | ✓ | ✓ | ✓ | ✓ | ✓ | ✓ | ✓ | ✗ | ✗ | ✗ | ✓ |
| 11 | ✓ | ✓ | ✗ | ✗ | ✗ | ✓ | ✓ | ✓ | ✓ | ✓ | ✓ | ✓ | ✓ | ✗ | ✗ | ✗ | ✓ | ✓ |
| 12 | ✓ | ✓ | ✓ | ✗ | ✗ | ✗ | ✓ | ✓ | ✓ | ✓ | ✓ | ✓ | ✗ | ✗ | ✗ | ✓ | ✓ | ✓ |
| 13 | ✓ | ✓ | ✓ | ✓ | ✗ | ✗ | ✗ | ✓ | ✓ | ✓ | ✓ | ✗ | ✗ | ✗ | ✓ | ✓ | ✓ | ✓ |
| 14 | ✓ | ✓ | ✓ | ✓ | ✓ | ✗ | ✗ | ✗ | ✓ | ✓ | ✗ | ✗ | ✗ | ✓ | ✓ | ✓ | ✓ | ✓ |
| 15 | ✓ | ✓ | ✓ | ✓ | ✓ | ✓ | ✗ | ✗ | ✗ | ✗ | ✗ | ✗ | ✓ | ✓ | ✓ | ✓ | ✓ | ✓ |
| 16 | ✓ | ✓ | ✓ | ✓ | ✓ | ✓ | ✓ | ✗ | ✗ | ✗ | ✗ | ✓ | ✓ | ✓ | ✓ | ✓ | ✓ | ✓ |
| 17 | ✓ | ✓ | ✓ | ✓ | ✓ | ✓ | ✓ | ✓ | ✗ | ✗ | ✓ | ✓ | ✓ | ✓ | ✓ | ✓ | ✓ | ✓ |
| 18 | ✓ | ✓ | ✓ | ✓ | ✓ | ✓ | ✓ | ✓ | ✓ | ✓ | ✓ | ✓ | ✓ | ✓ | ✓ | ✓ | ✓ | ✓ |

Table 8.1: *This figure represents error flags. The places marked with '✗' are areas which will have exhibited large errors, while the ones marked with '✓' are the ones with acceptable error levels.*

### 8.8.4 Point Clustering and Grid Generation

To generate regular subgrids out of the flagged points in the grid shown in Table 8.2, one needs a point clustering algorithm. Popular choices to accomplish this task include the bisection-merging approach, creating a minimal spanning set, etc. I have implemented the Berger and Rigoutsos algorithm as proposed in [57]. This algorithm is based on searching for inflection

points in the signatures of the supplied binary image. The idea is to split the grid into two subgrids, using one of the grids as the next input. One proceeds to split that into two and so on until some criterion is met. To determine whether to keep splitting the remaining grids, one defines a measure of efficiency for a given grid, to determine if an optimal grid has been attained. The efficiency of a grid is defined as,

$$r = \frac{\text{number of flagged cells}}{\text{total number of cells in the grid}} , \tag{8.39}$$

where clearly $0 \leq r \leq 1$.

Given a binary image $\mathcal{C}(x, y, z)$ in three dimensions, the signatures in each dimension $\mathcal{S}_x$, $\mathcal{S}_y$ and $\mathcal{S}_z$ are respectively defined as,

$$\mathcal{S}_x = \int_y \int_z \mathcal{C}(x, y, z)\, dz\, dy , \tag{8.40}$$

$$\mathcal{S}_y = \int_x \int_z \mathcal{C}(x, y, z)\, dz\, dx , \tag{8.41}$$

$$\mathcal{S}_z = \int_x \int_y \mathcal{C}(x, y, z)\, dy\, dx , \tag{8.42}$$

for the $x$, $y$ and $z$ directions respectively. One then proceeds by searching for inflection points in the signatures (8.40)–(8.42). The inflection points are associated with zero-crossings in the second derivative of the signatures.

The point with the highest inflection in the signature $\mathcal{S}_x$ presents a potential split point along the $x$ direction. Similarly the highest inflection point in $\mathcal{S}_y$ presents a potential split point in the $y$ direction and the same for $\mathcal{S}_z$. Since we are splitting the grid into two, one can only split at one point, along only one dimension, therefore the highest inflection among the three potential split points will be the actual split point in that dimension corresponding to the signature at which the highest inflection point was found. The algorithm itself is illustrated in Algorithm 2.

In the following, we present an example of the grid clustering algorithm in two dimensions. The input binary image is given in Table 8.2 and the output is given in Figure 8.2 for an efficiency threshold of 100% and in Figure 8.3 for an efficiency threshold of 70%. Clearly one requires the generated subgrids to have as high efficiency as possible, while simultaneously requiring that the generated subgrids be as minimal as possible to avoid having many subgrids to reintegrate. With this goal in mind, we note that an efficiency threshold of 100% is not necessarily the most computationally efficient. Typically the grid efficiency threshold is set to about 70%.

| | a | b | c | d | e | f | g | h | i | j | k | l | m | n | o | p | q | r |
|---|---|---|---|---|---|---|---|---|---|---|---|---|---|---|---|---|---|---|
| 1 | 0 | 0 | 0 | 0 | 0 | 0 | 0 | 0 | 0 | 0 | 0 | 0 | 0 | 0 | 0 | 0 | 0 | 0 |
| 2 | 0 | 0 | 0 | 0 | 0 | 0 | 0 | 0 | 1 | 1 | 0 | 0 | 0 | 0 | 0 | 0 | 0 | 0 |
| 3 | 0 | 0 | 0 | 0 | 0 | 0 | 0 | 1 | 1 | 1 | 1 | 0 | 0 | 0 | 0 | 0 | 0 | 0 |
| 4 | 0 | 0 | 0 | 0 | 0 | 0 | 1 | 1 | 1 | 1 | 1 | 1 | 0 | 0 | 0 | 0 | 0 | 0 |
| 5 | 0 | 0 | 0 | 0 | 0 | 1 | 1 | 1 | 0 | 0 | 1 | 1 | 1 | 0 | 0 | 0 | 0 | 0 |
| 6 | 0 | 0 | 0 | 0 | 1 | 1 | 1 | 0 | 0 | 0 | 0 | 1 | 1 | 1 | 0 | 0 | 0 | 0 |
| 7 | 0 | 0 | 0 | 1 | 1 | 1 | 0 | 0 | 0 | 0 | 0 | 0 | 1 | 1 | 1 | 0 | 0 | 0 |
| 8 | 0 | 0 | 1 | 1 | 1 | 0 | 0 | 0 | 0 | 0 | 0 | 0 | 0 | 1 | 1 | 1 | 0 | 0 |
| 9 | 0 | 1 | 1 | 1 | 0 | 0 | 0 | 0 | 0 | 0 | 0 | 0 | 0 | 0 | 1 | 1 | 1 | 0 |
| 10 | 0 | 1 | 1 | 1 | 0 | 0 | 0 | 0 | 0 | 0 | 0 | 0 | 0 | 0 | 1 | 1 | 1 | 0 |
| 11 | 0 | 0 | 1 | 1 | 1 | 0 | 0 | 0 | 0 | 0 | 0 | 0 | 0 | 1 | 1 | 1 | 0 | 0 |
| 12 | 0 | 0 | 0 | 1 | 1 | 1 | 0 | 0 | 0 | 0 | 0 | 0 | 1 | 1 | 1 | 0 | 0 | 0 |
| 13 | 0 | 0 | 0 | 0 | 1 | 1 | 1 | 0 | 0 | 0 | 0 | 1 | 1 | 1 | 0 | 0 | 0 | 0 |
| 14 | 0 | 0 | 0 | 0 | 0 | 1 | 1 | 1 | 0 | 0 | 1 | 1 | 1 | 0 | 0 | 0 | 0 | 0 |
| 15 | 0 | 0 | 0 | 0 | 0 | 0 | 1 | 1 | 1 | 1 | 1 | 1 | 0 | 0 | 0 | 0 | 0 | 0 |
| 16 | 0 | 0 | 0 | 0 | 0 | 0 | 0 | 1 | 1 | 1 | 1 | 0 | 0 | 0 | 0 | 0 | 0 | 0 |
| 17 | 0 | 0 | 0 | 0 | 0 | 0 | 0 | 0 | 1 | 1 | 0 | 0 | 0 | 0 | 0 | 0 | 0 | 0 |
| 18 | 0 | 0 | 0 | 0 | 0 | 0 | 0 | 0 | 0 | 0 | 0 | 0 | 0 | 0 | 0 | 0 | 0 | 0 |

Table 8.2: *A binary image representing error flags. The places marked with '1' are areas which will have exhibited large errors, while the ones marked with '0' are the ones with acceptable error levels.*

**Algorithm 2:** *A simple illustration of the Berger and Rigoutsos algorithm for point clustering and grid generation.*

```
Procedure cluster()
Input: float efficiency_threshold
Output: List of grids
if gridEfficiency < efficiency_threshold then
    compute signatures
    Find a hole or inflection point in the signatures, representing the best place to split
    the grid.
    if found position to split then
        split the grid in two.
        append new grid to the list of grids to split.
    else
        move to the next grid in the list
        i = i + 1
else
    move to the next grid in the list
    i = i + 1
return ;
```

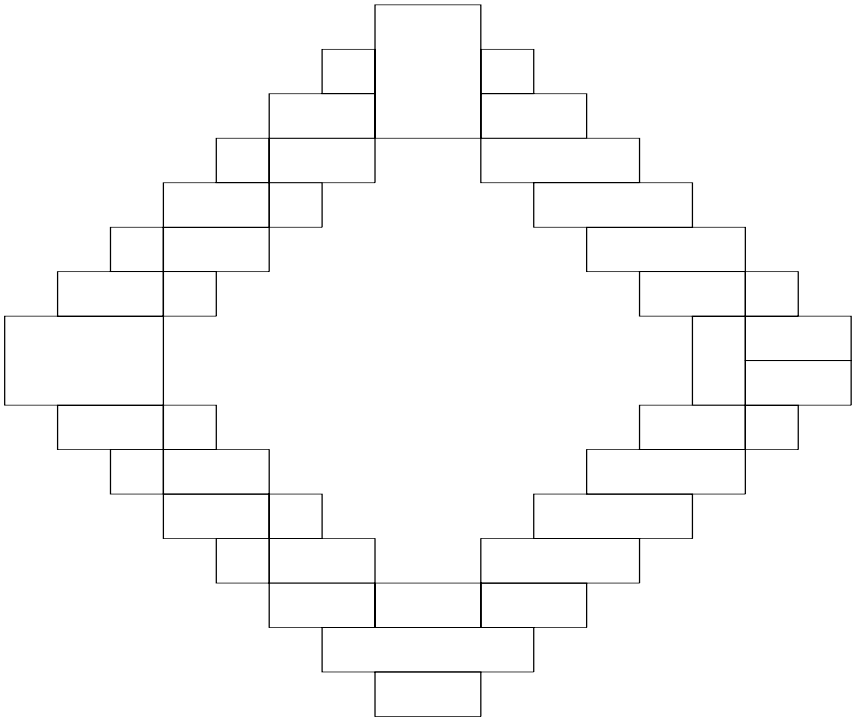

Figure 8.2: *Output from the clustering algorithm with efficiency threshold set to* 100%. *Note how the grids trace the binary image in Table 8.1*

### 8.8.5 Interpolation Operators

An implementation of mesh refinement without interpolation operators is incomplete since the algorithm relies heavily on interpolation to communicate data across different refinement levels due to differences in spatial resolution across the levels. An important aspect to consider here is that three dimensional interpolation is not cheap, computationally. Moreover, since we are interested in higher order convergent integration methods, the usual linear interpolation method is inadequate. In the following, we present some of the interpolation operators that are supported in our code. We note that although all the interpolating methods considered here fall under the theme of polynomial interpolation, the term itself is often reserved (with evident misuse of terminology) for the case where one solves the Vandermonde matrix.

#### Lagrange interpolation

We implement the barycentric form of the Lagrange interpolation polynomial [62]. To interpolate between function values $f_0, f_1, \cdots, f_n$, we use the interpolating polynomial, which is

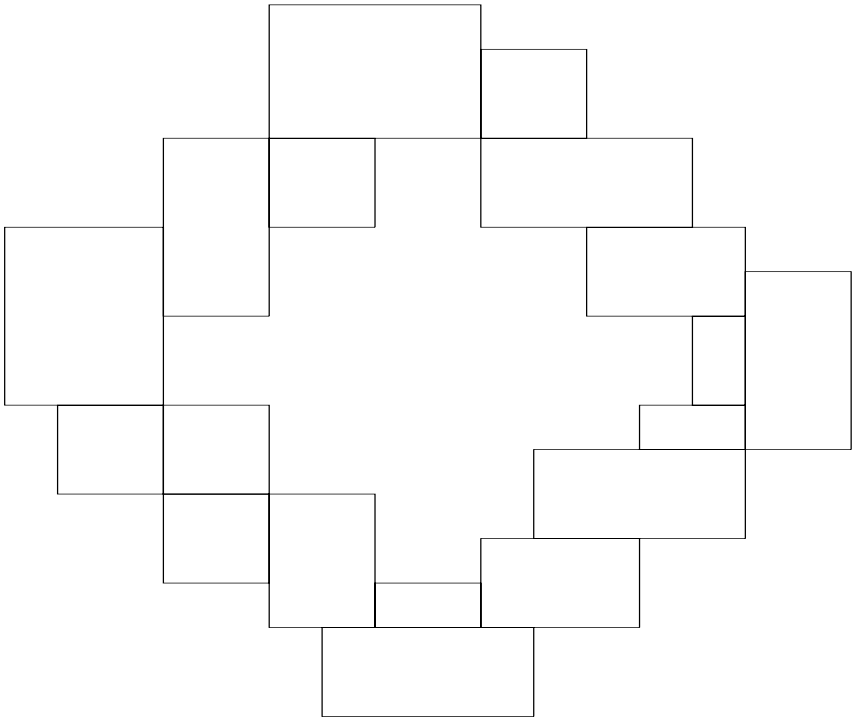

Figure 8.3: *Output from the clustering algorithm for the binary image given in Table 8.1. The efficiency threshold in this case was set to 70%. Note that there are fewer grids than in FIgure 8.2.*

given in one dimension as

$$p(x) = \frac{\sum_{j=0}^{n} \mathcal{A}_j f_j}{\sum_{j=0}^{n} \mathcal{A}_j} \,, \tag{8.43}$$

where

$$\mathcal{A}_j = \frac{w_j}{x - x_j} \qquad \text{and} \qquad w_j = \left( \prod_{\substack{k=0 \\ k \neq j}}^{N} (x_j - x_k) \right)^{-1} \,, \tag{8.44}$$

and the $x_i$ are the points corresponding to the function values $f_i$.

### Hermite interpolation

Hermite interpolation plays an important role in the construction of transition profiles. This is an important feature in the boundary treatment of our mesh refinement method which is detailed in Chapter 10. The main idea behind Hermite interpolation is not only to match the function values $f_i$ at the nodes $x_i$, but to simultaneously match the first $m$ derivatives $f', f'', f''', \cdots, f^{(m)}$ of the function $f$. This has the added property of the interpolation polynomial being smooth, but it comes with the extra requirement that the derivatives be

known at the nodes. This means in general one has to provide $n(m+1)$ values to attain an interpolant of order $n(m+1)-1$.

Directly relevant to our work is the case of constructing a transition profile between two points $x = a$ and $x = b$ along some dimension $x$. Assume further that the function value $P(x)$ takes on the values $P_0$ at $x = a$ and $P_1$ at $x = b$. The goal is to generate a weight function $f$ that will be used in linearly interpolating between the two end points,

$$P(x) = [1 - f(x)]P_0 + f(x)P_1 \ . \tag{8.45}$$

We parametrize the weight function $f(x)$ in terms of some variable $t$ that takes on the values $t_0 = 0$ and $t_1 = 1$ at the end points. The variable is given in terms of $x$, $a$, and $b$ as

$$t = \begin{cases} 0 & \text{if } \frac{x-a}{b-a} < 0 \\ 1 & \text{if } \frac{x-a}{b-a} > 1 \\ \frac{x-a}{b-a} & \text{otherwise} \ . \end{cases} \tag{8.46}$$

All derivatives of the weight function $f$ are constrained to be 0. This is summarized in Table 8.3.

| $x$ | $P(x)$ | $t$ | $f$ | $f'$ | $f''$ |
|---|---|---|---|---|---|
| $a$ | $P_0$ | 0 | 0 | 0 | 0 |
| $b$ | $P_1$ | 1 | 1 | 0 | 0 |

Table 8.3: *Transition values for a function $P(x)$ that varies from $P_0$ at $x = a$ to $P_1$ at $x = b$.*

We are now in a position to present the different transition profiles:

- ***Zeroth order interpolant***

  This case is simply given by the step function

$$f(t) = \begin{cases} f_0 & t \le t_c \ , \\ f_1 & t > t_c \ . \end{cases} \tag{8.47}$$

  for some $t_c$ intermediate between $t_0$ and $t_1$. This profile has sharp transitions between $t = 0$ and $t = 1$ at $t_c$. For later convenience we note that (8.47) is referred to simply as

a step profile.

- ***First order interpolant***

  An improvement upon the zeroth order interpolant is to use a smoother polynomial. To create a first order interpolant, one needs only match the function values at the end points. In particular, we start from the first order polynomial

  $$f(t) = a_0 + a_1 t \ . \tag{8.48}$$

  We proceed by imposing the conditions $f(0) = 0$ and $f(1) = 1$, leading to the interpolant

  $$f(t) = t \ . \tag{8.49}$$

  Because no derivative information was utilized in the derivation of this interpolant, one cannot guarantee smoothness at the end points. This profile is referred to as a boxstep profile.

- ***Third order interpolant***

  Starting with the third order polynomial,

  $$f(t) = a_0 + a_1 t + a_2 t^2 + a_3 t^3 \ , \tag{8.50}$$
  $$f'(t) = a_1 + 2a_2 t + 3a_3 t^2 \ , \tag{8.51}$$

  where the $a_i$ are constants, one can derive a third order smooth interpolant. We begin by imposing the conditions $f(0) = 0, f(1) = 1$ and $f'(0) = 0, f'(1) = 0$ at the end points, and solve the resulting system of equations. This results in the interpolating polynomial,

  $$f(t) = 3t^2 - 2t^3 \ . \tag{8.52}$$

  This is certainly smoother than the previous profiles. It is referred to as a smoothstep

profile.

- ***Fifth order interpolant***

  Similarly, by employing a fifth order polynomial,

$$f(t) = a_0 + a_1 t + a_2 t^2 + a_3 t^3 + a_4 t^4 + a_5 t^5 \ , \tag{8.53}$$

$$f'(t) = a_1 + 2a_2 t + 3a_3 t^2 + 4a_4 t^3 + 5a_5 t^4 \ , \tag{8.54}$$

$$f''(t) = 2a_2 + 6a_3 t + 12a_4 t^2 + 20a_5 t^3 \ , \tag{8.55}$$

  and imposing the appropriate conditions for the function $f$ and its first $f'$ and second derivative $f''$ as given in Table 8.3, one derives the fifth order interpolant given by

$$f(t) = 10t^3 - 15t^4 + 6t^5 \ . \tag{8.56}$$

  In reference to this being an improvement over the smoothstep profile, it is commonly known as smootherstep.

### Cubic Spline interpolation

We note that to apply Hermite interpolation of say third order of a function $f_i$ between two points $t_0$ and $t_1$, one needs the first derivatives of $f_i'$ at both points $t_0$ and $t_1$. However, one does not always have such derivative information available. A variant of (third order) Hermite interpolation called Catmull-Rom splines makes a provision to obtain derivatives at the end points by using finite differences. The essence of the method is that to interpolate between the points $t_0$ and $t_1$, one needs additional control points $t_{-1}$ and $t_2$ encompassing the points of interest. In order to avoid the formation of loops and self-intersections of the resulting curve, the control points are parametrized by the distance measure,

$$t_{i+1} = |\mathbf{P}_{i+1} - \mathbf{P}_i|^\alpha + t_i \ , \tag{8.57}$$

where the choices of $\alpha$ lead to the three types of Catmull-Rom splines given as

- Uniform: characterized by the choice $\alpha = 0$.
- Chordal: characterized by the choice $\alpha = 1$.
- Centripetal: characterized by the choice $\alpha = 1/2$.

With the Centripetal parametrization, the resulting spline has been shown to be free of the undesirable formation of loops and intersections [407]. In essence to calculate the point $C_{12}$ corresponding to some given $t$, one uses the formulas

$$L_{01} = f_0 \left( \frac{t_1 - t}{t_1 - t_0} \right) + f_1 \left( \frac{t - t_0}{t_1 - t_0} \right) , \tag{8.58}$$

$$L_{12} = f_1 \left( \frac{t_2 - t}{t_2 - t_1} \right) + f_2 \left( \frac{t - t_1}{t_2 - t_1} \right) , \tag{8.59}$$

$$L_{23} = f_2 \left( \frac{t_3 - t}{t_3 - t_2} \right) + f_3 \left( \frac{t - t_2}{t_3 - t_2} \right) , \tag{8.60}$$

$$L_{012} = L_{01} \left( \frac{t_2 - t}{t_2 - t_0} \right) + L_{12} \left( \frac{t - t_0}{t_2 - t_0} \right) , \tag{8.61}$$

$$L_{123} = L_{12} \left( \frac{t_3 - t}{t_3 - t_1} \right) + L_{23} \left( \frac{t - t_1}{t_3 - t_1} \right) , \tag{8.62}$$

$$C_{12} = L_{012} \left( \frac{t_2 - t}{t_2 - t_1} \right) + L_{123} \left( \frac{t - t_1}{t_2 - t_1} \right) . \tag{8.63}$$

**Polynomial and Least squares interpolation**

Given a set of data points $f_0, f_1, \cdots, f_n$ we want to find a polynomial of degree $n$ that goes through all the given points, see [315] for example. We start from the $n$-th order polynomial

$$p(x) = b_0 + b_1 x + \cdots + b_n x^n, \tag{8.64}$$

and impose the condition that the polynomial $p(x_i)$ reduce to the function values $f_i$ at the nodes $x_i$, $p(x_i) = f_i$. This requirement leads to the system of equations

$$\mathbf{A}\mathbf{b} = \mathbf{f} , \tag{8.65}$$

where $\mathbf{A}$ is called a Vandermonde matrix and is given in the equation (8.66), along with the vectors $\mathbf{b}$ and $\mathbf{f}$ as,

$$A = \begin{pmatrix} x_0^n & x_0^{n-1} & \cdots & x_0 & 1 \\ x_1^n & x_1^{n-1} & \cdots & x_1 & 1 \\ \vdots & \vdots & \vdots & \vdots & \vdots \\ x_n^n & x_n^{n-1} & \cdots & x_n & 1 \end{pmatrix} , \qquad b = \begin{pmatrix} b_n \\ b_{n-1} \\ \vdots \\ b_0 \end{pmatrix} , \qquad f = \begin{pmatrix} f_0 \\ f_1 \\ \vdots \\ f_n \end{pmatrix} . \tag{8.66}$$

It should be noted that the coeffients $b_i$ recovered from a numerical solution of the Vandermonde matrix can be unreliable. This stems from the fact that the Vandermonde matrix

is ill-conditioned. In [315], it is recommended that one use higher precision when handling interpolations of this nature.

A slightly related form of interpolation is that of least squares interpolation, characterized by the system of equations

$$(\mathbf{A}^T\mathbf{A})\mathbf{b} = \mathbf{A}^T\mathbf{f} \ , \tag{8.67}$$

instead of (8.65). With this type of interpolation, one is no longer guaranteed that the resulting polynomial will pass through all the points $f_i$ at the nodes $c_i$. In fact, with this method, one can employ a lower order polynomial to fit multiple data points than is allowed by the traditional interpolation approach. This has the added benefit of being smoother as it is not required to honor the data at all points.

## 8.9 The Code

In order to explore and carry out the aims of this thesis, we have decided to write a numerical relativity code from scratch. The primary aim for this endeavor is not necessarily to present an independent numerical relativity code but rather to eliminate the learning curve that comes with most numerical software. A useful rule-of-thumb is that if one is interested in studying the physics of a particular system, one is better off finding a well documented code that is already available and start from there. However, if one is interested in algorithmics and numerical methods, chances are one is less likely to find a code that will cater for all of ones programming idiosyncrasies. In addition, one would need to understand a significant aspect of how the code was written at the low level than for a user who simply needs a tool to compute certain results. In such cases one may waste a significant amount of time rewriting certain aspects of the available codes.

### Language choice

The language choice in this project was dictated by the choice of programming paradigm. When developing large codes, one ideally wants a system where large chunks of code fragments or modules can be discarded, replaced or modified independently without compromise to the structure of the remaining code. In principle for a procedural or modular paradigm, any of Fortran 90/95/2003/2008, C and/or C++ would have sufficed. However, our chosen paradigm was Object-Oriented programming (OOP). With this choice, C is not an option as it is not geared for OOP. Although the latest version of Fortran does support OOP, we had some trouble obtaining a reliable compiler. This has left the choice of C++.

It is often erroneously said that C++ is not good for scientific computation. However, C++ is just as efficient as C. In addition, with the use of template metaprogramming techniques, one can reach speeds comparable to that of Fortran.

### Parallelization

Parallelization is handled through the Message Passing Interface (MPI). The unigrid code runs across multiple processors. The mesh refinement module/class however is not yet fully parallelized. Programming an AMR/FMR code is already complex enough. When parallelizing, there are subtle issues related to domain decomposition that need a little more attention than the time we had available. But work is already underway to parallelize the full mesh refinement module.

### Matrix Algebra

The matrix computations involved in the code mostly involve 3-by-3 matrices. Routine calculations such as the inverse and determinant of such matrices can easily be hard-coded. For example, the determinant of a 3-by-3 matrix $A$ is given by the sarrus rule as

$$\det A = A_{00}(A_{11}A_{22} - A_{12}A_{21}) - A_{01}(A_{22}A_{10} - A_{12}A_{20}) + A_{02}(A_{10}A_{21} - A_{11}A_{20}) \,. \quad (8.68)$$

This avoids linking to specialized heavy modules such PetSc while also keeping in line with our philosophy of generating a simple light-weight code.

### IO system

We have adopted a very simple output system employing the ASCII format. The output is essentially parallel as each processor outputs to a separate file. The structure of the output system is outlined in Figure 8.4 for a case where only two processors are active.

In the input parameters of the code, there is a **outputStride** variable that sets how many iterations in time must the code wait for output. For example, if the output stride is set to 10, the output will occur after every 10 time steps. Therefore the code does not output results at each iteration. This helps against unnecessary resource wasting involved in writing large data to disk. Each output file is a frame in time, and can be visualized using any 3D tool of one's choice.

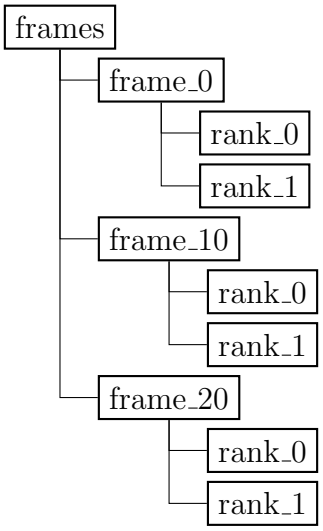


Figure 8.4: *File structure of the output system we employ.*

### Numerical Precision

In conventional computers, all numbers are stored in binary form, represented by a string of zeros and ones. Within this scheme, $N$ bits have the capacity to store integers between 0 and $2^N$. Taking the sign of the integer into account reduces the maximum to $2^{N-1}$. For example, 32 bits can represent integers between $[-2147483648, 2147483648]$. A classic problem in computing is how to represent an arbitrary number using a finite amount of memory space. We use the package MPFR (Multiple Precision Floating-Point Reliably), which is based on the GMP (GNU Multi-Precision) package to achieve arbitrary precision. We emphasize that at this stage, this is merely a debugging feature to help rule out round off effects whenever there is a bug in the code. In reality, runs with arbitrary precision are much slower than with the standard 64 bit precision.

# Chapter 9

# Time Marching and Order Reduction

## 9.1 Overview

The simplest time marching algorithm for an initial value problem is the Euler method. Consider the following initial value problem,

$$y_t = f(t, y(t)), \qquad y(t_0) = y_0 \ , \tag{9.1}$$

To advance (9.1) in time using the Euler method, one uses the update formula

$$y_{n+1} = y_n + hf(t, y) \ . \tag{9.2}$$

Evidently, this method is only first order accurate. For this reason, round-off error accumulation may soon render it unreliable. Moreover, it is unappealing for practical use because of its smaller region of absolute stability compared to higher order convergent methods (see §9.6 for stability analysis).

There exist methods with higher order of accuracy than just $\mathcal{O}(h)$. These methods rely on evaluating the right hand side of (9.1) at several other points to get an overall higher convergence rate. The most commonly used among these are often classified as being either Multilevel (also Multistep), Multiderivative, or Multistage methods. In general, Multistep methods are not self-starting, meaning that in addition to providing initial values, one must specify another method to compute the first few points of the solution. Multiderivative methods, which include Taylor methods, require evaluations of higher derivatives of the right-hand-side of the ODE system under consideration. We do not consider multistep or multiderivative methods in this work, we instead refer the reader to [196, 89] for details and rigor. We focus our attention solely on Multistage methods, in particular, explicit Runge

Kutta methods.

Using an $s$-stage explicit Runge-Kutta method to evolve (9.1), one employs the following update formula,

$$y_{n+1} = y_n + h \sum_{j=1}^{s} b_j k_j \,, \tag{9.3}$$

where the intermediate stages $k_i$ are given by

$$k_j = f\left( t_n + hc_j, y_n + h \sum_{i=1}^{j-1} a_{ij} k_i \right) \qquad j = 1, 2, \cdots, s \,. \tag{9.4}$$

and the $b_i$, $c_i$ and $a_{ij}$ are coefficients to be specified. Along with the method of lines discretization (§8.2), one can use this method to evolve time dependent PDEs. Ordinarily, one can reach higher convergence rates with Runge Kutta methods than is allowed by the Euler method for example. However, for general non-linear hyperbolic PDEs with time dependent Dirichlet boundary conditions[1], explicit Runge-Kutta methods suffer from the phenomenon of order reduction, where the order of convergence is governed by the stage order instead of the formal order of the scheme itself [100, 306]. For example, the classical four stage fourth order accurate Runge-Kutta method behaves like a first order method at the boundary, leading only to second order convergence globally. This order reduction phenomenon, at least in the hyperbolic case, has been traced to inconsistent application of boundary conditions for the intermediate Runge-Kutta stages [100, 1, 306]. For some linear problems, the negative effects induced by order reduction are likely to be negligible compared to those emanating from other sources. For example, the low order terms generated by inconsistent intermediate boundary treatment for the linear advection equation are smaller than the higher order errors for low resolution grids [100, 306]. However, this is not the norm for non-linear PDEs, as a result the convergence order for these problems is smaller than the formal order for a given scheme.

Implicit Runge-Kutta schemes are also prone to order reduction effects. When applied to differential algebraic equations (DAEs) or stiff systems of ODEs, they suffer from order reduction phenomena, even when the solution itself is regular [317, 88, 312, 87, 136, 142]. It is important to distinguish between order reduction effects arising from the discretization of hyperbolic PDEs and those arising from purely ODE or DAE systems. The former, which is the main focus of the present Chapter, is linked to the errors introduced in the application of boundary conditions, while the latter is related to the stiffness of the ODE system itself.

[1] This excludes periodic and outgoing boundary conditions. Although one may argue that they are time dependent, they are not Dirichlet type.

The concept of order reduction in the context of implicit Runge Kutta methods has been studied by several authors in the literature, see [195] and references therein.

For hyperbolic PDEs one could, in principle, avoid the issue of order reduction by considering linear multi-step methods. These have no intermediate stages, thus the problem of imposing boundary conditions is well defined. But these methods often have larger storage requirements and reduced stability limits compared to Runge-Kutta methods of the same order, see [221] for a comparison of fourth order Adams-Bashforth with the fourth order classical Runge-Kutta method.

In this Chapter we address the issue of consistent intermediate boundary application for explicit Runge Kutta schemes. We focus our treatment on the hyperbolic cases where explicit time discretizations are more appropriate. The Chapter is arranged as follows: we begin by summarizing some of the current boundary treatment methods in Section 9.2, we then review some background material that is relevant to the Runge Kutta algorithm in Sections 9.3 and 9.4 followed by our proposed method of application of boundary conditions in Section 9.5. Numerical examples and concluding remarks are presented in Sections 9.9 and 9.10, respectively.

## 9.2 Boundary Conditions and Order Reduction

Consider the method of lines discretization of the PDE,

$$y_t = \mathcal{F}(t, y(t)) \,, \qquad y(t_0) = y_0, \qquad t_0 \leq t < \infty \,, \tag{9.5a}$$

$$y \in \mathbb{R}^d, \qquad \text{and} \qquad t \in \mathbb{R} \tag{9.5b}$$

on some bounded spatial domain $\Omega \in \mathbb{R}^d$, where $\mathcal{F}$ is a differential operator. Additionally, consider the boundary conditions to be given by some time dependent function $g(t)$, $g \in \mathbb{R}^d$ which is a solution of (9.5). Following standard convention, we shall generally refer to the particular case $d = 1$ as scalar, and $d > 1$ as vector.

Using the $s$-stage explicit Runge Kutta algorithm (9.3) to advance the PDE system (9.5) in time, there arises the non-trivial question of how to apply boundary conditions in the computation of the intermediate stages (9.4). There are several methods currently in use but so far there has not been a method that achieves the optimal order for general hyperbolic problems with time dependent boundary conditions.

Intuitively, one can evaluate the boundary function at the time corresponding to the intermediate stage i.e. apply boundary values $g(t + c_i dt)$ for the intermediate stage $k_i$, a

scheme commonly referred to as the conventional method. Unfortunately, this leads to a slowly convergent error in the solution, resulting in second order convergence for non linear problems. Alternatively, one can integrate the ODE $y' = g'(t)$ at the boundary. However, this procedure leads to a similar reduction of convergence order. Another consideration is to apply boundary values only at the end of the time step. In the context of finite difference schemes, one can employ lop sided differencing operators at the boundary for the intermediate stages. While this method does retain the formal order of the scheme, it has undesirable effects on stability [100]. A strategy introduced in [100] essentially integrates (9.5) at the boundary, while replacing repetitive application of the differential operator $\mathcal{F}$ by repetitive time derivatives, i.e. replacing $\mathcal{F}^k$ by $d^k y/dt^k$. This setup works well when the differential operator $\mathcal{F}$ does not depend explicitly on time, otherwise one gets only up to third order accuracy [221, 306]. An intricate scheme that results in no order reduction for non-linear conservation laws of the form $u_t = f(u)u_x$ was derived in [306] by prescribing analytically those values that would have resulted from a Runge-Kutta scheme at the boundary. However, this is cumbersome even for relatively simple scalar PDEs. Moreover, it is not clear how one can generalize it to systems of PDEs, see also [221].

## 9.3 Rooted Trees and Order Conditions

The starting point in deriving a Runge Kutta method of order $p$ is the Taylor expansion of the exact solution about some time step size $h$,

$$y_{n+1} = y_n + hy'_n + \frac{1}{2}h^2 y''_n + \cdots + \frac{1}{p!}h^p y^{(p)} + \mathcal{O}(h^{p+1}) \,, \tag{9.6}$$

which in terms of $f(t, y(t))$ takes the form

$$y_{n+1} = y_n + hf + \frac{1}{2}h^2 \left(\frac{df}{dt}\right)_n + \cdots + \frac{1}{p!}h^p \left(\frac{d^{p-1}f}{dt^{p-1}}\right)_n + \mathcal{O}(h^{p+1}) \,. \tag{9.7}$$

One then proceeds by requiring that the approximate solution (9.3) reduce to the exact solution (9.7) up to order $p$. This requirement leads to the order conditions which place constraints on the $c_i$, $b_i$ and $a_{ij}$ coefficients appearing in equation (9.3) in the form of a non linear system of equations. The order conditions for a generic $s$-stage Runge Kutta method are given by Equation (9.8) in Theorem 9.3.1. The quantities appearing in Equation (9.8)

are given in terms of rooted tree notation in Table 9.1.

**Theorem 9.3.1 (Order Conditions [90])** *An $s$ stage Runge Kutta method is of order $p$ if and only if*

$$\sum_{j=1}^{s} b_j \Phi_j(t) = \frac{1}{\gamma(t)} , \tag{9.8}$$

*for all trees or order $\leq p$ .*

| Order | $\gamma$ | Tree | $\Phi$ |
|---|---|---|---|
| 1 | 1 |  | $\sum_i b_i$ |
| 2 | 2 |  | $\sum_i b_i c_i$ |
| 3 | 3 |  | $\sum_i b_i c_i^2$ |
| 3 | 6 |  | $\sum_{ij} b_i a_{ij} c_j$ |
| 4 | 4 |  | $\sum_i b_i c_i^3$ |
| 4 | 8 |  | $\sum_{ij} b_i c_i a_{ij} c_j$ |
| 4 | 12 |  | $\sum_{ij} b_i a_{ij} c_j^2$ |
| 4 | 24 |  | $\sum_{ijk} b_i a_{ij} a_{jk} c_k$ |

Table 9.1: *Trees and elementary differentials up to order $p = 4$.*

Whether such order conditions admit a solution is dependent on the number of stages $s$. For example one can achieve fourth order accuracy with four stages. But in order to reach order five accuracy, one needs at least six stages. Such relationships are summarized up to order eight in Table 9.2. As can be seen in the table, as one goes to higher order accuracy, more order conditions are needed. This makes dealing with higher order Runge-Kutta methods cumbersome. For reasons of efficiency, one wants a method with the highest convergence order possible, while requiring the least number of stages. For this reason, four stage fourth order methods are widely preferred.

| Order $p$ | 1 | 2 | 3 | 4 | 5 | 6 | 7 | 8 | 9 | 10 |
|---|---|---|---|---|---|---|---|---|---|---|
| Number of conditions | 1 | 2 | 4 | 8 | 17 | 37 | 85 | 200 | 486 | 1205 |
| Number of stages | 1 | 2 | 3 | 4 | 6 | 7 | 9 | 11 | | |

Table 9.2: *Number of order conditions required to achieve a given order $p$ for Explicit Runge-Kutta methods.*

In what follows, we consider four stage fourth order explicit Runge-Kutta methods characterized by the Butcher tableu,

$$\begin{array}{c|cccc} c_1 & & & & \\ c_2 & a_{21} & & & \\ c_3 & a_{31} & a_{32} & & \\ c_4 & a_{41} & a_{42} & a_{43} & \\ \hline & b_1 & b_2 & b_3 & b_4 \end{array} \tag{9.9}$$

Thus, to advance the ODE system (9.1) in time we have,

$$y_{n+1} = y_n + b_1 k_1 + b_2 k_2 + b_3 k_3 + b_4 k_4 \,, \tag{9.10}$$

where the intermediate stages $k_i$ are given by,

$$\begin{aligned} k_1 &= h f\left(x_n + c_1 h, Y_1\right) \,, \\ k_2 &= h f\left(x_n + c_2 h, Y_2\right) \,, \\ k_3 &= h f\left(x_n + c_3 h, Y_3\right) \,, \\ k_4 &= h f\left(x_n + c_4 h, Y_4\right) \,, \end{aligned} \tag{9.11}$$

and for later convenience, we have introduced the quantities $Y_i$,

$$\begin{aligned} Y_1 &= y_n \,, \\ Y_2 &= y_n + a_{21} k_1 \,, \\ Y_3 &= y_n + a_{31} k_1 + a_{32} k_2 \,, \\ Y_4 &= y_n + a_{41} k_1 + a_{42} k_2 + a_{43} k_3 \,. \end{aligned} \tag{9.12}$$

## 9.4 Taylor Expansions of the Approximate Solution

We proceed by examining the Taylor expansions of the approximate solution as given by Equation 9.10. Starting from the intermediate stages, we get

$$k_1 = hf \ , \tag{9.13a}$$

$$k_2 = hf + h^2 c_2 f_y f + \frac{h^3}{2} c_2^2 f_{yy}(f,f) + \frac{h^4}{6} c_2^3 f_{yyy}(f,f,f) + \mathcal{O}(h^5) \ , \tag{9.13b}$$

$$k_3 = hf + h^2 c_3 f_y f + \frac{h^3}{2} \left[ c_3^2 f_{yy}(f,f) + \left( 2 \sum_{j=1}^{4} a_{3j} c_j \right) f_y f_y f \right] \tag{9.13c}$$

$$+ h^4 \left[ \frac{1}{6} c_3^2 f_{yyy}(f,f,f) + \left( \sum_{j=1}^{4} c_3 a_{3j} c_j \right) f_{yy}(f, f_y f) + \frac{1}{2} \left( \sum_{j=1}^{4} a_{3j} c_j^2 \right) f_y f_{yy}(f,f) \right] + \mathcal{O}(h^5) \ , \tag{9.13d}$$

$$k_4 = hf + h^2 c_4 f_y f + h^3 \left[ \frac{1}{2} c_4^2 f_{yy}(f,f) + \left( \sum_{j}^{4} a_{4j} c_j \right) f_y f_y f \right] \tag{9.13e}$$

$$+ h^4 \left[ \frac{1}{6} c_4^3 f_{yyy}(f,f,f) + \left( \sum_{j=1}^{4} c_4 a_{4j} c_j \right) f_{yy}(f, f_y f) + \frac{1}{2} \left( \sum_{j=1}^{4} a_{4j} c_j^4 \right) f_y f_{yy}(f,f) \right. \tag{9.13f}$$

$$\left. + \left( \sum_{j,k=1}^{4} a_{4j} a_{jk} c_k \right) f_y f_y f_y f \right] + \mathcal{O}(h^5) \ , \tag{9.13g}$$

where upon application of Equation 9.10, and comparison with the Taylor approximation of the exact solution,

$$\begin{aligned} y_{n+1} = y_n + hf + \frac{h^2}{2} f_y f + \frac{h^3}{6} \left[ f_{yy}(f,f) + f_y f_y f \right] + \\ \frac{h^4}{24} \left[ f_{yyy}(f,f,f) + 3 f_{yy}(f, f_y f) + f_y f_{yy}(f,f) + f_y f_y f_y f \right] + \mathcal{O}(h^5) \, , \end{aligned} \tag{9.14}$$

results in the following order conditions,

$$b_1 + b_2 + b_3 + b_4 = 1 \,, \tag{9.15a}$$

$$b_2 c_2 + b_3 c_3 + b_4 c_4 = \frac{1}{2} \,, \tag{9.15b}$$

$$b_2 c_2^2 + b_3 c_3^2 + b_4 c_4^2 = \frac{1}{3} \,, \tag{9.15c}$$

$$b_3 a_{32} c_2 + b_4 a_{42} c_2 + b_4 a_{43} c_3 = \frac{1}{6} \,, \tag{9.15d}$$

$$b_2 c_2^3 + b_3 c_3^3 + b_4 c_4^3 = \frac{1}{4} \,, \tag{9.15e}$$

$$b_3 c_3 a_{32} c_2 + b_4 c_4 a_{42} c_2 + b_4 c_4 a_{43} c_3 = \frac{1}{8} \,, \tag{9.15f}$$

$$b_3 a_{32} c_2^2 + b_4 a_{42} c_2^2 + b_4 a_{43} c_3^2 = \frac{1}{12} \,, \tag{9.15g}$$

$$b_4 a_{43} a_{32} c_2 = \frac{1}{24} \,, \tag{9.15h}$$

which can be solved for the $c_i$, $b_i$ and $a_{ij}$ coefficients that populate the Butcher tableu (9.9). The elementary differentials appearing in equations (9.14) are Fréchet derivatives in $\mathbb{R}^d$, see for example [244]. Evidently, the Runge-Kutta algorithm relies on systematic error cancellations to arrive at the approximate solution. Should this systematic cancellation of error terms be compromised, the accuracy of the solution (9.14) is affected. In fact, when boundary conditions are applied in a way that is not consistent with the intermediate stages (9.13), the introduced error terms will not cancel out when computing the solution (9.14). This leads to a slowly convergent error in the solution, which is the essence of order reduction. We deal with how to avoid this problem in the next section.

The above scheme is certainly more verbose than the form given by Equations (9.11). Moreover, the expressions get cumbersome as the order increases. There actually is a more succinct formalism built around the idea of rooted trees, see Table 9.1. Within this formalism, one can write out Equations (9.13) and (9.14) in a general form. A thorough description may be found in e.g. [90].

## 9.5 Avoiding Order Reduction

By successive differentiation of $y' = f$, one can deduce the following useful relations,

$$y'' = f_y f \ , \tag{9.16}$$
$$y''' = f_{yy}(f,f) + f_y f_y f \ , \tag{9.17}$$
$$y'''' = f_{yyy}(f,f,f) + 3f_{yy}(f,f_y f) + f_y f_{yy}(f,f) + f_y f_y f_y f \ . \tag{9.18}$$

A more convenient form of Equations (9.13) can thus be obtained by using the above relations to eliminate some of the elementary differentials. We note that the scalar case is endowed with the simplification of the elementary derivatives $f_y f_{yy}(f,f) = f_{yy}(f,f_y f) = f_{yy} f_y f^2 \in \mathbb{R}$. In general however, $f_y f_{yy}(f,f) \neq f_{yy}(f,f_y f)$ and the simplifications that are commonplace for scalar problems are no longer possible. For practical purposes, this is not an issue since for most hyperbolic PDEs, one need only apply order $p-1$ boundary conditions to reach order $p$ in the interior domain [192]. With this in mind, one does not need to compute the $h^4$ terms above. Moreover, within the MoL discretization, boundary conditions for the stages $k_i$ are encoded in the quantities $Y_i$ given in Equations (9.12). Therefore, in order to follow the Runge Kutta scheme at the boundary points, we only need to compute the stages $k_1$, $k_2$, and $k_3$ to third order accuracy at the boundary resulting in,

$$\begin{aligned} k_1 &= hy' \ , \\ k_2 &= hy' + h^2 c_2 y'' + \frac{h^3}{2} c_2^2 \left(y''' - f_y y''\right) \ , \\ k_3 &= hy' + h^2 c_3 y'' + \frac{h^3}{2}\left[c_3^2 y''' - \left(c_3^2 - 2\sum_{j=1}^{4} a_{3j} c_j\right) f_y y''\right] \ . \end{aligned} \tag{9.19}$$

To illustrate the dependence of the boundary conditions on the chosen Runge Kutta scheme, we evaluate (9.19) for the following Runge Kutta methods

$$\begin{array}{c|cccc} 0 & & & & \\ 1/2 & 1/2 & & & \\ 1/2 & 0 & 1/2 & & \\ 1 & 0 & 0 & 1 & \\ \hline & 1/6 & 1/3 & 1/3 & 1/6 \end{array} \quad \Rightarrow \quad \begin{aligned} k_1 &= hy' \\ k_2 &= hy' + \frac{h^2}{2} y'' + \frac{h^3}{8}\left(y''' - f_y y''\right) \\ k_3 &= hy' + \frac{h^2}{2} y'' + \frac{h^3}{8}\left(y''' + f_y y''\right) \end{aligned} \tag{9.20}$$

$$
\begin{array}{c|cccc}
0 & & & & \\
1/4 & 1/4 & & & \\
1/2 & 0 & 1/2 & & \\
1 & 1 & -2 & 2 & \\
\hline
 & 1/6 & 0 & 2/3 & 1/6
\end{array}
\quad \Rightarrow \quad
\begin{aligned}
k_1 &= hy' \\
k_2 &= hy' + \frac{h^2}{4}y'' + \frac{h^3}{32}\left(y''' - f_y y''\right) \\
k_3 &= hy' + \frac{h^2}{2}y'' + \frac{h^3}{8}y'''
\end{aligned}
\tag{9.21}
$$

$$
\begin{array}{c|cccc}
0 & & & & \\
1/3 & 1/3 & & & \\
2/3 & -1/3 & 1 & & \\
1 & 1 & -1 & 1 & \\
\hline
 & 1/8 & 3/8 & 3/8 & 1/8
\end{array}
\quad \Rightarrow \quad
\begin{aligned}
k_1 &= hy' \\
k_2 &= hy' + \frac{h^2}{3}y'' + \frac{h^3}{18}\left(y''' - f_y y''\right) \\
k_3 &= hy' + \frac{2h^2}{3}y'' + \frac{h^3}{9}\left(2y''' + f_y y''\right)
\end{aligned}
\tag{9.22}
$$

Due to its popularity, at least in the numerical relativity literature, we shall restrict our attention to the classic RK4 scheme (9.20). We apply this scheme (together with equations 9.12) at the boundary to approximate the Runge-Kutta scheme of the interior. This strategy ensures proper cancellation of the error terms, thus achieving the required order of accuracy.

Of course, for practical implementations, one needs to evaluate the Jacobian matrix $f_y$ at the boundary. For scalar problems, one can trivially invert Equation 9.16 to get $f_y$, $f_y = y''/f$. This makes the implementation straightforward for scalar problems. However the situation is not so clear-cut for systems of coupled PDEs. For this case, Equation 9.16 constitutes $d$ equations for $d \times d$ unknowns, where $d$ is the number of variables within the PDE system. In this case, one has to devise other means to approximate $f_y$.

In principle, since the boundary is given as a function of time, one can make several evaluations in time and fit a multivariate polynomial in the variables. The resulting polynomial can then be analytically differentiated to obtain $f_y$. Another consideration is to use one sided lower order differencing to evaluate the Jacobian. In any case, one only has to approximate $f_y$ to $\mathcal{O}(h)$ accuracy since it appears at the $h^3$ term. A particularly appealing case arises in mesh refinement schemes where one already has coarser approximations of the intermediate stages $k_i$. Here, one can use these coarser approximations to make the approximation $f_y y'' = 4(k_3 - k_2)/h^3$ for the cancellation term. This is presented in more detail in Chapter 10.

## 9.6 Stability of Runge-Kutta Methods

The stability analysis of generic explicit Runge-Kutta schemes is carried out starting from the linear equation,

$$y' = \lambda y \ , \tag{9.23}$$

with some initial value $y(t_0) = y_0$ at the initial time $t_0$ and $\lambda \in \mathbb{C}$. The equation (9.23) admits the analytical solution $y(t) = y_0 e^{-\lambda(t-t_0)}$. Application of the classical fourth order Runge Kutta method results in the following intermediate stages,

$$\begin{aligned}
k_1 &= h\lambda y_n \ , && (9.24)\\
k_2 &= h\lambda y_n + \frac{(h\lambda)^2}{2} y_n \ , && (9.25)\\
k_3 &= h\lambda y_n + \frac{(h\lambda)^2}{2} y_n + \frac{(h\lambda)^3}{4} y_n \ , && (9.26)\\
k_4 &= h\lambda y_n + (h\lambda)^2 y_n + \frac{(h\lambda)^3}{2} y_n + \frac{(h\lambda)^4}{4} y_n \ , && (9.27)\\
& && (9.28)
\end{aligned}$$

which upon application of Equation 9.10 yields,

$$y_{n+1} = y_n + y_n \left( z + \frac{1}{2} z^2 + \frac{1}{6} z^3 + \frac{1}{24} z^4 \right) \ , \tag{9.29}$$

where we have replaced $z = h\lambda$. We follow standard practice and define, $\mathcal{P}(z) = y_{n+1}/y_n$, which results in the stability function

$$\mathcal{P}(z) = 1 + z + \frac{1}{2} z^2 + \frac{1}{6} z^3 + \frac{1}{24} z^4 \ . \tag{9.30}$$

The process of generating the stability function $\mathcal{P}(z)$ can be generalized for a generic explicit Runge Kutta method. This generalization leads to the stability function

$$\mathcal{P}(z) = 1 + z b^T (I - zA)^{-1} \mathbf{1} \ , \tag{9.31}$$

which can be rewritten as a polynomial in $z$,

$$\mathcal{P}(z) = \sum_{r=0}^{p} \frac{z^r}{r!} + \sum_{r=p+1}^{m} \alpha_j \frac{z^r}{r!} \ . \tag{9.32}$$

The region of absolute stability is given by the set $\{z \in \mathbb{C} : |\mathcal{P}(z)| \leq 1\}$. In Figure 9.1 we show the regions of absolute stability for Runge Kutta methods of orders 1, 2, 3 and 4.

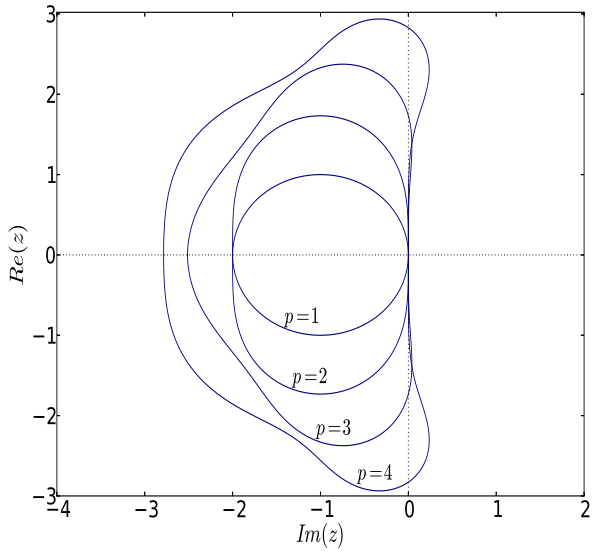


Figure 9.1: *Stability regions for Runge Kutta methods of order $p = 1$ through $p = 4$.*

## 9.7 Dispersion Relation

In this section we calculate the dispersion relation and phase velocity resulting in discretizing the wave equation with a fourth order stencil along with Runge Kutta time marching. We follow the approach (and notation) of [112] where a similar calculation was given using second order finite differences and iterative Crank-Nicholson time marching. The wave equation (10.11) can be written in matrix form as

$$V_t = \begin{pmatrix} 0 & 1 \\ \partial_{xx} & 0 \end{pmatrix} V \ , \tag{9.33}$$

where we have defined the vector $V$ as

$$V = \begin{pmatrix} \phi \\ \Pi \end{pmatrix} \ . \tag{9.34}$$

With this identification, we denote by $V_j^n$ the solution at time step $n$ and grid point $j$. The second derivative operator $\partial_{xx}$ appearing in the system (9.33) is given by the stencil,

$$\partial_{xx} V_i^n = \frac{-V_{i+2}^n + 16V_{i+1}^n - 30V_i^n + 16V_{i-1}^n - V_{i-2}^n}{12dx^2} \ . \tag{9.35}$$

For our analysis, we consider plane wave solutions for $V$, of the form,

$$V_j^n = We^{i\omega ndt} e^{-ikjdx}, \tag{9.36}$$

for some constant vector $W$. Using the classical fourth order Runge Kutta scheme to advance Equation (9.33) in time, results in the update rule,

$$V^{n+1}{}_j = MV^n{}_j \ . \tag{9.37}$$

Plugging in (9.36) to the above rule results in the relation,

$$e^{i\omega\Delta t} W = \begin{pmatrix} 1 - 2\Lambda^2 + \frac{2}{3}\Lambda^4 & \Delta t\left(1 - \frac{2}{3}\Lambda^2\right) \\ -\dfrac{4\Lambda^2(3 - 2\Lambda^2)}{3\Delta t} & 1 - 2\Lambda^2 + \frac{2}{3}\Lambda^4 \end{pmatrix} W \ , \tag{9.38}$$

where we have defined $\Lambda$ as,

$$\Lambda = \frac{\Delta t}{\Delta x}\sqrt{\frac{4}{3}\sin^2\left(\frac{k\Delta x}{2}\right) - \frac{1}{12}\sin^2\left(k\Delta x\right)} \ . \tag{9.39}$$

The system (9.38) represents an eigenvalue problem. In particular, $W$ is an eigenvector corresponding to the eigenvalue $e^{i\omega dt}$ for the matrix in (9.38). Further analysis shows the eigenvalues to be the pair,

$$e^{i\omega\Delta t} = 1 - 2\Lambda^2 + \frac{2}{3}\Lambda^4 \pm 2i\Lambda\left(1 - \frac{2}{3}\Lambda^2\right) \ . \tag{9.40}$$

This expression represents the dispersion relation, relating the frequency $\omega$ with the wave number $k$. For completeness we calculate the phase velocity, $v_p(\lambda) = \xi/k$ for $\xi = \text{Re}\ (\omega)$. From (9.40) we get,

$$\xi\Delta t = \arcsin\left(\frac{2\Lambda(3 - 2\Lambda^2)}{\sqrt{9 - 4\Lambda^6(2 - \Lambda^2)}}\right) \ . \tag{9.41}$$

Therefore the phase velocity $v_p$ is given by,

$$v_p(\lambda) = \frac{\lambda}{2\pi\Delta t}\arcsin\left(\frac{2\Lambda(3-2\Lambda^2)}{\sqrt{9-4\Lambda^6(2-\Lambda^2)}}\right) . \tag{9.42}$$

## 9.8 Dense Output

Dense output is an important concept in the studies and application of Runge Kutta methods. For higher order methods, one can generally take larger step sizes without compromising accuracy. In general, for a given step size $\Delta t$, the method will output points at times $t_n + \Delta t$. However, cases arise where one needs points at, say $\theta = t_n + c\Delta t$ for some $c \in \mathbb{R}$, $0 \leq c \leq 1$. Several options are available to achieve this. For example, one can construct a Hermite interpolating polynomial along the points $t_n + \Delta t$. Consider the points $t_n$ and $t_{n+1}$ with solutions $y_n$ and $y_{n+1}$ respectively. One can utilize the available derivative information $f_n = \Delta t f(y_n)$ and $f_{n+1} = \Delta t f(y_{n+1})$ to construct the following third order polynomial

$$\begin{aligned} y(\theta) &= (1-\theta)y_n + \theta y_{n+1} \\ &\quad + \theta(\theta-1)\Big[(1-2\theta)(y_{n+1}-y_n) + (\theta-1)\Delta t f_n + \theta\Delta t f_{n+1}\Big] . \end{aligned} \tag{9.43}$$

Although this polynomial is both continuous and $\mathcal{C}^1$, it has the undesirable property of requiring the derivative at the next time step. In a mesh refinement setting, one typically only has the points $y_n$, $y_{n+1}$ and $f(y_n)$ to interpolate to finer meshes before calculating the derivative $f_{n+1}$. For the classical fourth order Runge Kutta method, we have the following third order formula, based on the Runge Kutta order conditions [196],

$$y(\theta) = y_n + b_1(\theta)k_1 + b_2(\theta)k_2 + b_3(\theta)k_3 + b_4(\theta)k_4 , \tag{9.44}$$

where the $k_i$ are the current intermediate stages of the Runge Kutta method and the $b_i$ are polynomials in $\theta$ given by,

$$b_1 = \theta - \frac{3}{2}\theta^2 + \frac{2}{3}\theta^3 , \tag{9.45}$$

$$b_2 = \theta^2 - \frac{2}{3}\theta^3 , \tag{9.46}$$

$$b_3 = b_2 , \tag{9.47}$$

$$b_4 = -\frac{1}{2}\theta^2 + \frac{2}{3}\theta^3 . \tag{9.48}$$

This method forms a key component of time interpolation in our mesh refinement method (§10.3.1).

## 9.9 Numerical Examples

As our numerical examples, we adopt the non linear advection equation and the Einstein field equations. A key requirement in the numerical tests is that the boundary conditions to be imposed must be time dependent. We apply boundary conditions using two methods. The first method is the conventional method, characterized by evaluating the boundary function at the time corresponding to the intermediate stage in question. The second method is using our proposed scheme which we will label as 'non linear'.

### 9.9.1 Non-Linear Advection

We solve the non linear scalar advection equation,

$$u_t = 2uu_x\,, \tag{9.49a}$$

$$u(1,t) = \frac{0.5}{2-t}. \tag{9.49b}$$

on the domain $x \in [0,1]$, with the inflow boundary located at $x = 1$. One can solve (9.49a) analytically to obtain, [306]

$$u(x,t) = \frac{x}{2(2-t)}. \tag{9.50}$$

We use a pseudospectral approximation on $N+1$ Gauss-Chebyshev-Lobatto collocation points for the space discretization of Equation (9.49a). A numerical solution showing the evolution of $u(x,t)$ with $N = 10$ is shown in Figure 9.2. Figure 9.3 shows the convergence plot for the different boundary treatment methods. Here, we note that when Equation (9.20) is evaluated with $f_y = 0$, it will differ at the $h^3$ term with the Runge-Kutta algorithm for $k_2$ and $k_3$, leading only to third order convergence for non linear problems.

### 9.9.2 Gowdy Spacetime

For this test, we use the Einstein field equations in the ADM form, a system of coupled partial differential equations given by (7.27). We evolve an expanding polarized Gowdy spacetime on the domain $z \in [-0.5,\ 0.5]$. Although the solution has a $T^3$ spatial topology on this domain, we do not enforce periodic boundary conditions, but instead use the analytical solutions

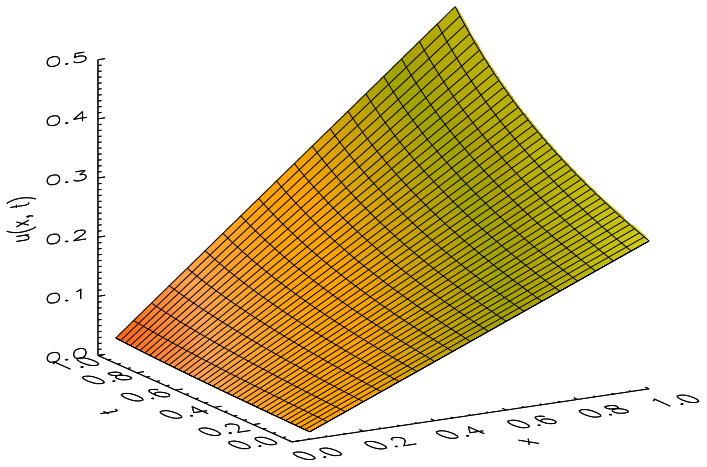


Figure 9.2: *Numerical solution of the non linear advection equation with initial and boundary equations derived from Equation (9.50).*

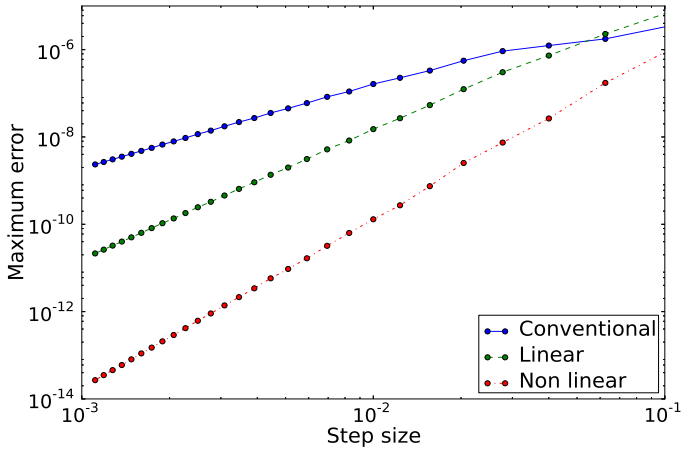


Figure 9.3: *Log-log plot of the $L_\infty$ error in the solution of the non linear advection equation (9.49a) for the conventional and non linear boundary treatment. The line marked 'linear' represents the non linear scheme with the Jacobian set to zero, $f_y = 0$.*

(9.54) to cast the boundary conditions into a time dependent Dirichlet form in order to use the scheme (9.19) for the intermediate steps. The polarized Gowdy metric is given by,

$$ds^2 = t^{-1/2}e^{\lambda/2}(-dt^2 + dz^2) + te^P dx^2 + te^{-P}dy^2, \tag{9.51}$$

with analytical solutions,

$$\begin{aligned}\lambda(z,t) &= 2\pi^2 t^2\left(J_0(2\pi t)^2 + J_1(2\pi t)^2\right) \\ &\quad -2\pi t J_0(2\pi t) J_1(2\pi t)\cos^2(2\pi z) \\ &\quad +\pi J_0(2\pi) J_1(2\pi) - 2\pi^2\left(J_0(2\pi)^2 + J_1(2\pi)^2\right)\end{aligned} \tag{9.52}$$

and

$$P(z,t) = J_0(2\pi t)\cos(2\pi z), \tag{9.53}$$

where $J_0$ and $J_1$ are Bessel functions of the first kind, see [16] and references therein. The initial conditions for the ADM variables $g_{ij}$ and $K_{ij}$ are derived from (9.51), (9.52) and (9.53) and are given by,

$$g_{xx} = te^{P}\ , \qquad K_{xx} = -\frac{1}{2}t^{1/4}e^{-\lambda/4}e^{P}(1+tP_{,t})\ , \tag{9.54}$$

$$g_{yy} = te^{-P}\ , \qquad K_{yy} = -\frac{1}{2}t^{1/4}e^{-\lambda/4}e^{-P}(1-tP_{,t})\ , \tag{9.55}$$

$$g_{zz} = t^{-1/2}e^{\lambda/2}\ , \qquad K_{zz} = \frac{1}{4}t^{-1/4}e^{\lambda/4}(t^{-1}-\lambda_{,t})\ . \tag{9.56}$$

The gauge condition is characterized by,

$$\alpha = \sqrt{g_{zz}} = t^{-1/4}e^{\lambda/4} \qquad \text{and} \qquad \beta_i = 0\ . \tag{9.57}$$

We make the following remarks about this test:

1. Because the metric is singular at $t = 0$, we start the evolution from $t = 1$ [293, 16].

2. Although the solution is essentially one dimensional, following [16], we evolve it in a three dimensional grid, with dimensions $[-0.5,\ 0.5] \times [-0.5,\ 0.5] \times [-0.5,\ 0.5]$.

3. The variable $\lambda(z,t)$ increases linearly with time, leading to exponential growth in $g_{zz}$ and $K_{zz}$. This causes the numerical solution to drift from the analytical solution with time.

4. In our adopted gauge (9.57), the speed of light is not constant along the trivial directions ($x$ and $y$), this affects the long term behavior of the numerical solution [71].

These and other issues present a challenge for most numerical relativity codes when numerically evolving the Gowdy spacetime [31].

We discretize the ADM equations using fourth order accurate finite differences in a 3D grid with four ghost zones in each of the trivial dimensions and only two along the $z$ dimension. Although it is customary to include artificial dissipation in numerical relativity codes, we do not add any here. This arrangement requires a minimum of eight grid points in each dimension. We therefore make the choice $N_x = N_y = 8,\ N_z = 25\rho,\ \rho \in \{1, 2, 4, 8, 16\}$. The numerical solutions for $\rho = 4$ ($N_z = 100$) are presented in Figure 9.4.

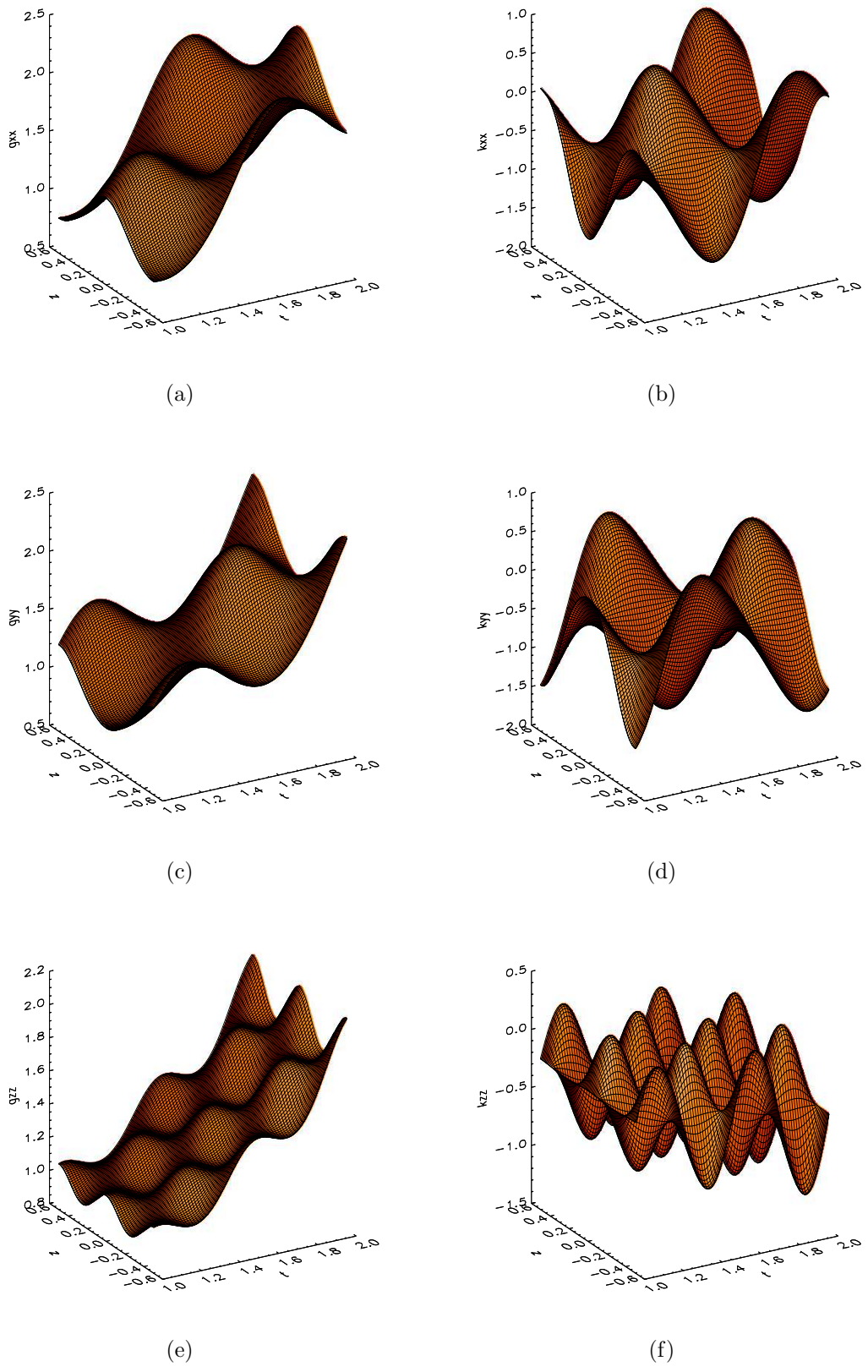


(a) (b)

(c) (d)

(e) (f)

Figure 9.4: *Numerical evolution of the Gowdy spacetime. (a), (b) and (c) show the metric functions respectively $g_{xx}, g_{yy}$ and $g_{zz}$ while (b), (d) and (f) show the extrinsic curvature components $K_{xx}, K_{yy}$ and $K_{zz}$ respectively.*

We use the quantity $\mathcal{E}_g$ as a measure of the error in the solution, [293]

$$\mathcal{E}_g = \sqrt{\left(\frac{g_{xx}}{\gamma_{xx}} - 1\right)^2 + \left(\frac{g_{yy}}{\gamma_{yy}} - 1\right)^2 + \left(\frac{g_{zz}}{\gamma_{zz}} - 1\right)^2}. \tag{9.58}$$

Where the $g_{ii}$ are numerical solutions and the $\gamma_{ii}$ are the analytic solutions. The convergence plot is shown in Figure 9.5. Note how the order reduction in the conventional method kicks in at smaller step sizes. In the lower resolution region, the boundary error is not the dominant source of error, however, as one goes to higher resolution, the boundary error starts to dominate as evidenced by a reduced rate of convergence.

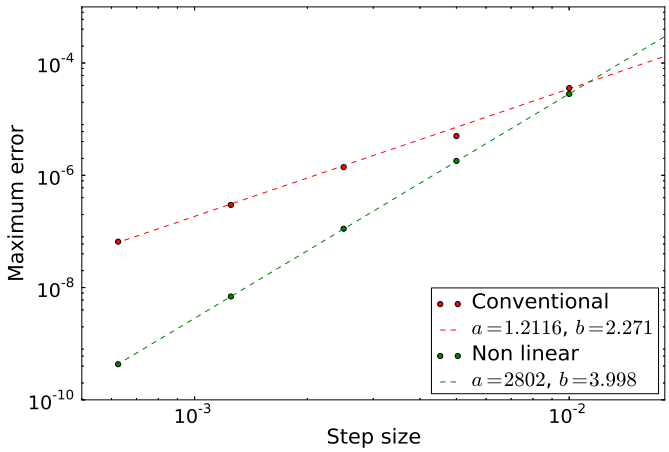


Figure 9.5: *Log-log plot of the $L_\infty$ error in the evolution of the Gowdy space time. We also fit a power law of the form $y = ax^b$, with $b$ representing the order of convergence. In this case, the conventional method has convergence rate* $2,271$ *while the non linear method gives the expected rate of convergence* $3.998$.

## 9.10 Summary

In this Chapter, we have presented a procedure for the consistent application of intermediate boundary conditions when using explicit Runge Kutta algorithms for non linear hyperbolic partial differential equations within the method of lines framework. By applying the boundary conditions in a way that follows the Runge Kutta scheme, the method retains its formal order of accuracy, and no order reduction effects are observed.

On the numerical cost of the schemes investigated, the conventional method is by far the cheapest. Of course, it also gives the worst convergence rate. The cost of the non linear scheme should be negligible for scalar problems. For systems of coupled PDEs, the cost

will depend on how the Jacobian matrix $f_y$ is estimated. Comprehensively, the boundary is usually much smaller than the domain of integration and should incur the least computational work by comparison, irrespective of the boundary scheme chosen. We emphasize that in comparing the computational work of the conventional method with the non-linear method presented here, one must take into account that, the former is effectively second order convergent, while the latter is fourth order convergent. Therefore, in order to reach the same level of accuracy one will require significantly smaller step sizes when employing the conventional method, which translates to a high computational cost.

For practical considerations we note that simplifications can often arise because of the following points,

1. It may happen that some quantities are not spatially differentiated in the PDE system, such quantities may not require the computation of boundary conditions.

2. For those quantities that do require boundary conditions, some may not actually be time dependent. The conventional method is then sufficient for such quantities.

3. The time derivatives of some quantities might not depend on all the variables, resulting in a sparse Jacobian matrix.

The non trivial question of how to apply boundary conditions for the Runge Kutta intermediate stages also arises in mesh refinement algorithms employing the Berger-Oliger-Colella time stepping [59, 58]. The incompatibility of high order Runge Kutta schemes with mesh refinement algorithms is discussed by several authors [248, 131, 80] in the context of numerical relativity. Basically one usually finds a slowly converging error in the interface boundaries, often resulting in artificial reflections across mesh refinement boundaries. Consequently the accuracy and convergence properties of the solution are compromised. This undesirable feature is not surprising, considering that the standard mesh refinement algorithm applies boundary conditions in the conventional way, which only works well for second order schemes. The work presented here acts as a stepping stone toward fourth order mesh refinement schemes, especially in the field of numerical relativity where one deals with non linear systems of hyperbolic PDEs. This issue is the subject of Chapter 10.

# Chapter 10

# Fourth Order Mesh Refinement

## 10.1 Introduction

Long term stable evolution of non linear hyperbolic partial differential equations often require techniques to efficiently deal with vast length scales while simultaneously resolving fine scale features. Indeed, many numerical simulations in computational astrophysics, cosmology, numerical relativity and fluid dynamics are confronted with processes that span a wide range of time and length scales. In the context of numerical relativity, these simulations are often performed in full three spatial dimensions without any symmetry assumptions. For these cases, running fine unigrid integrations is computationally expensive and often impractical. Recent establishments in the numerical solution of partial differential equations by finite difference techniques has seen an increasing use of nested grids and mesh refinement techniques in order to minimize the truncation error incurred with minimal computational and memory requirements [59, 58, 329].

The principle behind mesh refinement schemes is to recursively refine areas of the computational grid that are likely to induce higher discretization errors. This approach efficiently focuses computational effort and resources in places where it is needed compared to refining the entire grid. Extensive theory has since been developed for the method in different contexts, and mesh refinement algorithms have been widely adopted in the literature [263, 298, 334, 137, 409]. One of the key aspects in the implementation is the way in which the decision to add or remove levels of refinement is made. In this work we focus on the concept of fixed mesh refinement (FMR), where the grid hierarchy is created once and remains fixed for the duration of the computation [79, 334, 112]. This differs from adaptive mesh refinement (AMR), where the algorithm is endowed with error estimation routines that dynamically determines which areas need refinement. For most applications in numerical rel-

ativity, one can know before hand which areas within the computational domain require more refinement. As a result the FMR configuration is widely adopted in the field. In the context of numerical relativity, mesh refinement has seen application in studies of critical phenomena [113], single black hole space times [78, 412], binary black hole collisions [79, 204], black hole lattice universes [56, 55], neutron stars [365, 302] and core-collapse supernovae [299, 300], within the non linear framework of general relativty.

Another component of the scheme is the inter-level coupling among nested grids. While the coarse grid has to supply boundary conditions to finer grids during evolution, one can choose not to update the coarse grid solution with the fine grid solution. This is the basis of one way (parasitic) schemes. In this work we employ the two way (interactive) scheme, where we update coarser levels with finer levels once the finer levels have been integrated to the same time level as the coarser ones. See [197] for a comparison between parasitic and interactive coupling.

Traditionally, mesh refinement techniques were coupled to second order convergent methods. On the other hand, recent trends in the numerical simulation community has seen the coupling of higher order finite difference methods to the mesh refinement framework [342, 248, 131, 416, 314]. This combines the efficiency of local mesh refinement with the robustness and accuracy of higher order methods. However, there is an inherent incompatibility between high order time discretization schemes with the standard mesh refinement algorithm that may result in loss of convergence or even instabilities [248]. This issue is related to how the computation of boundary data for the refined grids is handled. A search for a stable high order mesh refinement implementation has resulted in several modifications to the standard method in an effort to address this subject. Most notably, [334] introduces the idea of buffer zones in the refined grids. In this setup, boundary conditions are not prescribed explicitly in the refined levels, the integration is only applied to a progressively smaller domain in the refined grids and the buffer zone is ultimately discarded. Another approach is the tapered boundary approach [248, 131]. Here, one performs the integration at level $l$ using the past domain of dependence of the child grid only. Other approaches have been to refine only in space while using the same time step for all levels [112]. In this work we use a framework where we refine both in space and time and the treatment of interface boundaries is dictated by the time marching algorithm, fourth order accurate Runge Kutta algorithm in this case.

In addition to issues of convergence and stability, one has to address the problem of spurious reflections off refinement boundaries that arise when propagating waves cross refinement boundaries. This is essential for gravitational wave source simulations as the waves are normally extracted at a large radius. Propagating waves will have crossed several refinement

boundaries, before reaching the radius of extraction. In [112], the idea of derivative matching was proposed in order to minimize spurious reflections for second order convergent schemes. Also, the concept of mesh adapted stencils (MAD) was introduced in [33]. However these implementations do not involve refinement in time. Other methods that have been applied in the Advanced Weather Research and Forecasting Model, Euler equations and Maxwell equations involve the use of sponge layers in the refined levels to ensure that the solution in the refined levels will be nudged towards that of the coarser grids at refinement boundaries. This typically involves the addition of artificial damping and dissipation terms in the system under consideration [197, 348]. See also the treatment of [318] in the case of first order convergent schemes. In this work we propose a simple scheme that is adopted from the animation and image processing community [148], to deal with transitions from fine to coarse grid solutions at refinement boundaries.

Finally, we note that high order mesh refinement implementations are often endowed with several lower order approximations in order to reduce the overall computational demand [80, 314, 416]. In the case where there is refinement in time, this often includes the use of lower order interpolations in time. This results in some savings in memory usage as the storage of past time levels is lower for lower order interpolations. For example, one typically needs $n+1$ past points in order to have a $n$-th order polynomial interpolant. In addition, one can reduce the number of buffer zones in the refinement boundaries by successively lowering the order of finite differencing as one approaches the refinement boundary. Other approaches in the case where artificial dissipation is needed, include the use of Kreiss-Oliger dissipation operators of order lower than that required by the finite differencing operator. This lowers the number of required ghost points as well as being cheaper computationally. Ultimately, these approximations have a bearing on the convergence order, the amount of spurious reflections induced at interface boundaries and the overall performance of a given implementation.

This Chapter is organized as follows: in Section 10.2 we convey the framework of our FMR approach. We review our boundary application method in §10.3.1 and introduce the transition zone in §10.3.2. Finally, we present our results and discussions in Section 10.4.

## 10.2 Generalities

Our FMR implementation follows the discussion in §8.8, without the adaptivity. In addition, we employ fourth order accurate finite differencing in space as discussed in §8.3. Time marching is handled through the classical four state fourth order accurate Runge Kutta scheme (Chapter 9).

## 10.3 Interface Boundary Treatment

The base grid consists of a ghost zone that serves to store boundary data. For refined grids, in addition to ghost zones, there is also a transition zone that ensures a smooth transition from the well resolved solution of the finer grids to the less resolved solution of the coarser grids. We discuss each in turn.

### 10.3.1 Ghost Zone

For a fourth order accurate computation of centered derivatives, we use two ghost zones on each side of a grid[1]. Outer boundary conditions on the base grid are supplied by the user, for example, the user may specify periodic or sommerfeld type boundary conditions. We distinguish between two types of boundary conditions for the finer levels, those that coincide with the outer boundary and those that simply border a cell from the underlying coarse grid.

If the ghost zones of refined grids coincide with those of the base grid, the boundary is filled using the prescribed procedure for outer boundaries. Otherwise, we use coarse grid data to fill the fine grid boundaries. In Chapter 9, we showed that using the conventional method of imposing boundary conditions, i.e, simply applying boundaries corresponding to the intermediate times of Runge Kutta methods leads to a loss of convergence for unigrid runs. We have found that this method, leads to unstable modes in the mesh refinement case. We instead use the Runge Kutta method itself to fill the ghost zones. We use Equations (9.12), where the $k_i$ are given by,

$$\begin{aligned} k_1 &= hy' \ , \\ k_2 &= hy' + \frac{h^2}{2}y'' + \frac{h^3}{8}\left(y''' - f_y y''\right) \ , \\ k_3 &= hy' + \frac{h^2}{2}y'' + \frac{h^3}{8}\left(y''' + f_y y''\right) \ . \end{aligned} \tag{10.1}$$

In the equations above, $y', y''$ and $y'''$ are time derivatives of the quantities under evolution while $f_y$ is the Jacobian matrix of the PDE system. See [283] for more details. The time derivatives can easily be obtained by polynomial interpolation methods since the coarse grid points at the advanced time will already have been computed before advancing the refined levels. However, a subtle issue arises in this case. To evolve the finer grids, at least four past points of the coarse grid solution are needed in order to obtain third order interpolants.

[1] However, our implementation is such that one needs the number of Ghost points to be odd for a staggered mesh and even otherwise. We will employ the staggered mesh in this Chapter and thus choose the number of Ghost points to be three.

This means each finer grid can only be initialed after the coarser grid has evolved at least four time steps. This is undesirable in the context of FMR. We opt to use the fact that the classical Runge Kutta method has a built-in interpolant, termed dense output (see §9.8). This interpolant is given by, [196]

$$y(t_n + \theta h) = y_n + \sum_{i=1}^{4} b_i(\theta) k_i + \mathcal{O}(h^4) \ , \tag{10.2}$$

with $0 \leq \theta \leq 1$ and the $b_i$ are polynomials in $\theta$,

$$b_i(\theta) = \theta - \frac{3}{2}\theta^2 + \frac{2}{3}\theta^3, \qquad b_2(\theta) = b_3(\theta) = \theta^2 - \frac{2}{3}\theta^3, \qquad \text{and} \qquad b_4(\theta) = -\frac{1}{2}\theta^2 + \frac{2}{3}\theta^3 \ . \tag{10.3}$$

One can verify that this dense output formula reduces to Equation (8.47) when $\theta = 1$. The required time derivatives are then computed from Equation (10.2) as,

$$\frac{d^{(m)}}{dt^{(m)}} y(t_n + \theta h) \quad = \quad \frac{1}{h^m} \sum_{i=1}^{s} k_i \frac{d^{(m)}}{d\theta^{(m)}} b_i(\theta) + \mathcal{O}(h^{4-m}) \ , \tag{10.4}$$

with $1 \leq m \leq 3$. One does not need to compute the Jacobian matrix $f_y$ explicitly since we are only interested in the product $f_y y''$ which can be computed from the system (10.1) as,

$$f_y y'' = \frac{4}{h^3} \left( k_3 - k_2 \right) \ . \tag{10.5}$$

See also, [280]. The implication is that we do not store the solution history of coarser grids but we store the four (current) intermediate $k_i$ values instead. Of course this is followed by spatial interpolation, for which we employ fourth order barycentric Lagrange interpolation (§8.8.5); higher than fourth order was found to be unreliable in some of the runs.

### 10.3.2 Transition Zone

To complete the specifications on treatment of the boundary, we examine what happens close to the refinement boundary. Consider a grid hierarchy with two levels $l_0$ and $l_1$. Parametrize the solution $F(x)$ on such a hierarchy as,

$$F(x) = (1 - w) f(x, l_0) + w f(x, l_1), \tag{10.6}$$

where $f(x, l_0)$ and $f(x, l_1)$ are the solutions on the base and refined grids respectively, and $w$ is a binary weight function which takes the value $w = 1$ if $x$ is within the refined region and $w = 0$ everywhere else. A plot of the weight function is depicted in Figure 10.1. Note the discontinuity at the transition points $x = 10$ where $w$ transitions from $w = 0$ to $w = 1$ indicating a switch from the solution $F(x) = f(x, l_0)$ to $F(x) = f(x, l_1)$. Also at $x = 90$, $w$ transitions from $w = 1$ to $w = 0$, indicating the switch from $F(x) = f(x, l_1)$ back to $F(x) = f(x, l_0)$.

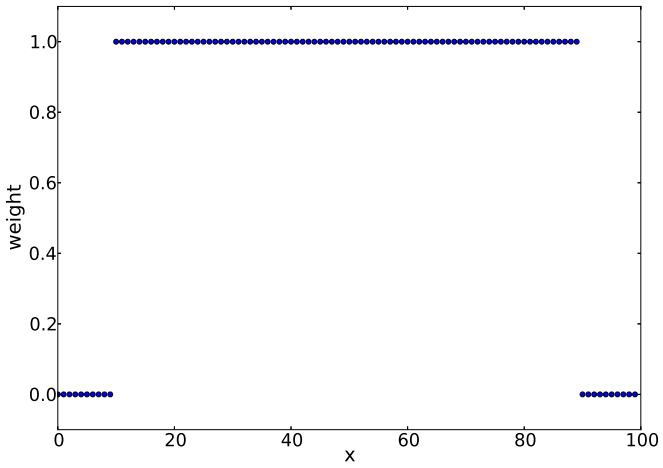


Figure 10.1: *Step function transition profile from $w = 0$ to $w = 1$. The refined region in this case is $x \in [10, 90]$. Note the discontinuity at $x = 10$ where the weight $w$ transitions from w=0 to w=1 and again at $x = 90$ where $w$ transitions from $w = 1$ to $w = 0$.*

Because of the dispersion relation for propagating waves (§9.7), there is a difference in phase speeds of propagating modes in the coarse and fine grid levels. As a result of the discontinuous transition in the weight function $w$, waves propagating from refined regions abruptly change their phase velocities when crossing refinement boundaries, creating a glitch that will seed spurious reflections. To circumvent this problem, we introduce a transition zone on the refined levels, within which the weight function $w = w(x)$ is allowed to vary smoothly from $w = 0$ to $w = 1$ across the refinement boundary. This can be accomplished by Hermite interpolation (see §8.8.5). For a transition beginning at $x = a$ and ending at $x = b$, one can derive the following profiles,

$$w(a, b, x) = t \qquad \text{(boxstep)} \tag{10.7}$$

$$w(a, b, x) = 3t^2 - 2t^3 \qquad \text{(smoothstep)} \tag{10.8}$$

$$w(a, b, x) = 10t^3 - 15t^4 + 6t^5 \qquad \text{(smootherstep)} \tag{10.9}$$

where the variable $t$ is defined as,

$$t = \begin{cases} 0 & \frac{x-a}{b-a} < 0 \\ 1 & \frac{x-a}{b-a} > 1 \\ \frac{x-a}{b-a} & \text{otherwise} \end{cases}$$

These profiles are shown in Figure 10.2. In this case the weight function varies continuously from $w = 0$ to $w = 1$, allowing the solution $F(x)$ to vary smoothly across the transition zone. This can also be interpreted as a smooth acceleration and deceleration of the associated phase speeds of propagating modes in the solution $F(x)$. See [148] for a discussion on transition profiles.

The procedure we follow to ensure a smooth transition from the fine grid solution to the coarse grid solution is as follows.

- Fill ghost zone points using the method outlined in §10.3.1.
- Fill the transition zone by blending values from the refined grid, with that of the coarse grid according to the weight function $w(x)$.

The transition zone is evolved along with the fine grid solution to ensure a smooth coupling with the refinement boundary and thus the coarse grid solution. However, for reasons of stability, we do not use transition zone values when updating the coarse grid solution with the fine grid solution. Unless otherwise specified, we take the width of the transition zone to be three through out this work. For this size, the smooth profiles given above are equivalent.

## 10.4 Numerical Results

For ease of exposition, we restrict to the case $\beta^i = 0$. The time step is given by $dt = cdx$ where $c = 0.25$ for all the runs considered here. Where refinement is used, we restrict to a refinement factor $r = 2$. All runs employ three ghost points and, where appropriate, three transition points.

### 10.4.1 Wave equation: Periodic boundaries

In this section, we carry out evolutions of the wave equation with mesh refinement. The wave equation in flat Cartesian coordinates is given by,

$$\partial_{tt}\phi = \partial^i \partial_i \phi. \tag{10.10}$$

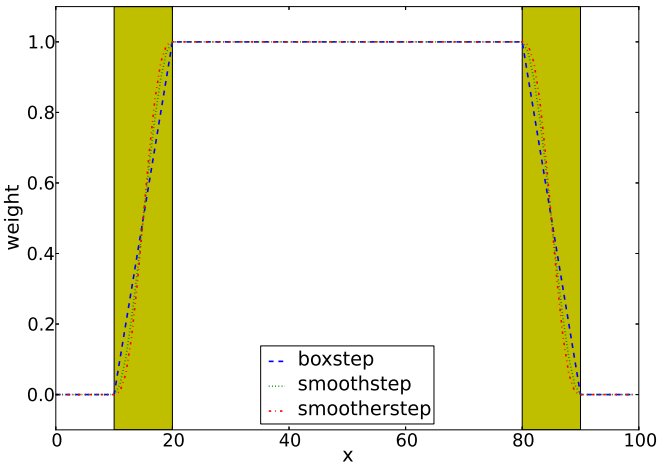


Figure 10.2: *Smooth transition profiles from $w = 0$ to $w = 1$. The refined region in this case is $x \in [10, 90]$ with the shaded regions representing the transition zone. We have exaggerated the width of the transition zone for ease of visualization. Compare with Figure 10.1.*

We instead cast it in an alternative form, by introducing a new auxiliary variable $\Pi = \partial_t \phi$,

$$\partial_t \phi = \Pi \tag{10.11a}$$

$$\partial_t \Pi = \partial^i \partial_i \phi \tag{10.11b}$$

As initial data, we choose a sinusoidal profile

$$\phi(x, y, z, t = 0) = \sin(2\pi(x - t)) \qquad \Pi(x, y, z, t = 0) = -2\pi \cos(2\pi(x - t)), \tag{10.12}$$

with periodic boundary conditions on the domain $x \in [-0.5, 0.5]$. The region $x \in [-0.25, 0.25]$ is refined by a factor of $r = 2$. Although the wave propagates essentially in one dimension, we evolve it using the full 3D grid with periodic boundary conditions for the outer boundaries. In Figure 10.3 we plot the solution errors for evolutions with resolution $dx = 1/25\rho$ for $\rho = 1, 2, 3$. The errors show fourth order convergence as desired.

### 10.4.2 Gauge Wave

We now evolve a non linear gauge wave using the BSSN system. The Gauge wave test is characterized by a line element which results from a non linear gauge transformation of the

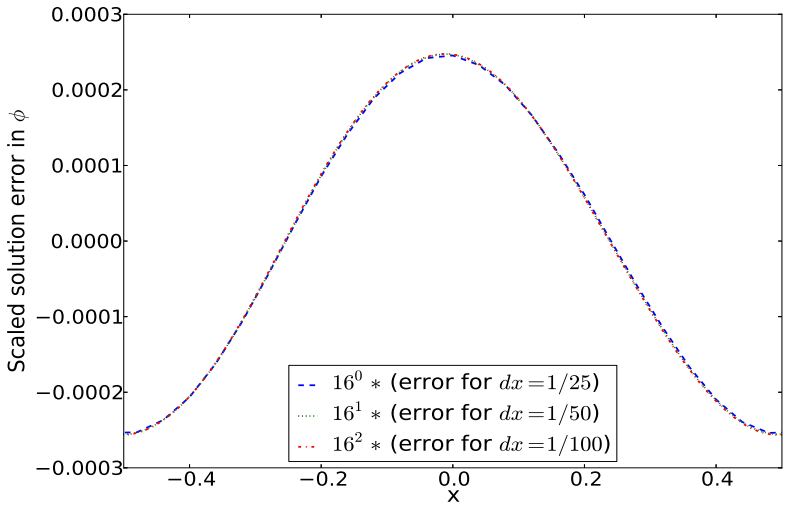


Figure 10.3: *Scaled solution errors for $\phi$ after 2 crossing times. The errors have been scaled with the resolution to highlight fourth order convergence.*

flat Minkowski space time in Cartesian coordinates, resulting in

$$ds^2 = -Hdt^2 + Hdx^2 + dy^2 + dz^2 \ , \tag{10.13}$$

where the function $H$ is given as,

$$H \equiv H(x-t) = 1 + A \sin\left(\frac{2\pi(x-t)}{d}\right) \ , \tag{10.14}$$

for some constant $A$, and $d$ is the wavelength. We evolve the above metric using the BSSN formulation with the Harmonic gauge condition,

$$\partial_t \alpha = -\alpha^2 K \ . \tag{10.15}$$

We choose the amplitude $A = 0.1$ and the wavelength $d = 1$. As in the last case, the simulation domain covers the range $x \in [-0.5 : 0.5]$ with refinement boundaries in the region $x \in [-0.25 : 0.25]$. Evolving the gauge wave initial data with the BSSN formulation requires the addition of artificial dissipation in order to achieve stable evolutions. This is true even for unigrid runs, see for example [31]. Our dissipation operator takes the form described in §8.5. In Figure 10.4 we plot the solution errors for evolutions with resolution $dx = 1/25\rho$ for $\rho = 1, 2, 3$. The errors scale according to fourth order convergence.

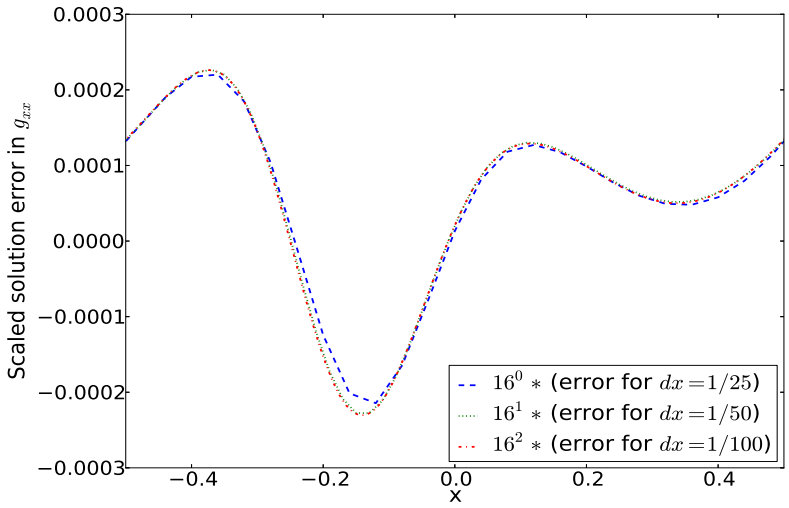


Figure 10.4: *Scaled solution errors for the $g_{xx}$ component of the gauge wave metric after 2 crossing times. The errors have been scaled with the resolution to highlight fourth order convergence.*

### 10.4.3 Wave equation: Gaussian pulse

In the following test we show how our proposed algorithm handles artificial reflections that often arise when a propagating wave crosses a mesh refinement boundary. We are interested in waves propagating outward from the fine grid across mesh refinement boundaries into the coarser grid. We evolve the wave equation, with initial data given by a Gaussian pulse centered at the origin,

$$\phi(x, y, z, t = 0) = A \exp(-x^2/\sigma^2) \qquad \Pi(x, y, z, t = 0) = 0, \tag{10.16}$$

with $\sigma = 0.25$ and $A = 1$. Although the wave propagates essentially in one dimension, we evolve it using the full 3D grid with periodic boundary conditions for the outer boundaries. The simulation domain covers $x \in [-4, 4]$. The region $x \in [-1, 1]$ is further refined by a factor of $r = 2$.

The solution is shown in Figure 10.5(a). The pulse starts initially at $x = 0$ with amplitude one and produces two pulses each with amplitude 0.5 traveling in opposite directions. In Figure 10.5(b) we show the result after the pulses have crossed refinement boundaries at $x = \pm 1$. When each pulse crosses a refinement boundary, spurious reflections are generated. These travel in a direction opposite that of the inducing pulse. When no transition zone is used, the spurious reflections reinforce at $x = 0$ and can exceed the discretization error in amplitude. Employing a transition zone significantly reduces these artificial reflections.

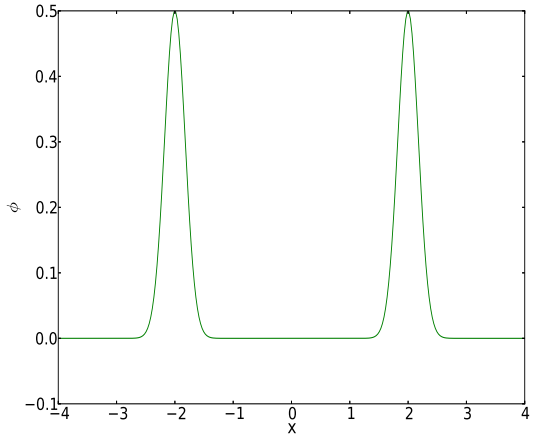


(a)

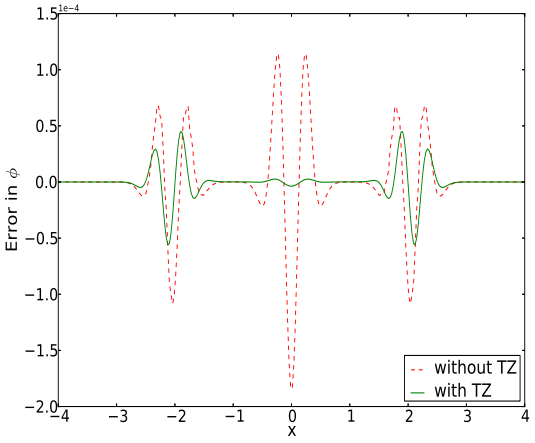


(b)

Figure 10.5: *Solution of the wave equation at $t = 2s$. (a) A plot showing $\phi$. (b) Error in $\phi$ computed from the analytic solution for two runs with the same resolution, with and without a transition zone. Note the artificial reflection at $x = 0$.*

### 10.4.4 Teukolsky Wave

In this section we evolve the Einstein field equations in three space dimensions, using the BSSN formulation (§7.6). As initial data, we use the Teukolsky solution for a quadrupole

$l = 2$, even parity $m = 0$ waves [368]. The metric for the quadrupole modes is given by,

$$ds^2 = -dt^2 + (1 + Af_{rr})dr^2 + (2Bf_{r\theta})r\,dr\,d\theta + (2Bf_{r\phi})\,r\,\sin\theta\,dr\,d\phi \tag{10.17}$$

$$+ \left(1 + Cf^{(1)}_{\theta\theta} + Af^{(2)}_{\theta\theta}\right) r^2\,d\theta^2 + [2(A - 2C)f_{\theta\phi}]r^2\sin\theta\,d\theta\,d\phi \tag{10.18}$$

$$+ \left(1 + Cf^{(1)}_{\phi\phi} + Af^{(2)}_{\phi\phi}\right) r^2\,\sin^2\theta\,d\phi^2\ . \tag{10.19}$$

The coefficients $A$, $B$ and $C$ are constructed via a generating function $F(x)$ and are given by,

$$A = 3\left[\frac{F^{(2)}}{r^3} + \frac{3F^{(1)}}{r^4} + \frac{3F}{r^5}\right]\ , \tag{10.20}$$

$$B = -\left[\frac{F^{(3)}}{r^2} + \frac{3F^{(2)}}{r^3} + \frac{6F^{(1)}}{r^4} + \frac{6F}{r^5}\right]\ , \tag{10.21}$$

$$C = \frac{1}{4}\left[\frac{F^{(4)}}{r} + \frac{2F^{(3)}}{r^2} + \frac{9F^{(2)}}{r^3} + \frac{21F^{(1)}}{r^4} + \frac{21F}{r^5}\right]\ . \tag{10.22}$$

We take $F(x)$ to be a superposition of ingoing $(x = t + r)$ and outgoing $(x = t - r)$ waves,

$$F = F_1(t - r) + F_2(t + r)\ , \tag{10.23}$$

and,

$$F^{(n)} = \left[\frac{d^n\,F(x)}{dx^n}\right]_{x=t-r} + (-1)^n\left[\frac{d^n\,F(x)}{dx^n}\right]_{x=t+r}\ , \tag{10.24}$$

where we have chosen the particular case $F_1(x) = -F_2(x) = \mathcal{A}e^{-x^2}$. The angular functions $f_{uv}$ for even parity $m = 0$ modes are given by

$$f_{rr} = 2 - 3\sin^2\theta\ , \tag{10.25a}$$

$$f_{r\theta} = -3\sin\theta\cos\theta\ , \tag{10.25b}$$

$$f_{r\phi} = 0\ , \tag{10.25c}$$

$$f^{(1)}_{\theta\theta} = 3\sin^2\theta\ , \tag{10.25d}$$

$$f^{(2)}_{\theta\theta} = -1\ , \tag{10.25e}$$

$$f_{\theta\phi} = 0\ , \tag{10.25f}$$

$$f^{(1)}_{\phi\phi} = -f^{(1)}_{\theta\theta}\ , \tag{10.25g}$$

$$f^{(2)}_{\phi\phi} = 3\sin^2\theta - 1\ . \tag{10.25h}$$

We note that this represents time symmetric data and so $K_{ij} = 0$ and $K = \gamma^{ij} K_{ij} = 0$ at the initial slice $t = 0$. We use an amplitude of $\mathcal{A} = 10^{-6}$ to complete the specification of initial data.

Because of the symmetries of the problem, we impose mirror symmetry boundary conditions along the planes $x = 0$, $y = 0$ and $z = 0$. We thus evolve the Octant $[0, 8] \times [0, 8] \times [0, 8]$ and use radiation boundary conditions at the outer boundary. We employ one refinement level and refine the cubic region $[0, 4] \times [0, 4] \times [0, 4]$.

The wave propagates radially outward crossing mesh refinement boundaries along the $x = 4$, $y = 4$ and $z = 4$ planes, eventually reaching the radiation boundary and leaving flat Minkowski spacetime. Although the Teukolsky wave is a routine problem for testing numerical relativistic codes, it is especially challenging for a mesh refinement code. This is mainly because the refined region is Cartesian, while the wave propagates spherically outward. As a result, the wavefront will not encounter the refinement boundaries at the same time. In Figures 10.6 we show the result at $t = 8$ for a run without a transition zone. Spurious ripples are generated when the wave initially hits the refinement boundary; the reflections continue to be generated until the wave has fully crossed the refinement boundary. These ripples are reflected toward the origin as expected. In Figure 10.7, we show a similar run using a transition zone. In this case, spurious reflections are significantly minimized.

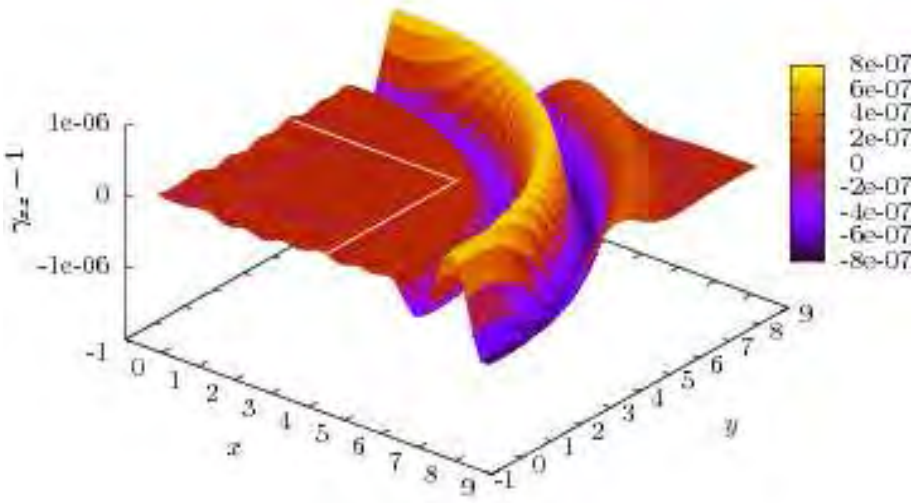


Figure 10.6: *Evolution of the $\gamma_{zz}$ component of the metric along the xy plane without a Transition zone. Note the spurious ripples in the refinement region. For ease of visualization, we mark the boundary of the refined grid with with white lines.*

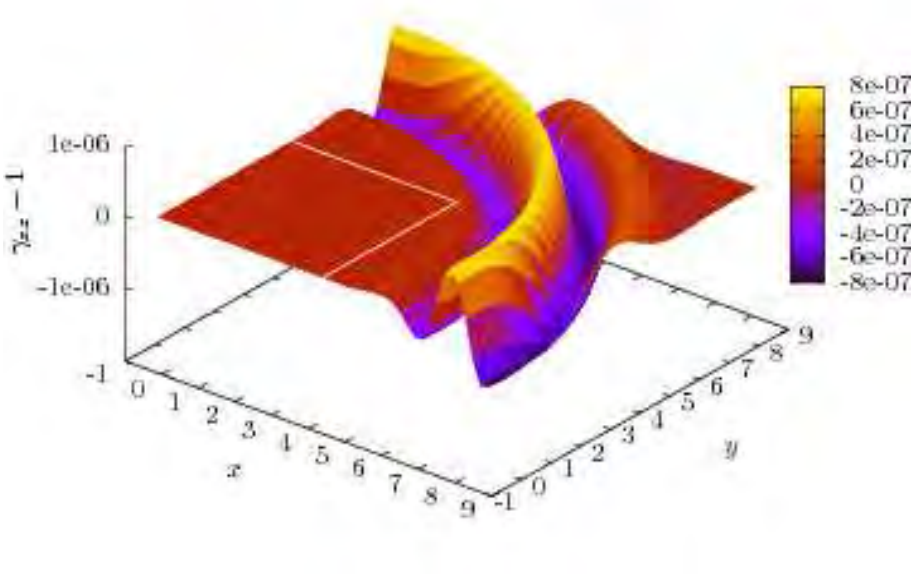


Figure 10.7: *Evolution of the $\gamma_{zz}$ component of the metric along the xy plane with a Transition zone. Note the absence of spurious ripples in the refinement region. For ease of visualization, we mark the boundary of the refined grid with with white lines. compare with Figure 10.6.*

# Chapter 11

# Conclusions and Future Outlook

## 11.1 Conclusions

Part II of the thesis was focused on presenting a new algorithm for higher order mesh refinement schemes for the solution of hyperbolic PDEs. It is known that during the implementation of such algorithms, several issues related to scalability, stability, loss of convergence, spurious reflections and loss of conservation may arise [22, 413, 334, 248, 33, 112]. We have addressed the issues of convergence and spurious reflections. In Chapter 9 we focused on deriving an algorithm for imposing time dependent boundary conditions in a manner that retains the convergence properties of a generic fourth order Runge Kutta method. We showed that our algorithm is fourth order convergent even when the PDE is non linear and the boundary conditions are time dependent. This presents a novel advance in solving the order reduction problem.

In Chapter 10 we have presented the full mesh refinement algorithm focusing in particular on the treatment of the interface boundary conditions. Our proposed scheme is both fourth order convergent and also significantly minimizes spurious reflections off refinement boundaries that are caused by differing levels of accuracy between two successive refinement levels. This is an important issue for the field of numerical relativity where the use of higher order finite differencing is becoming increasingly common [314, 139, 415]. For these higher order methods, the truncation error can become so small that the dominant error comes from spurious reflections. Our method is not restricted to any formulation of the Einstein field equations. Indeed one can apply it to any hyperbolic system of PDEs, as we have done also for the wave equation.

Because we are not using a buffer zone, our method requires a total of six halo points on each interface boundary, irrespective of the time integration method used. This differs from

employing buffer zones in that, for a fourth order accurate Runge Kutta algorithm, along with fourth order finite differencing involving lop-sided advection stencils such as the ones given by Equation (8.23), twelve points are needed along each boundary (the situation could be worse for higher order finite differencing) [217, 81]. This is a significant saving in memory usage, especially in three space dimensions where the buffer zone can be a significant part of the grid. In addition, the blending operation we employ to fill the transition zone is cheaper than having to repopulate the entire buffer zone after every time step.

We also note that the use of a transition zone is computationally cheaper than the sponge boundary method since one has to populate the sponge boundary at every intermediate Runge Kutta step, while the transition zone is only populated at the end of the time step. Moreover, there is often a level of experimentation required to determine how large a sponge zone one should use. Although one can have the transition zone as large as desired, we have found satisfactory results with a size that spans only three fine grid points.

The implementation described here uses Runge Kutta dense output formulas to interpolate in time, which avoids any potential issues with polynomial interpolation. In particular, because one does not have to couple fine grid solutions to the solution history of coarser grids, fine grids can be immediately initialized along with the base grid. This is especially attractive since fine grids can be initialized to the same accuracy as the base grid, by using the same initialization routine as the base grid. This method of time interpolation was also used in [280] for conservation laws and [111] for solving Maxwell's equations.

## 11.2 Future Work

The difficulty of spurious reflections off boundaries, is not unique to mesh refinement boundaries. Such reflections also occur at the outer boundary when applying outgoing boundary conditions [19]. In general, the notion of imposing bundary conditions at infinity presents distinct geometrical, numerical and overall physical challenges. An interesting possibility would be to investigate the efficiency of the transition zone idea in reducing reflections that arise in the case of radiative boundary conditions. In addition, it would be interesting to investigate the efficiency of the transition zone implementation in an adaptive context or whether it would minimize spurious reflections that are a result of shock waves crossing refinement boundaries. There is also the question of how it would affect conservation along interface boundaries in the context of conservation laws. These and other issues involving black hole spacetimes are a subject of further study.

Standardized testbed applications often facilitate the process of development and imple-

mentation of algorithms and code validation in general. This is notably seen from the apples with apples tests [16, 31] and the testbeds for apparent horizon finders [15]. The development of testbed problems for mesh refinement codes would be invaluable to the numerical relativity community in the quest for an efficient implementation. This could include testbed problems that aim to probe the convergence properties and the ability of the algorithm to handle spurious reflections.

The work presented here has featured the development of a new relativity code. Although the main aim behind such a venture was to make the debugging process easier, it did lead us to consider several aspects of code design. A case in point is the use of Expression Templates and other Template metaprogramming techniques to achieve better speed. We are also working towards a fully adaptive mesh refinement code equipped with error estimation routines. In this work, we have not addressed the challenges that arise in parallelising a mesh refinement code. In general issues of scalability arise because, by design, coarser grids have to wait while finer grids are integrated. This provides a bottle neck, especially when several refinement levels are added. The design of an efficient domain decomposition algorithm that would efficiently evolve the grid hierarchy in time would be invaluable.

Due to the complexity of dealing with black hole spacetimes, the distinction between the field of mathematical and numerical relativity has become more pronounced. One of the most interesting problems along the lines of mathematical relativity relates to the issues of Bowen-York initial data for rotating black holes. In particular, under what conditions would a slicing of a Kerr black hole be conformally flat. This question has been partially answered in [170, 241] under several restrictions. It is likely that such a question is related to the problem of finding interior solutions of rotating stars. It has been shown that the Wahlquist fluid, once thought to be a promising candidate for the interior solution of a rotating object, cannot describe an isolated rotating body [72]. This will be investigated in future work.

# Appendix A

# Cosmology

## A.1 Scalar Vector Tensor Decomposition

It is customary to decompose the perturbation variables into scalar, vector and tensor parts. This is simply a classification based on how the variables transform under coordinate transformations. We note that any vector $V_a$ can be split into a longitudinal (scalar) and a divergence free (vector) part according to,

$$V_a = V_a^{(S)} + V_a^{(V)}, \tag{A.1}$$

where curl $V_a^{(S)} = 0 = \mathrm{D}^a V_a^{(V)}$. Because scalar degrees of freedom are curl free, one can write $V_a^{(S)}$ as a divergence of some scalar field $\phi$

$$V_a = \mathrm{D}_a\phi + V_a^{(V)}, \tag{A.2}$$

Similarly, any tensor $U_{ab}$ can be decomposed onto a scalar, vector and tensor part according to

$$U_{ab} = U_{ab}^{(S)} + U_{ab}^{(V)} + U_{ab}^{(T)} \tag{A.3}$$

where $\mathrm{D}^a U_{ab}^{(T)} = 0$. If $U_{ab}$ is a symmetric trace free tensor, then the scalar and vector parts may be written as,

$$U_{ab}^{(S)} = \left(\partial_a\partial_b - \frac{1}{3}h_{ab}\partial^i\partial_i\right)\phi \tag{A.4}$$

$$U_{ab}^{(V)} = \partial_{(a}U_{b)} \tag{A.5}$$

## A.2 Harmonic Splitting

It is standard to decompose the perturbed variables harmonically in Fourier space; separating out the time and space variations [198, 3, 84]. The idea is to expand the quantities in terms of eigenfunctions of the Laplace-Beltrami operator. To this end, we introduce the helicity basis vectors $\mathbf{e}^{(-)}, \mathbf{e}^{(0)}$ and $\mathbf{e}^{(+)}$ defined by

$$e_a^{(\pm)} = -\frac{i}{\sqrt{2}}\left(e_a^1 \pm i e_a^2\right) \tag{A.6}$$

where $(\mathbf{e^1}, \mathbf{e^2}, \hat{\mathbf{k}})$ form a right-handed orthonormal system with $\mathbf{e_2} = \hat{\mathbf{k}} \times \mathbf{e_1}$ and we align $\mathbf{e}^0$ with $\hat{\mathbf{k}}$.

Using this basis, the scalar harmonic functions are given by,

$$Q^{(0)} = e^{ik_j x^j} \ . \tag{A.7}$$

Scalar type components of vectors and tensors are expanded in terms of harmonic functions defined from $Q^{(0)}$ as follows,

$$Q_a^{(0)} = -\frac{a}{k}\mathrm{D}_a Q^{(0)} = a\, i\hat{k}_a e^{ik_j x^j} \ , \tag{A.8}$$

$$Q_{ab}^{(0)} = \frac{a^2}{k^2}\mathrm{D}_{\langle a}\mathrm{D}_{b\rangle} Q^{(0)} = -a^2\left(\hat{k}_a\hat{k}_b - \frac{1}{3}\delta_{ab}\right) e^{ik_j x^j} \ . \tag{A.9}$$

Vector harmonics are given by

$$Q_a^{(\pm)} = e_a^{(\pm)} Q^{(0)} \ , \tag{A.10}$$

$$Q_{ab}^{(\pm)} = -\frac{a}{k}\mathrm{D}_{(a} e_{b)}^{(\pm)} Q^{(0)} = a\, i\hat{k}_{(a} e_{b)}^{(\pm)} e^{ik_j x^j} \ . \tag{A.11}$$

While tensor harmonics are defined as,

$$Q_{ab}^{\pm 2} = \sqrt{\frac{3}{2}} e_a^{(\pm)} e_b^{(\pm)} Q^{(0)} \ . \tag{A.12}$$

## A.3 Commutation Relations

### A.3.1 3-Scalar Derivatives

$$(\mathrm{D}_a f)\dot{}_\perp = \mathrm{D}_a \dot{f} + \dot{f}\mathcal{A}_a - \left(\frac{1}{3}\Theta h_{ab} + \sigma_{ab} + \epsilon_{abc}\omega^c\right)\mathrm{D}^b f \ , \tag{A.13}$$

$$\mathrm{D}_{[a}\mathrm{D}_{b]} f = \epsilon_{abc}\omega^c \dot{f} \tag{A.14}$$

### A.3.2 3-Vector Derivatives

$$\begin{aligned}(\mathrm{D}_a V_b)\dot{}_\perp = {} & \mathrm{D}_a \dot{V}_b + \mathcal{A}_a \dot{V}_b - \left(\frac{1}{3}\Theta h_{ac} + \sigma_{ac} + \epsilon_{acd}\omega^d\right) \times (\mathrm{D}^c V_b + V^c \mathcal{A}_b) \\ & + \epsilon_{bcd} H_a{}^c V^d - \frac{1}{2} q_b V_a + \frac{1}{2} h_{ab} q_c V^c \end{aligned} \tag{A.15}$$

$$(\mathrm{curl}\, V_a)\dot{}_\perp = \mathrm{curl}\, \dot{V}_a - \frac{1}{3}\Theta\, \mathrm{curl}\, V_a - \epsilon_{abc}\sigma^{bd}\mathrm{D}_d V^c + H_{ab}V^b - \frac{1}{3}\Theta\epsilon_{abc}V^b\mathcal{A}^c \ , \tag{A.16}$$

$$\tag{A.17}$$

### A.3.3 3-Tensor Derivatives

$$\mathrm{curl}\ \mathrm{curl}\ S_{ab} = -\mathrm{D}^2 S_{ab} + (\mu + \Lambda - \frac{1}{3}\Theta^2)S_{ab} + \frac{3}{2}\mathrm{D}_{\langle a}\mathrm{D}^c S_{b\rangle c} \ . \tag{A.18}$$

$$(\mathrm{D}_a S_{ab})\dot{}_\perp = \mathcal{A}_a \dot{S}_{bc} - \left(\frac{1}{3}\Theta h_{ad} + \sigma_{ad} + \omega_{ad}\right) \times \left(\mathcal{A}_b S^d{}_c + \mathcal{A}_c S^d{}_b + \mathrm{D}^d S_{bc}\right) \tag{A.19}$$

$$- \left(h_{a[f}q_{b]} - \epsilon_{fbd}H^d{}_a\right) S^f{}_c - \left(h_{a[f}q_{c]} - \epsilon_{fcd}H^d{}_a\right) S^f{}_b \tag{A.20}$$

# Appendix B

# Numerical Relativity

## B.1 $\chi$ and $W$ Formulations

The time evolution equations for the $\chi$ and $W$ formalisms for puncture spacetime are given by the system (B.2)–(B.6) [314], where

$$\hat{\phi}_\kappa = (\det \gamma_{ab})^{-1/\kappa} \,, \tag{B.1}$$

so that $\chi = \hat{\phi}_3$ and $W = \hat{\phi}_6$.

$$\partial_t \hat{\phi}_\kappa = \frac{2}{\kappa}\hat{\phi}_\kappa \alpha K + \beta^k \partial_k \hat{\phi}_\kappa - \frac{2}{\kappa}\hat{\phi}_\kappa \partial_k \beta^k, \tag{B.2}$$

$$\partial_t \tilde{\gamma}_{ij} = -2\alpha \tilde{A}_{ij} + \beta^k \partial_k \tilde{\gamma}_{ij} + \tilde{\gamma}_{ik}\partial_j \beta^k + \tilde{\gamma}_{jk}\partial_i \beta^k - \frac{2}{3}\tilde{\gamma}_{ij}\partial_k \beta^k, \tag{B.3}$$

$$\partial_t K = \alpha \left( \tilde{A}_{ij}\tilde{A}^{ij} + \frac{1}{3}K^2 \right) - \gamma^{ij} \mathrm{D}_i \mathrm{D}_j \alpha + \beta^k \partial_k K \tag{B.4}$$

$$\partial_t \tilde{A}_{ij} = \alpha \left( K\tilde{A}_{ij} - 2\tilde{A}_{ik}\tilde{A}^k{}_j \right) + (\hat{\phi}_\kappa)^{\kappa/3} \big( \alpha R_{ij} - \mathrm{D}_i \mathrm{D}_j \alpha \big)^{TF} + \beta^k \partial_k \tilde{A}_{ij} + \tilde{A}_{ik}\partial_j \beta^k + \tilde{A}_{jk}\partial_i \beta^k - \frac{2}{3}\tilde{A}_{ij}\partial_k \beta^k, \tag{B.5}$$

$$\partial_t \tilde{\Gamma}^i = 2\alpha \left( \tilde{\Gamma}^i_{jk}\tilde{A}^{jk} - \frac{2}{3}\tilde{\gamma}^{ij}K_{,j} - \frac{\kappa}{2}\tilde{A}^{ij}\frac{\partial_j \hat{\phi}_\kappa}{\hat{\phi}_\kappa} \right) - 2\tilde{A}^{ij}\alpha_{,j} + \tilde{\gamma}^{jk}\beta^i{}_{,jk} + \frac{1}{3}\tilde{\gamma}^{ij}\beta^k{}_{,jk} + \beta^j \tilde{\Gamma}^i{}_{,j} - \tilde{\Gamma}^j \beta^i{}_{,j} + \frac{2}{3}\tilde{\Gamma}^i \beta^j{}_{,j}. \tag{B.6}$$

## B.2 Fourth Order Stencils

In this section we present fourth order finite difference stencils including both centered and lopsided stencils, see [371] for example. For the first derivative

$$\partial_x \equiv \frac{1}{12\Delta x}\left[\,\cdots\,\right] \ . \tag{B.7}$$

we have the finite difference coefficients given in Table B.1 as a function of offset.

| Offset | $i-4$ | $i-3$ | $i-2$ | $i-1$ | $i$ | $i+1$ | $i+2$ | $i+3$ | $i+4$ |
|---|---|---|---|---|---|---|---|---|---|
| $-2$ | $[+3$ | $-16$ | $+36$ | $-48$ | $+25]$ | | | | |
| $-1$ | | $[-1$ | $+6$ | $-18$ | $+10$ | $+3]$ | | | |
| $0$ | | | $[+1$ | $-8$ | $0$ | $+8$ | $-1]$ | | |
| $+1$ | | | | $[-3$ | $-10$ | $+18$ | $-6$ | $+1]$ | |
| $+2$ | | | | | $[-25$ | $+48$ | $-36$ | $+16$ | $-3]$ |

Table B.1: *This table gives the coefficients for fourth order convergent finite difference approximation to the first derivative $\partial_x$ as a function of offset.*

The second derivative takes the form

$$\partial_{xx} \equiv \frac{1}{(12\Delta x)^2}\left[\,\cdots\,\right] \ . \tag{B.8}$$

where the finite difference coefficients are given in Table B.2.

| Offset | $i-5$ | $i-4$ | $i-3$ | $i-2$ | $i-1$ | $i$ | $i+1$ | $i+2$ | $i+3$ | $i+4$ | $i+5$ |
|---|---|---|---|---|---|---|---|---|---|---|---|
| $-2$ | $[-10$ | $+61$ | $-156$ | $+214$ | $-154$ | $+45]$ | | | | | |
| $-1$ | | $[+1$ | $-6$ | $+14$ | $-4$ | $-15$ | $+10]$ | | | | |
| $0$ | | | | $[-1$ | $+16$ | $-30$ | $+16$ | $-1]$ | | | |
| $+1$ | | | | | $[+10$ | $-15$ | $-4$ | $+14$ | $-6$ | $+1]$ | |
| $+2$ | | | | | | $[+45$ | $-154$ | $+214$ | $-156$ | $+61$ | $-10]$ |

Table B.2: *This table gives the coefficients for fourth order convergent finite difference approximation to the second derivative $\partial_{xx}$ as a function of offset.*

# Bibliography


[1] S. Abarbanel, D. Gottlieb, and M. Carpenter. On the removal of boundary errors caused by runge-kutta integration of nonlinear partial differential equations. *SIAM Journal on Scientific Computing*, 17(3):777–782, 1996http://dx.doi.org/10.1137/S1064827595282520. (Cited on pages 4, 131, and 150.)

[2] B. Abbott et al. LIGO: The Laser interferometer gravitational-wave observatory. *Rept.Prog.Phys.*, 72:076901, 2009 arXiv:0711.3041, [gr-qc]. (Cited on page 94.)

[3] L. F. Abbott and R. K. Schaefer. A general, gauge-invariant analysis of the cosmic microwave anisotropy. *Astrophys. J.*, 308:546–562, September 1986. (Cited on page 190.)

[4] A. M. Abrahams and C. R. Evans. Trapping a geon: Black hole formation by an imploding gravitational wave. *Phys. Rev. D*, 46:R4117–R4121, Nov 1992. (Cited on page 93.)

[5] T. Accadia et al. Virgo: a laser interferometer to detect gravitational waves. *Journal of Instrumentation*, 7:3012, March 2012. (Cited on page 94.)

[6] J. Adamek, C. de Rham, and R. Durrer. Mode Spectrum of the Electromagnetic Field in Open Universe Models. *Mon.Not.Roy.Astron.Soc.*, 423:2705–2710, 2012 arXiv:1110.2019, [gr-qc]. (Cited on page 36.)

[7] P. A. R. Ade et al. BICEP2 I: Detection Of B-mode Polarization at Degree Angular Scales. 2014 arXiv:1403.3985, [astro-ph.CO]. (Cited on page 28.)

[8] P. Ade et al. Planck 2013 results. XVI. Cosmological parameters. 2013 arXiv:1303.5076, [astro-ph.CO]. (Cited on pages xi, 12, 13, 18, 19, and 34.)

[9] P. Ade et al. Planck 2013 results. XXII. Constraints on inflation. 2013 arXiv:1303.5082, [astro-ph.CO]. (Cited on pages xi, 25, 27, and 29.)

[10] P. Ade et al. Planck 2013 results. XXIII. Isotropy and statistics of the CMB. 2013 arXiv:1303.5083, [astro-ph.CO]. (Cited on page 35.)

[11] J. Ahonen and K. Enqvist. Magnetic field generation in first order phase transition bubble collisions. *Phys. Rev. D*, 57:664–673, Jan 1998. (Cited on page 36.)

[12] T. Akahori, B. Gaensler, and D. Ryu. Statistical Techniques for Detecting the Intergalactic Magnetic Field from Large Samples of Extragalactic Faraday Rotation Data. 2014 arXiv:1406.3871, [astro-ph.CO]. (Cited on page 32.)

[13] A. Albrecht and P. J. Steinhardt. Cosmology for grand unified theories with radiatively induced symmetry breaking. *Phys. Rev. Lett.*, 48:1220–1223, Apr 1982. (Cited on pages 20 and 21.)

[14] M. Alcubierre. *Introduction to 3+1 Numerical Relativity*. International Series of Monographs on Physics. OUP Oxford, 2012. (Cited on page 71.)

[15] M. Alcubierre, S. Brandt, B. Bruegmann, C. Gundlach, J. Masso, et al. Test beds and applications for apparent horizon finders in numerical relativity. *Class.Quant.Grav.*, 17:2159–2190, 2000 arXiv:gr-qc/9809004, [gr-qc]. (Cited on pages 115 and 187.)

[16] M. Alcubierre, G. Allen, C. Bona, D. Fiske, T. Goodale, et al. Toward standard testbeds for numerical relativity. *Class.Quant.Grav.*, 21:589, 2004 arXiv:gr-qc/0305023, [gr-qc]. (Cited on pages 165 and 187.)

[17] M. Alcubierre, G. Allen, B. Bruegmann, G. Lanfermann, E. Seidel, et al. Gravitational collapse of gravitational waves in 3-D numerical relativity. *Phys.Rev.*, D61:041501, 2000 arXiv:gr-qc/9904013, [gr-qc]. (Cited on page 93.)

[18] M. Alcubierre, G. Allen, B. Brügmann, G. Lanfermann, E. Seidel, W.-M. Suen, and M. Tobias. Gravitational collapse of gravitational waves in 3d numerical relativity. *Phys. Rev. D*, 61:041501, Jan 2000. (Cited on page 109.)

[19] M. Alcubierre, B. Bruegmann, P. Diener, M. Koppitz, D. Pollney, et al. Gauge conditions for long term numerical black hole evolutions without excision. *Phys.Rev.*, D67:084023, 2003 arXiv:gr-qc/0206072, [gr-qc]. (Cited on pages 111, 127, and 186.)

[20] M. Alcubierre and B. Brügmann. Simple excision of a black hole in numerical relativity. *Phys. Rev. D*, 63:104006, Apr 2001. (Cited on pages 107, 109, and 112.)

[21] J. Anderson, R. Beck, M. Bell, G. de Bruyn, K. Chyzy, J. Eislöffel, T. Enßlin, A. Fletcher, M. Haverkorn, G. Heald, A. Horneffer, A. Noutsos, W. Reich, A. Scaife, and the LOFAR collaboration. The LOFAR Magnetism Key Science Project. *ArXiv e-prints*, March 2012 arXiv:1203.2467, [astro-ph.IM]. (Cited on page 89.)

[22] M. Anderson, E. Hirschmann, S. L. Liebling, and D. Neilsen. Relativistic MHD with Adaptive Mesh Refinement. *Class.Quant.Grav.*, 23:6503–6524, 2006 arXiv:gr-qc/0605102, [gr-qc]. (Cited on pages 3, 96, and 185.)

[23] S. Ando and A. Kusenko. Evidence for Gamma-ray Halos Around Active Galactic Nuclei and the First Measurement of Intergalactic Magnetic Fields. *Astrophys. J. Lett*, 722:L39–L44, October 2010 arXiv:1005.1924, [astro-ph.HE]. (Cited on page 35.)

[24] P. Anninos, D. Bernstein, S. Brandt, J. Libson, J. Massó, E. Seidel, L. Smarr, W.-M. Suen, and P. Walker. Dynamics of apparent and event horizons. *Phys. Rev. Lett.*, 74:630–633, Jan 1995. (Cited on page 115.)

[25] P. Anninos, K. Camarda, J. Libson, J. Masso, E. Seidel, et al. Finding apparent horizons in dynamic 3-D numerical space-times. *Phys.Rev.*, D58:024003, 1998 arXiv:gr-qc/9609059, [gr-qc]. (Cited on page 115.)

[26] P. Anninos, J. Massó, E. Seidel, W.-M. Suen, and J. Towns. Three-dimensional numerical relativity: The evolution of black holes. *Phys. Rev. D*, 52:2059–2082, Aug 1995. (Cited on page 111.)

[27] F. Arneodo. Dark Matter Searches. *ArXiv e-prints*, January 2013 arXiv:1301.0441, [astro-ph.IM]. (Cited on page 16.)

[28] R. L. Arnowitt, S. Deser, and C. W. Misner. The Dynamics of general relativity. *Gen.Rel.Grav.*, 40:1997–2027, 2008 arXiv:gr-qc/0405109, [gr-qc]. (Cited on page 100.)

[29] P. Astier et al. The Supernova legacy survey: Measurement of omega(m), omega(lambda) and W from the first year data set. *Astron.Astrophys.*, 447:31–48, 2006 arXiv:astro-ph/0510447, [astro-ph]. (Cited on page 31.)

[30] B. Aylott, J. G. Baker, W. D. Boggs, M. Boyle, P. R. Brady, et al. Testing gravitational-wave searches with numerical relativity waveforms: Results from the first Numerical INJection Analysis (NINJA) project. *Class.Quant.Grav.*, 26:165008, 2009 arXiv:0901.4399, [gr-qc]. (Cited on page 94.)

[31] M. Babiuc, S. Husa, D. Alic, I. Hinder, C. Lechner, et al. Implementation of standard testbeds for numerical relativity. *Class.Quant.Grav.*, 25:125012, 2008 arXiv:0709.3559, [gr-qc]. (Cited on pages 130, 165, 179, and 187.)

[32] J. G. Baker, J. Centrella, D.-I. Choi, M. Koppitz, and J. van Meter. Binary black hole merger dynamics and waveforms. *Phys.Rev.*, D73:104002, 2006 arXiv:gr-qc/0602026, [gr-qc]. (Cited on page 94.)

[33] J. G. Baker and J. R. van Meter. Reducing reflections from mesh refinement interfaces in numerical relativity. *Phys.Rev.*, D72:104010, 2005 arXiv:gr-qc/0505100, [gr-qc]. (Cited on pages 3, 96, 173, and 185.)

[34] A. B. Balakin and W.-T. Ni. Anomalous character of the axion-photon coupling in a magnetic field distorted by a pp-wave gravitational background. 2014 arXiv:1403.6711, [gr-qc]. (Cited on pages 71 and 87.)

[35] J. Balakrishna, G. Daues, E. Seidel, W.-M. Suen, M. Tobias, and E. Wang. Coordinate conditions in three-dimensional numerical relativity. *Classical and Quantum Gravity*, 13(12):L135, 1996. (Cited on page 127.)

[36] J. M. Bardeen. Gauge-invariant cosmological perturbations. *Phys. Rev. D*, 22:1882–1905, Oct 1980. (Cited on page 60.)

[37] A. Barnes. Cosmology of a charged universe. *Astrophys. J.*, 227:1–12, January 1979. (Cited on page 32.)

[38] J. D. Barrow. Graduated inflationary universes. *Physics Letters B*, 235(12):40 – 43, 1990. (Cited on page 26.)

[39] J. D. Barrow, P. G. Ferreira, and J. Silk. Constraints on a primordial magnetic field. *Phys.Rev.Lett.*, 78:3610–3613, 1997 arXiv:astro-ph/9701063, [astro-ph]. (Cited on page 34.)

[40] J. D. Barrow, R. Maartens, and C. G. Tsagas. Cosmology with inhomogeneous magnetic fields. *Phys.Rept.*, 449:131–171, 2007 arXiv:astro-ph/0611537, [astro-ph]. (Cited on page 50.)

[41] J. D. Barrow and C. G. Tsagas. Slow decay of magnetic fields in open Friedmann universes. *Phys.Rev.*, D77:107302, 2008 arXiv:0803.0660, [astro-ph]. (Cited on page 36.)

[42] N. Bartolo, E. Komatsu, S. Matarrese, and A. Riotto. Non-Gaussianity from inflation: Theory and observations. *Phys.Rept.*, 402:103–266, 2004 arXiv:astro-ph/0406398, [astro-ph]. (Cited on pages 21, 23, 24, 25, and 26.)

[43] B. Bassett and R. Hlozek. *Baryon acoustic oscillations*, page 246. Cambridge University Press, 2010 arXiv:0910.5224, [astro-ph.CO]. (Cited on page 30.)

[44] E. Battaner and E. Florido. Magnetic fields in the early Universe In *IAU Symposium*. K. G. Strassmeier, A. G. Kosovichev, and J. E. Beckman, editors, volume 259 of *IAU Symposium*, pages 529–538, April 2009. (Cited on page 79.)

[45] E. Battaner, E. Florido, and J. Jimenez-Vicente. Magnetic fields and large scale structure in a radiation dominated universe. *Astron.Astrophys.*, 326:13–22, 1997 arXiv:astro-ph/9602097, [astro-ph]. (Cited on page 2.)

[46] E. Battaner and H. Lesch. On the physics of primordial magnetic fields. *Annales Phys.(France)*, 2000 arXiv:astro-ph/0003370, [astro-ph]. (Cited on pages 1, 32, 36, and 90.)

[47] D. Baumann et al. CMBPol Mission Concept Study: Probing Inflation with CMB Polarization. *AIP Conf.Proc.*, 1141:10–120, 2009 arXiv:0811.3919, [astro-ph]. (Cited on page 71.)

[48] T. W. Baumgarte and S. L. Shapiro. On the numerical integration of Einstein's field equations. *Phys.Rev.*, D59:024007, 1999 arXiv:gr-qc/9810065, [gr-qc]. (Cited on page 105.)

[49] T. W. Baumgarte and S. L. Shapiro. Numerical relativity and compact binaries. *Physics Reports*, 376(2):41 – 131, 2003. (Cited on pages 100 and 108.)

[50] T. Baumgarte and S. Shapiro. *Numerical Relativity: Solving Einstein's Equations on the Computer*. Cambridge University Press, 2010. (Cited on page 71.)

[51] R. Beck. Future Observations of Cosmic Magnetic Fields with the SKA and its Precursors. *ArXiv e-prints*, November 2011 arXiv:1111.5802, [astro-ph.CO]. (Cited on page 89.)

[52] R. Beck and R. Wielebinski. *Magnetic Fields in Galaxies*, page 641. Springer Netherlands, 2013. (Cited on page 33.)

[53] S. V. Beckwith, M. Stiavelli, A. M. Koekemoer, J. A. Caldwell, H. C. Ferguson, et al. The Hubble Ultra Deep Field. *Astron.J.*, 132:1729–1755, 2006 arXiv:astro-ph/0607632, [astro-ph]. (Cited on pages xi and 11.)

[54] C. Bennett et al. First year Wilkinson Microwave Anisotropy Probe (WMAP) observations: Preliminary maps and basic results. *Astrophys.J.Suppl.*, 148:1, 2003 arXiv:astro-ph/0302207, [astro-ph]. (Cited on page 18.)

[55] E. Bentivegna and M. Korzynski. Evolution of a periodic eight-black-hole lattice in numerical relativity. *Class.Quant.Grav.*, 29:165007, 2012 arXiv:1204.3568, [gr-qc]. (Cited on pages 94, 113, and 172.)

[56] E. Bentivegna and M. Korzynski. Evolution of a family of expanding cubic black-hole lattices in numerical relativity. *Class.Quant.Grav.*, 30:235008, 2013 arXiv:1306.4055, [gr-qc]. (Cited on pages 94 and 172.)

[57] M. Berger and I. Rigoutsos. An algorithm for point clustering and grid generation. *Systems, Man and Cybernetics, IEEE Transactions on*, 21(5):1278 –1286, sep/oct 1991. (Cited on page 137.)

[58] M. J. Berger and P. Colella. Local adaptive mesh refinement for shock hydrodynamics. *Journal of Computational Physics*, 82:64–84, May 1989. (Cited on pages 133, 136, 169, and 171.)

[59] M. J. Berger and J. Oliger. Adaptive Mesh Refinement for Hyperbolic Partial Differential Equations. *Journal of Computational Physics*, 53:484, March 1984. (Cited on pages 3, 133, 136, 169, and 171.)

[60] L. Bergstrom. Nonbaryonic dark matter: Observational evidence and detection methods. *Rept.Prog.Phys.*, 63:793, 2000 arXiv:hep-ph/0002126, [hep-ph]. (Cited on page 16.)

[61] M. L. Bernet, F. Miniati, S. J. Lilly, P. P. Kronberg, and M. Dessauges-Zavadsky. Strong magnetic fields in normal galaxies at high redshifts. *Nature*, 454:302–304, 2008 arXiv:0807.3347, [astro-ph]. (Cited on page 35.)

[62] J. Berrut and L. Trefethen. Barycentric lagrange interpolation. *SIAM Review*, 46(3):501–517, 2004http://dx.doi.org/10.1137/S0036144502417715. (Cited on page 140.)

[63] G. Bertone, D. Hooper, and J. Silk. Particle dark matter: Evidence, candidates and constraints. *Phys.Rept.*, 405:279–390, 2005 arXiv:hep-ph/0404175, [hep-ph]. (Cited on page 16.)

[64] G. Betschart, P. K. Dunsby, and M. Marklund. Cosmic magnetic fields from velocity perturbations in the early universe. *Class.Quant.Grav.*, 21:2115–2126, 2004 arXiv:gr-qc/0310085, [gr-qc]. (Cited on page 36.)

[65] G. Betschart, C. Zunckel, P. Dunsby, and M. Marklund. Primordial magnetic seed field amplification by gravitational waves. *Phys.Rev.*, D72:123514, 2005 arXiv:gr-qc/0503006, [gr-qc]. (Cited on pages 2, 69, 70, 71, 74, 80, 87, and 88.)

[66] G. Betschart, C. Zunckel, P. K. Dunsby, and M. Marklund. Response to "Comment on 'Primordial magnetic seed field amplification by gravitational waves' ". *Phys.Rev.*, D75:087902, 2007 arXiv:gr-qc/0702104, [gr-qc]. (Cited on page 88.)

[67] H. Beyer and O. Sarbach. Well-posedness of the baumgarte-shapiro-shibata-nakamura formulation of einstein's field equations. *Phys. Rev. D*, 70:104004, Nov 2004. (Cited on page 105.)

[68] K. Bolejko, M.-N. Célérier, and A. Krasiński. Inhomogeneous cosmological models: exact solutions and their applications. *Classical and Quantum Gravity*, 28(16):164002, August 2011 arXiv:1102.1449, [astro-ph.CO]. (Cited on page 20.)

[69] C. Bona, J. Massó, E. Seidel, and J. Stela. New formalism for numerical relativity. *Phys. Rev. Lett.*, 75:600–603, Jul 1995. (Cited on pages 110 and 111.)

[70] J. M. Bowen and J. W. York. Time-asymmetric initial data for black holes and black-hole collisions. *Phys. Rev. D*, 21:2047–2056, Apr 1980. (Cited on page 121.)

[71] M. Boyle, L. Lindblom, H. Pfeiffer, M. Scheel, and L. E. Kidder. Testing the accuracy and stability of spectral methods in numerical relativity. *Phys.Rev.*, D75:024006, 2007 arXiv:gr-qc/0609047, [gr-qc]. (Cited on pages 95, 128, and 165.)

[72] M. Bradley, G. Fodor, M. Marklund, and Z. Perjes. The Wahlquist metric cannot describe an isolated rotating body. *Class.Quant.Grav.*, 17:351–359, 2000 arXiv:gr-qc/9910001, [gr-qc]. (Cited on page 187.)

[73] R. H. Brandenberger. Is the Spectrum of Gravitational Waves the "Holy Grail" of Inflation? *ArXiv e-prints*, April 2011 arXiv:1104.3581, [astro-ph.CO]. (Cited on page 71.)

[74] A. Brandenburg and K. Subramanian. Astrophysical magnetic fields and nonlinear dynamo theory. *Phys.Rept.*, 417:1–209, 2005 arXiv:astro-ph/0405052, [astro-ph]. (Cited on page 36.)

[75] K. Brecher and G. R. Blumenthal. On the Origin of Cosmic Magnetic Fields. *Astrophysical Letters*, 6:169, July 1970. (Cited on page 32.)

[76] D. R. Brill and R. W. Lindquist. Interaction energy in geometrostatics. *Phys.Rev.*, 131:471–476, 1963. (Cited on page 115.)

[77] G. Brodin, M. Marklund, and P. K. Dunsby. Nonlinear gravitational wave interactions with plasmas. *Phys.Rev.*, D62:104008, 2000 arXiv:gr-qc/0006030, [gr-qc]. (Cited on pages 71, 87, and 89.)

[78] B. Bruegmann. Adaptive mesh and geodesically sliced Schwarzschild space-time in (3+1)-dimensions. *Phys.Rev.*, D54:7361–7372, 1996 arXiv:gr-qc/9608050, [gr-qc]. (Cited on page 172.)

[79] B. Bruegmann. Binary black hole mergers in 3-d numerical relativity. *Int.J.Mod.Phys.*, D8:85, 1999 arXiv:gr-qc/9708035, [gr-qc]. (Cited on pages 133, 171, and 172.)

[80] B. Bruegmann, J. A. Gonzalez, M. Hannam, S. Husa, U. Sperhake, et al. Calibration of Moving Puncture Simulations. *Phys.Rev.*, D77:024027, 2008 arXiv:gr-qc/0610128, [gr-qc]. (Cited on pages 3, 169, and 173.)

[81] B. Bruegmann, J. A. Gonzalez, M. Hannam, S. Husa, U. Sperhake, et al. Calibration of Moving Puncture Simulations. *Phys.Rev.*, D77:024027, 2008 arXiv:gr-qc/0610128, [gr-qc]. (Cited on page 186.)

[82] B. Bruegmann, W. Tichy, and N. Jansen. Numerical simulation of orbiting black holes. *Phys.Rev.Lett.*, 92:211101, 2004 arXiv:gr-qc/0312112, [gr-qc]. (Cited on page 94.)

[83] J.-P. Bruneton and J. Larena. Dynamics of a lattice Universe: The dust approximation in cosmology. *Class.Quant.Grav.*, 29:155001, 2012 arXiv:1204.3433, [gr-qc]. (Cited on page 94.)

[84] M. Bruni, P. K. S. Dunsby, and G. F. R. Ellis. Cosmological perturbations and the physical meaning of gauge-invariant variables. *Astrophys. J.*, 395:34–53, August 1992. (Cited on pages 65, 68, 76, and 190.)

[85] M. Bruni, L. Gualtieri, and C. F. Sopuerta. Two-parameter nonlinear space-time perturbations: Gauge transformations and gauge invariance. *Class. Quant. Grav.*, 20:535–556, 2003 arXiv:gr-qc/0207105. (Cited on pages 2, 60, and 69.)

[86] T. Bunch and P. Davies. Quantum Field Theory in de Sitter Space: Renormalization by Point Splitting. *Proc.Roy.Soc.Lond.*, A360:117–134, 1978. (Cited on page 26.)

[87] K. Burrage and L. Petzold. On order reduction for rungekutta methods applied to differential/algebraic systems and to stiff systems of odes. *SIAM Journal on Numerical Analysis*, 27(2):447–456, 1990. (Cited on page 150.)

[88] K. Burrage and R. P. K. Chan. On smoothing and order reduction effects for implicit runge-kutta formulae. *J. Comput. Appl. Math.*, 45(1-2):17–27, April 1993. (Cited on page 150.)

[89] J. C. Butcher. *Numerical Methods for Ordinary Differential Equations, Second Edition*. Wiley, 2008. (Cited on page 149.)

[90] J. Butcher. *Numerical Methods for Ordinary Differential Equations*. Wiley, 2003. (Cited on pages 153 and 156.)

[91] G. Calabrese, I. Hinder, and S. Husa. Numerical stability for finite difference approximations of Einstein's equations. *J.Comput.Phys.*, 218:607–634, 2006 arXiv:gr-qc/0503056, [gr-qc]. (Cited on page 130.)

[92] R. Caldwell. A Phantom menace? *Phys.Lett.*, B545:23–29, 2002 arXiv:astro-ph/9908168, [astro-ph]. (Cited on page 19.)

[93] S. Camera, C. Fedeli, and L. Moscardini. Magnification bias as a novel probe for primordial magnetic fields. *JCAP*, 3:27, March 2014 arXiv:1311.6383, [astro-ph.CO]. (Cited on page 34.)

[94] M. Campanelli, C. O. Lousto, P. Marronetti, and Y. Zlochower. Accurate evolutions of orbiting black-hole binaries without excision. *Phys. Rev. Lett.*, 96:111101, Mar 2006. (Cited on page 113.)

[95] M. Campanelli, C. O. Lousto, and Y. Zlochower. Last orbit of binary black holes. *Phys. Rev. D*, 73:061501, Mar 2006. (Cited on pages 94 and 96.)

[96] C. Caprini and R. Durrer. Gravitational wave production: A Strong constraint on primordial magnetic fields. *Phys.Rev.*, D65:023517, 2001 arXiv:astro-ph/0106244, [astro-ph]. (Cited on pages 34 and 37.)

[97] C. Caprini and R. Durrer. Limits on stochastic magnetic fields: A Defense of our paper [1]. *Phys.Rev.*, D72:088301, 2005 arXiv:astro-ph/0504553, [astro-ph]. (Cited on pages 34 and 37.)

[98] C. Caprini, R. Durrer, and G. Servant. The stochastic gravitational wave background from turbulence and magnetic fields generated by a first-order phase transition. *JCAP*, 0912:024, 2009 arXiv:0909.0622, [astro-ph.CO]. (Cited on page 36.)

[99] S. Carloni, P. K. Dunsby, S. Capozziello, and A. Troisi. Cosmological dynamics of $R^n$ gravity. *Class.Quant.Grav.*, 22:4839–4868, 2005 arXiv:gr-qc/0410046, [gr-qc]. (Cited on page 58.)

[100] M. Carpenter, D. Gottlieb, S. Abarbanel, and W. Don. The theoretical accuracy of rungekutta time discretizations for the initial boundary value problem: A study of the boundary error. *SIAM Journal on Scientific Computing*, 16(6):1241–1252, 1995. (Cited on pages 4, 132, 150, and 152.)

[101] S. M. Carroll. The Cosmological constant. *Living Rev.Rel.*, 4:1, 2001 arXiv:astro-ph/0004075, [astro-ph]. (Cited on page 19.)

[102] S. M. Carroll and L. Mersini-Houghton. Can we live in a selftuning universe? *Phys.Rev.*, D64:124008, 2001 arXiv:hep-th/0105007, [hep-th]. (Cited on page 19.)

[103] S. M. Carroll, W. H. Press, and E. L. Turner. The cosmological constant. *Annual Review of Astronomy and Astrophysics*, 30(1):499–542, 1992. (Cited on page 19.)

[104] S. Carroll. *Spacetime and Geometry: An Introduction to General Relativity*. Addison-Wesley Longman, Incorporated, 2004. (Cited on page 30.)

[105] C. Cattoen and M. Visser. Cosmography: Extracting the Hubble series from the supernova data. 2007 arXiv:gr-qc/0703122, [gr-qc]. (Cited on pages 29 and 31.)

[106] X. Chen. Primordial Non-Gaussianities from Inflation Models. *Advances in Astronomy*, 2010, 2010 arXiv:1002.1416, [astro-ph.CO]. (Cited on page 26.)

[107] B. Cheng and A. V. Olinto. Primordial magnetic fields generated in the quark-hadron transition. *Phys. Rev.*, pages 2421–2424, August 1994. (Cited on page 34.)

[108] B.-l. Cheng, A. V. Olinto, D. N. Schramm, and J. W. Truran. Constraints on the strength of primordial magnetic fields from big bang nucleosynthesis revisited. *Phys.Rev.*, D54:4714–4718, 1996 arXiv:astro-ph/9606163, [astro-ph]. (Cited on page 34.)

[109] C. Cherubini and S. Filippi. Using FEMLAB for gravitational problems: Numerical simulations for all. *J.Korean Phys.Soc.*, 49:S829–S834, 2006 arXiv:gr-qc/0509099, [gr-qc]. (Cited on pages 95 and 128.)

[110] T. Chiba and T. Nakamura. The Luminosity distance, the equation of state, and the geometry of the universe. *Prog.Theor.Phys.*, 100:1077–1082, 1998 arXiv:astro-ph/9808022, [astro-ph]. (Cited on page 31.)

[111] S. Chilton. *A fourth order adaptive mesh refinement solver for Maxwell's Equations*. PhD thesis, University of California, Berkeley, 2013. (Cited on page 186.)

[112] D.-I. Choi, J. David Brown, B. Imbiriba, J. Centrella, and P. MacNeice. Interface conditions for wave propagation through mesh refinement boundaries. *Journal of Computational Physics*, 193:398–425, January 2004arXiv:physics/0307036. (Cited on pages 3, 96, 133, 160, 171, 172, 173, and 185.)

[113] M. W. Choptuik. Universality and scaling in gravitational collapse of a massless scalar field. *Phys. Rev. Lett.*, 70:9–12, Jan 1993. (Cited on pages 94 and 172.)

[114] M. W. Choptuik, E. W. Hirschmann, S. L. Liebling, and F. Pretorius. Critical collapse of the massless scalar field in axisymmetry. *Phys.Rev.*, D68:044007, 2003 arXiv:gr-qc/0305003, [gr-qc]. (Cited on page 133.)

[115] A. J. Christopherson, K. A. Malik, and D. R. Matravers. Vorticity generation at second order in cosmological perturbation theory. *Phys. Rev. D.*, 79(12):123523, June 2009 arXiv:0904.0940, [astro-ph.CO]. (Cited on page 66.)

[116] M. Cirelli. Indirect searches for dark matter. *Pramana*, 79:1021–1043, November 2012 arXiv:1202.1454, [hep-ph]. (Cited on page 16.)

[117] C. Clarkson. Local gauge-invariance at any order in cosmological perturbation theory. *ArXiv e-prints*, August 2011 arXiv:1108.4513, [astro-ph.CO]. (Cited on page 89.)

[118] C. Clarkson, G. F. R. Ellis, A. Faltenbacher, R. Maartens, O. Umeh, and J.-P. Uzan. (Mis)interpreting supernovae observations in a lumpy universe. *MNRAS*, 426:1121–1136, October 2012 arXiv:1109.2484, [astro-ph.CO]. (Cited on page 20.)

[119] C. Clarkson and R. Maartens. Inhomogeneity and the foundations of concordance cosmology. *Classical and Quantum Gravity*, 27(12):124008, June 2010 arXiv:1005.2165, [astro-ph.CO]. (Cited on pages 31 and 54.)

[120] C. Clarkson, G. Ellis, J. Larena, and O. Umeh. Does the growth of structure affect our dynamical models of the universe? the averaging, backreaction, and fitting problems in cosmology. *Reports on Progress in Physics*, 74(11):112901, 2011. (Cited on page 20.)

[121] C. A. Clarkson and R. K. Barrett. Does the isotropy of the cmb imply a homogeneous universe? some generalized egs theorems. *Classical and Quantum Gravity*, 16(12):3781, 1999. (Cited on page 67.)

[122] C. A. Clarkson. Density fluctuations and gravity waves: A Covariant approach to gauge - invariant non-linear cosmological perturbation theory. *Phys.Rev.*, D70:103524, 2004 arXiv:astro-ph/0311505, [astro-ph]. (Cited on pages 65, 73, and 89.)

[123] C. A. Clarkson, M. Marklund, G. Betschart, and P. Dunsby. The electromagnetic signature of black hole ringdown. *Astrophys.J.*, 613:492–505, 2004 arXiv:astro-ph/0310323, [astro-ph]. (Cited on pages 2, 69, and 94.)

[124] T. Clifton, P. G. Ferreira, A. Padilla, and C. Skordis. Modified gravity and cosmology. *Phys. Rep.*, 513:1–189, March 2012 arXiv:1106.2476, [astro-ph.CO]. (Cited on page 20.)

[125] A. A. Coley. Dynamical systems in cosmology. 1999 arXiv:gr-qc/9910074, [gr-qc]. (Cited on page 58.)

[126] G. B. Cook and Others. Boosted three-dimensional black-hole evolutions with singularity excision. *Phys. Rev. Lett.*, 80:2512–2516, Mar 1998. (Cited on page 112.)

[127] G. B. Cook. Initial data for numerical relativity. *Living Reviews in Relativity*, 3(5), 2000. (Cited on pages 116 and 119.)

[128] A. Cooray, W. Hu, D. Huterer, and M. Joffre. Measuring angular diameter distances through halo clustering. *Astrophys.J.*, 557:L7, 2001 arXiv:astro-ph/0105061, [astro-ph]. (Cited on page 30.)

[129] J. M. Cornwall. Speculations on primordial magnetic helicity. *Phys. Rev. D*, 56:6146–6154, Nov 1997. (Cited on page 36.)

[130] R. Courant, K. Friedrichs, and H. Lewy. On the partial difference equations of mathematical physics. *IBM J. Res. Dev.*, 11:215–234, 1967. (Cited on page 129.)

[131] P. Csizmadia. Fourth order AMR and nonlinear dynamical systems in compactified space. *Class.Quant.Grav.*, 24:S369–S379, 2007. (Cited on pages 3, 169, and 172.)

[132] L. Dai, D. Jeong, M. Kamionkowski, and J. Chluba. The Pesky Power Asymmetry. *Phys.Rev.*, D87(12):123005, 2013 arXiv:1303.6949, [astro-ph.CO]. (Cited on page 35.)

[133] A.-C. Davis, M. Lilley, and O. Tornkvist. Relaxing the bounds on primordial magnetic seed fields. *Phys.Rev.*, D60:021301, 1999 arXiv:astro-ph/9904022, [astro-ph]. (Cited on page 35.)

[134] J. C. de Araujo and R. Opher. A Possible dynamical effect of a primordial magnetic field. *Astrophys.J.*, 1997 arXiv:astro-ph/9707303, [astro-ph]. (Cited on page 34.)

[135] A. De Felice and S. Tsujikawa. $f(R)$ theories. *Living Rev.Rel.*, 13:3, 2010 arXiv:1002.4928, [gr-qc]. (Cited on page 20.)

[136] K. Debrabant and K. Strehmel. Convergence of rungekutta methods applied to linear partial differential-algebraic equations. *Applied Numerical Mathematics*, 53(24):213 – 229, 2005. (Cited on page 150.)

[137] L. Debreu, C. Vouland, and E. Blayo. Agrif: Adaptive grid refinement in fortran. *Comput. Geosci.*, 34(1):8–13, January 2008. (Cited on pages 96 and 171.)

[138] R. H. Dicke and P. J. E. Peebles. The big-bang cosmology-enigmas and nostrums. In *General relativity: an Einstein centenary survey*, volume 1, pages 504–517, 1979. (Cited on page 21.)

[139] P. Diener, E. N. Dorband, E. Schnetter, and M. Tiglio. New, efficient, and accurate high order derivative and dissipation operators satisfying summation by parts, and applications in three-dimensional multi-block evolutions. *J.Sci.Comput.*, 32:109–145, 2007 arXiv:gr-qc/0512001, [gr-qc]. (Cited on pages 131 and 185.)

[140] P. Diener, F. Herrmann, D. Pollney, E. Schnetter, E. Seidel, et al. Accurate evolution of orbiting binary black holes. *Phys.Rev.Lett.*, 96:121101, 2006 arXiv:gr-qc/0512108, [gr-qc]. (Cited on page 94.)

[141] A. Dolgov. Magnetic fields in cosmology. 2003 arXiv:astro-ph/0306443, [astro-ph]. (Cited on pages 1 and 36.)

[142] C. Donald and W. Enright. Implications of order reduction for implicit runge-kutta methods. *Numerical Algorithms*, 2(3):351–369, 1992. (Cited on page 150.)

[143] P. K. S. Dunsby, B. A. C. C. Bassett, and G. F. R. Ellis. Covariant analysis of gravitational waves in a cosmological context. *Class. Quant. Grav.*, 14:1215–1222, 1997 arXiv:gr-qc/9811092. (Cited on page 67.)

[144] R. Durrer. *The Cosmic Microwave Background*. Cambridge University Press, 2008. (Cited on page 60.)

[145] R. Durrer. Is the mystery of cosmic magnetic fields solved? *Science*, 311(5762):787–788, 2006. (Cited on page 89.)

[146] G. Dvali and S. Kachru. Large scale power and running spectral index in New Old Inflation. *ArXiv High Energy Physics - Phenomenology e-prints*, October 2003hep-ph/0310244. (Cited on page 26.)

[147] G. Dvali and S. Kachru. New old inflation. 2003 arXiv:hep-th/0309095, [hep-th]. (Cited on page 26.)

[148] D. S. Ebert, K. F. Musgrave, D. Peachey, K. Perlin, and S. Worley. *Texturing and Modeling: A Procedural Approach*. Morgan Kaufmann, 2002. (Cited on pages 173 and 177.)

[149] J. Ehlers, P. Geren, and R. Sachs. Isotropic solutions of the Einstein-Liouville equations. *J.Math.Phys.*, 9:1344–1349, 1968. (Cited on page 54.)

[150] J. Ehlers. Contributions to the relativistic mechanics of continuous media. *General Relativity and Gravitation*, 25(12):1225–1266, 1993. (Cited on pages 17 and 42.)

[151] D. J. Eisenstein, W. Hu, and M. Tegmark. Cosmic Complementarity: H 0 and Omega M from Combining Cosmic Microwave Background Experiments and Redshift Surveys. *Astrophys. J.*, 504:L57, September 1998astro-ph/9805239. (Cited on page 30.)

[152] G. F. R. Ellis. Relativistic cosmology. In *General Relativity and Cosmology*. R. K. Sachs, editor, pages 104–182. 1971. (Cited on pages 39, 48, 50, and 83.)

[153] G. F. R. Ellis. Inhomogeneity effects in cosmology. *Classical and Quantum Gravity*, 28(16):164001, August 2011 arXiv:1103.2335, [astro-ph.CO]. (Cited on page 20.)

[154] G. F. R. Ellis and M. Bruni. Covariant and gauge-invariant approach to cosmological density fluctuations. *Phys. Rev. D*, 40(6):1804–1818, Sep 1989. (Cited on pages 2 and 64.)

[155] G. F. R. Ellis, M. Bruni, and J. Hwang. Density-gradient-vorticity relation in perfect-fluid robertson-walker perturbations. *Phys. Rev. D*, 42:1035–1046, Aug 1990. (Cited on page 77.)

[156] G. F. R. Ellis and H. van Elst. Cosmological models. *NATO Adv. Study Inst. Ser. C. Math. Phys. Sci.*, 541:1–116, 1999 arXiv:gr-qc/9812046. (Cited on pages 39, 67, and 83.)

[157] G. F. Ellis. Issues in the philosophy of cosmology. In *Philosophy of Physics*. J. Butterfield and J. Earman, editors. Elsevier, 2006 arXiv:astro-ph/0602280, [astro-ph]. (Cited on page 17.)

[158] G. F. Ellis, H. van Elst, J. Murugan, and J.-P. Uzan. On the Trace-Free Einstein Equations as a Viable Alternative to General Relativity. *Class.Quant.Grav.*, 28:225007, 2011 arXiv:1008.1196, [gr-qc]. (Cited on page 15.)

[159] G. Ellis. On the definition of distance in general relativity: I. m. h. etherington (philosophical magazine ser. 7, vol. 15, 761 (1933)). *General Relativity and Gravitation*, 39(7):1047–1052, 2007. (Cited on page 30.)

[160] G. Ellis, R. Maartens, and M. MacCallum. *Relativistic Cosmology*. Relativistic Cosmology. Cambridge University Press, 2012. (Cited on pages 39 and 52.)

[161] K. Eppley. Evolution of Time Symmetric Gravitational Waves: Initial Data and Apparent Horizons. *Phys.Rev.*, D16:1609–1614, 1977. (Cited on page 115.)

[162] L. Evans. *Partial Differential Equations*. Graduate studies in mathematics. American Mathematical Society, 2010. (Cited on page 102.)

[163] V. Faraoni. Extension of the EGS theorem to metric and Palatini f(R) gravity. *ArXiv e-prints*, November 2008 arXiv:0811.1870, [gr-qc]. (Cited on page 54.)

[164] S. February, J. Larena, M. Smith, and C. Clarkson. Rendering dark energy void. *MNRAS*, 405:2231–2242, July 2010 arXiv:0909.1479, [astro-ph.CO]. (Cited on page 20.)

[165] E. Fenu and R. Durrer. Interactions of cosmological gravitational waves and magnetic fields. *Phys. Rev.*, D79:024021, 2009 arXiv:0809.1383, [astro-ph]. (Cited on pages 71, 84, and 87.)

[166] E. Fenu, C. Pitrou, and R. Maartens. The seed magnetic field generated during recombination. *Mon.Not.Roy.Astron.Soc.*, 414:2354–2366, 2011 arXiv:1012.2958, [astro-ph.CO]. (Cited on pages 35 and 36.)

[167] E. Fermi. On the origin of the cosmic radiation. *Phys. Rev.*, 75:1169–1174, Apr 1949. (Cited on page 33.)

[168] B. Fornberg. Calculation of weights in finite difference formulas. *SIAM Rev*, 40:685–691, 1998. (Cited on page 129.)

[169] J. Frauendiener. Conformal infinity. *Living Reviews in Relativity*, 7(1), 2004. (Cited on page 95.)

[170] A. Garat and R. H. Price. Nonexistence of conformally flat slices of the kerr spacetime. *Phys. Rev. D*, 61:124011, May 2000. (Cited on pages 121 and 187.)

[171] D. Garfinkle. Harmonic coordinate method for simulating generic singularities. *Phys. Rev. D*, 65:044029, Jan 2002. (Cited on page 110.)

[172] D. Garfinkle. Inhomogeneous spacetimes as a dark energy model. *Class.Quant.Grav.*, 23:4811–4818, 2006 arXiv:gr-qc/0605088, [gr-qc]. (Cited on page 20.)

[173] M. Gasperini, M. Giovannini, and G. Veneziano. Primordial magnetic fields from string cosmology. *Phys. Rev. Lett.*, 75:3796–3799, Nov 1995. (Cited on pages 36 and 66.)

[174] B. Giacomazzo and L. Rezzolla. WhiskyMHD: A New numerical code for general relativistic magnetohydrodynamics. *Class.Quant.Grav.*, 24:S235–S258, 2007 arXiv:gr-qc/0701109, [gr-qc]. (Cited on page 94.)

[175] M. Giovannini. The Magnetized universe. *Int.J.Mod.Phys.*, D13:391–502, 2004 arXiv:astro-ph/0312614, [astro-ph]. (Cited on page 1.)

[176] K. Glazebrook and C. Blake. Measuring the cosmic evolution of dark energy with baryonic oscillations in the galaxy power spectrum. *Astrophys.J.*, 631:1–20, 2005 arXiv:astro-ph/0505608, [astro-ph]. (Cited on page 30.)

[177] R. J. Gleiser, C. O. Nicasio, R. H. Price, and J. Pullin. Evolving the bowen-york initial data for spinning black holes. *Phys. Rev. D*, 57:3401–3407, Mar 1998. (Cited on page 121.)

[178] R. Gopal and S. Sethi. Generation of magnetic field in the pre-recombination era. *Mon.Not.Roy.Astron.Soc.*, 363:521–528, 2005 arXiv:astro-ph/0411170, [astro-ph]. (Cited on page 35.)

[179] R. Gopal and S. K. Sethi. Generation of magnetic field in the pre-recombination era. *MNRAS*, 363(2):521–528, 2005. (Cited on page 88.)

[180] E. Gourgoulhon. 3+1 formalism and bases of numerical relativity. 2007 arXiv:gr-qc/0703035, [gr-qc]. (Cited on pages 100 and 108.)

[181] E. Gourgoulhon. Construction of initial data for 3+1 numerical relativity. *Journal of Physics: Conference Series*, 91(1):012001, 2007. (Cited on page 116.)

[182] P. Grandclment and J. Novak. Spectral methods for numerical relativity. *Living Reviews in Relativity*, 12(1), 2009. (Cited on pages 95 and 128.)

[183] D. Grasso and H. R. Rubinstein. Revisiting nucleosynthesis constraints on primordial magnetic fields. *Phys.Lett.*, B379:73–79, 1996 arXiv:astro-ph/9602055, [astro-ph]. (Cited on page 34.)

[184] D. Grasso and H. R. Rubinstein. Magnetic fields in the early universe. *Phys.Rept.*, 348:163–266, 2001 arXiv:astro-ph/0009061, [astro-ph]. (Cited on page 2.)

[185] G. Greenstein. Primordial Helium Production in "Magnetic" Cosmologies. *Nature*, 223:938–939, August 1969. (Cited on page 33.)

[186] H. Grote and LIGO Scientific Collaboration. The GEO 600 status. *Classical and Quantum Gravity*, 27(8):084003, April 2010. (Cited on page 94.)

[187] A. Gruppuso, P. Natoli, F. Paci, F. Finelli, D. Molinari, et al. Low Variance at large scales of WMAP 9 year data. *JCAP*, 1307:047, 2013 arXiv:1304.5493, [astro-ph.CO]. (Cited on page 35.)

[188] C. Gundlach. Pseudospectral apparent horizon finders: An efficient new algorithm. *Phys. Rev. D*, 57:863–875, Jan 1998. (Cited on page 114.)

[189] C. Gundlach. Critical phenomena in gravitational collapse. *Living Reviews in Relativity*, 2(4), 1999. (Cited on page 94.)

[190] C. Gundlach and J. M. Martín-García. Symmetric hyperbolicity and consistent boundary conditions for second-order einstein equations. *Phys. Rev. D*, 70:044032, Aug 2004. (Cited on page 105.)

[191] B. Gustafsson, H. Kreiss, and J. Oliger. *Time Dependent Problems and Difference Methods*. A Wiley-Interscience Publication. Wiley, 1995. (Cited on pages 102 and 131.)

[192] B. Gustafsson. The convergence rate for difference approximations to mixed initial boundary value problems. *Mathematics of Computation*, 29(130):pp. 396–406, 1975. (Cited on page 157.)

[193] A. H. Guth. Inflationary universe: A possible solution to the horizon and flatness problems. *Phys. Rev. D*, 23:347–356, Jan 1981. (Cited on pages 20 and 21.)

[194] S. G. Hahn and R. W. Lindquist. The two-body problem in geometrodynamics. *Annals of Physics*, 29:304–331, September 1964. (Cited on page 93.)

[195] E. Hairer and G. Wanner. *Solving Ordinary Differential Equations II: Stiff and Differential-Algebraic Problems*. Solving ordinary differential equations. Springer, 2010. (Cited on page 151.)

[196] E. Hairer, S. P. Nørsett, and G. Wanner. *Solving Ordinary Differential Equations I: Nonstiff Problems (Springer Series in Computational Mathematics) (v. 1)*. Springer, 2nd edition, December 2009. (Cited on pages 149, 162, and 175.)

[197] L. M. Harris and D. R. Durran. An Idealized Comparison of One-Way and Two-Way Grid Nesting. *Monthly Weather Review*, 138:2174–2187, June 2010. (Cited on pages 172 and 173.)

[198] E. R. Harrison. Normal modes of vibrations of the universe. *Rev. Mod. Phys.*, 39(4):862–882, Oct 1967. (Cited on page 190.)

[199] E. R. Harrison. Generation of magnetic fields in the radiation era. *MNRAS*, 147:279, 1970. (Cited on page 35.)

[200] W. Hasse and V. Perlick. On spacetime models with an isotropic hubble law. *Classical and Quantum Gravity*, 16(8):2559, 1999. (Cited on page 31.)

[201] S. W. Hawking. Perturbations of an Expanding Universe. *Astrophys. J.*, 145:544, August 1966. (Cited on page 64.)

[202] S. Hawking and G. Ellis. *The Large Scale Structure of Space-Time*. Cambridge Monographs on Mathematical Physics. Cambridge University Press, 1973. (Cited on pages 9, 54, and 114.)

[203] F. Herrmann, D. Shoemaker, and P. Laguna. Unequal Mass Binary Black Hole Plunges and Gravitational Recoil. 2006 arXiv:gr-qc/0601026, [gr-qc]. (Cited on page 94.)

[204] F. Herrmann, I. Hinder, D. M. Shoemaker, P. Laguna, and R. A. Matzner. Binary Black Holes: Spin Dynamics and Gravitational Recoil. *Phys.Rev.*, D76:084032, 2007 arXiv:0706.2541, [gr-qc]. (Cited on page 172.)

[205] J. Hesthaven and T. Warburton. *Nodal Discontinuous Galerkin Methods: Algorithms, Analysis, and Applications*. Texts in Applied Mathematics. Springer, 2008. (Cited on page 130.)

[206] I. Hinder. The current status of binary black hole simulations in numerical relativity. *Classical and Quantum Gravity*, 27(11):114004, 2010. (Cited on page 94.)

[207] M. Hindmarsh and A. Everett. Magnetic fields from phase transitions. *Phys.Rev.*, D58:103505, 1998 arXiv:astro-ph/9708004, [astro-ph]. (Cited on page 36.)

[208] S. Hobbs and P. K. Dunsby. Dynamical systems approach to magnetized cosmological perturbations. *Phys.Rev.*, D62:124007, 2000 arXiv:gr-qc/0007010, [gr-qc]. (Cited on page 2.)

[209] P. Hobson, G. Efstathiou, and A. Lasenby. *General Relativity: An Introduction for Physicists*. Cambridge University Press, 2006. (Cited on pages 4, 9, 11, 23, 29, and 115.)

[210] C. J. Hogan. Magnetohydrodynamic Effects of a First-Order Cosmological Phase Transition. *Phys. Rev. Lett.*, 51:1488–1491, 1983. (Cited on page 36.)

[211] L. Hollenstein, C. Caprini, R. Crittenden, and R. Maartens. Challenges for creating magnetic fields by cosmic defects. *Phys. Rev.*, D77:063517, 2008 arXiv:0712.1667, [astro-ph]. (Cited on page 36.)

[212] H. J. Hortua, L. Castañeda, and J. M. Tejeiro. Evolution of magnetic fields through cosmological perturbation theory. *Phys. Rev. D*, 87:103531, May 2013. (Cited on page 73.)

[213] A. M. Howard and R. M. Kulsrud. The Evolution of a primordial galactic magnetic field. *Astrophys.J.*, 483:648–665, 1997 arXiv:astro-ph/9609031, [astro-ph]. (Cited on page 35.)

[214] E. Hubble. A Relation between Distance and Radial Velocity among Extra-Galactic Nebulae. *Proceedings of the National Academy of Science*, 15:168–173, March 1929. (Cited on page 10.)

[215] S. A. Hughes. Gravitational wave astronomy and cosmology. 2014 arXiv:1405.0504, [gr-qc]. (Cited on page 71.)

[216] S. A. Hughes, C. R. Keeton, P. Walker, K. T. Walsh, S. L. Shapiro, and S. A. Teukolsky. Finding black holes in numerical spacetimes. *Phys. Rev. D*, 49:4004–4015, Apr 1994. (Cited on page 116.)

[217] S. Husa, J. A. Gonzalez, M. Hannam, B. Bruegmann, and U. Sperhake. Reducing phase error in long numerical binary black hole evolutions with sixth order finite differencing. *Class.Quant.Grav.*, 25:105006, 2008 arXiv:0706.0740, [gr-qc]. (Cited on page 186.)

[218] S. Husa, I. Hinder, and C. Lechner. Kranc: A Mathematica application to generate numerical codes for tensorial evolution equations. *Comput.Phys.Commun.*, 174:983–1004, 2006 arXiv:gr-qc/0404023, [gr-qc]. (Cited on page 124.)

[219] K. Ichiki, K. Takahashi, H. Ohno, H. Hanayama, and N. Sugiyama. Cosmological magnetic field: A fossil of density perturbations in the early universe. *Science*, 311(5762):827–829, 2006. (Cited on pages 35, 79, and 85.)

[220] J. Isenberg. *Initial Value Problem in General Relativity*, pages 303–321. Springer Berlin Heidelberg, 2013 arXiv:1304.1960, [gr-qc]. (Cited on page 118.)

[221] M. Johansson. Loss of high order spatial accuracy due to boundary error caused by runge-kutta time integration. Technical Report 2000-013, Department of Information Technology, Uppsala University, May 2000. (Cited on pages 151 and 152.)

[222] P. Jordan, J. Ehlers, and W. Kundt. Republication of: Exact solutions of the field equations of the general theory of relativity. *General Relativity and Gravitation*, 41(9):2191–2280, 2009. (Cited on pages 57 and 104.)

[223] R. Joshi and H. Chand. Dependence of Residual Rotation Measure (RRM) on Intervening MgII Absorbers at Cosmic Distances. *MNRAS*, 434:3566, 2013 arXiv:1307.2678, [astro-ph.CO]. (Cited on page 35.)

[224] A. Kandus, K. E. Kunze, and C. G. Tsagas. Primordial magnetogenesis. *Phys.Rept.*, 505:1–58, 2011 arXiv:1007.3891, [astro-ph.CO]. (Cited on page 33.)

[225] R. Kantowski and R. K. Sachs. Some Spatially Homogeneous Anisotropic Relativistic Cosmological Models. *Journal of Mathematical Physics*, 7:443–446, March 1966. (Cited on page 72.)

[226] I. Kazes, T. H. Troland, and R. M. Crutcher. Zeeman splitting of H I toward high velocity clouds and NGC 1275. *Astronomy and Astrophysics*, 245:L17–L19, May 1991. (Cited on page 33.)

[227] P. J. Kernan, G. D. Starkman, and T. Vachaspati. Big bang nucleosynthesis constraints on primordial magnetic fields. *Phys.Rev.*, D54:7207–7214, 1996 arXiv:astro-ph/9509126, [astro-ph]. (Cited on page 34.)

[228] R. Khanna. On the magnetohydrodynamic description of a two-component plasma in the Kerr metric. *MNRAS*, 294:673, March 1998arXiv:astro-ph/9803088. (Cited on page 78.)

[229] L. E. Kidder, M. A. Scheel, S. A. Teukolsky, E. D. Carlson, and G. B. Cook. Black hole evolution by spectral methods. *Phys. Rev. D*, 62:084032, Sep 2000. (Cited on pages 95 and 128.)

[230] E.-J. Kim, A. V. Olinto, and R. Rosner. Generation of Density Perturbations by Primordial Magnetic Fields. *Astrophys. J.*, 468:28, September 1996astro-ph/9412070. (Cited on pages 2 and 34.)

[231] R. P. Kirshner. Hubble's diagram and cosmic expansion. In *Proceedings of the National Academy of Sciences of the United States of America (PNAS)*, volume 101, January 2004. (Cited on page 12.)

[232] T. Kobayashi, R. Maartens, T. Shiromizu, and K. Takahashi. Cosmological magnetic fields from nonlinear effects. *Phys. Rev.*, D75:103501, 2007 arXiv:astro-ph/0701596. (Cited on page 35.)

[233] H. Kodama and M. Sasaki. Cosmological perturbation theory. *Progress of Theoretical Physics Supplement*, 78:1–166, 1984. (Cited on page 60.)

[234] L. Kofman, A. D. Linde, and A. A. Starobinsky. Reheating after inflation. *Phys.Rev.Lett.*, 73:3195–3198, 1994 arXiv:hep-th/9405187, [hep-th]. (Cited on page 21.)

[235] T. Kolatt. Determination of the primordial magnetic field power spectrum by Faraday rotation correlations. *Astrophys.J.*, 495:564–591, 1998 arXiv:astro-ph/9704243, [astro-ph]. (Cited on page 32.)

[236] E. Kolb and M. Turner. *The Early Universe*. Frontiers in Physics. Addison-Wesley Longman, Incorporated, 1990. (Cited on page 21.)

[237] O. Korobkin, B. Aksoylu, M. Holst, E. Pazos, and M. Tiglio. Solving the Einstein constraint equations on multi-block triangulations using finite element methods. *Class.Quant.Grav.*, 26:145007, 2009 arXiv:0801.1823, [gr-qc]. (Cited on pages 95 and 128.)

[238] A. Kosowsky and A. Loeb. Faraday Rotation of Microwave Background Polarization by a Primordial Magnetic Field. *Astrophys.J.*, 469:1, September 1996astro-ph/9601055. (Cited on page 34.)

[239] H. Kreiss, H. Kreiss, J. Oliger, and G. A. R. P. J. O. Committee. *Methods for the approximate solution of time dependent problems*. GARP publications series. International Council of Scientific Unions, World Meteorological Organization, 1973. (Cited on page 130.)

[240] P. P. Kronberg. Extragalactic magnetic fields. *Rept. Prog. Phys.*, 57:325–382, 1994. (Cited on page 32.)

[241] J. A. V. Kroon. Nonexistence of conformally flat slices in kerr and other stationary spacetimes. *Phys. Rev. Lett.*, 92:041101, Jan 2004. (Cited on pages 121 and 187.)

[242] M. Kuhlen, S. E. Woosley, and G. A. Glatzmaier. Carbon ignition in type ia supernovae. ii. a three-dimensional numerical model. *The Astrophysical Journal*, 640(1):407, 2006. (Cited on page 30.)

[243] S. Kuroyanagi, H. Tashiro, and N. Sugiyama. A numerical study of primordial magnetic field amplification by inflation-produced gravitational waves. *Phys. Rev.*, D81:023510, 2010 arXiv:0909.0907, [astro-ph.CO]. (Cited on pages 78, 83, 84, and 87.)

[244] J. D. Lambert. *Numerical methods for ordinary differential systems: the initial value problem*. John Wiley & Sons, Inc., New York, NY, USA, 1991. (Cited on page 156.)

[245] K. Land and J. Magueijo. The Axis of evil. *Phys.Rev.Lett.*, 95:071301, 2005 arXiv:astro-ph/0502237, [astro-ph]. (Cited on page 35.)

[246] W. Landry. Implementing a high performance tensor library. *Sci. Program.*, 11(4):273–290, December 2003. (Cited on page 124.)

[247] W. Landry and S. A. Teukolsky. An Efficient method for fully relativistic simulations of coalescing binary neutron stars. 1999 arXiv:gr-qc/9912004, [gr-qc]. (Cited on page 110.)

[248] L. Lehner, S. L. Liebling, and O. Reula. AMR, stability and higher accuracy. *Class.Quant.Grav.*, 23:S421–S446, 2006 arXiv:gr-qc/0510111, [gr-qc]. (Cited on pages 3, 96, 133, 169, 172, and 185.)

[249] A. R. Liddle. An Introduction to cosmological inflation. pages 260–295, 1999 arXiv:astro-ph/9901124, [astro-ph]. (Cited on pages xi and 22.)

[250] J. E. Lidsey, A. R. Liddle, E. W. Kolb, E. J. Copeland, T. Barreiro, et al. Reconstructing the inflation potential : An overview. *Rev.Mod.Phys.*, 69:373–410, 1997 arXiv:astro-ph/9508078, [astro-ph]. (Cited on page 21.)

[251] E. Lifshitz. On the gravitational stability of the expanding universe. *J. Phys. (Moscow)*, 10:116, 1946. (Cited on pages 58 and 60.)

[252] E. Lifshitz and I. Khalatnikov. Investigations in relativistic cosmology. *Advances in Physics*, 12(46):185–249, 1963. (Cited on pages 58 and 60.)

[253] A. C. Limache and P. S. Rojas Fredini. A Tensor Library for Scientific Computing In *High Performance Computing in Computational Mechanics*. Alberto Cardona and Mario Storti and Carlos Zuppa, editor, pages 2907–2925, 2008. (Cited on page 124.)

[254] A. D. Linde. Hybrid inflation. *Phys.Rev.*, D49:748–754, 1994 arXiv:astro-ph/9307002, [astro-ph]. (Cited on page 26.)

[255] A. D. Linde. Fast roll inflation. *JHEP*, 0111:052, 2001 arXiv:hep-th/0110195, [hep-th]. (Cited on page 26.)

[256] R. W. Lindquist and J. A. Wheeler. Dynamics of a lattice universe by the schwarzschild-cell method. *Rev. Mod. Phys.*, 29:432–443, Jul 1957. (Cited on page 94.)

[257] M. Livio. The world according to the Hubble Space Telescope. 2003 arXiv:astro-ph/0303500, [astro-ph]. (Cited on page 12.)

[258] F. Lucchin and S. Matarrese. Power-law inflation. *Phys. Rev. D*, 32:1316–1322, Sep 1985. (Cited on page 26.)

[259] D. H. Lyth and M. Mukherjee. Fluid-flow description of density irregularities in the universe. *Phys. Rev. D*, 38:485–489, Jul 1988. (Cited on page 64.)

[260] D. Lyth and A. Liddle. *The Primordial Density Perturbation: Cosmology, Inflation and the Origin of Structure*. Cambridge University Press, 2009. (Cited on pages 22 and 23.)

[261] P. G. Macedo and A. H. Nelson. Propagation of gravitational waves in a magnetized plasma. *Phys. Rev. D*, 28:2382–2392, Nov 1983. (Cited on page 87.)

[262] A. J. Maciejewski and M. Szydiowski. Bianchi cosmologies as dynamical systems. *Celestial Mechanics and Dynamical Astronomy*, 73(1-4):17–24, 1999. (Cited on page 58.)

[263] P. MacNeice, K. M. Olson, C. Mobarry, R. de Fainchtein, and C. Packer. PARAMESH: A parallel adaptive mesh refinement community toolkit. *Computer Physics Communications*, 126:330–354, April 2000. (Cited on pages 96 and 171.)

[264] M. S. Madsen. Magnetic fields in cosmology. *MNRAS*, 237:109–117, March 1989. (Cited on page 34.)

[265] K. Maeda, S. Benetti, M. Stritzinger, F. K. Röpke, G. Folatelli, J. Sollerman, S. Taubenberger, K. Nomoto, G. Leloudas, M. Hamuy, M. Tanaka, P. A. Mazzali, and N. Elias-Rosa. An asymmetric explosion as the origin of spectral evolution diversity in type Ia supernovae. *NATURE*, 466:82–85, July 2010 arXiv:1006.5888, [astro-ph.CO]. (Cited on page 30.)

[266] S. Maeda, S. Kitagawa, T. Kobayashi, and T. Shiromizu. Primordial magnetic fields from second-order cosmological perturbations:Tight coupling approximation. *Class. Quant. Grav.*, 26:135014, 2009 arXiv:0805.0169, [astro-ph]. (Cited on pages 35 and 80.)

[267] M. Maggiore. Gravitational wave experiments and early universe cosmology. *Phys.Rept.*, 331:283–367, 2000 arXiv:gr-qc/9909001, [gr-qc]. (Cited on page 71.)

[268] K. A. Malik and D. R. Matravers. Comments on gauge-invariance in cosmology. *General Relativity and Gravitation*, 45:1989–2001, October 2013 arXiv:1206.1478, [astro-ph.CO]. (Cited on page 2.)

[269] K. A. Malik and D. Wands. Cosmological perturbations. *Phys.Rept.*, 475:1–51, 2009 arXiv:0809.4944, [astro-ph]. (Cited on page 63.)

[270] G. D. Mallinson and G. de Vahl Davis. The Method of the False Transient for the Solution of Coupled Elliptic Equations. *Journal of Computational Physics*, 12:435–461, August 1973. (Cited on page 127.)

[271] M. Marklund, G. Brodin, and P. K. S. Dunsby. Radio wave emissions due to gravitational radiation. *Astrophys. J.*, 536:875–879, 2000 arXiv:astro-ph/9907350. (Cited on pages 71 and 87.)

[272] M. Marklund and C. Clarkson. The general relativistic MHD dynamo. *Mon. Not. Roy. Astron. Soc.*, 358:892, 2005 arXiv:astro-ph/0411140. (Cited on page 78.)

[273] M. Marklund, P. K. Dunsby, and G. Brodin. Cosmological electromagnetic fields due to gravitational wave perturbations. *Phys.Rev.*, D62:101501, 2000 arXiv:gr-qc/0007035, [gr-qc]. (Cited on pages 71, 87, and 88.)

[274] P. Marronetti, W. Tichy, B. Brügmann, J. González, and U. Sperhake. High-spin binary black hole mergers. *Phys. Rev. D*, 77:064010, Mar 2008. (Cited on page 114.)

[275] J. Martin. Everything you always wanted to know about the cosmological constant problem (but were afraid to ask). *Comptes Rendus Physique*, 13:566–665, July 2012 arXiv:1205.3365, [astro-ph.CO]. (Cited on page 19.)

[276] J. Martin and J. Yokoyama. Generation of Large-Scale Magnetic Fields in Single-Field Inflation. *JCAP*, 0801:025, 2008 arXiv:0711.4307, [astro-ph]. (Cited on page 36.)

[277] J. M. Martín-García. xPerm: fast index canonicalization for tensor computer algebra. *Computer Physics Communications*, 179:597–603, October 2008 arXiv:0803.0862, [cs.SC]. (Cited on page v.)

[278] S. Matarrese, S. Mollerach, A. Notari, and A. Riotto. Large-scale magnetic fields from density perturbations. *Phys.Rev.*, D71:043502, 2005 arXiv:astro-ph/0410687, [astro-ph]. (Cited on page 88.)

[279] J. J. Matese and R. F. O'Connell. Production of Helium in the Big-Bang Expansion of a Magnetic Universe. *Astrophys.J.*, 160:451, May 1970. (Cited on page 33.)

[280] P. McCorquodale and P. Colella. A high-order finite-volume method for hyperbolic conservation laws on locally-refined grids. *Communications in Applied Mathematics and Computational Science*, 6:1–25, 2011. (Cited on pages 175 and 186.)

[281] C. W. Misner, K. S. Thorne, and J. A. Wheeler. *Gravitation*. San Francisco: W.H. Freeman and Co., 1973, 1973. (Cited on pages 4 and 5.)

[282] C. W. Misner. Mixmaster universe. *Phys. Rev. Lett.*, 22:1071–1074, May 1969. (Cited on page 22.)

[283] B. Mongwane. On Convergence of High Order Runge-Kutta Time Discretizations for Non-Linear Hyperbolic Problems. *Under Review*. (Cited on page 174.)

[284] G. Montani, M. Battisti, and R. Benini. *Primordial Cosmology*. World Scientific, 2010. (Cited on page 9.)

[285] H. J. Mosquera Cuesta. Gravitational-to-electromagnetic wave conversion and gamma-ray bursts calorimetry: The grb980425/sn 1998bw $\sim 10^{49}$erg radio emission. *Phys. Rev. D*, 65:064009, Feb 2002. (Cited on page 1.)

[286] A. Moss, D. Scott, J. P. Zibin, and R. Battye. Tilted physics: A cosmologically dipole-modulated sky. *Phys. Rev. D*, 84(2):023014, July 2011 arXiv:1011.2990, [astro-ph.CO]. (Cited on page 35.)

[287] P. Mosta, C. Palenzuela, L. Rezzolla, L. Lehner, S. Yoshida, et al. Vacuum Electromagnetic Counterparts of Binary Black-Hole Mergers. *Phys.Rev.*, D81:064017, 2010 arXiv:0912.2330, [gr-qc]. (Cited on page 94.)

[288] V. F. Mukhanov, H. A. Feldman, and R. H. Brandenberger. Theory of cosmological perturbations. *Physics Reports*, 215(5):203–333, 1992. (Cited on page 64.)

[289] A. G. Muslimov. On the scalar field dynamics in a spatially flat friedman universe. *Classical and Quantum Gravity*, 7(2):231, 1990. (Cited on page 26.)

[290] P. Msta, B. C. Mundim, J. A. Faber, R. Haas, S. C. Noble, et al. GRHydro: A new open source general-relativistic magnetohydrodynamics code for the Einstein Toolkit. *Class.Quant.Grav.*, 31:015005, 2014 arXiv:1304.5544, [gr-qc]. (Cited on page 94.)

[291] K. Nakamura. Second-order gauge invariant cosmological perturbation theory: Einstein equations in terms of gauge invariant variables. *Prog.Theor.Phys.*, 117:17–74, 2007 arXiv:gr-qc/0605108, [gr-qc]. (Cited on page 66.)

[292] K. Nakamura. Second-order Gauge-Invariant Cosmological Perturbation Theory: Current Status. *Adv.Astron.*, 2010:576273, 2010 arXiv:1001.2621, [gr-qc]. (Cited on page 2.)

[293] K. C. New, K. Watt, C. W. Misner, and J. M. Centrella. Stable three level leapfrog integration in numerical relativity. *Phys.Rev.*, D58:064022, 1998 arXiv:gr-qc/9801110, [gr-qc]. (Cited on pages 165 and 168.)

[294] U. S. Nilsson, C. Uggla, J. Wainwright, and W. C. Lim. An Almost Isotropic Cosmic Microwave Temperature Does Not Imply an Almost Isotropic Universe. *Astrophys. J. Lett*, 522:L1–L3, September 1999astro-ph/9904252. (Cited on page 67.)

[295] S. C. Noble, J. H. Krolik, and J. F. Hawley. Direct calculation of the radiative efficiency of an accretion disk around a black hole. *Astrophys.J.*, 692:411–421, 2009 arXiv:0808.3140, [astro-ph]. (Cited on page 94.)

[296] P. W. Northrop, P. Ramachandran, W. E. Schiesser, and V. R. Subramanian. A robust false transient method of lines for elliptic partial differential equations. *Chemical Engineering Science*, 90(0):32 – 39, 2013. (Cited on page 127.)

[297] D. W. Olson. Density perturbations in cosmological models. *Phys. Rev. D*, 14:327–331, Jul 1976. (Cited on page 64.)

[298] B. W. O'Shea, G. Bryan, J. Bordner, M. L. Norman, T. Abel, R. Harkness, and A. Kritsuk. Introducing Enzo, an AMR Cosmology Application. *ArXiv Astrophysics e-prints*, March 2004arXiv:astro-ph/0403044. (Cited on pages 96 and 171.)

[299] C. D. Ott, E. Abdikamalov, P. Mösta, R. Haas, S. Drasco, E. P. O'Connor, C. Reisswig, C. A. Meakin, and E. Schnetter. General-relativistic Simulations of Three-dimensional Core-collapse Supernovae. *Astrophys.J.*, 768:115, May 2013 arXiv:1210.6674, [astro-ph.HE]. (Cited on page 172.)

[300] C. D. Ott, E. Schnetter, A. Burrows, E. Livne, E. O'Connor, and F. Löffler. Computational models of stellar collapse and core-collapse supernovae. *Journal of Physics Conference Series*, 180(1):012022, July 2009 arXiv:0907.4043, [astro-ph.HE]. (Cited on page 172.)

[301] D. Paoletti and F. Finelli. CMB Constraints on a Stochastic Background of Primordial Magnetic Fields. *Phys.Rev.*, D83:123533, 2011 arXiv:1005.0148, [astro-ph.CO]. (Cited on page 34.)

[302] V. Paschalidis, Y. T. Liu, Z. Etienne, and S. L. Shapiro. Merger of binary white dwarf-neutron stars: Simulations in full general relativity. *Phys. Rev. D*, 84(10):104032, November 2011 arXiv:1109.5177, [astro-ph.HE]. (Cited on page 172.)

[303] V. Paschalidis, S. M. Halataei, S. L. Shapiro, and I. Sawicki. Constraint propagation equations of the 3+1 decomposition of f(R) gravity. *Class.Quant.Grav.*, 28:085006, 2011 arXiv:1103.0984, [gr-qc]. (Cited on page 95.)

[304] A. Passamonti, M. Bruni, L. Gualtieri, and C. F. Sopuerta. Coupling of Radial and Non-radial Oscillations of Neutron Stars In *NATO ASIB Proc. 210: The Electromagnetic Spectrum of Neutron Stars*. A. Baykal, S. K. Yerli, S. C. Inam, & S. Grebenev, editor, page 83, January 2005arXiv:gr-qc/0411021. (Cited on pages 2 and 69.)

[305] A. Passamonti, M. Bruni, L. Gualtieri, and C. F. Sopuerta. Coupling of radial and non-radial oscillations of relativistic stars: gauge-invariant formalism. *Phys. Rev.*, D71:024022, 2005 arXiv:gr-qc/0407108. (Cited on pages 2 and 69.)

[306] D. Pathria. The correct formulation of intermediate boundary conditions for runge–kutta time integration of initial boundary value problems. *SIAM Journal on Scientific Computing*, 18(5):1255–1266, 1997. (Cited on pages 4, 150, 152, and 163.)

[307] R. Penrose. Gravitational collapse: The role of general relativity. *Riv. Nuovo Cimento*, 1:252–276, 1969. (Cited on page 94.)

[308] R. Penrose. The question of cosmic censorship. *Journal of Astrophysics and Astronomy*, 20(3-4):233–248, 1999. (Cited on page 94.)

[309] W. J. Percival et al. Parameter constraints for flat cosmologies from CMB and 2dF-GRS power spectra. *Mon.Not.Roy.Astron.Soc.*, 337:1068, 2002 arXiv:astro-ph/0206256, [astro-ph]. (Cited on page 19.)

[310] S. Perlmutter et al. Measurements of Omega and Lambda from 42 high redshift supernovae. *Astrophys.J.*, 517:565–586, 1999 arXiv:astro-ph/9812133, [astro-ph]. (Cited on pages 19 and 29.)

[311] L. I. Petrich, S. L. Shapiro, and S. A. Teukolsky. Oppenheimer-snyder collapse with maximal time slicing and isotropic coordinates. *Phys. Rev. D*, 31:2459–2469, May 1985. (Cited on page 112.)

[312] L. Petzold. Order results for implicit rungekutta methods applied to differential/algebraic systems. *SIAM Journal on Numerical Analysis*, 23(4):837–852, 1986. (Cited on page 150.)

[313] Planck Collaboration, R. Adam, P. A. R. Ade, N. Aghanim, M. Arnaud, J. Aumont, C. Baccigalupi, A. J. Banday, R. B. Barreiro, J. G. Bartlett, and et al. Planck intermediate results. XXX. The angular power spectrum of polarized dust emission at intermediate and high Galactic latitudes. *ArXiv e-prints*, September 2014 arXiv:1409.5738. (Cited on page 28.)

[314] D. Pollney, C. Reisswig, E. Schnetter, N. Dorband, and P. Diener. High accuracy binary black hole simulations with an extended wave zone. *Phys.Rev.*, D83:044045, 2011 arXiv:0910.3803, [gr-qc]. (Cited on pages 172, 173, 185, and 193.)

[315] W. H. Press, S. A. Teukolsky, W. T. Vetterling, and B. P. Flannery. *Numerical Recipes 3rd Edition: The Art of Scientific Computing*. Cambridge University Press, New York, NY, USA, 3 edition, 2007. (Cited on pages 145 and 146.)

[316] F. Pretorius. Evolution of Binary Black-Hole Spacetimes. *Physical Review Letters*, 95(12):121101, September 2005gr-qc/0507014. (Cited on page 112.)

[317] A. Prothero and A. Robinson. On the Stability and Accuracy of One-Step Methods for Solving Stiff Systems of Ordinary Differential Equations. *Math. Comput.*, 28(125):145–162, 1974. (Cited on page 150.)

[318] M. M. Rai. A conservative treatment of zonal boundaries for euler equation calculations. *Journal of Computational Physics*, 62(2):472 – 503, 1986. (Cited on page 173.)

[319] S. Räsänen. Backreaction: directions of progress. *Classical and Quantum Gravity*, 28(16):164008, August 2011 arXiv:1102.0408, [astro-ph.CO]. (Cited on page 20.)

[320] S. Rasanen. Dark energy from backreaction. *JCAP*, 0402:003, 2004 arXiv:astro-ph/0311257, [astro-ph]. (Cited on page 20.)

[321] B. Ratra. Cosmological 'seed' magnetic field from inflation. *Astrophys J. Lett*, 391:L1–L4, May 1992. (Cited on page 36.)

[322] B. Ratra and P. J. E. Peebles. Cosmological consequences of a rolling homogeneous scalar field. *Phys. Rev. D*, 37:3406–3427, Jun 1988. (Cited on page 19.)

[323] M. J. Reid and E. M. Silverstein. OH masers and the Galactic magnetic field. *Astrophys.J.*, 361:483–486, October 1990. (Cited on page 33.)

[324] O. A. Reula. Hyperbolic methods for einstein's equations. *Living Reviews in Relativity*, 1(3), 1998. (Cited on pages 95, 104, and 108.)

[325] A. G. Riess et al. Observational evidence from supernovae for an accelerating universe and a cosmological constant. *Astron.J.*, 116:1009–1038, 1998 arXiv:astro-ph/9805201, [astro-ph]. (Cited on pages 19 and 29.)

[326] A. G. Riess et al. Type Ia supernova discoveries at $z > 1$ from the Hubble Space Telescope: Evidence for past deceleration and constraints on dark energy evolution. *Astrophys.J.*, 607:665–687, 2004 arXiv:astro-ph/0402512, [astro-ph]. (Cited on page 31.)

[327] W. Rindler. *Relativity: Special, General, and Cosmological*. Relativity: Special, General, and Cosmological. Oxford University Press, 2001. (Cited on page 9.)

[328] T. Robishaw, E. Quataert, and C. Heiles. Extragalactic Zeeman Detections in OH Megamasers. 2008 arXiv:0803.1832, [astro-ph]. (Cited on page 33.)

[329] A. M. Roma, C. S. Peskin, and M. J. Berger. An adaptive version of the immersed boundary method. *Journal of Computational Physics*, 153(2):509 – 534, 1999. (Cited on page 171.)

[330] A. Ruzmaikin, D. Sokolov, and A. Shukurov. Magnetism of spiral galaxies. *NATURE*, 336:341–347, November 1988. (Cited on page 35.)

[331] M. Salgado and D. Martinez-del Rio. The Initial value problem of scalar-tensor theories of gravity. *J.Phys.Conf.Ser.*, 91:012004, 2007 arXiv:0712.2260, [gr-qc]. (Cited on page 95.)

[332] A. Sandage and G. A. Tammann. Steps toward the Hubble constant. VIII - The global value. *Astrophys. J.*, 256:339–345, May 1982. (Cited on page 29.)

[333] M. A. Scheel, H. P. Pfeiffer, L. Lindblom, L. E. Kidder, O. Rinne, et al. Solving Einstein's equations with dual coordinate frames. *Phys.Rev.*, D74:104006, 2006 arXiv:gr-qc/0607056, [gr-qc]. (Cited on page 94.)

[334] E. Schnetter, S. H. Hawley, and I. Hawke. Evolutions in 3-D numerical relativity using fixed mesh refinement. *Class.Quant.Grav.*, 21:1465–1488, 2004 arXiv:gr-qc/0310042, [gr-qc]. (Cited on pages 3, 96, 133, 171, 172, and 185.)

[335] R. Schrader. On the electromagnetic response to gravitational waves. *Physics Letters B*, 143(46):421 – 426, 1984. (Cited on pages 71 and 87.)

[336] M. Schroeder. *Number Theory in Science and Communication: With Applications in Cryptography, Physics, Digital Information, Computing, and Self-Similarity*. Springer series in information sciences. Springer, 2008. (Cited on page 114.)

[337] D. J. Schwarz, G. D. Starkman, D. Huterer, and C. J. Copi. Is the low-l microwave background cosmic? *Phys.Rev.Lett.*, 93:221301, 2004 arXiv:astro-ph/0403353, [astro-ph]. (Cited on page 35.)

[338] J. M. M. Senovilla. New class of inhomogeneous cosmological perfect-fluid solutions without big-bang singularity. *Phys. Rev. Lett.*, 64:2219–2221, May 1990. (Cited on page 20.)

[339] M. Servin, G. Brodin, and M. Marklund. Cyclotron damping and Faraday rotation of gravitational waves. *Phys.Rev.*, D64:024013, 2001 arXiv:gr-qc/0102031, [gr-qc]. (Cited on page 87.)

[340] S. K. Sethi and K. Subramanian. Primordial magnetic fields in the post-recombination era and early reionization. *Mon.Not.Roy.Astron.Soc.*, 356:778–788, 2005 arXiv:astro-ph/0405413, [astro-ph]. (Cited on page 34.)

[341] J. R. Shaw and A. Lewis. Constraining primordial magnetism. *Phys. Rev. D*, 86:043510, Aug 2012. (Cited on page 34.)

[342] C. Shen, J.-M. Qiu, and A. Christlieb. Adaptive mesh refinement based on high order finite difference weno scheme for multi-scale simulations. *J. Comput. Phys.*, 230(10):3780–3802, May 2011. (Cited on pages 3 and 172.)

[343] M. Shibata. Fully general relativistic simulation of coalescing binary neutron stars: Preparatory tests. *Phys. Rev. D*, 60:104052, Oct 1999. (Cited on page 127.)

[344] M. Shibata and T. Nakamura. Evolution of three-dimensional gravitational waves: Harmonic slicing case. *Phys.Rev.*, D52:5428–5444, 1995. (Cited on page 105.)

[345] M. Shibata and H. Yoshino. Nonaxisymmetric instability of rapidly rotating black hole in five dimensions. *Phys. Rev. D*, 81:021501, Jan 2010. (Cited on page 95.)

[346] H.-a. Shinkai and G. Yoneda. Reformulating the Einstein equations for stable numerical simulations. 2002 arXiv:gr-qc/0209111, [gr-qc]. (Cited on pages 95, 104, and 108.)

[347] D. Shoemaker, K. Smith, U. Sperhake, P. Laguna, E. Schnetter, and D. Fiske. Moving black holes via singularity excision. *Classical and Quantum Gravity*, 20:3729–3743, August 2003gr-qc/0301111. (Cited on page 112.)

[348] W. C. Skamarock, J. B. Klemp, J. Dudhia, D. O. Gill, D. M. Barker, W. Wang, and J. G. Powers. A description of the advanced research wrf version 2. *Available from NCAR; P.O. Box 3000; Boulder, co*, 88:7–25, 2001. (Cited on page 173.)

[349] L. Smarr. Space-Time Generated by Computers: Black Holes with Gravitational Radiation In *Eighth Texas Symposium on Relativistic Astrophysics*. M. D. Papagiannis, editor, volume 302 of *Annals of the New York Academy of Sciences*, page 569, December 1977. (Cited on page 93.)

[350] Y. Sofue, M. Fujimoto, and K. Kawabata. Faraday Rotation by Metagalactic Magnetic Field. *Publications of the Astronomical Society of Japan*, 20:388, 1968. (Cited on page 32.)

[351] D. T. Son. Magnetohydrodynamics of the early universe and the evolution of primordial magnetic fields. *Phys. Rev. D*, 59:063008, Feb 1999. (Cited on page 36.)

[352] C. F. Sopuerta, M. Bruni, and L. Gualtieri. Non-Linear N-Parameter Spacetime Perturbations: Gauge Transformations through the Baker-Campbell-Hausdorff Formula. *Phys. Rev.*, D70:064002, 2004 arXiv:gr-qc/0306027. (Cited on pages 2, 58, 60, and 69.)

[353] T. P. Sotiriou and V. Faraoni. f(R) Theories Of Gravity. *Rev.Mod.Phys.*, 82:451–497, 2010 arXiv:0805.1726, [gr-qc]. (Cited on page 20.)

[354] D. Spergel et al. First year Wilkinson Microwave Anisotropy Probe (WMAP) observations: Determination of cosmological parameters. *Astrophys.J.Suppl.*, 148:175–194, 2003 arXiv:astro-ph/0302209, [astro-ph]. (Cited on pages 18 and 19.)

[355] A. A. Starobinskii. Spectrum of relict gravitational radiation and the early state of the universe. *ZhETF Pisma Redaktsiiu*, 30:719–723, December 1979. (Cited on page 71.)

[356] H. Stephani, D. Kramer, M. MacCallum, C. Hoenselaers, and E. Herlt. *Exact Solutions of Einstein's Field Equations*. Cambridge University Press, 2003. (Cited on page 57.)

[357] J. M. Stewart. Perturbations of friedmann-robertson-walker cosmological models. *Classical and Quantum Gravity*, 7(7):1169, 1990. (Cited on page 58.)

[358] J. M. Stewart and M. Walker. Perturbations of space-times in general relativity. *Royal Society of London Proceedings Series A*, 341:49–74, October 1974. (Cited on pages 2, 60, and 69.)

[359] W. R. Stoeger, R. Maartens, and G. F. R. Ellis. Proving almost-homogeneity of the universe: an almost Ehlers-Geren-Sachs theorem. *Astrophys. J.*, 443:1–5, April 1995. (Cited on page 67.)

[360] L. E. Strigari. Galactic searches for dark matter. *Phys. Rep.*, 531:1–88, October 2013 arXiv:1211.7090, [astro-ph.CO]. (Cited on page 16.)

[361] P. Szekeres. A Class of Inhomogeneous Cosmological Models. *Commun.Math.Phys.*, 41:55, 1975. (Cited on page 20.)

[362] M. Szydlowski. Dynamical systems in cosmology. *Classical and Quantum Gravity*, 14(9), 1997. (Cited on page 58.)

[363] K. Takahashi, K. Ichiki, H. Ohno, and H. Hanayama. Magnetic field generation from cosmological perturbations. *Phys.Rev.Lett.*, 95:121301, 2005 arXiv:astro-ph/0502283, [astro-ph]. (Cited on pages 35, 79, 83, and 85.)

[364] R. Takahashi and the TAMA Collaboration. Status of tama300. *Classical and Quantum Gravity*, 21(5):S403, 2004. (Cited on page 94.)

[365] K. Takami, L. Rezzolla, and L. Baiotti. Constraining the Equation of State of Neutron Stars from Binary Mergers. *Phys.Rev.Lett.*, 113(9):091104, 2014 arXiv:1403.5672, [gr-qc]. (Cited on page 172.)

[366] F. Tavecchio, G. Ghisellini, G. Bonnoli, and L. Foschini. Extreme TeV blazars and the intergalactic magnetic field. *MNRAS*, 414:3566–3576, July 2011 arXiv:1009.1048, [astro-ph.HE]. (Cited on page 35.)

[367] L. F. A. Teodoro, D. A. Diver, and M. A. Hendry. A cautionary note on cosmological magnetic fields. *MNRAS: Letters*, 383(1):L35–L39, 2008. (Cited on page 79.)

[368] S. A. Teukolsky. Linearized quadrupole waves in general relativity and the motion of test particles. *Phys. Rev. D*, 26:745–750, Aug 1982. (Cited on page 182.)

[369] J. Thornburg. Coordinates and boundary conditions for the general relativistic initial data problem. *Classical and Quantum Gravity*, 4(5):1119, 1987. (Cited on page 112.)

[370] J. Thornburg. Finding apparent horizons in numerical relativity. *Phys.Rev.*, D54:4899–4918, 1996 arXiv:gr-qc/9508014, [gr-qc]. (Cited on page 114.)

[371] J. Thornburg. A (3+1) computational scheme for dynamic spherically symmetric black hole space-times. 2. Time evolution. *Phys.Rev.D*, 1999 arXiv:gr-qc/9906022, [gr-qc]. (Cited on page 194.)

[372] J. Thornburg. Event and apparent horizon finders for 3+1 numerical relativity. *Living Reviews in Relativity*, 10(3), 2007. (Cited on page 115.)

[373] P. Tourrenc. Effect of a gravitational wave on electromagnetic radiation confined in a cavity: Ii. intrinsic coupling. *General Relativity and Gravitation*, 9(2):141–153, 1978. (Cited on pages 71 and 87.)

[374] P. Trivedi, K. Subramanian, and T. Seshadri. Primordial Magnetic Field Limits from CMB Trispectrum - Scalar Modes and Planck Constraints. *Phys.Rev.*, D89:043523, 2014 arXiv:1312.5308, [astro-ph.CO]. (Cited on page 34.)

[375] M. Trodden and S. M. Carroll. TASI lectures: Introduction to cosmology. pages 703–793, 2004 arXiv:astro-ph/0401547, [astro-ph]. (Cited on page 30.)

[376] C. Tsagas and R. Maartens. Magnetized cosmological perturbations. *Phys.Rev.*, D61:083519, 2000 arXiv:astro-ph/9904390, [astro-ph]. (Cited on page 2.)

[377] C. G. Tsagas. Electromagnetic fields in curved spacetimes. *Class.Quant.Grav.*, 22:393–408, 2005 arXiv:gr-qc/0407080, [gr-qc]. (Cited on page 50.)

[378] C. G. Tsagas. Resonant amplification of magnetic seed fields by gravitational waves in the early universe. *Phys.Rev.*, D72:123509, 2005 arXiv:astro-ph/0508556, [astro-ph]. (Cited on page 83.)

[379] C. G. Tsagas. On constraint-consistency, covariant operators, gauge-invariance, etc. 2007 arXiv:gr-qc/0703005, [gr-qc]. (Cited on page 88.)

[380] C. G. Tsagas. Primordial magnetic seed field amplification by gravitational waves: Comment on gr-qc/0503006. *Phys.Rev.*, D75:087901, 2007 arXiv:gr-qc/0503042, [gr-qc]. (Cited on page 88.)

[381] C. G. Tsagas, P. K. Dunsby, and M. Marklund. Gravitational wave amplification of seed magnetic fields. *Phys.Lett.*, B561:17–25, 2003 arXiv:astro-ph/0112560, [astro-ph]. (Cited on pages 71, 83, and 87.)

[382] C. G. Tsagas and A. Kandus. Superadiabatic-type magnetic amplification in conventional cosmology. *Phys.Rev.*, D71:123506, 2005 arXiv:astro-ph/0504089, [astro-ph]. (Cited on page 36.)

[383] C. G. Tsagas and R. Maartens. Cosmological perturbations on a magnetized Bianchi I background. *Class.Quant.Grav.*, 17:2215–2242, 2000 arXiv:gr-qc/9912044, [gr-qc]. (Cited on pages 72 and 73.)

[384] S. Tsujikawa. Quintessence: A Review. *Class.Quant.Grav.*, 30:214003, 2013 arXiv:1304.1961, [gr-qc]. (Cited on page 19.)

[385] M. S. Turner and L. M. Widrow. Inflation-produced, large-scale magnetic fields. *Phys. Rev. D*, 37:2743–2754, May 1988. (Cited on page 36.)

[386] T. Vachaspati. Magnetic fields from cosmological phase transitions. *Physics Letters B*, 265(34):258 – 261, 1991. (Cited on page 36.)

[387] D. Vandevoorde and N. Josuttis. *C++ Templates: The Complete Guide*. Pearson Education, 2002. (Cited on page 125.)

[388] T. L. Veldhuizen. Expression templates. 7(5):26–31, June 1995. Reprinted in C++ Gems, ed. Stanley Lippman. (Cited on page 125.)

[389] G. L. Verschuur. Zeeman Effect Observations of H i Emission Profiles. II. Results of an Attempt to Confirm Previous Claims of Field Detections. *Astrophys.J.*, 451:645, October 1995. (Cited on page 33.)

[390] F. H. Vincent, E. Gourgoulhon, and J. Novak. 3+1 geodesic equation and images in numerical spacetimes. *Class.Quant.Grav.*, 29:245005, 2012 arXiv:1208.3927, [gr-qc]. (Cited on page 116.)

[391] M. Visser. Cosmography: Cosmology without the Einstein equations. *Gen.Rel.Grav.*, 37:1541–1548, 2005 arXiv:gr-qc/0411131, [gr-qc]. (Cited on pages 14 and 31.)

[392] J. Wainwright and G. Ellis. *Dynamical Systems in Cosmology*. Cambridge University Press, 1997. (Cited on page 58.)

[393] R. M. Wald. *General relativity*. Chicago, University of Chicago Press, 1984, 504 p., 1984. (Cited on pages 4, 5, 11, and 100.)

[394] I. Wasserman. On the origins of galaxies, galactic angular momenta, and galactic magnetic fields. *Astrophys. J.*, 224:337–343, September 1978. (Cited on page 34.)

[395] S. Weinberg. *Gravitation and cosmology: principles and applications of the general theory of relativity*. Wiley, 1972. (Cited on pages 29 and 30.)

[396] S. Weinberg. *Cosmology*. Cosmology. OUP Oxford, 2008. (Cited on page 30.)

[397] L. M. Widrow. Origin of galactic and extragalactic magnetic fields. *Rev.Mod.Phys.*, 74:775–823, 2002 arXiv:astro-ph/0207240, [astro-ph]. (Cited on pages 32 and 33.)

[398] H. Witek, H. Okawa, V. Cardoso, L. Gualtieri, C. Herdeiro, et al. Higher dimensional Numerical Relativity: code comparison. 2014 arXiv:1406.2703, [gr-qc]. (Cited on page 95.)

[399] A. M. Wolfe, R. A. Jorgenson, T. Robishaw, C. Heiles, and J. X. Prochaska. An 84 microGauss Magnetic Field in a Galaxy at Redshift $z = 0.692$. *Nature*, 455:638, 2008 arXiv:0811.2408, [astro-ph]. (Cited on page 33.)

[400] T. Yamamoto, M. Shibata, and K. Taniguchi. Simulating coalescing compact binaries by a new code (sacra). *Phys. Rev. D*, 78:064054, Sep 2008. (Cited on page 94.)

[401] H.-J. Yo, T. W. Baumgarte, and S. L. Shapiro. Improved numerical stability of stationary black hole evolution calculations. *Phys.Rev.*, D66:084026, 2002 arXiv:gr-qc/0209066, [gr-qc]. (Cited on page 107.)

[402] C.-M. Yoo and H. Okawa. Black hole universe with a cosmological constant. *Phys.Rev.*, D89(12):123502, 2014 arXiv:1404.1435, [gr-qc]. (Cited on page 113.)

[403] C.-M. Yoo, H. Okawa, and K.-i. Nakao. Black Hole Universe: Time Evolution. *Phys.Rev.Lett.*, 111:161102, 2013 arXiv:1306.1389, [gr-qc]. (Cited on page 94.)

[404] J. W. York. Kinematics and Dynamics of General Relativity In *Sources of Gravitational Radiation*. Larry L. Smarr, editor, pages 83–126, 1979. (Cited on page 110.)

[405] J. W. York, Jr. *Initial data for collisions of black holes and other gravitational miscellany.*, pages 89–109. Cambridge University Press, 1989. (Cited on page 114.)

[406] J. W. York. Conformal "thin-sandwich" data for the initial-value problem of general relativity. *Phys. Rev. Lett.*, 82:1350–1353, Feb 1999. (Cited on page 119.)

[407] C. Yuksel, S. Schaefer, and J. Keyser. On the parameterization of catmull-rom curves. In *2009 SIAM/ACM Joint Conference on Geometric and Physical Modeling*, SPM '09, pages 47–53, New York, NY, USA, 2009. ACM. (Cited on page 145.)

[408] I. B. Zeldovich and I. D. Novikov. *Relativistic astrophysics. Volume 2 - The structure and evolution of the universe /Revised and enlarged edition/.* Chicago, IL, University of Chicago Press, 1983, 751 p. Translation., 1983. (Cited on page 34.)

[409] U. Ziegler. The nirvana code: Parallel computational mhd with adaptive mesh refinement. *Computer Physics Communications*, 179(4):227 – 244, 2008. (Cited on pages 96 and 171.)

[410] M. Zilhão, V. Cardoso, C. Herdeiro, L. Lehner, and U. Sperhake. Collisions of charged black holes. *Phys. Rev. D*, 85:124062, Jun 2012. (Cited on page 94.)

[411] M. Zilhao, H. Witek, U. Sperhake, V. Cardoso, L. Gualtieri, et al. Numerical relativity for D dimensional axially symmetric space-times: formalism and code tests. *Phys.Rev.*, D81:084052, 2010 arXiv:1001.2302, [gr-qc]. (Cited on page 95.)

[412] M. Zilho, V. Cardoso, C. Herdeiro, L. Lehner, and U. Sperhake. Testing the nonlinear stability of Kerr-Newman black holes. *Phys.Rev.*, D90:124088, 2014 arXiv:1410.0694, [gr-qc]. (Cited on page 172.)

[413] M. Zilho and S. C. Noble. Dynamic fisheye grids for binary black hole simulations. *Class.Quant.Grav.*, 31:065013, 2014 arXiv:1309.2960, [gr-qc]. (Cited on pages 3, 96, and 185.)

[414] I. Zlatev, L.-M. Wang, and P. J. Steinhardt. Quintessence, cosmic coincidence, and the cosmological constant. *Phys.Rev.Lett.*, 82:896–899, 1999 arXiv:astro-ph/9807002, [astro-ph]. (Cited on page 19.)

[415] Y. Zlochower, J. Baker, M. Campanelli, and C. Lousto. Accurate black hole evolutions by fourth-order numerical relativity. *Phys.Rev.*, D72:024021, 2005 arXiv:gr-qc/0505055, [gr-qc]. (Cited on page 185.)

[416] Y. Zlochower, M. Ponce, and C. O. Lousto. Accuracy issues for numerical waveforms. *Phys. Rev. D*, 86:104056, Nov 2012. (Cited on pages 172 and 173.)

[417] C. Zunckel, G. Betschart, P. K. Dunsby, and M. Marklund. On inhomogeneous magnetic seed fields and gravitational waves within the MHD limit. *Phys.Rev.*, D73:103509, 2006 arXiv:gr-qc/0602036, [gr-qc]. (Cited on pages 2, 69, 71, 74, 78, 87, and 88.)